Layer-by-Layer Assembled Nanoparticles for Drug Delivery Through Skin

THESIS

Submitted in partial fulfillment

of the requirements for the degree of

DOCTOR OF PHILOSOPHY

by

SUMAN LABALA

ID. No. 2012PHXF505H

Under the supervision of

Dr. VENKATA VAMSI KRISHNA VENUGANTI

BITS Pilani

Pilani | Dubai | Goa | Hyderabad

BIRLA INSTITUTE OF TECHNOLOGY AND SCIENCE, PILANI

2016

BIRLA INSTITUTE OF TECHNOLOGY AND SCIENCE, PILANI

CERTIFICATE

This is to certify that the thesis entitled "**Layer-by-Layer Assembled Nanoparticles for Drug Delivery Through Skin**" and submitted by **Suman Labala** ID. No. **2012PHXF505H** for award of Ph.D. of the Institute embodies original work done by him under my supervision.

Signature of the supervisor :

Name in capital letters : VENKATA VAMSI KRISHNA VENUGANTI

Designation : Assistant Professor

Date :

ACKNOWLEDGEMENTS

I would like to express my special appreciation and thanks to my supervisor, Dr. Venkata Vamsi Krishna Venuganti, Assistant Professor, Department of Pharmacy, BITS Pilani, Hyderabad Campus. He has been a tremendous mentor for me. I would like to thank him for encouraging my research and for allowing me to grow as a researcher. His advice on both research as well as on my career have been invaluable. To work with him, has been a great and inexplicable experience that will go along a long way in my life. It is with affection and reverence that I acknowledge my indebtness to him and his outstanding dedication, often far beyond the call of duty. I can't forget the financial assistance provided by him and I wouldn't have completed this project without his support.

I am extremely obliged to Prof. Punna Rao Ravi, Department of Pharmacy, BITS-Pilani Hyderabad, who acted as Doctoral Advisory Committee (DAC) member. I would like to thank him for his valuable suggestions during my proposal and departmental presentations. Working with him as a teaching assistant is a memorable experience to me.

I am extremely obliged to Prof. P. Yogeeswari, Associate Dean, Sponsored Research and Consultancy Division, BITS-Pilani Hyderabad, who acted as Doctoral Advisory Committee (DAC) member and gave her valuable suggestions whenever needed.

I also expressed my profound gratitude to Prof. Shrikant Yashwant Charde, Associate Professor and Head, Department of Pharmacy, for his support and extending the facilities to work at the institute.

My special thanks to Dr. Onkar Prakash Kulkarni, Assistant Professor, Department of Pharmacy, BITS-Pilani Hyderabad for sharing his vast experience and technical knowledge with me at needy times.

I am grateful to Prof. D. Sriram, Prof. A. Sajeli Begum, Dr. Swati Biswas, Dr. Balaram Ghosh and Dr. Arti Dhar, Faculty, Department of Pharmacy for their invaluable suggestions and support.

My sincere thanks to Prof. Souvik Bhattacharyya, Vice Chancellor, Prof. V. S. Rao, Director, BITS Pilani, Hyderabad Campus, Prof. M. M. S. Anand, Registrar, Prof. Sanjay Kumar Verma, Dean, Academic Research, Prof. M. B. Srinivas, Dean, General Administration and Prof. Vidya Rajesh, Associate Dean, Academic Research (Ph.D. Programme) BITS-Pilani, Hyderabad, for providing necessary support to accomplish my research work.

My lab mates Mr. Praveen, Mr. Anup, Ms. Shubhmita, Dr. Sudeep, Mr. Omkar, Ms. Preeti, Mr. Vishnu, Mr. Himanshu, deserve special thanks for making congenial environment in the lab. It would be incomplete if I failed to thank Mr. Shailender, Mr. Gangadhar, Mr. Poorna, Mr. Srikanth, Mr. Santhosh, Ms. Prakruti, Ms. Hasitha, Ms. Priyanka Suryadevara, Mr. Brahmam, Mr. Bobesh, Ms. Reshma, Ms. Nikhila, Ms. Prasanthi, Mr. Shubham, Mr. Siva Krishna, Mr. Suresh, Ms. Priyanka Reddy, Ms. Rimpy, Ms. Ekta Prasanthi, Ms. Padma Sridevi, Ms. Jaspreet, Ms. Renuka, Dr. Madhubabu, Dr. Saketh, Dr. Mahibalan, Dr. Koushik, Dr. Rukaiyya S Khan, Dr. N. Aditya, Dr. Rahul Vats, Dr. Mallika, Mr. Abinav, Mr. Shareef, Mr. Sumeet, Ms. Aashma, Ms Aswini, Mr. Kunal and Ms. Neeraja for giving me overwhelming support all these days.

My heartfelt thanks to supporting staff Ms. Saritha, Mr. Rajesh, Mr. Praveen, Ms. Laxmi, Mr. Narendra Verma, Mr. Srinivas and Ms. Rekha, their extra-ordinary support.

I appreciate the Department of Science and Technology (DST) and Department of Biotechnology (DBT) for providing funding to pursue doctoral studies.

I also thank Science and Engineering Research Board (SERB), Department of Science and Technology (DST), Indian Council of Medical Research (ICMR) and Centre for International Co-operation in science (CICS) for providing me international travel support grant to present my research work at various conferences.

I bow down with reverence and offer my heartfelt thanks to my parents Leelavathi and Jayarao, sister Indira, brother in law Murali, for their moral support, encouragement and patience absolutely needed to complete my entire study. It was the blessing of them that gave me courage to face the challenges and made my path easier.

I am indebted infinitely to care, support and trust being shown by my wife Pavithra, who has taken a lot of pains to keep me free from domestic responsibilities. I am very much thankful to my beloved son Digvijay Sai, for forgiving me with his cute smile for not spending enough time with him.

Suman Labala

July, 2016

ABSTRACT

Advances in the drug discovery science resulted in the development of various therapeutic molecules. Drug delivery through oral route is considered to be the most convenient method for drug administration. But many small and macromolecules therapeutics (nucleic acids, proteins and vaccines) cannot be delivered through oral route due to enzymatic degradation in gastric environment. Over the past few decades topical route of drug delivery is gaining much attention for delivery of drugs through the skin due to its convenience, dose termination and elimination of first pass effect. However drug transport through skin is challenging due to barrier function of stratum corneum. Various nanocarriers were explored for drug delivery through the skin. Recently, Layer-by-layer (LbL) assembly technique gained greater interest for drug delivery application. Essentially, the LbL technique involves sequential adsorption of oppositely charged polyelectrolytes on a template. In the present work spherical gold nanoparticles (AuNP) were used as template for fabrication of layer-by-layer gold nanoparticles (LbL-AuNP). LbL assembly also offers co-delivery of various therapeutic agents.

To this end, the overall objective of the study is the development of LbL-AuNP for topical delivery of small and macromolecule therapeutics. In the present study melanoma was taken as model to prove our hypothesis. Imatinib mesylate (IM) and small interference RNA (siRNA) and were taken as model small and macromolecule therapeutics, respectively. Imatinib mesylate is a c-kit tyrosine kinase inhibitor approved for treatment of melanoma. Signal transducer and activator of transcription 3 (STAT3) is over expressed in melanoma, hence we used siRNA against STAT3 for treatment of melanoma. Iontophoresis was used for topical application of LbL-AuNP.

The first objective of this study was to investigate the feasibility of using LbL-AuNP as a carrier for topical iontophoretic delivery of imatinib mesylate (IM) for treatment of melanoma. LbL-AuNP were prepared by sequential adsorption of cationic polyethylene imine (PEI) and anionic poly(styrenesulfonate) (PSS). We studied the stability of AuNP and LbL-AuNP in biological media. In-vitro release of IM was performed in phosphate buffered saline (PBS). In-vitro skin penetration of IM was studied by passive and iontophoresis application using excised porcine ear skin. Finally the toxicity of LbL-AuNP was determined using B16F10 murine melanoma cell line and cell uptake studies are also conducted. But we observed that blank LbL-AuNP showed significant reduction in viability of B16F10 cells, and this toxicity could be associated with PEI used in fabrication of LbL-AuNP.

The second objective of our study is to replace PEI with chitosan (Mw 15kDa) due to its natural origin and biocompatibility. The prepared chitosan stabilized gold nanoparticles (AuNP-CS) were used for delivery of STAT3 siRNA. The AuNP-CS were then sequentially layered with siRNA and chitosan to form AuNP-CS/siRNA/CS. In-vitro release of siRNA was performed in PBS. We also studied cell viability, cell uptake of LbL-AuNP-CS in B16F10 cells. In addition we also performed studies to determine apoptotic potential and mechanism of cell uptake of LbL-AuNP by flow cytometry. We also studied skin penetration of siRNA delivered by LbL-AuNP-CS using confocal microscopy. In-vitro gene silencing studies were also performed using B16F10. We observed that STAT3 delivered using LbL-AuNP-CS showed significant knockdown of STAT3 protein and iontophoresis application also improved skin penetration of siRNA.

In the third objective of this study we explored co-delivery of IM with STAT3 siRNA using LbL-AuNP-CS. In-vivo application of LbL-AuNP-CS was also performed using C57BL/6 mouse model for melanoma. It was observed co-delivery of siRNA and IM using LbL-AuNP-CS was able to silence STAT3 and reduced tumor volume compared to other

treatments groups. Taken together, LbL-AuNP can be developed as a carrier for iontophoretic delivery of small molecules and siRNA based therapeutics for treatment of melanoma and other skin conditions.

TABLE OF CONTENTS

LIST OF TABLES

LIST OF FIGURES

LIST OF ABBREVIATIONS AND SYMBOLS

AuNP	Gold nanoparticles
BRAF	Murine sarcoma viral (v-raf) oncogene homolog B1
DLS	Dynamic light scattering
DMEM	Dulbecco's modified eagle’s medium
DNA	deoxyribonucleic acid
DSC	Differential scanning calorimeter
EDTA	Ethylene diamine tetra acetic acid
EE	Encapsulation efficiency
ERK	Extracellular signal-regulated kinases
FBS	Fetal bovine serum
FDA	Food and drug administration
FTIR	Fourier transform infrared spectroscopy
g	Gram
h	Hour
HPLC	High performance liquid chromatography
IM	Imatinib mesylate
J	Joules

L	Litre
LbL	Layer-by-layer
M	Molar
MAPK	Mitogen-activated protein kinase
mg	Milligram
min	Minute
mm	Millimetre
MW	Molecular weight
PBS	Phosphate buffered saline
PDI	Polydispersity index
PEI	Polyethylene imine
PSS	Poly(styrene-4-sulphonic acid)
R^2	Regression coefficient
RNAi	Ribonucleic acid interference
RP-HPLC	Reverse phase – high performance liquid chromatography
RT	Room temperature (25 ± 2 ºC/60 ± 5% RH)
s	Seconds
SA	Sodium alginate
SC	Stratum corneum

SD	Standard deviation
SDS	Sodium dodecyl sulphate
SDS-PAGE	Sodium dodecyl sulphate polyacrylamide gel electrophoresis
SEM	Scanning electron microscopy
siRNA	Small interference ribonucleic acid
STAT3	Signal transducer and activator of transcription 3
TBE	Tris Borate EDTA buffer
TEM	Transmission electron microscopy
TEMED	N, N‘tetra methyl ethylene diamine
UV	Ultraviolet
ζ-potential	Zeta-potential
λ_{max}	Wavelength maxima for UV-absorbance
µg	Microgram
^{o}C	Degree centigrade

Chapter 1

Introduction

1. INTRODUCTION

The skin is an easily accessible site for the administration of therapeutics (Cevc et al., 1997). The field of transdermal drug delivery aims at developing safe, efficacious and non-invasive modes of delivery of drugs across the skin. Drugs are delivered mainly through oral and parenteral routes (Sudhakar et al., 2007). The oral route has several advantages such as convenience to patient for self-administration of predetermined doses of drugs (Tanner et al., 2008). Various small molecule drugs and macromolecules such as proteins (vaccines, growth factors, insulin, monoclonal antibodies etc.), nucleic acids (small interference RNA, DNA vaccines, micro RNA) are not delivered by the oral route, due to rapid degradation in the stomach by proteases and nucleases (Hejazi et al., 2003; Lowman et al., 1999). The high molecular weight macromolecules are not able to transport across the epithelium. Hence, the primary mode of administering macromolecules like proteins, antibodies, vaccines are therefore via injection (Mitragotri et al., 2014; Borges et al., 2013). Rationally, the conventional routes of drug delivery have several inherent limitations, which could potentially be addressed by advanced drug delivery methodologies such as non-invasive topical and transdermal drug delivery (Alkilani et al., 2015, Tibbitt et al., 2016). Understanding the structure and physiology of skin aids in designing new technologies for efficient delivery of small and macromolecule therapeutics to /across skin.

1. 1. Structure and physiology of skin

The skin is the largest organ in the human body. The large surface area of skin is suitable for delivery of drugs for topical and systemic application. The skin is divided into three layers: epidermis, dermis and hypodermis.

1.1.1. Epidermis

The outer layer, epidermis mainly consists of keratinocytes. The thickness of epidermis is approximately 50–150 μm and is made up of distinct layers of stratified squamous epithelial tissue. These layers, starting with the outermost, are the stratum corneum (SC), stratum lucidum, stratum granulosum, stratum spinosum, and stratum basale (Gauglitz et al., 2013).

The outermost layer, SC forms a natural barrier composed of 10–15 layers of keratinized cells with a thickness of 10-20 μm (Langer et al., 1990). SC prevents excessive water loss and entry of exogenous chemicals, which limits the use of the transdermal route as a means of systemic drug delivery (Proksch et al., 2008; Micali et al., 2001). The SC undergoes a total turnover, every 2–3 weeks. SC keratinocytes are surrounded by a continuous lipid phase known as the intercellular lipid lamellae and arranged in a "bricks and mortar" model (Foldvari et al., 2000). The major components in the stratum corneum lipid lamellae are ceramides, cholesterol and fatty acids (Harding et al., 2004). Apart from these cells, the antigen-presenting Langerhans cells are also located in the epidermis (Katz et al., 1979).

1.1.2. Dermis

The dermis, which is about 2–3 mm thick and consists of connective tissues, which adhere to the epidermis and the hypodermis (Philandrianos et al., 2012). Blood vessels, lymphatic vessels, sensory nerve endings, pilosebaceous units and sweat glands are located in the dermis (Khavkin et al., 2011). The dermis represents the bulk of the skin and contains collagen fibres and a smaller amount of elastin. This fibrous network gives tensile strength and elasticity to the skin and also provides support for nerve and vascular networks. In the

upper papillary region of the dermis, the collagen fibres are small and loosely distributed. The deep, reticular region contains densely packed, bundled collagen fibres mainly running parallel to the skin surface and along certain directions, called Langer's lines (Pawar et al., 2012).

1.1.3. Hypodermis

The hypodermis or subcutaneous layer is the deepest layer of the skin and consists of a network of fat cells (Haake et al., 2001). It is the contact layer between the skin and the

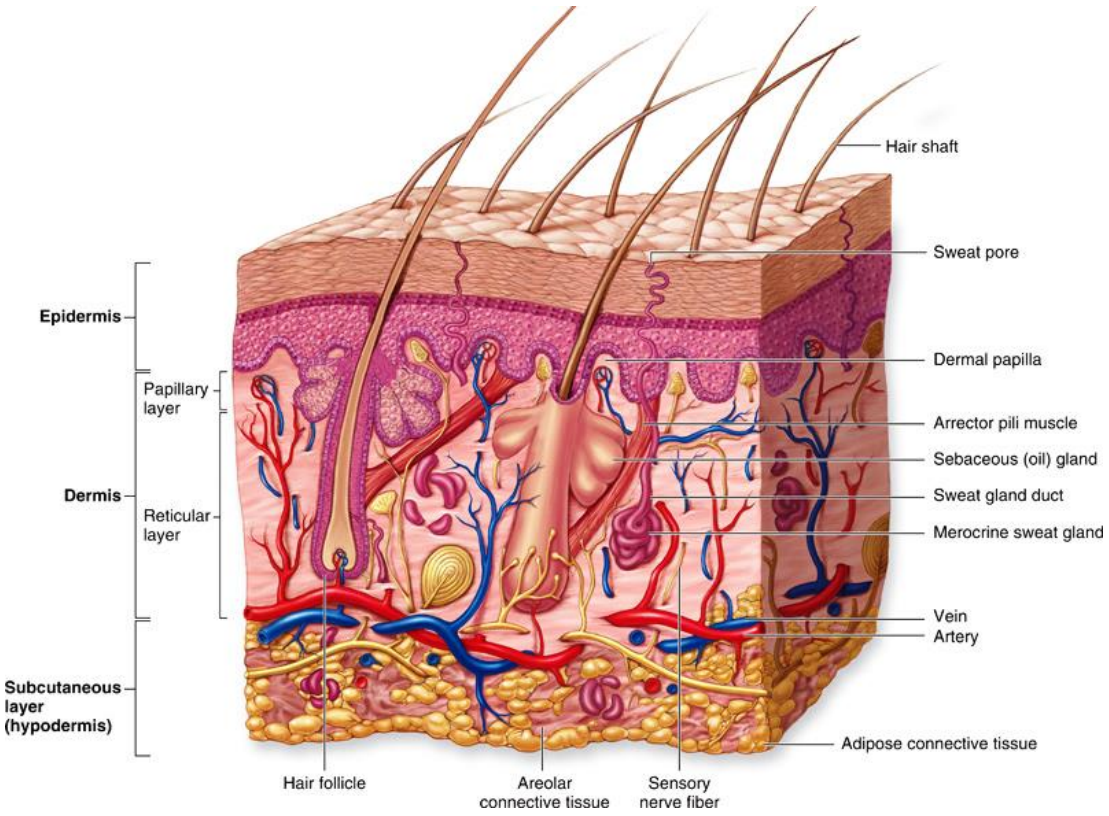

Fig.1.1. Anatomy of the skin. Reproduced from web page http://cosbiology.pbworks.com.

underlying tissues of the body, such as muscles and bone. Therefore, the major functions of the hypodermis are protection against physical shock, heat insulation, support and

conductance of the vascular and neural signals of the skin (Benson et al 2012). Hypodermis resident fat cells account for approximately 50% of the body's fat and also consisting of fibroblasts and macrophages (Figure 1.1).

1.2. Localized diseases of skin

Most of diseases affecting the skin originate in the layers of the skin, such abnormalities are also important factors in the diagnosis of a variety of internal diseases. Like other tissues, skin is also affected by all types of pathological changes, including hereditary, inflammatory, benign and malignant, endocrine, hormonal, traumatic, and degenerative processes. The common diseases of skin are eczema, dermatitis, psoriasis, urticaria (Antony et al., 2014, Lane et al., 2013).

1.2.1. Eczema

The eczema is an inflammatory process in the dermis and epidermis of skin (Hoare et al., 2000). The epidermis exhibits swelling of the keratinocytes and retention of fluid between them, this condition is called spongiosis (Erkinjuntti et al., 1996). In chronic forms of eczema, the prominent changes are thickening of the epidermis and marked hyperkeratosis. These changes may lead to lichenification, roughening and scaling of the skin surface (Mansouri et al., 2011). The impervious barrier functions of SC are seriously impaired, with two important consequences: loss of water from the skin leads to desiccation of SC, which in turn leads to cracking, increased scaling, and soreness.

1.2.2. Dermatitis

The term dermatitis is also an inflammatory process in the dermis and epidermis of the skin. The classification of dermatitis includes contact dermatitis and atopic dermatitis.

Contact dermatitis is further classified as allergic or non-allergic (Shaffer et al., 2000). Non-allergic contact dermatitis occurs in response to skin irritants, and usually affects the hands. Acids, alkalis, oils, detergents, solvents, and even repeated exposure to water are among the numerous causes. Allergic contact dermatitis is a less common cause of occupational skin disease but is frequently found among the general population. Allergic contact dermatitis occurs only in persons sensitized to the offending chemicals or antigen (Kimber et al., 2002). Common antigens include nickel, chromium, rubber, and paraphenyline diamine. The langerhans cells of the epidermis are responsible for recognizing the antigen (Liu et al., 2001; Gunther et al., 2007).

Atopic dermatitis is characterized by sensitization of the skin to a wide range of common antigens. In addition to eczematous changes, persons with atopic dermatitis may also often have diminished, absent, or paradoxical cutaneous vascular reactions to vasodilating and vasoconstricting drugs and also having impaired immunity to fungal and viral infections (Leung et al., 2004).

1.2.3. Psoriasis

Psoriasis is a proliferative and an inflammatory disorder, but less common than atopic dermatitis. Psoriasis is characterized by rapid proliferation of the keratinocytes, which results in the formation of raised scaly plaques in areas (Feldman et al., 2008). Psoriatic persons may suffer from arthritis that affects joints in the fingers and spine (Helliwell et al., 2015). Whether the increased rate of keratinocyte proliferation is due to increased activity of a growth-promoting factor or to lack of a growth inhibitor is unknown. As an inflammatory disorder, psoriasis is characterized by nests of neutrophil leukocytes in the epidermis called microabscesses. Possible mediators that attract this cell type are leukotrienes and fragments derived from activated blood peptide components called complement (Tursun et al., 2015).

1.2.4. Skin infections and infestations

Healthy skin harbours a resident, harmless bacterial population that includes *Micrococcaceae, Propionibacteriaceae,* and *Aerobic diphtheroids* and pathogenic form of *Staphylococci* (Zuniga et al., 2013). These staphylococci strains are often resistant to antibiotics. Signs of bacterial infection appear after the organisms have been introduced into the dermis. Some organisms, such as staphylococci and streptococci, produce a pustular infection in which the main features are acute inflammation and the accumulation of large numbers of white blood cells. Other organisms, including *Mycobacterium tuberculosis* and *Treponema pallidum*, may cause more chronic inflammatory changes without pus but involving a characteristic arrangement of mononuclear inflammatory cells called histiocytes. Whereas leprosy is a cutaneous bacterial granulomatous disease in which the causative organism, *Mycobacterium leprae,* resides in the neural tissue in the skin, producing the characteristic features of nerve thickening and numbness (Geluk et al., 2014).

1.2.5. Urticaria

Urticaria features an area of central redness, on which is superimposed an irregular wheal, caused by local edema and surrounded by a bright pink flare (Asero et al., 2014). The wheals are usually multiple and remain visible for short duration. The reaction is due to release of histamine from cellular stores within the skin and is usually accompanied by itching. Common causes include allergies to shellfish, strawberries and nuts or to drugs such as penicillin; but physical factors such as cold, exercise, and sunlight may also produce the response (Antonova et al., 2015).

1.2.6. Metabolic disorders

A metabolic disorder that dramatically affects the skin is porphyria, an enzyme defect that causes haemoglobin precursors, or porphyrins to accumulate in the skin. Porphyrins are abnormally sensitive to long wavelength ultraviolet light. The accumulation of porphyrins results in severe sun sensitivity with blistering, increased skin fragility and scarring on the areas exposed to light (Egan et al., 2015). The most common form, porphyria cutanea tarda is usually caused by a combination of a hereditary enzyme defect and chronic alcoholism.

1.2.7. Skin cancer

Skin cancer is one of the most common forms of cancer in humans resulting in significant mortality (Jemal et al., 2011). The incidence and prevalence of skin cancer can be greatly reduced by simple preventive measures, such as avoidance of exposure to the sun and to excessive ionizing radiation. Primary skin cancers can be divided into basal cell carcinoma, squamous cell carcinoma and malignant melanoma.

1.2.7. 1. Basal cell carcinoma

Basal cell carcinoma is the most common form of skin tumor and arises from the undifferentiated basal keratinocytes of the epidermis (Sekulic et al., 2012). Although multiple basal cell carcinomas may develop early in life as an inherited trait, most arise in middle age and later. These cancers rarely metastasize but may be highly invasive locally. The lesions occur in fair-skinned persons and on areas of skin that receive the greatest exposure to sunlight. Treatment with inorganic arsenical drugs and exposure to ionizing radiation (X rays, radium) may also contribute to some cases. Avoidance of excessive sunlight and careful control of ionizing radiation significantly lowers the incidence of basal cell carcinoma. Although metastases are rare, the cancer may spread locally and invade surrounding tissues. When this occurs, treatment may be difficult and lengthy (Velema et al., 2014).

1.2.7. 2. Squamous cell carcinoma

Squamous cell carcinoma is less common than basal cell carcinoma but has a higher rate of metastasis (Hawrot et al., 2003). It is common in children with xeroderma pigmentosum, who are unable to repair DNA damage caused by ultraviolet irradiation. In most persons this inability is due to the deficiency of an endonuclease enzyme. In adults, squamous cell carcinoma rarely occurs in the absence of an external cause. Excessive exposure to sunlight is the usual cause, but chronic scarring from burns, as well as reactions to vaccinations, radiation dermatitis and chronic ulceration may contribute to some cases (Ibeto et al., 2016).

Squamous cell carcinoma is also an occupational hazard (Mitragotri et al., 2014). Skin lesions that precede squamous cell carcinoma include white patches in the mucous membranes of the mouth and genitalia.

1.2.7. 3. Malignant melanoma

Melanoma arises from melanocytes, neural crest-derived cells which are located in the basal layer of the epidermis (Barckhausen et al., 2014). Melanocytes, synthesizes melanin pigment and exporting it to the adjacent keratinocytes play a key role in protecting the skin from the damaging effects of ultraviolet (UV) and other solar radiation (Bandarchi et al., 2013; Pfeifer et al., 2012). The mutations in regulatory genes, production of autocrine growth factors and the loss of adhesion receptors all contribute to disrupt intracellular signaling in melanocytes, allowing them to escape their tight regulation by keratinocytes. Consequently, melanocytes can proliferate and spread, leading to formation of a naevus or common mole. Melanocyte proliferation can be restricted to the epidermis (junctional naevus), the dermis (dermal naevus) or overlapping components of both (compound naevus). Naevi are generally

benign but can progress to the radial-growth-phase (RGP) melanoma, an intra-epidermal lesion that can involve some local micro invasion of the dermis (Means et al., 2015; Masterpol et al., 2013). RGP cells can progress to the vertical-growth phase (VGP), a more dangerous stage in which the cells have metastatic potential, with nodules or nests of cells invading the dermis.

Considering the growth patterns, four histological types of melanoma have been historically recognized: superficial spreading melanoma (SSM), lentigo malignant melanoma (LMM), nodular melanoma (NM) and acral lentiginous melanoma (ALM). Comparative genomic hybridization revealed that several genomic regions (mostly, 11q13, 22q11-13, and 5p15) were abnormally amplified in ALM; such regions were different from those found altered in superficial SSM or NM (mainly, 9p21 and 1p22).

Recently, a new classification of melanoma including the site of primary tumor and the degree of chronic sun-induced damage of the surrounding skin has been introduced. Based on these criteria, melanomas are classified into four groups; melanoma on skin with chronic sun-damage (CSD melanoma), melanoma on skin without chronic sun-damage (non-CSD melanoma), melanoma on palms, soles and nail bed (acral melanoma), and melanoma on mucous membrane (mucosal melanoma) (Russak et al., 2012). There are an estimated 2–3 million cases of skin cancer across the world each year, and although melanoma only accounts for about 132,000 of these (World Health Organization), it is the most dangerous form, accounting for most skin cancer deaths (Gray-Schopfer et al., 2007). If melanoma is diagnosed early it can be cured by surgical resection. However, metastatic malignant melanoma is largely refractory to existing therapies and has a very poor prognosis, with a median survival rate of 6 months, so new treatment strategies are urgently needed (Ruiz et al., 2011).

1.3. Melanoma signaling pathways

The management of melanoma requires an in-depth understanding of the biology underlying its initiation and progression (Smalle et al., 2006). Comprehensive strategies such as comparative genomic hybridization and mutation analysis by gene sequencing have identified some of the crucial cell-signalling pathways are discussed below.

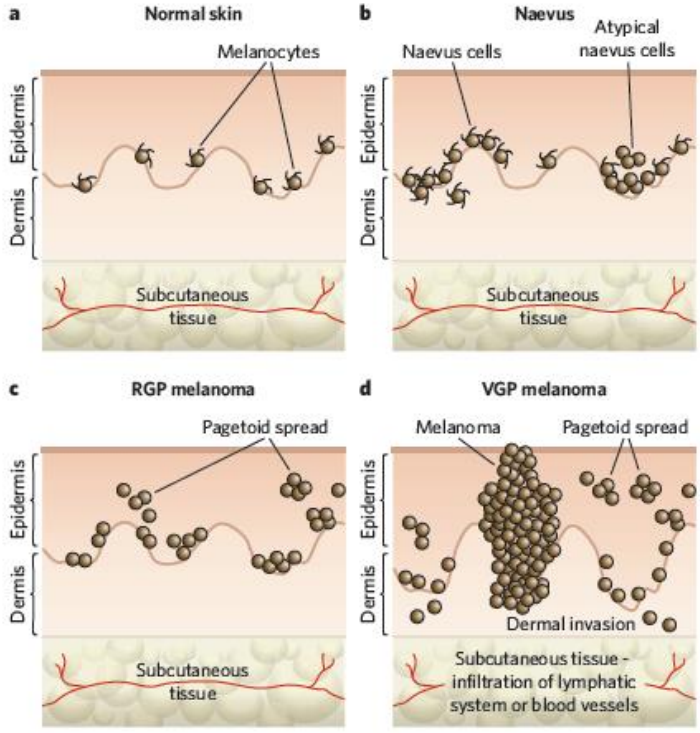

Fig.1.2. Progression of melanocyte transformation. **a**, Normal skin, showing an even distribution of dendritic melanocytes within the basal layer of the epidermis. **b**, Naevus, in the early stages, benign melanocytic naevi occur with increased numbers of dendritic melanocytes. **c**, Radial-growth-phase (RGP) melanoma. **d**, Vertical-growth-phase (VGP) melanoma. Reproduced from Schopfer et al., 2007.

1.3.1. BRAF and MAPK pathway

The mitogen-activated protein kinase (MAPK) signal transduction pathway regulates cell growth, survival, and invasion. MAPK signaling is initiated by receptor tyrosine kinases (RTKs) binding ligand adhesion to extracellular matrix, which transmits activation signals via RAS on the inner surface of cell membrane (Fig. 1.3.). RAS proteins are small GTPases that are activated by extracellular stimuli and regulate signal transduction of the BRAF-MAPK-

ERK and AKT/PI3K pathways, controlling crucial cellular processes such as proliferation, differentiation, cell adhesion, apoptosis and cell migration (Davies et al., 2002; Sumimoto et al., 2006).

The RAF (Rapidly Accelerated Fibrosarcoma) kinase family consists of ARAF, BRAF and CRAF, all of which can phosphorylate protein kinases followed by activation of the extracellular signal-regulated kinase (ERK) downstream protein. In melanoma, *BRAF* gene is the most commonly mutated; the prevalent *BRAF* mutation is due to substitution of valine with glutamic acid at position 600 (V600E) (Chapman et al., 2011). Mutated *BRAF* induces constitutive ERK activation followed by activation of ERK and translocate to the nucleus for transcription of a variety of genes associated with cell growth, proliferation and survival. ERK activation seems to be implicated in melanoma growth, survival and resistance to apoptosis. High levels of activated ERK increases the expression of integrins which inturn promotes invasion (Solit et al., 2006). *BRAF* activation is necessary but not sufficient for the development of melanoma and additional co-operating genetic events are required to achieve full malignancy (Satyamoorthy et al., 2003).

1.3.2. Ras–ERK and phosphoinositide-3-OH kinase signaling

Phosphoinositides are membrane lipids that are converted to secondary messengers through phosphorylation by phosphoinositide-3-OH kinase PI (3) Ks. The lipid second messengers activate various downstream pathways and signaling is terminated PTEN (phosphate and tensin homologue). In melanoma, hyper activated PI (3) K signaling increases melanoma cell survival, growth. PI(3)K mutations occur in 3% of metastatic melanomas, PTEN function is lost in between 5% and 20% cases of late-stage melanomas (Meier et al., 2001). The PI(3)K effector protein kinase B (PKB or Akt) is overexpressed in up to 60% of human melanomas (Downward et al., 2003; Blume-Jensen et al., 2001) .

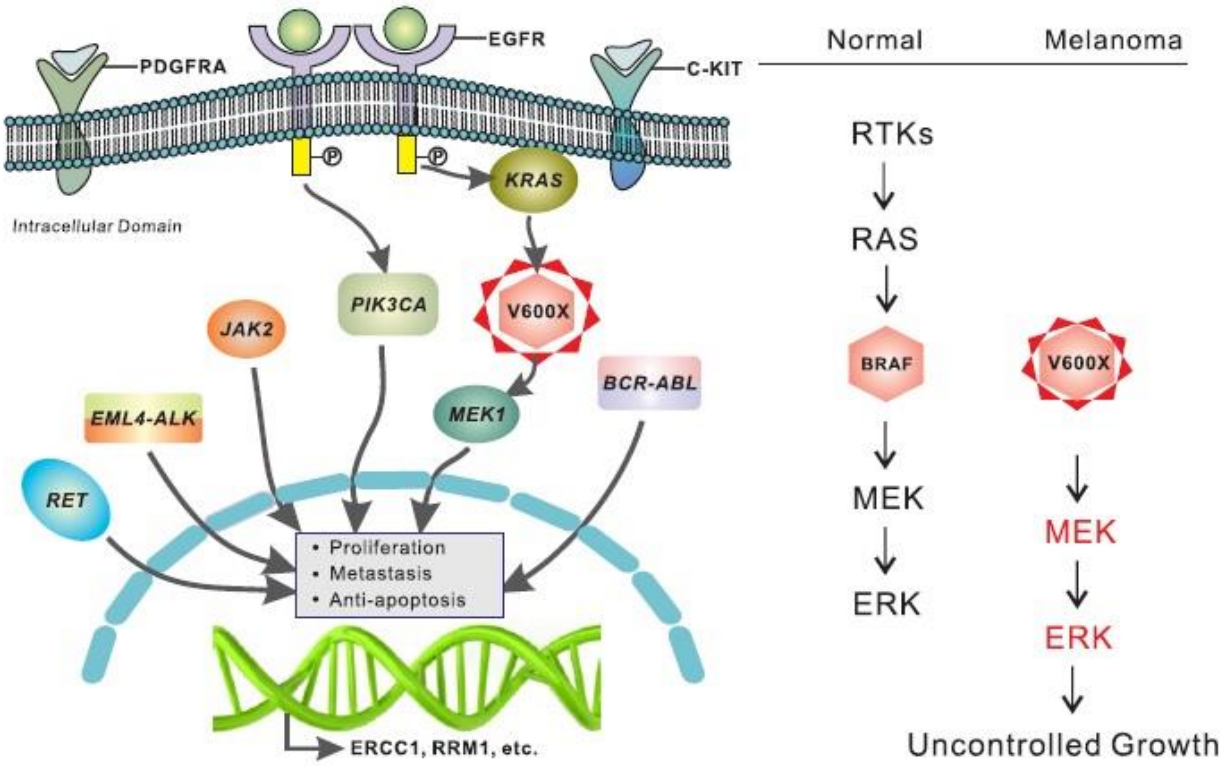

Fig.1.3. BRAF signaling in melanoma. Reproduced from Wang et al., 2015.

1.3.3. CDKN2A and senescence/apoptosis pathways

The cyclin-dependent kinase inhibitor 2 (CDKN2A) located at chromosome 9p21 encodes tumor suppressors ($p16^{CDKN2A}$ and $p14^{CDKN2A}$) genes due to alternative splicing. The cyclins are regulatory effector proteins which are able to bind and activate the cyclin-dependent kinases (CDKs). Cyclin D/CDK4 complex leads the passage from the pre-replicative cell cycle phase (G1) to the DNA duplication (S) phase. The Cyclin E/CDK2 complex promotes cell cycle progression through S phase and the Cyclin B/CDK1 complex induces mitosis. $p16^{CDKN2A}$ and $p14^{CDKN2A}$ act as inhibitors of the cell cycle, negatively interfering with the activity of the cyclin/CDK complexes and, in this way, ensuring the

control of the cell replication. In particular, $p16^{CDKN2A}$ is part of the G1–S cell cycle checkpoint mechanism that involves the retinoblastoma-susceptibility tumor suppressor protein (pRb). The $p16^{CDKN2A}$ inhibits the Cyclin D/CDK4 complex, which, in turn, phosphorylates pRb and allows progression through the G1–S checkpoint. The Cyclin D (CCND1) and CDK4 genes are found altered in less than 5% of total melanomas. A reduced expression of the $p16^{CDKN2A}$ protein is associated with tumor invasion, varying from 5% to about 15% in benign melanocytic lesions, from 10% to 50% in primary melanomas, and from 50% to 60% in melanoma metastases. The CDKN2A gene is frequently mutated at germ line level in patients with a strong familial history of melanoma indicating that it represents a key susceptibility gene for familial melanoma (Gray-Schopfer et al., 2007).

1.3.4. PTEN and MTOR pathways

Phosphatase and tensin homolog deleted in chromosome ten (PTEN) is involved in cellular signal transduction by decreasing intracellular phosphatidylinositol [3, 4-bisphosphate (PIP2) and 3, 4, 5-triphosphate (PIP3)] which are produced by the activation of PI3K (Xu et al., 2004). There is a balance between PIP2 and PIP3 which is maintained by the opposite activities of PTEN and PI3K. Upon growth stimulation, mainly obtained by triggering the RAS kinase, PI3K is constitutively activated resulting in an increase of intracellular levels of PIP3 and a consequent activation of AKT by phosphorylation (Dai et al., 2005). Activated AKT in turn phosphorylates its substrate, the serine/threonine kinase mTOR, leading to increased synthesis of target proteins that promote cell division and survival as well as apoptotic escapes (fig. 1.4.). The AKT suppress apoptosis by the phosphorylation and inactivation of pro-apoptotic proteins (BAD -Bcl-2 antagonist of cell death) and activation of NF-kB (Dolcet et al., 2005).

1.3.5. MITF and melanocytic differentiation

The microphthalmia-associated transcription factor (MITF) is a transcription factor involved in development, differentiation and maintenance of melanocytes. MITF is activated by the MAPK pathway and cyclic adenosine monophosphate cAMP pathway. The *MITF* gene is over expressed in melanoma and causes increased resistance to chemotherapy (Levy et al., 2006; Goding et al., 2000).

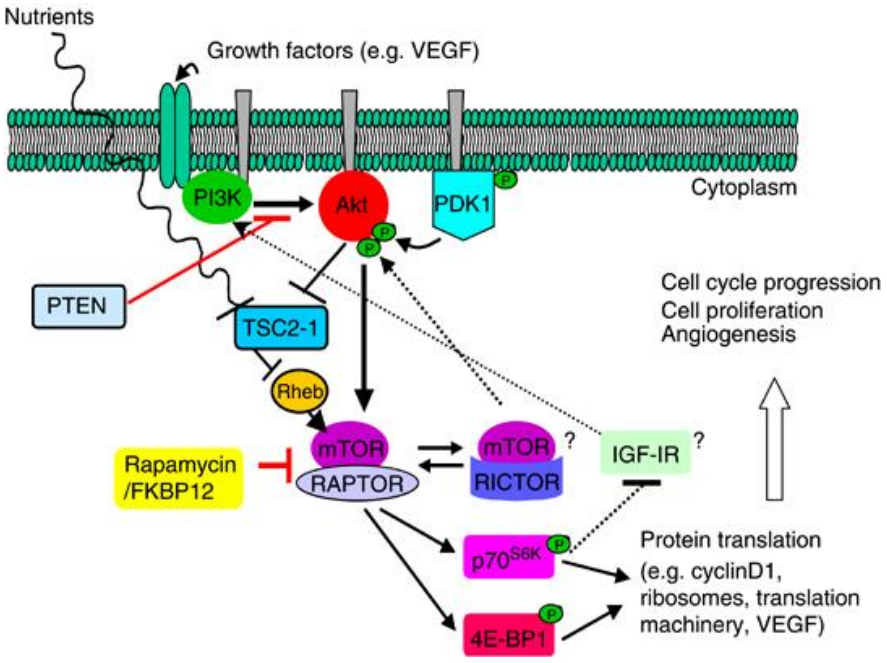

Fig.1.4. PI3K/Akt/mTOR pathway. Reproduced from Wang et al., 2012.

1.3.6. iNOS and NF-kB pathways

Inducible nitric oxide synthase (iNOS) enzyme is expressed by human melanoma cells and is responsible for synthesis of nitric oxide (NO). Melanoma is promoted due to excess levels of NO by sustained protection of the tumor from apoptosis. Higher levels of iNOS have been found in subcutaneous and lymph node metastases of melanoma (Filip et al.,

2013). The constitutive iNOS expression in melanoma cells might be induced by activation of the MAPK pathway through stimulation of Nuclear Factor-kB (NF-kB) activity.

NF-kB is a transcriptional factor and exists as cytoplasmic hetero- or homo dimers associated with members of the inhibitor of kB (IkB) proteins (IkB*a*, Ik*Bb* and IkB*e*), which form complexes sequestering NF-kB into the cytoplasm. Upon stimulation, IkB proteins are phosphorylated and undergo ubiquitination followed by degradation in the proteasome. This causes nucleus translocation of NF-kB and binds to target DNA loci, induces transcription of genes associated with immune response, angiogenesis, proliferation and apoptosis. In melanoma, NF-kB is constitutively activated since expression of the IkB proteins seems to be significantly reduced in comparison to nevi (Madonna et al., 2012).

1.3.7. cKIT and tyrosin kinase receptors

cKIT is a transmenbrane receptor tyrosine kinase which comprises of five immunoglobulin (Ig) like motifs (Guo et al., 2011). Under physiological conditions, binding of the cKIT ligand stem-cell factor (SCF) to the extracellular domain of the receptor leads to dimerization, activation of the intracellular tyrosine kinase domain through auto phosphorylation of specific tyrosine residue (Zsebo et al., 1990). The intracellular signaling through cKIT plays a critical role in the development of several mammalian cells, including growth, differentiation, migration, and proliferation of melanocytes (fig. 1.5.). cKIT recruits and activates a number of intracellular signaling pathways implicated in tumor progression, such as MAPK, PI3K/AKT, Src, signal transducer and activators of transcription (STAT), and phospholipase-C (PLC) (Montone et al., 1997).

Specific mutations within the cKIT gene cause constitutive phosphorylation and activation of the kinase domain resulting in uncontrolled cell proliferation. Sequencing of cKIT exons 11, 13, 17 and 18 revealed the most prevalent mutation to be K642, L576P, D816H, V559A (Rivera et al., 2008). The cKIT mutations are more common in cutaneous melanomas. High

expression levels of cKIT and CDK4 proteins have been identified in another subset of melanomas lacking *BRAF* mutations.

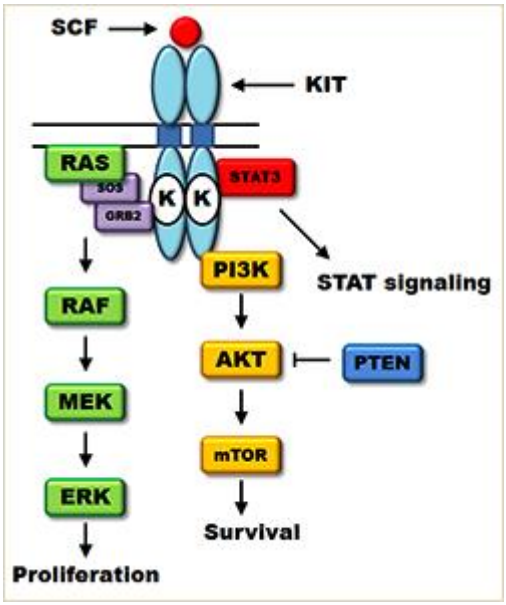

Fig.1.5. cKIT signaling in melanoma. Reproduced from Lartigue et al., 2011.

1.3.8. CTLA-4 and T-cell activation

Melanoma antigens that are bound to the major histocompatibility complex (MHC) on antigen-presenting cells (APCs) require the co-stimulation of CD28 receptor on T-cells by CD80/CD86 ligands on APCs (Lapointe et al., 2003). The cytotoxic T-lymphocyte antigen-4 (CTLA-4) binds to CD80 and CD86, and disrupts the co-stimulatory signal provided by APCs and alters functions of CTLA-4 (fig. 1.6.). In particular, Ipilimumab is a recombinant human IgG1 monoclonal antibody that binds to CTLA-4 and blocks binding to CD80 or CD86 on APCs, thus increasing activation and proliferation of T cells (Alegre et al., 2001).

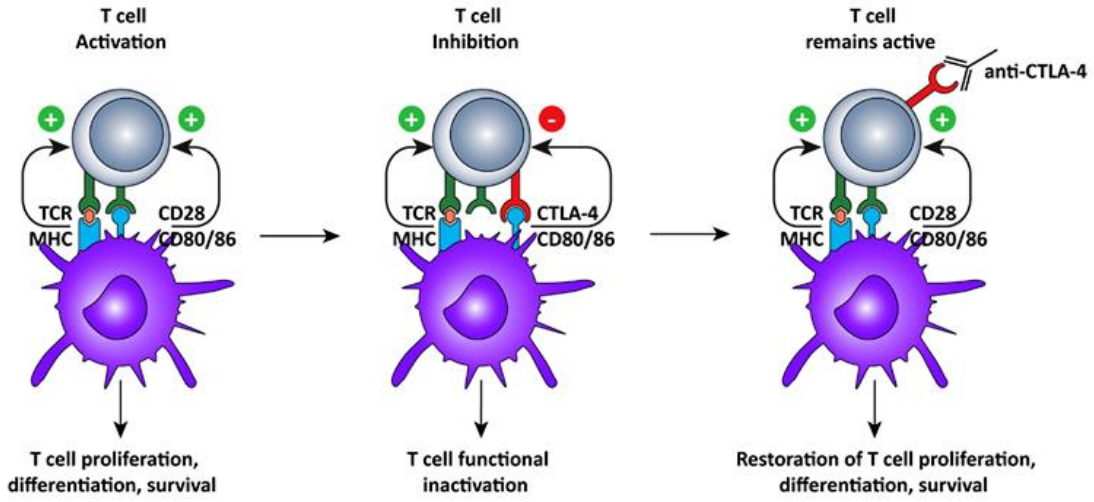

Fig.1.6. CTLA-4 and T-cell activation. Reproduced from Vasaturo et al., 2013.

1.3.9. STAT3 (Signal Transducer and Activator of Transcription) signaling

The STAT family comprises of STAT1, STAT2, STAT3, STAT4, STAT5a, STAT5b and STAT6. The STAT2, STAT4 and STAT6 are activated through a small number of cytokines and involved in T-cell development and Interferon- γ (IFN-γ) signaling. Whereas STAT1, STAT3 and STAT5 are influenced by various ligands and have a key role in promoting oncogenesis. Among STAT3 family of transcription factors, STAT3 controls numerous physiological processes including development, differentiation, immunity, metabolism and is overexpressed in cancer. STAT3 is constitutively phosphorylated in malignant melanoma cells (Kortylewski et al., 2005; Xie et al., 2006).

Several cytokines and growth factors (IL-6 and EGF), hepatocyte growth factor (HGF) activates STAT3 by phosphorylation (Niu et al., 2002). Interleukin-6 (IL-6) signaling serves as an autocrine growth factor for advanced metastatic stages of melanoma in-vivo. STAT3 is mainly implicated in effects mediating IL-6-induced growth inhibition of normal melanocytes and early-stage melanoma cells and promoting advanced malignant melanoma.

Binding of IL-6 to STAT3 receptor causes dimerization of a signal transducer protein, gp130 in the cytoplasm. This is followed by induction of Janus-kinase (JAK) and STAT3 phosphorylation. The JAK family of tyrosine-kinases especially JAK1 mediates the activation of STAT3. Phosphorylated STAT3 monomers combine to form dimers and translocate to nucleus for transcription of genes involved in melanoma cell survival and proliferation (fig. 1.7.). Constitutively activated STAT3 increase expression of anti-apoptotic B-cell lymphoma/leukemia-2 (BCL2) family gene BCLXL and inhibits apoptosis (Taga et al., 1997).

Targeting STAT3 in melanoma tumor models induces tumor cell death/tumor regression, inhibits angiogenesis, prevents metastasis and activates antitumor immune responses (Burdelya et al., 2005). As the majority of melanoma cell lines and tumor specimens display constitutively-activated STAT3, targeting STAT3 is expected to affect a significant population of melanoma patients. Most of the oncogenic proteins converge upon a limited set of nuclear transcription factors for progression of malignancy. Hence targeting a single transcription factor such as STAT3 by various means could neutralize the oncogenic potential of various upstream genetic aberrations. However, combination therapy using inhibitors against STAT3 together with inhibitors of other oncogenic signalling pathways prominently activated in melanoma may lead to better antitumor effects.

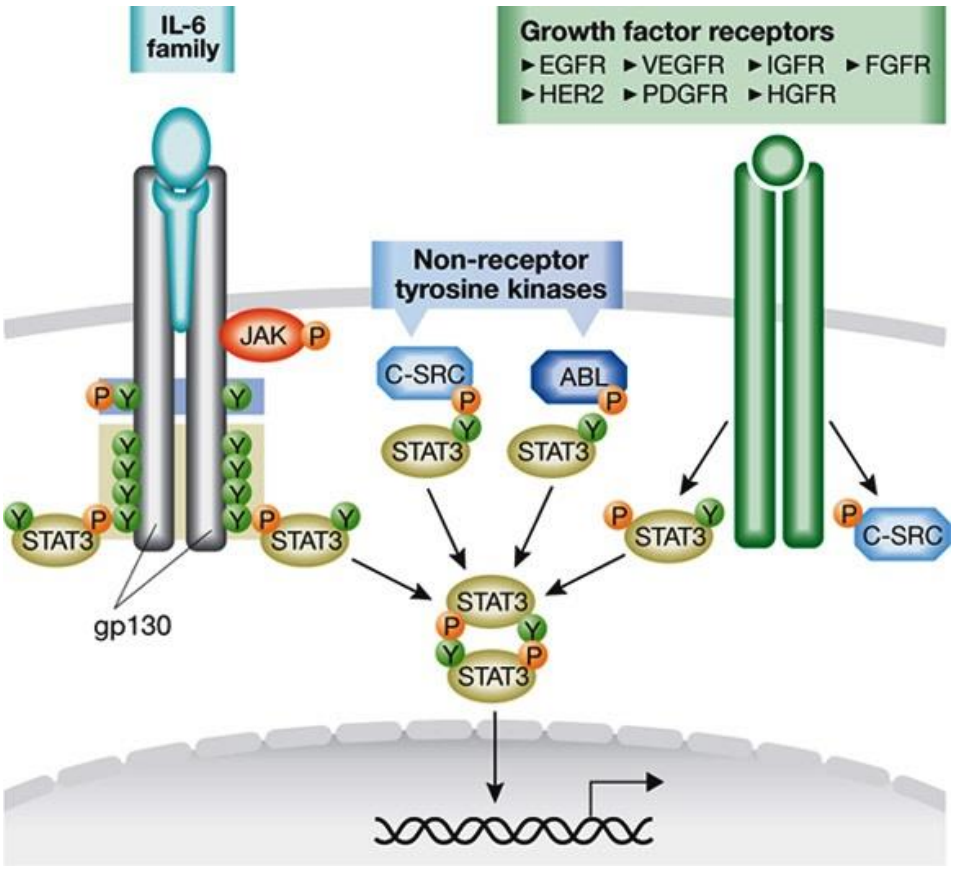

Fig.1.7. STAT3 signaling in melanoma. Reproduced from Bollrath et al., 2009.

1.4. Current treatment options for melanoma

1.4.1. Radiation therapy

Radiation therapy uses high-energy rays (such as X-rays) or particles to kill cancer cells. External beam radiation therapy focuses radiation from outside the body on the skin tumor. This type of radiation therapy is used to treat some patients with melanoma.

1.4.2. Stereotactic radiosurgery (SRS)

SRS is a type of radiation therapy that can sometimes be used for melanoma tumors that have spread to the brain. In this treatment, a machine called a Gamma Knife® focuses

about 200 beams of radiation on the tumor from different angles over a few minutes to hours. The head is kept in the same position by placing it in a rigid frame. In another version, a linear accelerator (a machine that creates radiation) that is controlled by a computer moves around the head to deliver radiation to the tumor from many different angles (Fraker et al., 1996).

1.4.3. Mohs surgery

In this procedure, the skin (including the melanoma) is removed in very thin layers. Each layer is then viewed under a microscope for cancer cells. The procedure continues until a layer shows no signs of cancer. In theory, this allows the surgeon to remove the cancer while saving as much of the surrounding normal skin as possible. If melanoma has spread from the skin to distant organs such as the lungs or brain, the cancer is very unlikely to be curable by surgery.

1.4.4. Isolated limb perfusion/isolated limb infusion

Isolated limb perfusion (ILP) is a limb salvaging therapy for widespread regional cutaneous and subcutaneous metastases. In ILP, high doses of chemotherapeutic agents are delivered to the patient under an extracorporeal circuit that isolates the affected limb to avoid systemic toxicity (Deroose et al., 2012). ILP is most commonly performed with the alkylating agent melphalan, under hyperthermic conditions which potentiates action of melphalan. More recently, the addition of tumor necrosis factor (TNF) and interferon (IFN)-γ to melphalen perfusion has been found to increase overall response to ILP (Fraker et al., 1996).

1.4.5. Cryo therapy

In cryo therapy, liquid nitrogen is generally used for non-invasive target treatment of melanoma. Theoretically, this therapy results in tumor antigen release through local trauma to

the area and thus has the potential to elicit a systemic anti-melanoma immune response. However, the tumor specific immune response following cryo therapy seems to be inferior when compared to other destructive modalities (Bahner et al., 2013).

1.4.6. Chemotherapy Agents

Early stages of melanoma can be easily cured by chemotherapy. There are few chemotherapeutic agents approved for treatment of melanoma.

1.4.6.1. Dacarbazine (DTIC)

DTIC is a class of alkylating agent imidazole carboxamide derivative and approved by FDA for the treatment of stage IV melanoma. It is administered as an intravenous infusion. Dacarbazine is bio- activated to diazomethane in liver by demethylases (Schadendorf et al., 2006).

1.4.6.2. Temozolomide

Temozolomide is an oral form of dacarbazine. This medication is not FDA-approved for the treatment of melanoma, but is often used in Stage IV of malignant melanoma (Kirkwood et al., 2012).

1.4.7. Targeted therapy

Drugs are developed with the goal of destroying cancer cells while leaving normal cells intact. These drugs are designed to interfere with the specific molecules that are driving the growth and spread of the tumor. Because they are “targeted” to the tumor, these therapies may be more effective and associated with fewer side effects compared to chemotherapy. This facilitates personalized treatment as patients receive drugs based on the unique genetic

profile, or subtype of tumor. Fig. 1.8 depicts various treatment options available for treating melanoma.

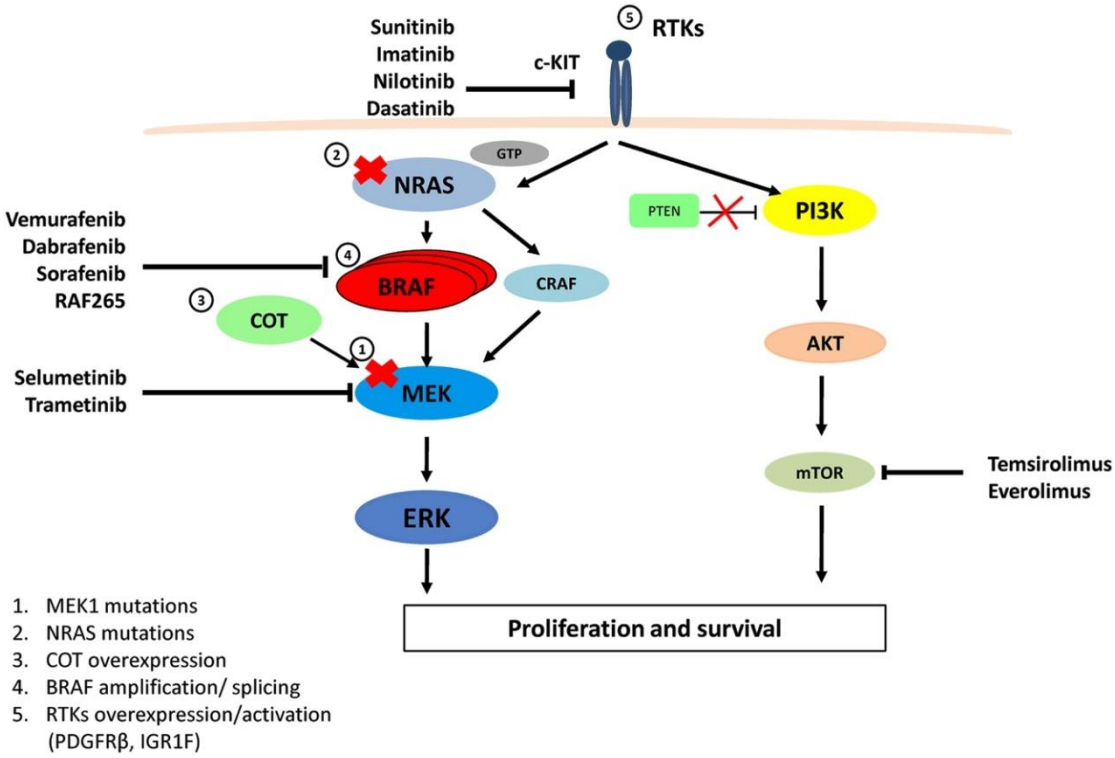

Fig.1.8. Targeted therapy of melanoma. Reproduced from Klinac et al., 2013.

1.4.7.1. Ipilimumab (Yervoy®)

Ipilimumab stimulates T cells and was approved by the FDA in 2011. It was the first drug in 13 years to be approved for the treatment of metastatic melanoma. Randomized trials have shown an improvement in overall survival in patients with either previously treated or untreated advanced melanoma (Fellner et al., 2012).

1.4.7.2. Vemurafenib (Zelboraf®) and Dabrafenib (Tafinlar®)

These drugs are approved by the FDA in 2011 and 2013 respectively, for the treatment of BRAF V600E mutant melanoma that cannot be removed by surgery. This drug is only approved for those patients who have tested positive for the BRAF mutation (Davis et al., 2014).

1.4.7.3. Trametinib (Mekinist®)

Trametinib was approved by the FDA in 2013 for the treatment of BRAF V600E or V600K mutations. It is a first-in-class MEK inhibitor approved for the treatment of unresectable or metastatic melanoma. It is not indicated for the treatment of patients who have received a prior BRAF inhibitor therapy (Robert et al., 2015).

1.4.7.4. Pembrolizumab (Keytruda®)

Pembrolizumab is a therapeutic antibody that blocks the inhibitory ligand of programmed cell death 1 receptor (PD 1). It received FDA approval in 2014 for demonstrating durable responses in patients whose disease has progressed following ipilimumab and dabrafenib treatment (Poole et al., 2014).

1.4.7.5. Nivolumab (Opdivo®)

Nivolumab was approved in November 2015 as a first line therapy for melanoma patients who do not have a positive BRAF V600 mutation. It is the second anti-PD-1 drug to be approved for the treatment of unresectable or metastatic melanoma, but the only anti-PD-1 therapy approved as a single agent for first-line use in patients with advanced BRAF V600 wild-type melanoma (Deeks et al., 2014).

1.4.7.6. Imatinib (Gleevec)

Imatinib (Gleevec) acts by selective inhibition of *C-KIT*. It revolutionized the treatment of chronic myelogenous leukemia and has now been included in the National Comprehensive Cancer Network Clinical Practice Guidelines for Melanoma (Iqbal et al., 2014).

1.4.8. Immunotherapy

1.4.8.1. Interferon alpha 2-b

Interferon alpha 2-b was approved by FDA for patients with metastatic melanoma that has been surgically resected and that are at high risk for recurrence. Analyses of randomized trials of interferon used in an adjuvant show that it can lengthen the time of melanoma recurrence, but it does not appear to prolong survival (Litvin et al., 2015).

1.4.8.2. Interleukin-2 (IL-2)

IL-2 was the first immunotherapeutic agent to be approved for metastatic melanoma (1998) and was approved on the basis of long-lasting complete response (Rosenberg et al., 1999).

1.5. Stages of melanoma diagnosis

Staging of melanoma is the process used to describe the extent of the disease progression. The staging takes into account the tumor thickness, tumor depth and metastasis to the lymph nodes or other parts of the body. Staging helps to provide specific treatment to patients. A detailed knowledge on disease condition, factors associated with its progression would help in designing suitable drug delivery systems.

Table. 1.1. Stages of diagnosis in melanoma (Berrocal et al., 2014).

Stage	Description	Treatment Option
0	The tumor is confined to the epidermis and has not entered the dermis. This stage of melanoma is also called melanoma *in situ.*	The tumor and some surrounding tissue are removed surgically. Usually no further treatment is necessary; however, skin examination to evaluate for a new melanoma or other skin cancer should continue.
I	The tumor is less than 1 mm thick. The outer layer of skin does not look cracked or ulcerated. It has not spread to any lymph nodes or other organs.	The tumor and some surrounding tissue are removed surgically. Usually no further treatment is necessary; however, skin examination to evaluate for a new melanoma or other skin cancer should continue.
II	The tumor is more than 4 mm thick and is ulcerated. These are aggressive tumors that are more likely to spread.	The tumor and some surrounding tissue are removed surgically. Additional treatment(s) may be recommended.
III	The tumor may be of any thickness. It may or may not be ulcerated. The cancer cells have spread either to a few nearby lymph nodes, or to some tissue just outside the tumor but not the distant organs.	The tumor and lymph nodes that have cancer cells are removed surgically. Additional treatment(s) may be recommended. Yervoy® and Imygic®, both immunotherapies, were approved in October 2015 as adjuvant therapies for patients with Stage III melanoma.
IV	The cancer cells have spread to the lymph nodes, other organs in the body, or areas far from the original site of the tumor. This is called metastatic melanoma.	The tumor and lymph nodes that have cancer cells are removed surgically. Additional treatment(s), like immunotherapy, tar geted therapy or clinical trials may be recommen ded.

1.6. Drug delivery

Drug delivery refers to approaches, formulations and technologies for transporting a pharmaceutical compound in the body safely to elicit its desired pharmacological effect (Allen et al., 2004). Drug delivery technologies involve modification of drug release, absorption, distribution and elimination for improving product efficacy and safety. Most drugs are delivered via oral and invasive parenteral route. The oral route of delivery is considered to be the most convenient and acceptable route for drug administration. But many drugs such as macromolecule therapeutics (nucleic acids, proteins, vaccines) cannot be delivered through oral route due to enzymatic degradation in gastric environment or may not be absorbed into the systemic circulation efficiently due to its high molecular size (Niemeyer et al., 2001)

Over the past few decades topical route of drug delivery has gained much attention for delivery of drugs. Topical delivery can be defined as the application of drug formulation to body surfaces, such as skin or mucous membranes to prevent or treat diseases. Topical route can be further classified into extra topical and intra topical route. In extra topical route, the formulation is directly applied on to the cutaneous tissue or skin. Whereas in intra topical route, the formulation is applied into the local cavities of body for therapeutic action; example vagina, rectum and buccal cavity. Most of these topical formulations are generally used for localized effect at the site of drug delivery.

Some of the advantages of drug delivery through skin over conventional routes are as follows:

1. Eliminates the risk and inconvenience with intravenous therapy
2. Usually provides less chance of an overdose or under dose
3. Permits both local and systemic effects
4. Reduces dosing frequency

5. Avoids hepatic first pass elimination and gastrointestinal irritation
6. Non-invasive drug delivery system
7. Improves physiological and pharmacological responses
8. Reduction of fluctuations in plasma levels of drugs
9. Allows easy termination
10. Utilization of drug candidates with short half-life and low therapeutic index
11. Reduction of dosing frequency and patient compliance
12. Transdermal delivery not only provides controlled and constant administration of the drug, but also allows continuous input of drugs with short biological half-lives and eliminates pulsed entry into systemic circulation which often causes undesirable side effects (Naik et al., 2000).

1.7. Routes of penetration of drugs into skin

The drug enters into blood vasculature through epidermis, hair follicles with their associated sebaceous glands and the sweat ducts (fig.1.9.). The major routes of penetration are discussed below.

1.7.1. Transcellular penetration

Intracellular macromolecular matrix within the stratum corneum abounds in keratin, which does not contribute directly to the skin diffusive barrier but supports mechanical stability and thus intactness of the stratum corneum. Transcellular diffusion is practically unimportant for transdermal drug transport (Silva et al., 2014). The narrow aqueous trans epidermal pathways have been observed using confocal laser scanning microscopy. Here, regions of poor cellular and intercellular lipid packing coincide with wrinkles on skin surface and are simultaneously the sites of lowest skin resistance to the transport of hydrophilic entities (Bolzinger et al., 2012). This lowest-resistance pathway leads between clusters of corneocytes at the locations where such cellular groups show no lateral overlap.

The contribution to transdermal drug transport can increase with pathway widening or multiplication, e.g., that which is caused by exposing the stratum corneum to a strong electrical (electroporation/iontophoresis), mechanical (sonoporation/ sonophoresis), or thermal stimulus, or suitable skin penetrants.

1.7.2. Intercellular penetration

Interlamellar regions in the stratum corneum, including linker regions, contain less ordered lipids and more flexible hydrophobic chains. This is the reason for the non-planar spaces between crystalline lipid lamellae and their adjacent cells' outer membrane. Fluid lipids in skin barrier are crucially important for trans epidermal diffusion of the lipidic and amphiphilic molecules, occupying those spaces for the insertion and migration through intercellular lipid layers of such molecules (Silva et al., 2014). The hydrophilic molecules diffuse predominantly "laterally" along surfaces of the less abundant water-filled interlamellar spaces or through such volumes; polar molecules can also use the free space between a lamella and a corneocyte outer membrane to the same end (Lane et al., 2013).

1.7.3. Transappendegeal penetration

This is also called as the shunt pathway. In this route, the drug molecule may transverse through the hair follicles, the sebaceous pathway of the pilosebaceous apparatus or the aqueous pathway of the salty sweat glands (Hayat et al., 2014). The transappendegeal pathway is considered to be of minor importance because of its relatively small area (less than 0.1% of total surface). However, this route may be of some importance for large polar compounds.

The route through which permeation occurs is largely dependent on physical and chemical characteristics of penetrant, most importantantly being the relative ability to partition into each skin phase (Mittal et al., 2015). The transdermal permeation can be visualized as a composite of a series in sequence as:

1. Adsorption of a penetrant molecule onto the surface layers of stratum corneum.

2. Diffusion through stratum corneum and through viable epidermis.

3. Finally, through the papillary dermis into the microcirculation.

The viable tissue layer and the capillaries are relatively permeable and the peripheral circulation is sufficiently rapid. Hence, diffusion through the stratum corneum is the rate-limiting step. The stratum corneum acts like a passive diffusion medium. So for transdermal drug diffusion, the various skin tissue layers can be represented by a simple multilayer model.

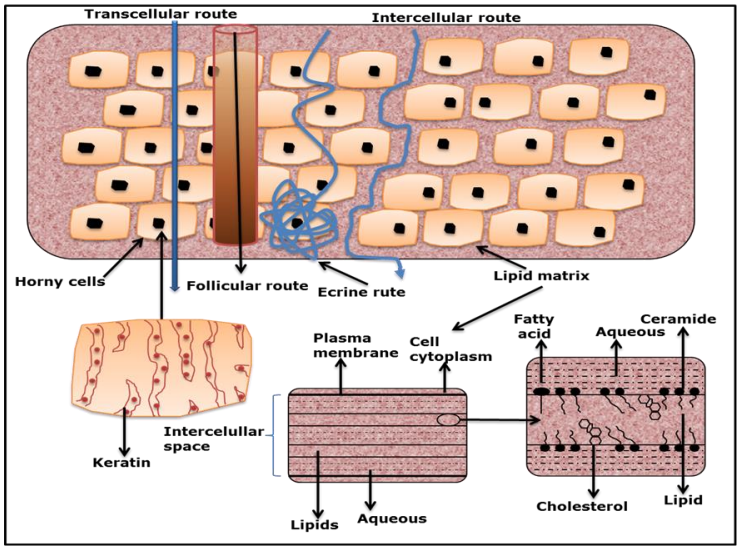

Fig.1.9. Possible drug penetration routes across human skin. Reproduced from Chavez et al., 2012.

Drug delivery through the skin via topical/transdermal application of drugs is an important approach for delivery of potent drugs such as chemotherapeutic agents and macromolecule therapeutics. However, passive application of drugs is not sufficient to maintain systemic concentrations of drugs; hence it is necessary to improve the skin penetration of topically applied drugs. Therapeutic concentrations of drugs in the skin can be maintained using chemical enhancers or by applying external electrical or mechanical energy

for enhancing skin penetration. However, electromechanical devices used for delivery should be safe, easy to use, and compatible with drug formulation, and affordability for regular use.

There is significant improvement in drug delivery device technologies for systemic delivery of drugs by a minimally invasive or non-invasive manner. Drug delivery systems that employ external devices to enhance skin penetration include ultra-sonication, iontophoresis and micro needles, and these devices are expected to be in common use in the near future (Barry et al., 2001).

1.8. Techniques for enhancement of skin permeabilization

Various passive and active methodologies (fig. 1.10.) are used to modify the barrier properties of the stratum corneum.

1.8.1. Passive methods of drug penetration

Passive methods include the influencing of drug, vehicle interactions and optimization of formulation, in order to modify the stratum corneum structure (Benson et al., 2005).

1.8.1.1. Chemical penetration enhancers

One of the most widely used passive approaches is the use of chemical penetration enhancers which facilitate drug permeation across the skin by increasing drug partitioning into the barrier domain of the stratum corneum, without long-term damage to the skin. Penetration enhancers acts by various mechanisms of action such as: increasing the fluidity of the stratum corneum lipid bilayers and interaction with intercellular proteins, disruption or extraction of intercellular lipids, increase of the drug's thermodynamic activity and increase in stratum corneum hydration. Several types of penetration enhancers are known and they can be divided into several groups based on their chemical structure, rather than their mechanism of action. Most of these have mixed modes of action so it is difficult to classify them according to this characteristic. Examples of commonly investigated

penetration enhancers are alcohols, sulphoxides, azone, pyrrolidones, essential oil, terpenes and terpenoids, fatty acids, water and urea (Benson et al., 2005). However, the major limitation for penetration enhancers is that their efficacy is often closely correlated with the occurrence of skin irritation.

1.8.2. Active methods of drug penetration

The active methods for skin permeabilization include ultrasound, electrically assisted methods (electroporation and iontophoresis), velocity based devices (powder injection, jet injectors), thermal approaches (lasers and radio-frequency heating) and mechanical methodologies such as micro needles (MN) and tape stripping.

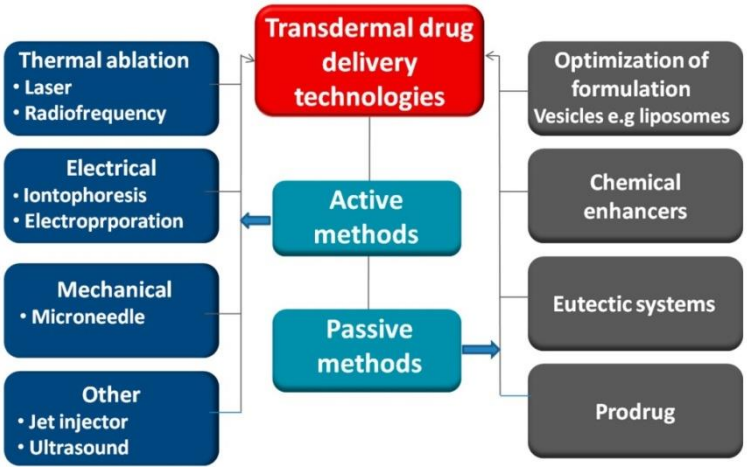

Fig.1.10. Approaches for enhancing drug transport across the skin. Reproduced from Alkilani et al., 2015.

These approaches allow a broader class of drugs to be delivered into the skin. Active methods involve the use of external energy to act as a driving force for drug transport across the skin or by physically disrupting the stratum corneum. These techniques greatly expand the range of drugs that can be delivered effectively across the skin. This in turn will significantly enhance the value of the transdermal delivery market and will be increasingly important over the coming years as the number of new drugs of biological origin continues

to increase. In addition, active methods also offer more reproducible control over the delivery profiles of the medications, thus overcoming lag times between the application and the drug reaching the systemic circulation when compared to passive methods. Some of these active methodologies will be described in detail below.

1.8.2.1. Ultrasound Devices

Ultrasound is an oscillating sound pressure wave that has long been used for many research areas including physics, chemistry, biology, engineering and others in a wide range of frequencies (Mitragotri et al., 1995). Ultrasound, sonophoresis, or phonophoresis can be defined as the transport of drugs across the skin by application of ultrasound perturbation at frequencies of 20 kHz–16 MHz which has a sufficient intensity to reduce the resistance of skin (Azagury et al., 2014). The use of ultrasound has resulted in the effective delivery of various different categories and classes of drugs, regardless of their electrical characteristics, by increasing skin permeability. These drugs have included hydrophilic and large molecular weight drugs (Herwadkar et al., 2012). However, the mechanism of action is still not clearly understood or characterized. The proposed mechanisms by which ultrasound affects tissues and cells includes thermal effects and cavitation effects caused by collapse and acoustic streaming which can be explained as oscillation of cavitation bubbles in the ultrasound field. Ultrasound can increase the temperature of the insonated medium (the skin) by the absorption of the sound waves with a frequency greater than the upper limit of the human hearing range (Wong et al., 2014). All recent studies point out that cavitation is believed to be the predominant mechanism in the enhancement of transdermal drug delivery (TDD) via ultrasound treatment.

The concept of ultrasound for use in TDD was initially reported by Fellinger and Schmidt in 1950 for the successful treatment of polyarthritis using hydrocortisone ointment combined with sonophoresis. However, the first ultrasound device for transdermal application

was approved in 2004 by the FDA for the delivery of local dermal anaesthesia by the Sontra Medical, SonoPrep® (fig. 1.11) (Kim et al., 2012; Mitragotri et al., 2004.)

Fig.1.11. The SonoPrep® ultrasound device. Reproduced from Mitragotri et al., 2004.

1.8.3. Electrical Techniques

1.8.3.1. Electroporation

In electroporation, cells are temporarily exposed to high intensities of electric pulses that lead to the formation of aqueous pores in the lipid bilayers of the stratum corneum, thus allowing the diffusion of drugs across skin (Zorec et al., 2013). The technique was first described by Neumann et al. in 1982. Usage of high voltage pulses (50–500 V) for short times of only one second have been shown to increase transport across the skin for different molecular weight drugs ranging from small e.g., fentanyl, timolol, orcalcein, to high molecular weight drugs such as LHRH, calcitonin, heparin or FITC–dextran with molecular weights up to 40 kDa (Denet et al., 2004). However, the main drawbacks are the lack of quantitative delivery, cell death with high fields and potential damage to labile drugs, e.g., those of protein origin (Junginger et al., 1999).

1.8.3.2. Iontophoresis

Iontophoresis involves the application of physiologically acceptable electrical currents (0.1–1.0 mA/cm^2) to drive charged permeants into the skin through electrostatic effects and make ionic drugs pass through the skin by its potential gradient (Singh et al., 1993). Unlike other transdermal enhancement methodologies, it acts mainly by involving a second driving force, the electrical potential gradient as companion to the concentration gradient across the skin since uncharged species can also be delivered through electro osmosis (Yan et al., 2015).

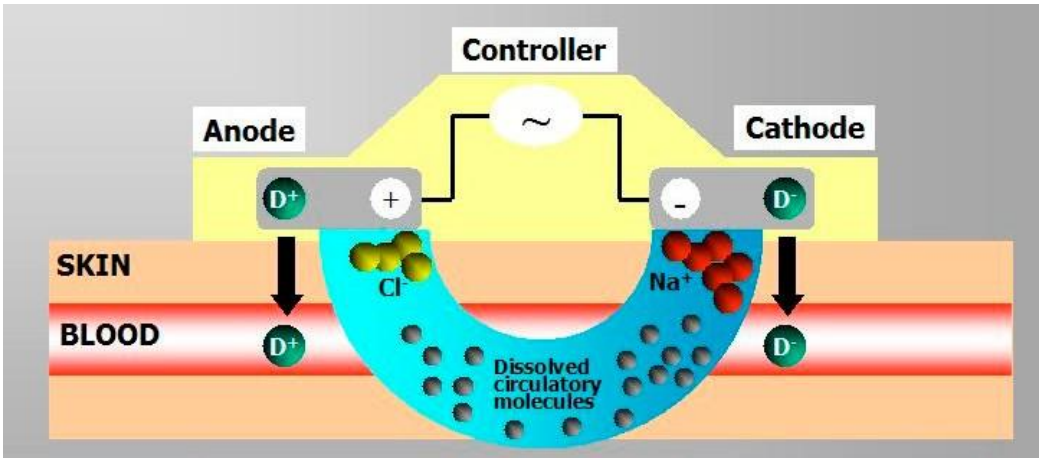

Fig.1.12. Schematic representation of an iontophoresis application. Reproduced from Tyle et al., 1986.

Phoresor®, Lidosite®, and E-trans® are examples of three commercially developed iontophoretic delivery systems. The first approved commercial iontophoretic patch system was LidoSite®, which was developed to deliver lidocaine for fast dermal anesthesia (Sharma et al., 2015; Kalaria et al., 2012). The system was composed of a disposable pre-filled patch, re-usable battery-powered controller and a flexible interconnect module. Iontophoresis has a minor effect on skin structure over short treatment periods due to the low-voltage nature of the applied electric current, when compared to electroporation. Several factors affect iontophoretic delivery of drugs, including pH of the donor solution,

electrode type, buffer concentration, current strength and the type of current employed. The molecular size of the solute/drug is an important factor in determining its feasibility for successful iontophoretic delivery. The flux of smaller and more hydrophilic ions is faster than larger ions. There is a linear relationship between the current and drug flux across the skin but the current is limited to 1 mA in order to facilitate patient comfort and consider safety concerns as with increasing current, the risk of nonspecific vascular reactions also increases (Gratieri et al., 2011). The maximum physiologically acceptable iontophoretic current is 0.5 mA/cm^2. The current should be adequately high to provide a desired flux rate but it should not irritate the skin. The use of continuous direct current (DC) can decrease the drugs flux due to its polarization effect on the skin. In order to overcome this problem, pulsed current has been used. The maximum molecular weight for iontophoretic delivery has not been extensively studied, although it is estimated that molecules with a molecular weight less than 12,000 Da may be successfully delivered across skin via iontophoresis. In order to deliver molecules greater than 12,000 Da, an alternate means of overcoming the barrier properties of the stratum corneum must be sought. However, it was found that a small protein, cytochrome *c* (12.4 kDa) was delivered non-invasively across intact skin (Cázares et al., 2007). Afterwards, ribonuclease A, with isoelectric point of 8.64 (13.6 kDa), was successfully delivered across porcine and human skin (Dubey et al., 2010). More recently, it was shown that transdermal iontophoresis was also able to deliver biologically active human basic fibroblast growth factor (17.4 kDa) in therapeutically relevant amounts corresponding to those used in clinical trials and animal studies. Iontophoresis has been used in various diagnostic applications e.g. diagnosing cystic fibrosis and recently for monitoring blood glucose levels. The major advantage of iontophoresis in diagnostic applications is that there is no mechanical penetration or disruption of the skin involved in this approach.

1.8.4. Velocity Based Devices

Velocity based devices, either powder or liquid jet injections employ a high-velocity jet with velocities ranging from 100 to 200 m/s to puncture the skin and deliver drugs using a power source mainly compressed gas or a spring (Mitragotri et al., 2013). The concept of jet injectors for use in drug delivery was first explored in the early of 1930s by Arnold Sutermesiter. Since then, interest in this method of drug delivery has expanded significantly and two types of liquid jet injectors have been developed; single-dose jet injectors (disposable cartridge jet injectors) and multi-use-nozzle jet injectors (MUNJIs) (Arora et al., 2008). Jet injections have been used for more than 50 years for parenteral delivery of vaccines, as well as small molecules, such as anesthetics and antibiotics. A jet injector is a needle free device capable of delivering electronically controlled doses of medication which result in improved consistency of delivery and reduced pain for the patient (Figure 1.13).

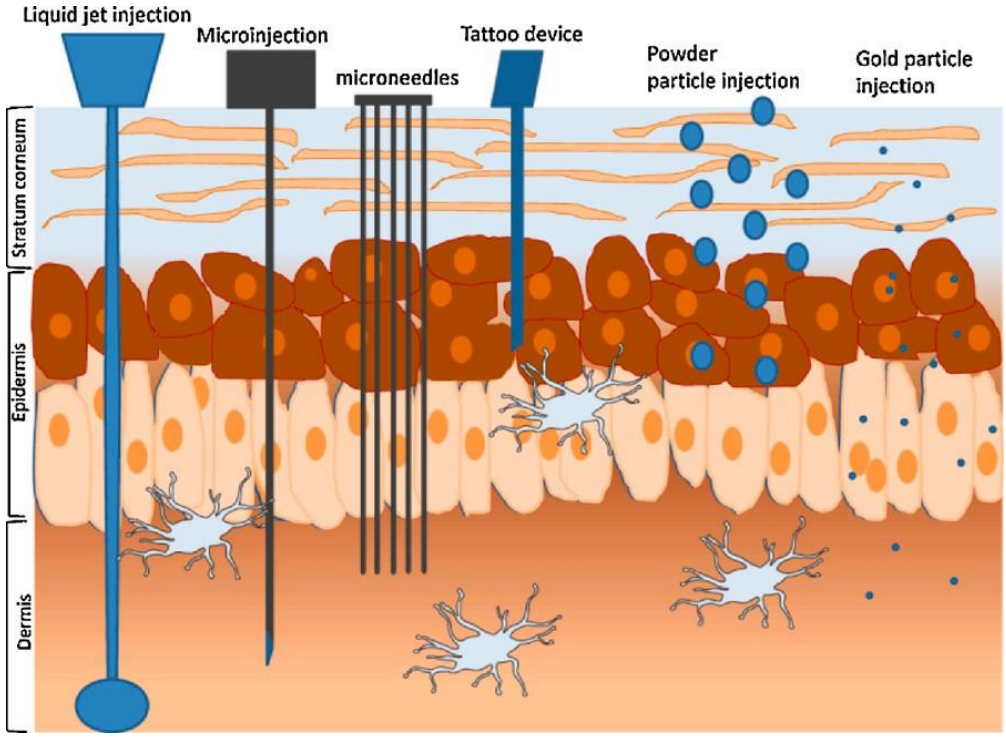

Fig.1.13. Methods for intradermal injection. Reproduced from Kis et al., 2012.

Liquid-jet injectors propel liquid from a nozzle with an orifice diameter ranging from 50 to 360 μm, which is much smaller than the outer diameter of a standard hypodermic needle (810 μm for a 21G needle). The jet can deliver drug into different layers of skin e.g., intradermal, subcutaneous, intramuscular by changing the jet velocity and orifice diameter (Schramm et al., 2002). The major advantage of using needle free devices relates to concerns regarding safe needle disposal and avoidance of accidental needle stick injuries. However, the risk of cross contamination is not excluded, since splash back of interstitial liquid from the skin may contaminate the nozzle (Bhosle et al., 2011). Therefore the use of multi-use nozzle jet injectors has been terminated and such devices are now only used for multi-dose drug delivery to the same individual, e.g., the Tjet® device which delivers somatropin (human growth hormone (hGH)).

Fig.1.14. Commercially available jet injector Tjet® device. Reproduced from Taberner et al., 2012.

Powder jet injectors have an advantage over liquid jet injectors of delivering solid drugs or vaccines to the skin, so the stability of the formulation will be increased and the necessity for cold storage will be avoided, which simplifies transportation and reduces associated costs (Arora et al., 2008). Powder jet injectors may be formulated from nano-or micro-particles containing the active or lyophilized drugs and antigens. Excellent bioavailability for a number of drugs has been reported but the intermittent pain and bruising

caused to patients has restricted wide acceptance of jet injectors.

1.8.5. Thermal Approaches

Thermal ablation is a method used to deliver drugs systemically through the skin by heating the surface of the skin, which depletes the stratum corneum selectively at that site of heating only, without damaging deeper tissues (Rossi et al., 1994). Many methods could be used to cause thermal ablation such as laser, radiofrequency, in addition to electrical heating elements. In order to generate the high temperatures needed to ablate the stratum corneum without damaging the underlined epidermis, the thermal exposure should be short, so the temperature gradient across the stratum corneum can be high enough to keep the skin surface extremely hot but the temperature of the viable epidermis does not experience a significant temperature rise (Goldberg et al., 2008).

1.8.5.1. Laser Thermal Ablation

Laser methodologies have been used in clinical therapies for the treatment of dermatological conditions such as pigmented lesions (Welch et al., 1991; Zhao et al., 2010). The main mechanism of laser thermal ablation of the skin is the selective removal of the stratum corneum without damaging deeper tissues, thus enhancing the delivery of lipophilic and hydrophilic drugs into skin layers. Lasers ablate the stratum corneum by deposition of optical energy, which causes evaporation of water and formation of microchanels in the skin (Gómez et al., 2011). In addition, such approaches have been used to extract interstitial fluid for subsequent measurement of glucose levels in diabetic patients. However, the degree of barrier disruption achieved is controlled by wavelength, pulse length, tissue thickness, pulse energy, tissue absorption coefficient, pulse number, duration of laser exposure and pulse repetition rate.

1.8.5.2. Radiofrequency (RF) thermal Ablation

Radiofrequency (RF) thermal ablation involves use of a thin, needle-like electrode

directly into the skin and application of high frequency alternating current (~100 kHz) which produces microscopic pathways in the stratum corneum, through which drugs can permeate. Exposure of skin cells to a high frequency (100–500 kHz) causes ionic vibrations within the tissue which attempts to localize the heating to a specific area of the skin and thus ablate the cells in that region, resulting in drug transport across the skin. This technology may enable transdermal delivery of a wide variety of hydrophilic drugs and macromolecules using a low-cost, fully disposable device (Sintov et al., 2003; Arora et al., 2008).

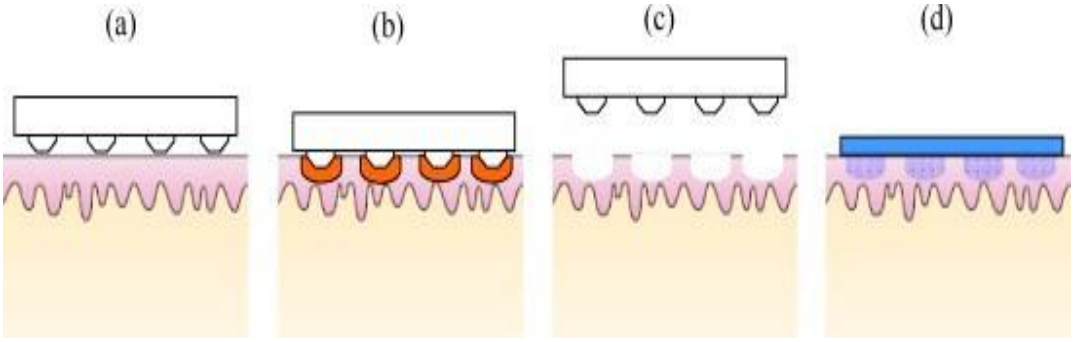

Fig.1.15. Schematic diagram of drug delivery using thermal ablation: **a**, micro-electrodes are pressed against the skin; **b**, skin is ablated via heating due to RF energy or resistive heating in the electrodes, **c**, after removing the ablation device, **d**, micro-pores formed. Reproduced from Arora et al., 2008.

1.8.6. Mechanical approaches to mediate skin permeation

The use of hypodermic needles is often associated with phobia, pain and the risk of needle-stick injuries. To overcome some of the delivery limitations often experienced when delivering macromolecular compounds, some innovative methodologies including tape stripping and the use of micro needles (MN) have been used. These concepts will be described further below.

1.8.6.1. Microneedle (MN) Arrays

MN arrays, minimally invasive drug delivery systems, were developed to overcome some of the disadvantages commonly associated with hypodermic needle usage and in order to address and improve patient compliance (Wermeling et al., 2008). MN arrays have the potential to be used as an alternative to hypodermic and subcutaneous needle technologies. As MN combine the ease of use of a transdermal patch with the effectiveness of delivery achieved using conventional hypodermic needle and syringes (Donnelly et al., 2009) .

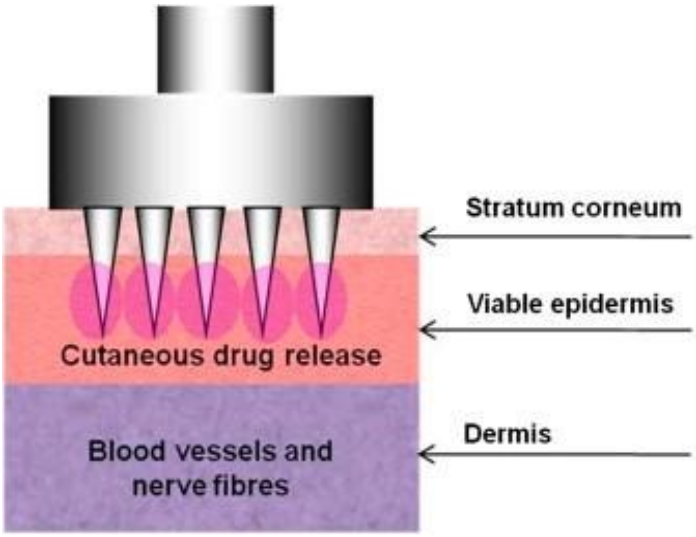

Fig.1.16. Schematic representation of the mechanism of action of a microneedle. Reproduced from Alkilani et al., 2015.

MN are multiple microscopic projections typically assembled on one side of a supporting base or patch, generally ranging from 25 to 2000 μm in height, 50 to 250 μm in base width and 1 to 25 μm in tip diameter (Yan et al., 2010). The needles should be of suitable length, width and shape to avoid nerve contact when inserted into skin layers. They are usually designed in arrays in order to improve the surface contact with the skin and facilitate penetration of therapeutic molecules into the skin. MN are designed to create transient aqueous conduits across the skin, thereby enhancing flux of the molecules ranging from small hydrophilic molecules such as

alendronate to macromolecules, including low molecular weight heparins, insulin and vaccines, in a pain-free manner (Koutsonanos et al., 2009). Besides the aspect of pain-free delivery, there are many other advantages of MN technologies, such as: the fact that they do not cause bleeding; eliminate transdermal dosing variability of small molecules; only minimal introduction of pathogens through MN-induced holes; potential for self-administration; the potential to overcome and reduce instances of accidental needle-sticks injuries and the risk of transmitting infections (Donnelly et al., 2009) .

The first two commercially marketed MN-based products are Intanzia® and Micronjet® which are based on metal and silicon MN, respectively (Alkilani et al., 2015). Intanza® is the first influenza vaccine that targets the dermis, a highly immunogenic area It was developed and licensed by Sanofi Pasteur MSD Limited and is being marketed in two strengths; Intanza® 9 µg for adults aged between 18 and 59 years and Intanza® 15 µg for adults of 60 years and above. The Intanza® influenza vaccine system has a needle length of 1.5 mm. MicronJet is a single use, MN-based device for intradermal delivery of vaccines and drugs. It was developed and licensed by NanoPass.

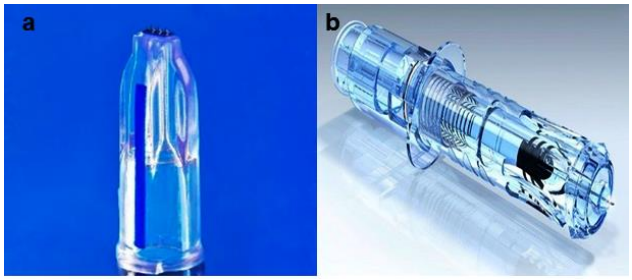

Fig.1.17. Current commercial MNs-based products (**a**) Intanza® and (**b**) MicronJet®. Reproduced from Alkilani et al., 2015.

1.9. Nanocarriers for transdermal delivery

Nano carriers such as vesicular systems (liposomes, transferosomes, ethosomes, solid lipid nanoparticles), polymer nanoparticles, dendrimers and metal based nanoparticles have demonstrated increased drug absorption, penetration, half-life, bioavailability, stability (Escobar et al., 2012). Nanocarriers are so small to be detected by immune system and they can deliver the drug in the target organ using lower drug doses in order to reduce side effects (Mura et al., 2013).

1.9.1. Nanoparticle based systems

1.9.1.1. Liposomes

Liposomes are spherical vesicles that comprise one or more lipid bilayer structures enclosing an aqueous core (Touitou et al., 1994). They are structures made of cholesterol and phospholipids. They can have different properties depending on the excipients included and the process of their elaboration (Barry et al., 2001). There are small unilamellar vesicles (25 nm to 100nm), medium-sized unilamellar vesicles (100 nm and 500nm), large unilamellar vesicles, giant unilamellar vesicles, oligolamellar vesicles, large multilamellar vesicles and multivesicular vesicles (500 nm to microns). The thickness of the membrane measures approximately 5 to 6 nm. These shapes and sizes depend of the preparation technique, the lipids used and process variables (Schreier 1994; Samad, 2007). They protect encapsulated drugs from degradation. Liposomes can also be functionalized to improve cell targeting and solubility.

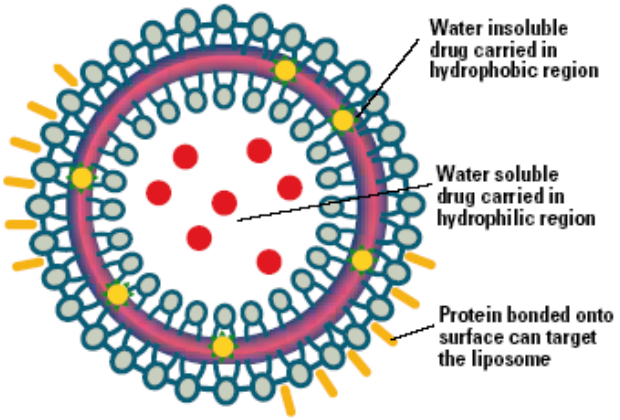

Fig.1.18. Structure of liposome. Reproduced from web page www.azonano.com/Article ID1222.

1.9.1.2. Transfersomes

Transfersomes have been defined as specially designed vesicular particles, consisting of at least one inner aqueous compartment surrounded by a lipid bilayer with appropriately tailored properties (Cevc et al., 1994). Transfersomes resemble lipid vesicles, liposomes, in morphology but, functionally, transfersomes are sufficiently deformable to penetrate pores much smaller than their own size (Kong et al., 2015). They are metastable, which makes the vesicle membrane ultraflexible, and, thus, the vesicles are highly deformable. It is chiefly the unusually strong membrane adaptability that allows the transfersomes vesicles to accommodate to a confining pore and thus trespass such a pore. Typical transfersomes are, therefore, characterized by at least one order of magnitude more elastic membrane than that of conventional lipid vesicles, liposomes. In order to change liposomes into transfersomes, one can incorporate one or more edge-active substance(s) into the vesicular membrane, surfactants were suggested as examples of such edge-activator. Another specific difference between transfersomes and liposomes is the higher hydrophilicity of the former, which allows transfersome membrane to swell more than conventional lipid vesicle bilayers (Vinod et al., 2012).

1.9.1.3. Ethosomes

Ethosomes are lipid vesicular carriers embodying ethanol in relatively high concentrations for enhanced skin permeation of drugs. They are composed mainly of phospholipids, ethanol and water. The high concentration of ethanol, which essentially differentiates ethosomes from other vesicular carriers, acts to enhance skin permeation in order to release the entrapped drug particles into deeper layers and systemic circulation (Ainbinder et al., 2016). Structurally, an ethosomal vesicle is composed a phospholipid bilayer and an aqueous inner core containing the entrapped active ingredient. They are soft and malleable (Ascenso et al., 2015). The size of an ethosome vesicle lies within the nanometer range. In addition, the size of ethosome vesicle is smaller than that of a liposome when prepared under the same conditions, due to the high alcohol content. The size decreased as alcohol increased from 20% to 45%. This reduction in size was attributed to the conferment of a net negative charge on the vesicle surface by ethanol. Ethosomes permeate through the stratum corneum barrier and possess significantly high transdermal flux unlike classical liposomes. These effects of combined phospholipids and high concentration of ethanol in vesicular formulations have been suggested to be responsible for deeper distribution and penetration in the skin lipid bilayers (Uchechi et al., 2014).

1.9.1.4. Dendrimers

Dendrimers are monodisperse populations that are structurally and chemically uniform. They allow conjugation with numerous functional groups due to the nature of their branches. The amount of branches increases exponentially and dendrimers growth is typically about 1 nm per generation (Svenson et al., 2012). The dendrimers classification is based on the number of generations. After the creation of a core, the stepwise synthesis is called first generation; after that, every stepwise addition of monomers creates the next

generation. This approach allows an iterative synthesis, providing the ability to control both molecular weight and architecture.

The kind of polymer chosen to construct the dendrimer by polymerization is very important with regard to the final architecture and features (Caminade et al., 2015). In addition, the use of branched monomers has the peculiarity of providing tailored loci for site-specific molecular recognition and encapsulation. Notably, 3D and fractal architecture, as well as the peripheral functional groups, provide dendrimers with important characteristic physical and chemical properties. In comparison with linear polymers, dendritic structures have “dendritic voids” that give these molecules important and useful features. These spaces inside dendrimers can mimic the molecular recognition performed by natural proteins (Ma et al., 2013).

Furthermore, dendrimers have a high surface-charge density due to ionizable groups that help them to attach drugs by electrostatic forces, regardless of the stoichiometry. This dendrimer-drug association provides drugs with better solubility, increasing their transport through biological membranes and sometimes increasing drug stability. The number of molecules that can be incorporated into dendrimers is related to the number of surface functional groups; therefore, later-generation dendrimers are more easily incorporated into dendritic structure. However, not all the functional groups are available for interaction due to steric volume, molecule rotation or stereochemistry effects (Yang et al., 2015). Dendrimers can have positive and negative charges, which allows them to complex different types of drugs. The permeability of dendrimers through the skin depends on physicochemical characteristics like generation size, molecular weight, surface charge, composition, and concentration.

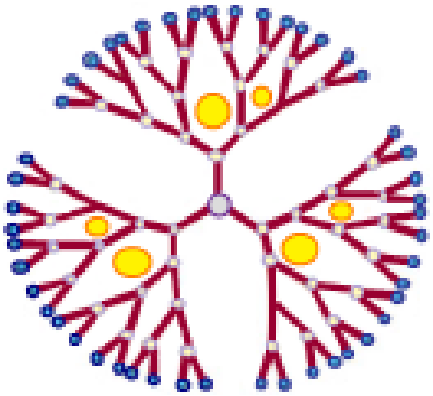

Fig.1.19. Structure of dendrimers. Reproduced from Escobar-Chávez et al., 2012.

1.9.1.5. Lipid nanoparticles

Lipid nanoparticles include solid lipid nanoparticles (SLN), nanostructured lipid carriers, lipid drug conjugates and are colloidal drug carrier systems (Lobovkina et al., 2013). The liquid lipid used in emulsions is replaced by a lipid solid at room temperature in SLN including high-melting point glycerides or waxes. Lipid nanoparticles are good candidates for transdermal delivery. They can be prepared in different sizes and it is possible to modify surface polarity in order to improve skin penetration. From the upper skin, nanoparticles can reach deeper skin regions because they exhibit mechanical flexion (Sachdeva et al., 2014).

1.9.1.6. Nanostructured lipid carriers (NLC)

NLC are colloidal carriers characterized by a solid lipid core consisting of a mixture of solid and liquid lipids, and having a mean particle size in the nanometer range. They consist of a lipid matrix with a special nanostructure. This nanostructure improves drug loading and firmly retains the drug during storage (Tamjidi et al., 2013). NLC system minimizes some problems associated with SLN such as low payload for some drugs; drug expulsion on storage and high water content of SLN dispersions. The conventional method for the production of NLC involves mixing of spatially very different lipid molecules, i.e.

blending solid lipids with liquid lipids (Vitorino et al., 2014). The resulting matrix of the lipid particles shows a melting point depression compared with the original solid lipid but the matrix is still solid at body temperature. Depending on the method of production and the composition of the lipid blend, different types of NLC are obtained. The basic idea is that by giving the lipid matrix a certain nanostructure, the payload for active compounds is increased and expulsion of the compound during storage is avoided. Ability to trigger and even control drug release should be considered while mixing lipids to produce NLC (Gönüllü et al., 2015).

1.9.1.7. Solid lipid nanoparticles

Solid lipid nanoparticles (SLN) are formed by a matrix of lipids which are biodegradable raw materials that are physiologically well tolerated (Gönüllü et al., 2015). The main advantages of these systems include protection of labile substances from chemical degradation, control of the release of substances due to the solid state of the lipid matrix, and formation of films over the skin showing occlusive properties. Additional features are the avoidance of organic solvents during the preparation and amenability to large scale production and sterilization. Further- more, the great ability of SLNs to facilitate the contact of active substances with the stratum corneum, because of the small size of the particles and consequently the high surface area, leads to the high permeation of the carried substances through the viable skin (Raj et al., 2015).

1.9.1.8. Polymeric nanoparticles

Polymeric nanoparticles are prepared from biocompatible and biodegradable polymers with size between 10-1000 nm, where the drug is dissolved, entrapped, encapsulated or attached to a polymer nanoparticle matrix. The penetration and transport extent of these systems through the skin depends on the ingredients' chemical composition, the encapsulation mechanism influencing the drug release, the size of nanoparticles and on the viscosity of the formulations

(Elsabahy et al., 2012). The polymeric nanoparticles are able to modify the activity of drugs, delay and control the drug release, and increase the drug adhesivity or its time of permanence in the skin. Briefly, the nanoparticles can be useful as reservoirs of lipophilic drugs to deliver them in the stratum corneum becoming an important strategy to control their permeation into the skin (Zhang et al., 2013).

1.9.1.9. Carbon nanotubes (CNT)

Carbon nanotubes are stable carbon nanoparticles with potential anti-oxidant ability and cytoprotective effect (Volder 2013). Carbon nanotubes have extremely small mean diameters (<100 nm). Their large inner volume allows the loading of small biomolecules while their outer surface can be chemically modified to render themselves various novel features that can be used to load proteins and genes for effective drug delivery, even through the skin (He et al., 2013)

1.9.1.10. Gold nanoparticles

In recent years, gold nanoparticles (AuNP) have received considerable attention due to their unique physical and chemical properties. Their surfaces are easy for chemical modification, and can be modified by many bioactive molecules. These properties enable them to be used extensively in various biological applications: photothermal therapy, delivery of drugs and genes and bio-imaging (Pissuwan et al., 2012; Lee et al., 2015).

The interactions of AuNP with various mammalian cells have been studied in the past few years. Recently, the uptake of gold particles across the skin barrier has attracted appreciable interest. It has been shown that cellular uptake of AuNP is dependent upon their size, shape, and chemical surface. It appears that these properties also affect the absorption and penetration of AuNP into the skin. It has been recently reported that AuNP have a high potential to “overwhelm” the skin barrier. The penetrative ability of small-sized AuNP could arise from their induction of lipid modulation (Albanese et al., 2012).

The combination between AuNP and deoxyribonucleic acid (DNA) vaccines was reviewed by Dean et al. DNA-coated gold particles could enhance the penetration of vaccines from the outer layer of the skin to Langerhans cells (Dykman et al., 2012).

For the first time, AuNP were used in nano fiber cosmetic facial masks for co delivery of free radical scavenger L–ascorbic acid (Fathi-Azarbayjani et al., 2010). Recent studies showed that AuNP in combination with cationic liposomes prepared with egg phosphatidyl choline and DOTAP showed enhanced penetration in to skin (Pornpattananangkul et al., 2010). The use of AuNP for percutaneous delivery of "protein drugs" was reported by Huang et al. It is observed that AuNP of mean size 5 nm were used to deliver proteins (45-kDa horseradish peroxidase; 460-kDa β-galactosidase). After exposure of mouse skin to the gold–protein mixture for 2 h, both types of proteins co-administered with AuNP could penetrate the SC (Huang et al., 2010).

1.10. Layer-by-layer (LbL) self-assembled nanoparticles

The sequential adsorption of oppositely charged colloids was reported in a seminal paper in 1966 by R. Iler. The technique did not receive much credit or attention from the scientific community until it was reintroduced in 1991 by Decher et al as a solution for deposition of charged polymers on planar surfaces. Later, this technique was used by Mohwald group for deposition of self-assembled polymer layers on spherical surfaces. Since its re-development in 1991, the LbL assembly technique has become one of the most preferred techniques for fabrication of thin films and has been practiced by numerous research groups worldwide. Self-assembly is now employed for the fabrication of ultrathin films from charged polymers (polyions) and nanoparticles (metallic, semiconducting, magnetic, ferroelectric, insulating), nanoplates, proteins, dyes and other supramolecular species.

The main idea of the method consists of the resaturation of polyion adsorption, resulting in the alternation of the terminal charge after each layer deposition. This idea is general and implies that there is no principle restriction on the choice of polyelectrolytes. It is possible to design composite polymeric films in the range of 5 to 1000 nm, with precision better than 1 nm and a definite knowledge of their compositions. For the successful assembly of nanoparticle or protein multilayers, an alternation with linear or polyion layers is important. Flexible linear polyions penetrate between nanoparticles and act as electrostatic glue. The concept of "electrostatic polyion glue", which keeps together neighboring arrays of nanoparticles, is central to this approach.

The build-up of poly electrolyte mutlilayers (PEM) is driven by the electrostatic attraction between the oppositely charged constituents (Iler et al., 1996) or hydrogen bonding (Fu et al., 2002; Kharlampieva et al., 2005), hydrophobic interactions (Kotov et al., 1999) and van der Waals forces (Sato et al., 2005). Generally, LbL self-assembly proceeds as follows: (1) A charged substrate is immersed in a solution of an oppositely-charged colloid to adsorb the first monolayer, (2) a washing cycle follows to remove unbound material and preclude contamination of the subsequent oppositely-charged colloid, (3) in which the coated substrate is submerged to deposit a second layer and the multilayered structure is formed (Lvov et al., 1999). A schematic of the LbL assembly process is shown in Figure 1.20.

Polyions predominately used in the assembly are as follows: polycations - poly(ethylenimine) (PEI), poly(dimethyldiallylammonium chloride) (PDDA), poly(allylamine) (PAH), polylysine, chitosan; polyanions - poly(styrenesulfonate) (PSS), poly(vinylsulfate), poly(acrylic acid), heparin, DNA. One can grow polymer nanocomposites with necessary alternation of different material monolayers using hundreds of commercially available polyions.

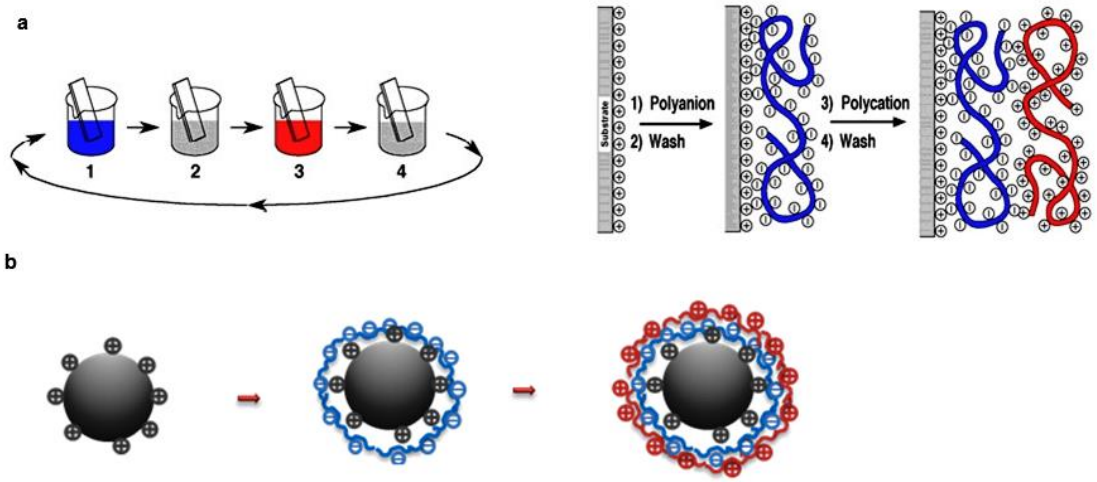

Fig. 1.20. Schematic representation of polyanion/polycation alternate assembly on planar surfaces (a); spherical substrates (b).

1.10.1. Influence of experimental parameters on LbL adsorption

The formation of polyelectrolyte layer-by-layer self-assembly depends on electrostatic interactions between substrate and subsequent polyelectrolyte layers. Along with electrostatic interactions other processing parameters play a significant role and are briefly discussed here:

1.10.1.1. Poly electrolyte concentration

The concentration of polymer should be high enough for successful adsorption and to prevent depletion during layering (Decher et al., 1997). Concentration should exceed the minimum threshold concentration for attachment and to reverse charge polarity for each

adsorbed layer. The threshold is dependent on solubility and charge density of polymer. Above the threshold, concentration was irrelevant to adsorption; however, result in an exponential increase in the thickness of the monolayers (Szarpak et al., 2008).

1.10.1.2. Ion concentration and pH of the medium

In LbL process, electrostatic interactions between polyelectrolytes play important role for successful polyelectrolyte multilayer growth. The layer thickness can increase exponentially or linearly with each step, with linear growth taking place when the polyelectrolytes in the solution interact exclusively with the outer layer of the multilayer film (Laugel et al., 2006). The thickness of adsorbed layer is mainly influenced by salt concentration or ion concentration and pH of the medium (Decher et al., 1997). Generally, an increase in ionic concentration results in an increase in layer thickness due to polyelectrolyte charge compensation resulting in more globular rather than extended polyelectrolyte structure (Kolarik et al., 1999; Guzmán et al., 2009). Furthermore diffusion of polyelectrolyte chains into interior results in exponential increase in thickness. However, beyond threshold, with increase in salt concentration, all charges compensate and polyelectrolyte form turbid, coagulated dispersions (Bharadwaj et al., 2006; Buron et al., 2009). At these conditions successful multilayer formation will be difficult. A change in pH of the solution will alter the dissociation of the polyelectrolytes and ions, which will further alter the successive adsorption process. Thickness of polyelectrolyte layers prepared by strong polyelectrolytes can be improved by adjusting salt concentration, whereas layers prepared by weak polyelectrolytes are improved by optimization of solution pH.

1.10.1.3 Working medium

The working medium should enable the polyelectrolyte coating and PEM integrity. It is reported that polarity of working medium influences the efficiency of LbL process. Water

soluble polyelectrolytes are mostly used as coating materials for effective layer-by-layer adsorption. Water, as working medium can ionize the water soluble polyelectrolytes, since the ionic interactions are important contributors for layer-by-layer assembly. Non-aqueous systems also investigated as working medium for an azo-polyelectrolyte in N,N-dimethylformamide (Tuo et al., 2005), PSS/PAH/formamide combinations (Kamineni et al., 2007) and PSS/PAH/chloroform systems (Hirsjärvi et al., 2006).

1.10.1.4. Washing

In the process of LbL adsorption, coated substrate is washed after each polyelectrolyte adsorption to remove unbound polyelectrolytes and to prevent the cross-contamination of solutions (Hoogeveen et al., 1996). Washing solution should be compatible with polyelectrolytes used and should not damage the LbL construction. Mostly the layers formed with strong polyelectrolytes are strong and not influenced by washing solution. However, weak polyelectrolyte layers may be stripped off and limits successful LbL assembly (Linford et al., 1998).

1.11. Advantages of LbL self-assembly

The LbL self-assembly methods have advantages compared to the more conventional coating methods, including

1. The simplicity of the LbL process and equipment
2. Its suitability to coating most surfaces
3. The availability of an abundance of natural and synthetic colloids
4. The flexible application to objects with irregular shapes and sizes
5. Coating thickness can be tailored in the nm-μm range

6. Surface labeling with targeting molecules is possible

7. Stabilization and surface protection of submicron particles

8. LbL coating eases the use of thermodynamically unstable mechanically-micronized particles

9. Compared to a minimum of ~10% of colloids and/or polymers needed with conventional coating techniques, much smaller amounts of colloids polymers (1 %) is needed to produce a functional LbL assembled coating.

1.12. Objectives

Layer-by-layer (LbL) assembly technique, involves sequential adsorption of oppositely charged polyelectrolytes on planar or spherical substrates by electrostatic interactions. LbL assembly technique has gained tremendous potential over the last decade due to versatility of applications ranging from drug delivery to bio-sensor applications. Any charged entity, small molecules or macromolecule therapeutics can be encapsulated using this technique. With this technique, co-delivery of multiple therapeutic agents can be achieved.

To this end, the overall objective of this study is to investigate the feasibility of using layer-by-layer polymer coated gold nanoparticles (LbL-AuNP) as a carrier for topical iontophoretic delivery of small and macromolecule therapeutics. In the present study melanoma was taken as model to prove our hypothesis. Imatinib mesylate (IM) and small interference RNA (siRNA) were taken as model small and macromolecule therapeutics, respectively. Imatinib mesylate is a c-kit tyrosine kinase inhibitor approved for treatment of melanoma. Signal transducer and activator of transcription 3 (STAT3) is over expressed in melanoma, hence we used siRNA against STAT3.

Objective I. LbL-AuNP for topical iontophoretic delivery of imatinib mesylate to treat melanoma.

Specific aims:

(i) To study the preparation, stabilization and surface functionalization of gold nanoparticles (AuNP) for fabrication of LbL-AuNP.

(ii) To study the encapsulation and in-vitro release of IM from LbL-AuNP.

(iii) To study the in-vitro cytotoxicity and cell uptake of LbL-AuNP using B16F10 murine melanoma cells.

(iv) To study the skin permeation of LbL-AuNP after passive, anodal iontophoresis application.

Objective II. LbL-AuNP for topical iontophoretic delivery of STAT3 siRNA to treat melanoma.

Specific aims:

(i) To study the preparation and characterization of LbL-AuNP for delivery of siRNA.

(ii) To study the in-vitro cytotoxicity, cell uptake and mechanism of cell uptake of LbL-AuNP in B16F10 murine melanoma cells.

(iii) To study the apoptotic potential and in-vitro gene silencing of STAT3 siRNA delivered using LbL-AuNP.

(iv) To study the skin penetration of siRNA delivered using LbL-AuNP.

Objective III. LbL-AuNP for topical iontophoretic co-delivery of STAT3 siRNA and imatinib mesylate to treat melanoma.

Specific aims:

(i) To study the preparation and characterization of LbL-AuNP for co-delivery of Imatinib mesylate and siRNA.

(ii) To study the in-vitro gene silencing and apoptotic potential of STAT3 siRNA and IM co-delivered using LbL-AuNP.

(iii) To study the efficacy of IM and siRNA co-delivered using LbL-AuNP for melanoma treatment.

Chapter 2

LbL-AuNP for topical iontophoretic delivery of imatinib mesylate to treat melanoma

Graphical abstract

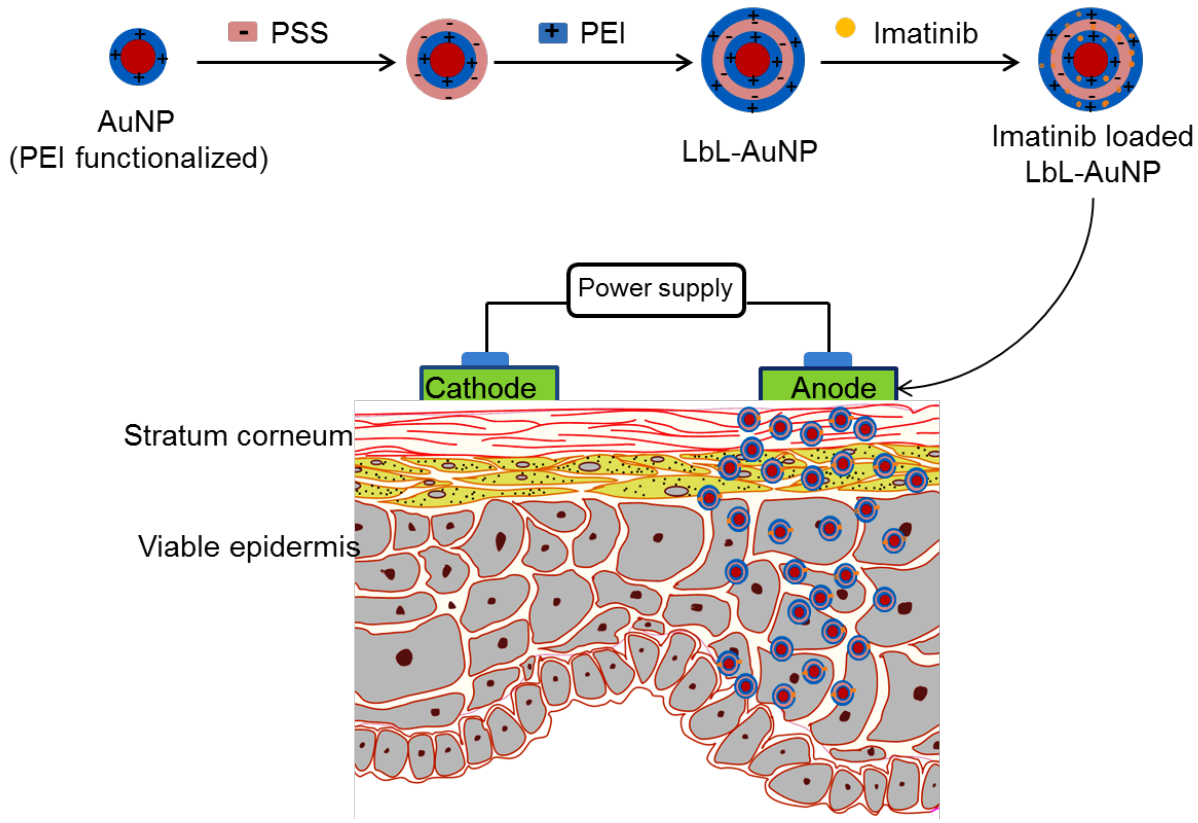

2.1. INTRODUCTION

Over the past few decades, transcutaneous drug delivery has been primed as a potential alternative to traditional oral drug delivery systems. The ease of application and dose termination, large surface area, patient compliance, less enzymatic and pH based drug degradation are potential advantages of topical drug delivery. The current global transdermal market is valued at $30 billion which is held by only a handful of molecules (Wiedersberg et al., 2014). This fewer number of molecules delivered through topical route is unequivocally attributed to the formidable skin barrier (Elias et al., 1975). Outermost layer of skin, stratum corneum evolved to limit the transport of extraneous compounds into skin. To increase the number of molecules transported across and into skin membrane, researchers have developed and studied permeation enhancement techniques (Barry et al., 2001). These included chemical and physical methods of permeation enhancement. While chemical penetration enhancers such as Azone® and oleic acid have consistently showed penetration enhancement, they are limited by skin irritation potential (Williams et al., 2012). In case of physical techniques, iontophoresis has been the only technique to attain maturity with few commercial products (Prausnitz et al., 2008). Iontophoresis utilizes a small electric current ($\leq$0.5 mA/cm^2) to enhance skin penetration of charged molecules. Iontophoresis involves electro-migration and electro-osmosis to transport molecules inside skin (Marro et al., 2001; Pikal et al., 2001).

Recently, more attention is being laid on nanocarrier systems for transcutaneous delivery of actives. Nanocarriers such as nanoparticles, polymeric systems, liposomes and micelles have been studied for their skin penetration and drug carrier properties. Nanocarrier systems are expected to penetrate the minute pores in the stratum corneum lipid matrix and skin appendages to get access to viable tissues (Schneider et al., 2009). While there have been controversial

claims, majority researchers observed that nanoparticles would penetrate only superficial layers of skin tissue (Prow et al., 2011; Campbell et al., 2012). This could be a limitation for transdermal delivery where the active compounds are expected to be in systemic circulation. On the other hand, stratum corneum deep penetration of nanocarriers could reasonably improve dermatopharmacokinetic and localized pharmacodynamic response of active compounds.

Particle size of nanocarriers is an important factor to optimize for skin transport studies. Often nanocarriers including liposomes, polymer and lipid-based spherical nanoparticles have size range beyond 100 nm. On the other hand, micelles and metal-based nanoparticles can be prepared with particle size <100 nm (Prow et al., 2011). Metals including gold, silver, iron, titanium and zinc among others have been used for preparation of nanoparticles (Labouta et al., 2013). Gold nanoparticles (AuNP) have shown potential in varied biomedical applications such as nanocarrier systems and imaging agents (Mieszawska et al., 2013). Initial interest in topical application of AuNP was directed to study nano-toxicology (Arruebo et al., 2013). Later, few studies reported AuNP as nanocarriers to deliver siRNA and protein products inside skin (Larese Filon et al., 2011; Huang et al., 2010). One of the bottle necks in developing AuNP for drug delivery is to load the cargo in AuNP. Traditionally surface conjugation has been the predominant approach where actives are ligated to AuNP using thiol linkage (Zheng et al., 2012; Asadishad et al., 2010). This involves complex chemistry and often the resulting drug conjugated AuNP are unstable in ionic medium (Kim et al., 2010). To overcome these limitations, we have developed layer-by-layer polyelectrolyte coated AuNP (LbL-AuNP). It is expected that LbL-AuNP would allow greater drug loading compared to chemical conjugation techniques. Furthermore, LbL-AuNP possesses greater surface charge density that could be utilized for its iontophoretic transport into skin.

The hypothesis of this study was that iontophoresis application would enhance the skin penetration of nanosized LbL-AuNP and the nanoparticles themselves would be rapidly taken-up by the skin cells. To enhance the skin penetration of LbL-AuNP we have applied anodal iontophoresis. Imatinib mesylate (IM), an anticancer agent was used as model small molecule for skin transport. IM is a c-kit tyrosine kinase receptor inhibitor indicated for the treatment of chronic myelogenous leukemia. Currently IM is being investigated to treat melanoma in a Phase II clinical study (Tournebize et al., 2012). In-vitro skin transport studies were performed to study the iontophoretic skin permeation of IM loaded LbL-AuNP. Furthermore, cell uptake and cell viability studies were performed in murine melanoma (B16F10) cells to understand the potential of IM loaded LbL-AuNP to inhibit cancer cell growth.

2.2. MATERIALS AND METHODS

Tetrachloro aurate trihydrate ($HAuCl_4$ $3H_2O$), polyethylene imine branched (PEI, MW: 25 kDa), poly(styrene sulfonate) (PSS, MW: 70 kDa), poly(N-vinyl pyrrolidone) (PVP K-30, MW: 40 kDa), sodium citrate dihydrate, imatinib mesylate (IM), sodium dodecyl sulfate (SDS), Tris base, boric acid, sodium chloride, ethylenediamine tetraacetic acid dihydrate (EDTA), potassium chloride, disodium hydrogen orthophosphate anhydrous, potassium di-hydrogen orthophosphate, fluorescein isothiocyanate (FITC), acetonitrile, agarose, sodium bicarbonate, methanol, chloroform, ammonia solution, paraformaldehyde, Triton X-100, DAPI and dimethyl sulfoxide (DMSO) were purchased from Sigma Aldrich Chemical Company (Bangalore, India). Dulbecco's modified Eagle's medium (DMEM), Dulbecco's phosphate buffered saline, fetal bovine serum (FBS) and thiazolyl blue tetrazolium bromide (MTT) were purchased from

Himedia Laboratories (Mumbai, India). All the chemicals were used without further purification. Milli-Q (Millipore Corporation, CA, USA) water was used for all the experiments.

2.2.1. Preparation of gold nanoparticles (AuNP)

To synthesize gold nanoparticles, tetrachloroaurate trihydrate ($HAuCl_4$) was used as a metal precursor and sodium citrate dihydrate was used as reducing agent. $HAuCl_4$ (0.25 mM) was heated to 100 ^oC and 1 % sodium citrate dihydrate (38.8 mM) was added. This reaction mixture was allowed to boil for 30 min under continuous agitation until the color turns deep red indicating formation of AuNP. Later poly(N-vinyl pyrrolidone) (PVP) was added as a capping agent for stabilization of AuNP. Different molar ratios ranging from 20 to 100 PVP / $HAuCl_4$ were used to optimize concentration of capping agent. An aqueous solution of PVP was added drop wise to AuNP solution and stirred for 4 h. The optimized PVP concentration for stabilization of AuNP was found to be 60:1 molar ratio of PVP monomer to $HAuCl_4$. Then PVP stabilized AuNP were functionalized by addition of PEI (0.8 mM) to the reaction mixture and allowed to stir at 500 rpm for 24 h.

2.2.2. Layer-by-layer coating of PEI functionalized AuNP

PEI functionalized AuNP solution (10 mL, ~$9x10^{11}$ AuNP) was centrifuged at 15000 rpm for 20 min at 20 ^oC. After centrifugation, AuNP were washed and re-suspended in 9 mL of 10 mM NaCl solution. PSS (10 mg/mL; 10 mM NaCl; pH 7.4) was added drop wise to the mixture to form second layer. The mixture was incubated for 4 h under constant stirring at 500 rpm. Then the unadsorbed PSS was removed by centrifugation (15000 rpm; 20 min). A final layer of PEI was formed after incubating PSS-coated AuNP in PEI solution (10 mg/mL; 10 mM

NaCl; pH 7.4) for 4 h at room temperature. The LbL-AuNP were then centrifuged and used for encapsulation of imatinib mesylate (IM).

2.2.3. Encapsulation of IM in LbL-AuNP

LbL-AuNP were dispersed in 1 mL of 10 mg/mL IM solution and incubated for 24 h at room temperature. After incubation, IM loaded LbL-AuNP were centrifuged at 15000 rpm for 20 min and the supernatant was analyzed by RP-HPLC. IM was separated by C8 column (150 x 4.6 mm; Phenomenex, CA, USA) using mobile phase of acetonitrile: 0.02 M KH_2PO_4 (30:70) at a flow rate of 1 mL/min. IM concentration was determined by measuring absorbance at 256 nm and comparing with IM standard curve (0.1 to 60 µg/mL, R^2 – 0.998). The loading efficiency (EE) of IM was calculated by using Equation (1)

$$\text{Loading efficiency (\%)} = \frac{\text{Concentration of IM in LbL-AuNP}}{\text{Concentration of LbL-AuNP}} \times 100 \qquad (1)$$

2.2.4. Characterization of free and IM loaded LbL-AuNP

For TEM analyses, samples were prepared by placing a drop of LbL-AuNP preparation on a carbon-coated copper grid, followed by evaporation of solvent. TEM images were acquired using JEM-2100F (JEOL Ltd., Japan).

Particle size and zeta-potential after adsorption of each polymeric layer were determined using Zetasizer (Nano ZS, Malvern Instruments, UK). For particle size analyses, samples were dispersed in deionized water. For zeta-potential measurement, samples were dispersed in deionized water, and 0.75 mL of sample solution was injected into clear folded capillary cell (DTS1060). Zeta-potential measurement was carried out at 25 ^{o}C using Smoluchowski model in automatic mode. AuNP are known to show strong optical absorption/scattering of UV-visible

radiation due to the excitation of localized surface plasmon resonance (SPR). The UV-visible absorption spectra of free AuNP and after adsorption of each polymeric layer were recorded using UV-visible spectrophotometer (SpectraMax M4, Molecular Devices Inc., California, USA).

Sequential adsorption of polymers on to AuNP was studied using Fourier transform infrared (FTIR) spectrometer (FT/IR-4200, Jasco Inc, USA). Furthermore, FTIR was also used to characterize the encapsulation of IM in LbL-AuNP. Samples (1 mg) were mixed with potassium bromide at 1:100 ratio and a pellet was prepared using high pressure hydraulic press (Riken Seiki, Tokyo, Japan) after application of 20 MPa pressure. Spectra were recorded within the range of 4000–400 cm^{-1} at a spectral resolution of 2 cm^{-1}.

Differential scanning calorimeter (DSC-60, Shimadzu, Japan) was used to study the thermal transitions of free AuNP and LbL-AuNP. Furthermore, DSC was also used to study the encapsulation of IM in LbL-AuNP. Sample (3 mg) was placed in an aluminum pan and sealed with a lid using a press. Thermograms were recorded at a heating rate of 10 ^{o}C per min from ambient temperature up to 400 ^{o}C.

2.2.5. In-vitro release of IM from LbL-AuNP

In-vitro release studies of IM from LbL-AuNP were performed using Franz diffusion cell apparatus (Permegear Inc., Pennsylvania, USA). Dialysis membrane (molecular weight cut-off of 12–14 kDa, Spectrum Labs, Houston, USA) was mounted between the donor and receptor compartments of a diffusion cell. The effective diffusional area was 0.637 cm^2 and the volume of receptor compartment was 5 mL. PBS (pH 7.4) was used as receptor medium and maintained at 37±0.5 ^{o}C using heated water circulator. Donor compartment was charged with IM loaded LbL-

AuNP dispersed in 0.2 mL of PBS (pH 7.4). Samples (0.3 mL) were withdrawn from receptor compartment at predetermined time intervals, including 0.25, 0.5, 1, 2, 4, 6, 8 and 12 h, and replaced with fresh media maintained at 37 ^{o}C. In-vitro diffusion of equivalent concentrations of free IM across dialysis membrane was also performed. Samples were analyzed using RP-HPLC equipped with UV-detector. Absorbance of IM was recorded at 256 nm. The amount of IM released was determined using standard calibration curve with a concentration range of 0.1 to 60 µg/mL and a correlation coefficient of 0.998.

2.2.6. Skin permeation of IM

Porcine ears were procured immediately after kill from local abattoir. Ears were cleaned under tap water and hair on the dorsal side was removed using hair clipper (HC70, Remington Inc., Germany). Then the full thickness skin was carefully excised using scalpel and forceps. Later the underlying fat tissue was scrapped off using a blunt scalpel. The full thickness skin samples were stored at -80 ^{o}C for a maximum of 8 weeks.

The skin thickness was measured using digital micrometer (Baker gauges India Pvt. Ltd., Mumbai, India). The skin resistance (R) was measured by applying current (I, 1 mA) across the skin using DC power supply unit (V-care Meditech Pvt. Ltd., Bangalore, India) and voltage drop (V) was determined by digital multimeter (17B, Fluke Corporation, WA, USA). The resistance (R) was calculated using Ohm's law (V=IR).

Skin permeation of free IM and IM loaded LbL-AuNP was performed on excised porcine ear skin using Franz diffusion cell apparatus. Skin sample was mounted between receptor and donor compartments of a diffusion cell with stratum corneum facing donor compartment. The effective diffusional area was 0.637 cm^2 and the volume of receptor

compartment was 5 mL. PBS (pH 7.4) was used as receptor medium and maintained at 37±0.5 ^{o}C. Donor compartment was charged with IM (400 µg) loaded LbL-AuNP dispersed in 0.2 mL of PBS (pH 7.4). Samples (0.3 mL) were withdrawn from receptor compartment at predetermined time intervals, including 0.25, 0.5, 1, 2, 4, 6, 8, 12, 24, 36 and 48 h and were replaced with fresh media maintained at 37 ^{o}C. Samples were analyzed using RP-HPLC method as described above.

The skin permeation parameters were calculated from cumulative amount of IM permeated vs. time profile. Flux (J) was calculated from the slope of linear portion of the cumulative amount of IM permeated – time profile. Lag time (t_{lag}) was calculated by extrapolating the linear portion of the curve to time axis. Permeability coefficient (K_p) was calculated using Equation (2).

$$\text{Permeability coefficient } (K_p) = \frac{\text{Flux}}{\text{Concentration of IM}} \qquad (2)$$

To determine the amount of IM retained in skin, samples were tape striped using scotch book tape (845, 3M, St. Paul, USA). After each tape strip, the weight of SC removed was measured using a microbalance (XP6, Excellence plus, Mettler Toledo Inc., USA). Skin resistance was measured before and after tape striping.

2.2.7. Iontophoresis application

Free IM (400 µg) or IM loaded LbL-AuNP were dispersed in 0.2 mL of PBS (pH 7.4) and charged in the donor compartment. Anodal iontophoresis (current density of 0.47 mA/cm^2) was applied for 4 h using silver electrode placed in donor and silver chloride electrode placed in receptor compartment. A salt bridge was used to avoid direct contact of silver wire with LbL-AuNP. Salt bridge was prepared using 1 % of agarose containing 2 mM of NaCl.

2.2.8. Cell uptake studies

Cell uptake of LbL-AuNP was studied using B16F10 murine melanoma cells. For visualization of cells under fluorescence microscope, the outer layer of LbL-AuNP was coated with FITC labeled PEI. For FITC labeling of PEI, 10 mol excess of FITC was dissolved in DMSO and added drop wise to PEI solution (0.1 M sodium carbonate buffer, pH 9.0). The reaction mixture was incubated for 24 h at room temperature. Later, the conjugate was dialyzed (regenerated cellulose membrane, molecular weight cut-off of 12–14 kDa, SpectraPor Inc., CA, USA) to remove unconjugated FITC. Complete removal of free FITC was confirmed by thin layer chromatography using 5:4:1 of chloroform: methanol: water as mobile phase. The PEI-FITC conjugate was characterized using UV-visible spectroscopy, fluorescence spectroscopy and FTIR.

B16F10 murine melanoma cells (1×10^5) were seeded in 12-well plates and incubated at 37 ^oC and 5 % CO_2. After 24 h, cells were treated with FITC labeled LbL-AuNP and incubated for 5, 15, 30 and 60 min. Later, cells were washed thrice with ice cold PBS and fixed using 4 % paraformaldehyde. Cells were permeabilized using 0.2 % Triton X-100 and were incubated for 5 min in DAPI (1 µg/mL). Fluorescence images were acquired after excitation of FITC using 488 nm laser and DAPI using 358 nm under 10X objective lens (Olympus IX53, Olympus Corporation, Tokyo, Japan). Image analyses were performed using Image J software (version 1.47 V, National Institutes of Health, USA).

2.2.9. Cell viability studies

Cell viability in the presence of free AuNP, LbL-AuNP, free IM and IM loaded AuNP was studied in B16F10 murine melanoma cells. Cells were cultured in Dulbecco's modified Eagle's medium (DMEM) supplemented with 10 % fetal bovine serum (FBS) and 1% penicillin/streptomycin solution, and incubated at 37 ^{o}C with 5% CO_2. Cells (1 x 10^4) were seeded in 96-well plates 24 h before incubation with formulations.

Samples were prepared in DMEM containing 2 % FBS at Au concentration range of 1 to 250 µM for AuNP, LbL-AuNP, free IM and IM loaded LbL-AuNP. The equivalent IM concentration range was 0.31 to 77.5 µM. Cells were treated for 48 h at 37 ^{o}C. Later, cell viability was determined using thiazolyl blue tetrazolium bromide (MTT) assay with absorbance of DMSO solubilized formazan measured at 572 nm wavelength using multimode plate reader (SpectraMax M4, Molecular Devices, California, USA).

2.2.10. Statistical analysis

All the results were presented as mean ± standard deviation. Significance between groups was determined by Student's t test or analysis of variance (Graphpad Prism, USA), where $p<0.05$ was considered to be significant.

2.3. RESULTS

2.3.1. Preparation and characterization of LbL-AuNP

Fig. 2.1a shows images of free AuNP obtained from transmission electron microscope. The average particle size of AuNP from dynamic light scattering studies was found to be 34.5±0.9 nm (PDI: 0.44 ± 0.09). The particle size increased to 98.5±4.3 nm (PDI: 0.29 ± 0.07) after LbL adsorption of polymers.

Fig. 2.1b shows representative particle size distribution of LbL-AuNP. Zeta-potential of PEI stabilized AuNP was found to be 35.2±5.4 mV which decreased and increased with sequential adsorption of PSS and PEI respectively (Fig. 2.1c). Further, overall positive surface charge associated with LbL-AuNP was also confirmed using agarose gel electrophoresis. Fig. 2.2 shows migration of LbL-AuNP toward negative electrode up on application of 100 V for 1 h.

The formation of AuNP was further confirmed by characteristic localized surface plasmon resonance (SPR) at 518 nm. Fig. 2.1d shows shift in SPR of AuNP after sequential adsorption of polymers. LbL adsorption of PSS and PEI onto AuNP showed red shift at 525 nm and 530 nm, respectively. The SPR wavelength of AuNP in different NaCl concentrations (10 to 500 mM) and PBS was 520 nm (Fig. 2.3; Fig. 2.4). The average particle size of AuNP increased from 33.2 ± 0.1 nm (PDI; 0.49 ± 0.01) to 48.9 ± 2.5 nm (PDI; 0.18 ± 0.11) after incubation in NaCl (10 to 500 mM) (Table 2.1). Further increase in NaCl concentration from 10 mM to 500 mM decreased zeta-potential of AuNP from 12.5 ± 0.8 to 2.9 ± 0.8 mV, respectively.

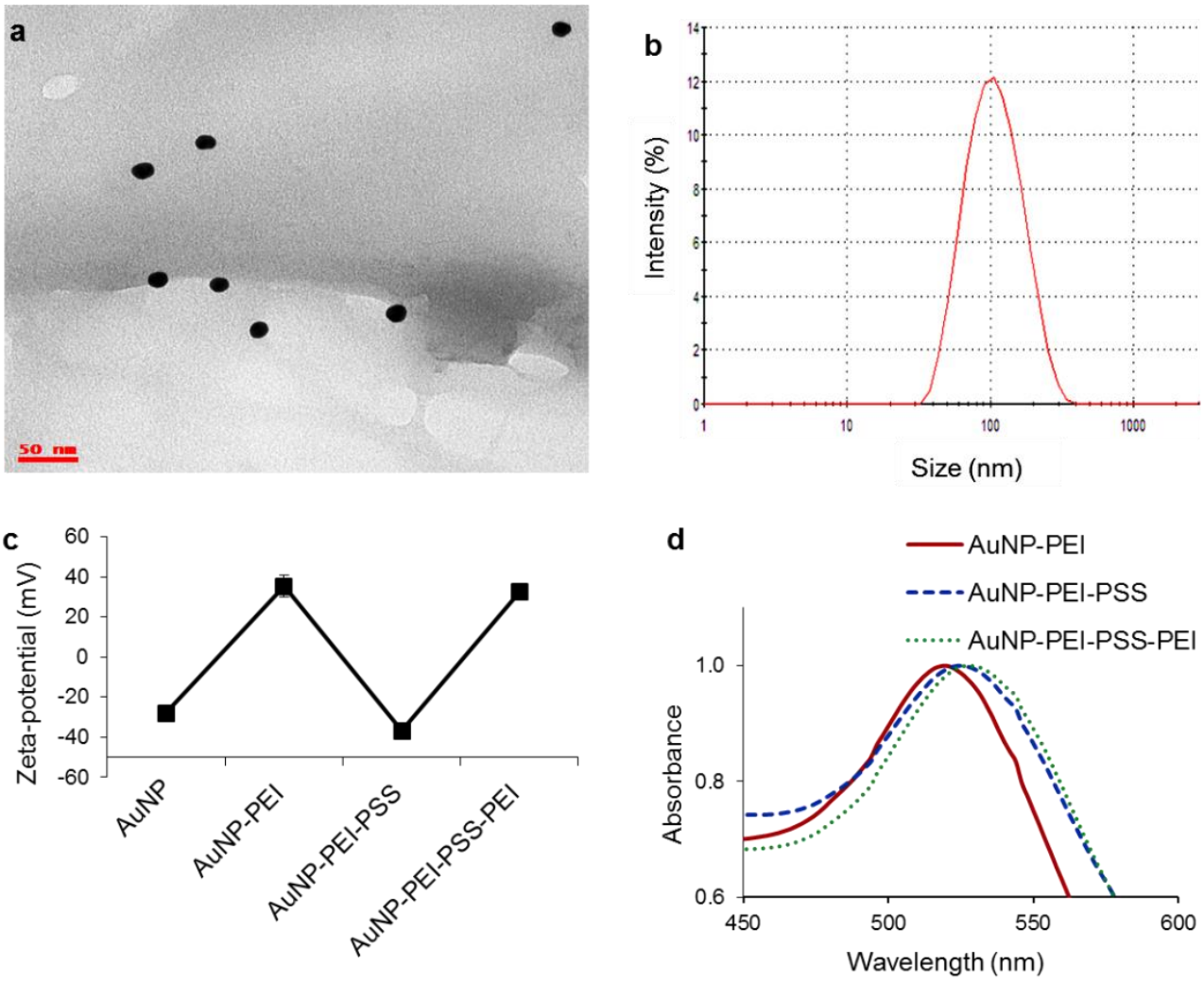

Fig. 2.1. Characterization of gold nanoparticles. **a**, transmission electron micrograph of polyethylene imine coated AuNP; **b**, representative intensity weighted particle size distribution of LbL-AuNP from dynamic light scattering study; **c**, zeta-potential measured after sequential adsorption of PEI and PSS polymers on AuNP; **d**, spectra obtained from surface plasmon resonance upon adsorption of PSS and PEI polymers on AuNP. Values in "c" and "d" represent average (n=3) ± SD.

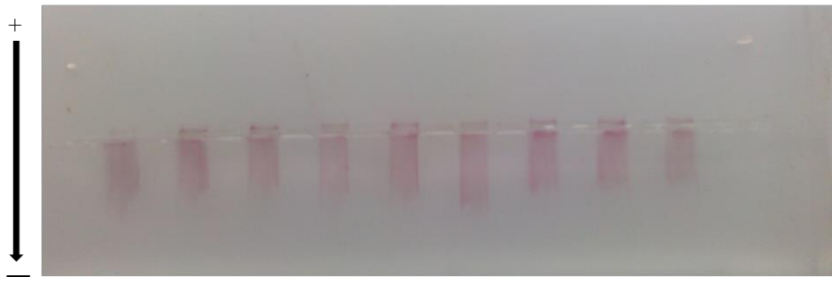

Fig. 2.2. Electrophoretic mobility of LbL-AuNP in 0.4 % agarose. All the bands represent only LbL-AuNP.

a.

b.

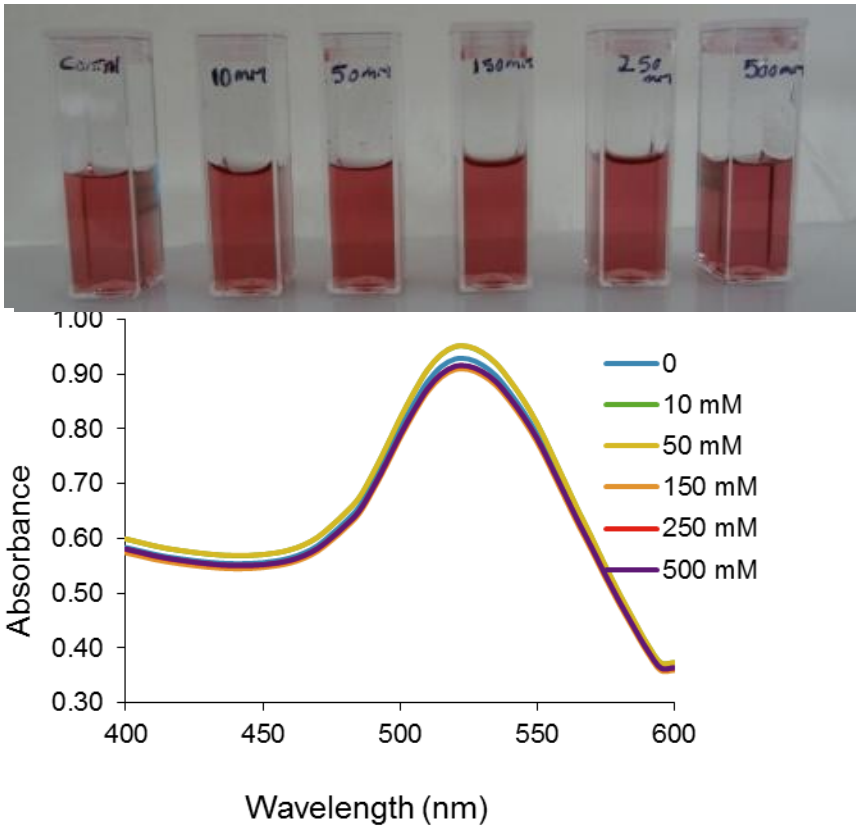

Fig. 2.3. a, Effect of NaCl concentration on localized surface plasmon resonance (SPR) wavelength of AuNP; **b**, Photograph of effect of NaCl concentration on stability of AuNP.

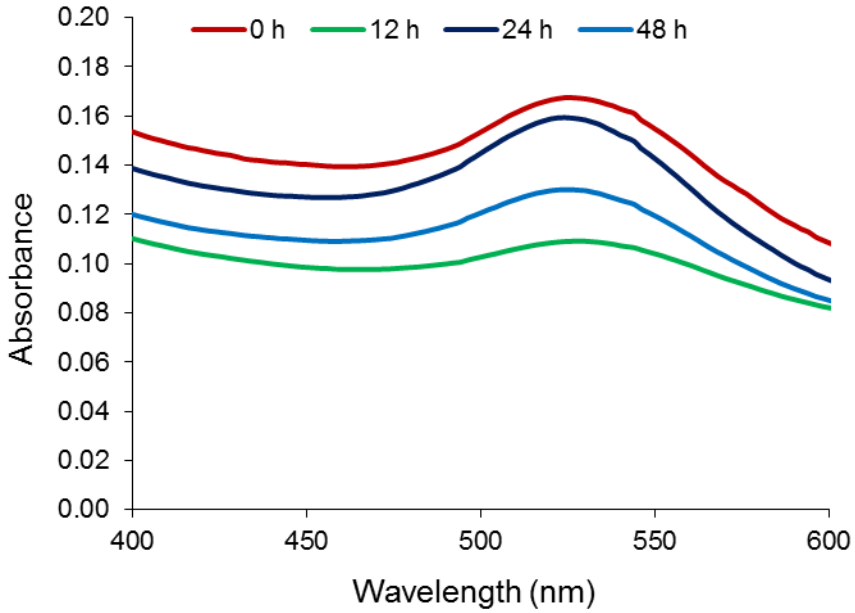

Fig. 2.4. Effect of PBS on localized surface plasmon resonance (SPR) wavelength of AuNP incubated at different time points.

Table 2.1. Particle size and zeta-potential measurements of AuNP incubated in different concentrations of NaCl.

NaCl concentration (mM)	Particle size (nm)	Zeta-potential (mV)
0	32.6±3.3 (0.49±0.03)	36.9±4.7
10	33.2±0.1 (0.49±0.01)	12.5±0.8
50	39.1±2.5 (0.43±0.01)	5.6±1.2
150	35.9±1.4 (0.44±0.03)	3.6±0.6
250	42.5±6.7 (0.34±0.16)	3.1±0.8
500	48.9±2.5 (0.18±0.11)	2.9±0.8

Data were presented as mean ± standard deviation (n =3).Values in parentheses represent polydispersity index (PDI) ± standard deviation.

After incubation of AuNP in PBS and DMEM containing 2% FBS for 48 h, the particle size was found to be 49.5±3.7 nm (PDI: 0.54±0.11) and 93.9±10.5 nm (PDI: 0.60±0.01), respectively (Table 2.2). Zeta-potential of AuNP in PBS and DMEM with 2% FBS was found to be -0.4±0.5 mV and -5.5±0.3 mV respectively after incubation for 48 h (Table 2.2). Similar stability studies were also performed for LbL-AuNP incubated in PBS, DMEM with 2% FBS and NaCl. LbL-AuNP in PBS showed SPR wavelength at 528 nm and particle size of 140.3±22.7 nm (PDI: 0.49±0.17) after 48 h incubation. Zeta-potential of LbL-AuNP decreased from 32.3±1.3 mV to -2.5±0.2 mV after 48 h incubation in PBS. The stability studies of LbL-AuNP in DMEM containing 2 % FBS showed particle size and zeta-potential of 137.9±9.2 nm (PDI: 0.43±0.08), -6.5±0.2 mV respectively after 48 h incubation (Table 2.2).

Fig. 2.5 shows FTIR spectrum of neat PVP, neat PEI, neat PSS. PVP showed characteristic peaks at 1687 cm^{-1} (C=O stretch) and 1285 cm^{-1} (C-N stretch) wave numbers respectively. PVP stabilized AuNP showed a shift in C=O stretching to 1651 cm^{-1}. Functionalization of PVP stabilized AuNP with PEI was confirmed by the presence of characteristic absorbance peaks at 1053 cm^{-1} (C-N stretch) and 3565 cm^{-1} (N-H stretch) wave numbers respectively (Fig. 2.6).

Table 2.2. Particle size and zeta-potential measurement of AuNP and LbL-AuNP in presence of phosphate buffered saline (PBS) and DMEM medium containing 2 % FBS.

Parameter	Incubation time (h)	AuNP		LbL-AuNP	
		PBS	DMEM	PBS	DMEM
Particle size (nm)	0	45.8 ± 2.1 (0.36 ± 0.01)	45.8 ± 2.1 (0.36 ± 0.01)	88.1 ± 17.7 (0.33 ± 0.02)	88.1 ± 17.7 (0.33 ± 0.02)
	12	45.7 ± 3.9 (0.37 ± 0.02)	45.7 ± 5.1 (0.55 ± 0.04)	153.7 ± 15.3 (0.40 ± 0.05)	104.2 ± 7.2 (0.44 ± 0.10)
	24	49.2 ± 2.0 (0.37 ± 0.02)	42.6 ± 2.9 (0.47 ± 0.02)	131.0 ± 33.5 (0.36 ± 0.18)	132.3 ± 8.0 (0.42 ± 0.10)
	48	49.5 ± 3.7 (0.54 ± 0.11)	93.9 ± 10.5 (0.60 ± 0.01)	140.3 ± 22.7 (0.49 ± 0.17)	137.9 ± 9.2 (0.43 ± 0.08)
Zeta-potential (mV)	0	35.2 ± 5.5	35.2 ± 5.5	32.3 ± 1.3	32.3 ± 1.3
	12	-1.2 ± 1.4	-5.1 ± 0.3	-6.7 ± 0.4	-6.2 ± 0.5
	24	-0.6 ± 0.8	-5.6 ± 0.2	-5.5 ± 0.4	-6.3 ± 0.2
	48	-0.4 ± 0.5	-5.5 ± 0.3	-2.5 ± 0.2	-6.5 ± 0.2

Data are presented as mean ± standard deviation (n =3).Values in parentheses represent polydispersity index (PDI) ± standard deviation.

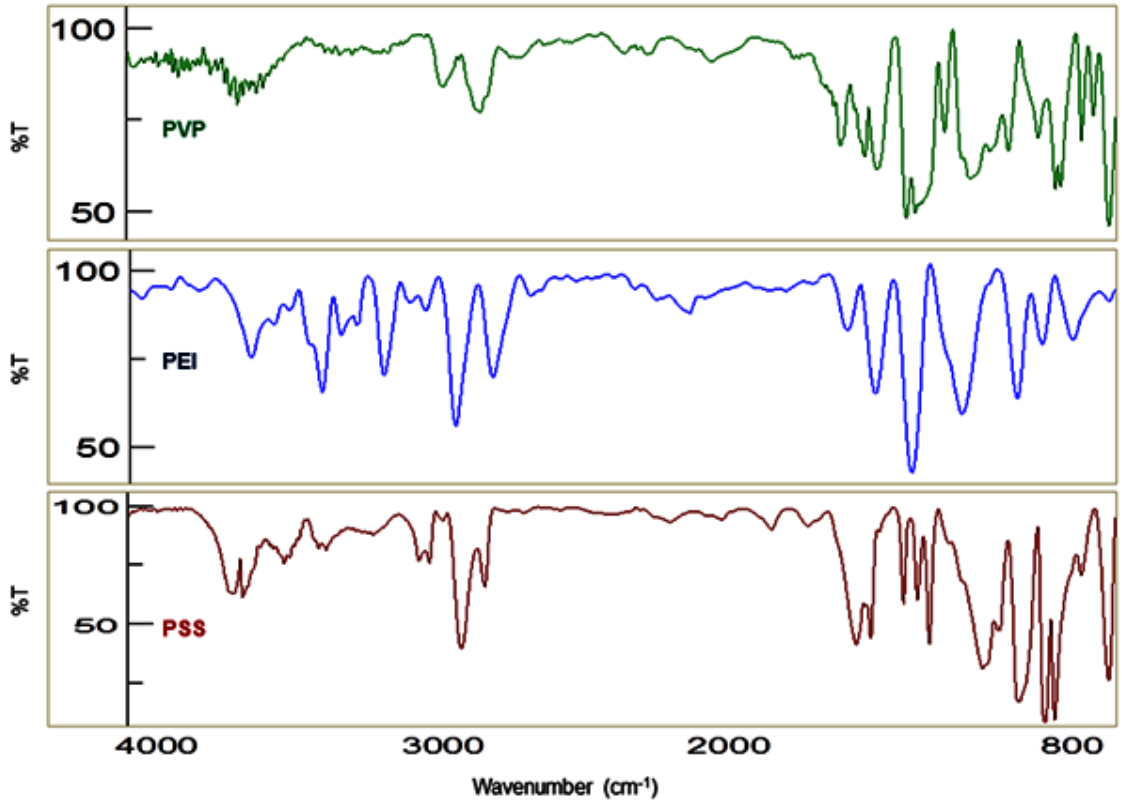

Fig. 2.5. FTIR spectra of neat PVP, neat PEI, neat PSS

LbL adsorption of polymers on to AuNP surface showed shift in characteristic peaks of PSS and PEI polymers. In case of PSS, wave numbers of 1040 cm^{-1}, 1184 cm^{-1} were shifted to 1033 cm^{-1} and 1179 cm^{-1} respectively. In case of PEI, 3532 cm^{-1} (N-H stretch), 1119 cm^{-1} (C-N stretch) were shifted to 3565 cm^{-1} and 1124 cm^{-1} respectively.

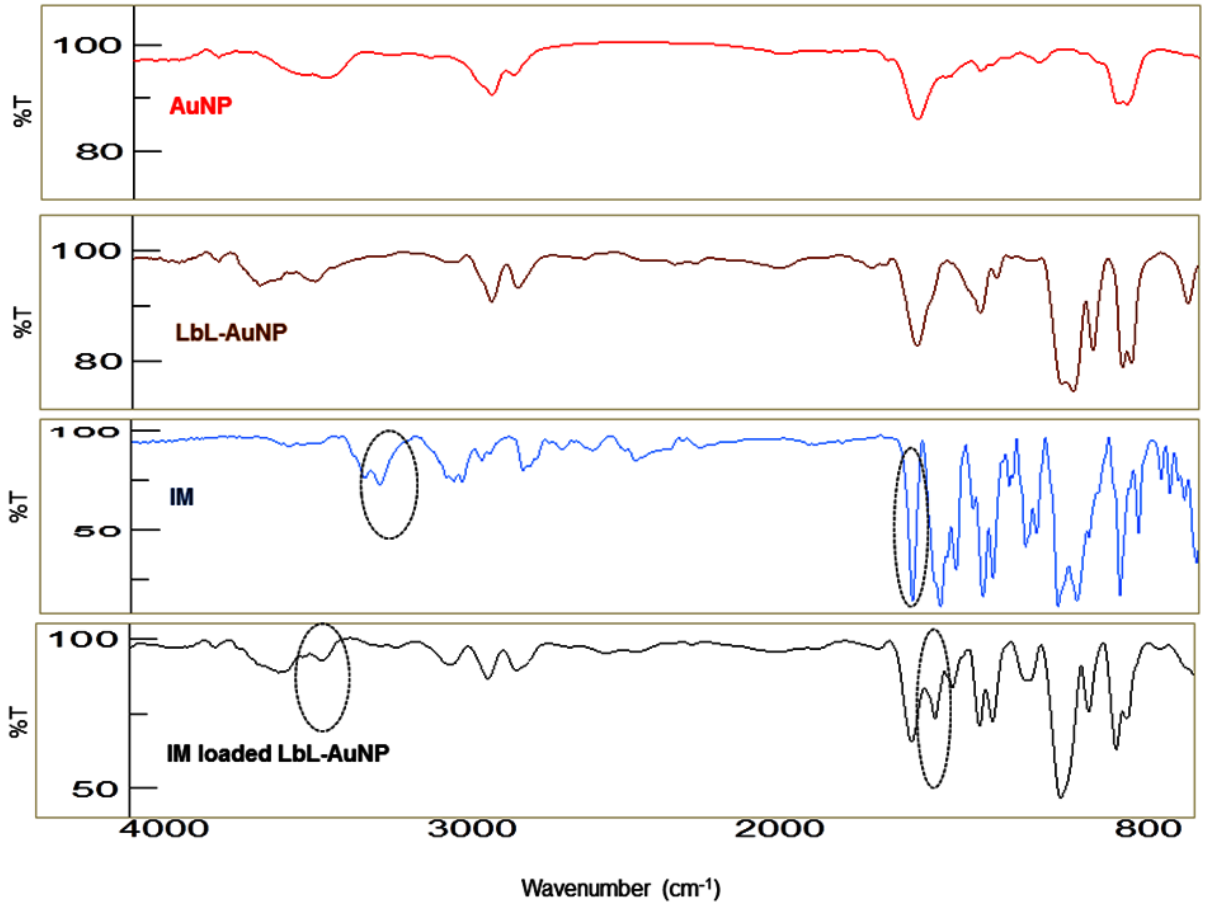

Fig. 2.6. FTIR spectra of AuNP, LbL-AuNP, neat IM and IM loaded LbL-AuNP. Spectra were representative of at least three different experiments. The dotted circle represents characteristic absorbance peaks of IM.

DSC studies showed glass transition temperature (T_g) for PSS at 86.9 ^oC and melting temperature (T_m) at 238.5 ^oC. For PEI, T_g and T_m were observed at 110.0 ^oC and 336.4 ^oC respectively. AuNP did not show any characteristic thermal transition up to 400 ^oC. DSC studies for LbL-AuNP showed shift in T_g for both PSS and PEI at 67.94 ^oC and shift in T_m of PSS and PEI to 284.8 ^oC and 381.5 ^oC respectively (Fig. 2.7).

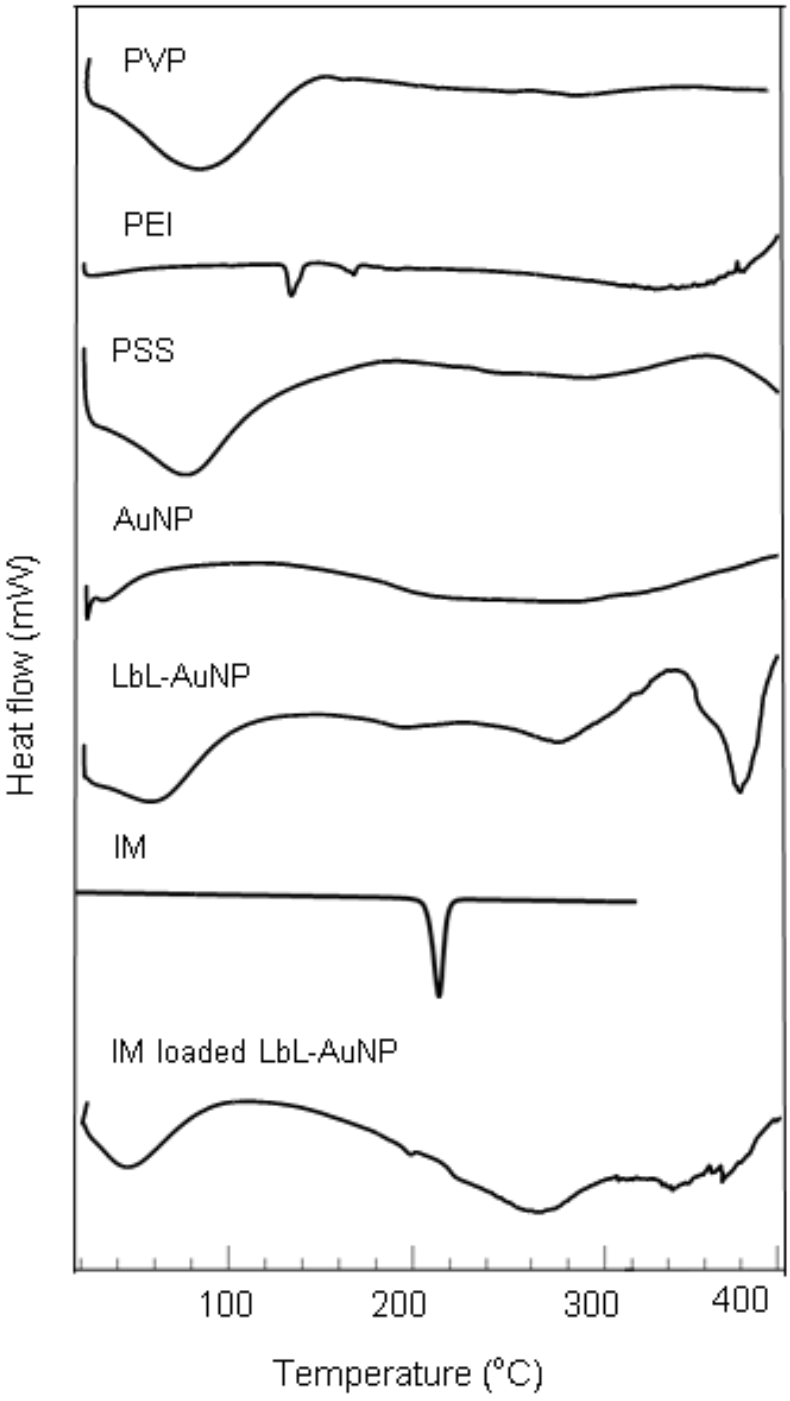

Fig. 2.7. DSC Thermograms of neat PVP, neat PEI, neat PSS, AuNP, LbL-AuNP, neat IM and IM loaded LbL-AuNP. Thermograms were representative of at least three different experiments.

2.3.2. Encapsulation and in-vitro release of IM in LbL-AuNP

Encapsulation of IM in LbL-AuNP was characterized by FTIR and DSC. FTIR studies showed shift in absorbance peak of IM after encapsulation, where 1658 cm^{-1} (C=O stretch) shifted to 1652 cm^{-1} and 3256 cm^{-1} (N-H stretch) shifted to 3400 cm^{-1} (Fig. 2.6). Similarly, DSC thermograms showed shift in melting temperature (T_m) of free IM from 226.5 ^oC to 229.9 ^oC after encapsulation (Fig. 2.7). The loading efficiency (%) of IM in LbL-AuNP was found to be 28.3 ± 2.3 %.

Fig. 2.8 shows In-vitro release profiles of IM from LbL-AuNP and diffusion of free IM across dialysis membrane. IM release from LbL-AuNP was controlled up to 8 h, while 100% free IM diffused across membrane within 2 h. The in-vitro release profiles were fitted into kinetic models of zero-order, first-order, Higuchi, Hixon-Crowell and Korsmeyer-Peppas. Correlation coefficients of regression analyses were found to be 0.860, 0.965, 0.962, 0.920, and 0.961 for zero-order, first-order, Higuchi, Hixon-Crowell and Korsmeyer-Peppas models, respectively. The release exponent "n" obtained from Korsmeyer-Peppas model was found to be 0.612. Therefore it can be said that IM showed zero order release mechanism (Fig. 2.9).

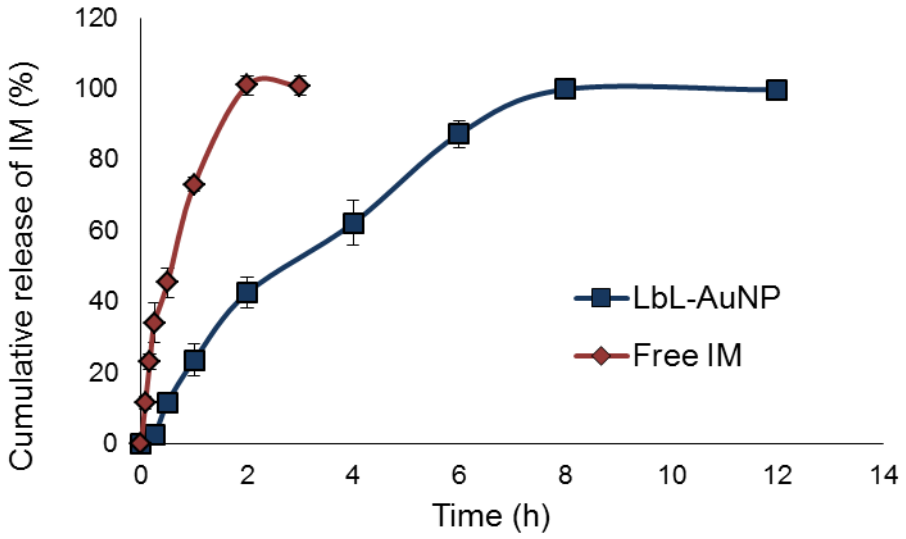

Fig. 2.8. In-vitro release profile of IM release from LbL-AuNP and diffusion of free IM.Data was presented as mean (n=3) ± SD.

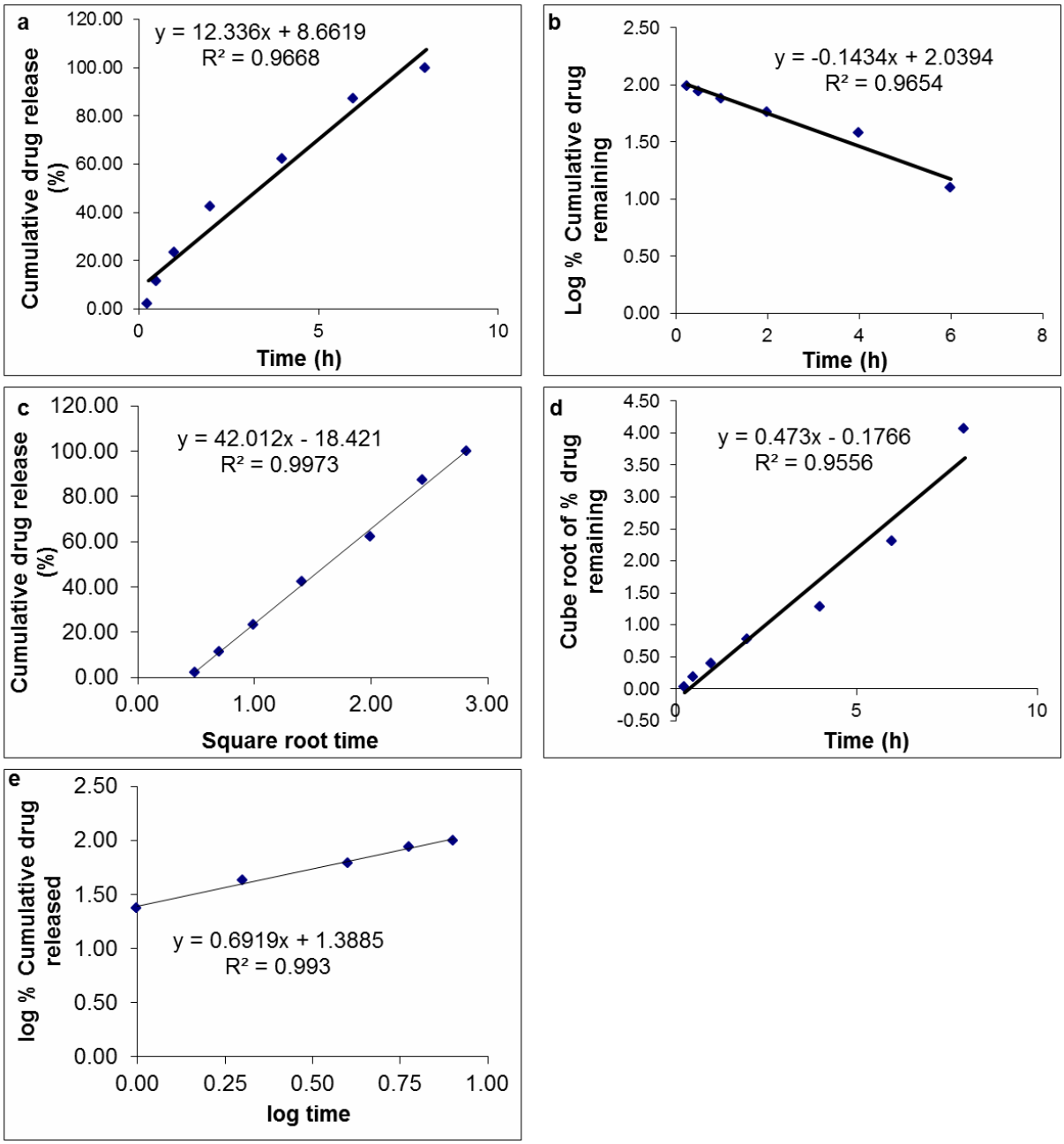

Fig. 2.9. Model fitting of cumulative amount of IM released from LbL-AuNP in zero-order (a), first-order (b), Higuchi model (c), Hixon-Crowell model (d) and Korsmeyer-Peppas model (e).

2.3.3. Skin permeation of IM loaded LbL-AuNP

Skin permeation studies were performed on excised porcine ear skin. The average resistance offered by skin samples before experimentation was 4.48 ± 1.01 kΩ (n=12). Table 2.3 shows skin permeation parameters of IM after 4 and 48 h treatment. After 4 h passive application, free IM showed a flux of 0.94±0.18 μg/cm^2/h in comparison to 1.10±0.30 μg/cm^2/h for IM loaded LbL-AuNP. Anodal iontophoresis showed flux of 1.64 ± 0.21 and 6.37±0.66 μg/cm^2/h for IM delivered as free form or loaded in LbL-AuNP. The lag time for free IM permeation was reduced from 3.38 ± 0.45 after passive application to 0.82 ± 0.17 after iontophoresis. Fig. 2.10 shows cumulative amount of IM permeated across skin and time profile. Similar reduction in lag time was also showed after iontophoresis application of LbL-AuNP. Iontophoresis of LbL-AuNP showed greatest cumulative amount of IM permeated at 31.7 ± 4.80 μg/cm^2 (Table 2.3). After 48 h passive treatment, cumulative amount of IM permeated was 129.8 ± 6.55 μg/cm^2 for LbL-AuNP compared to 267.6 ± 64.6 μg/cm^2 for free drug. Table 2.3 also shows the permeability coefficient for passive and iontophoretic application of free IM and IM loaded LbL-AuNP.

Tape striping of stratum corneum reduced skin resistance from 4.48±1.01 kΩ to 1.39±0.25 kΩ. Fig. 2.11 shows amount of IM retained in stratum corneum and viable epidermis after 4 h passive or iontophoresis application of LbL-AuNP. The amount of IM retained within stratum corneum after 4 h passive application of free IM and IM loaded LbL-AuNP was 0.07 ±0.03 and 0.2 ± 0.03 μg/mg, respectively. On the other hand, 4 h iontophoresis application showed 0.15 ± 0.02 and 1.17 ± 0.14 μg/mg of IM in stratum corneum for free IM and IM loaded LbL-AuNP, respectively. Similarly, iontophoresis application significantly ($p<0.05$) enhanced retention of IM in viable epidermis after treatment with IM loaded LbL-AuNP (0.69 ± 0.10 μg/mg) compared with passive application

of IM loaded LbL-AuNP (0.08 ± 0.02 µg/mg) and iontophoresis of free IM (0.14 ± 0.01 µg/mg).

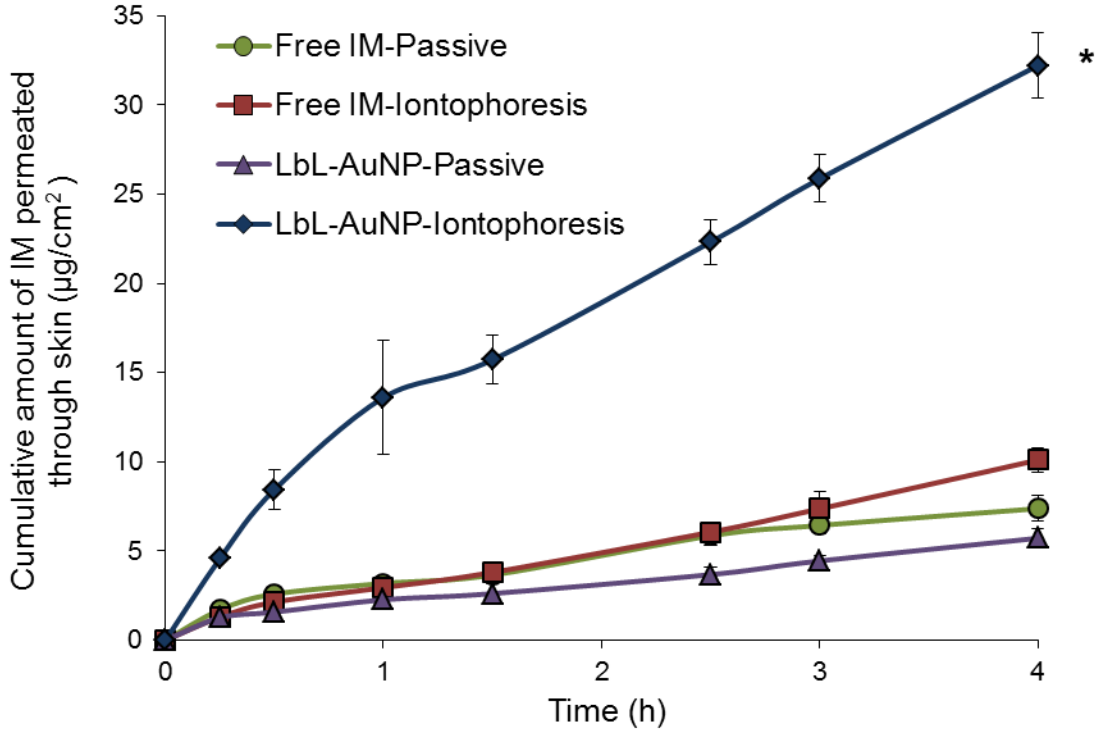

Fig. 2.10. Cumulative amount of IM permeated across excised porcine skin after treatment with respective formulation for 4 h.

Table 2.3. Skin permeation parameters of IM permeated through LbL-AuNP with and without iontophoresis in comparison with free drug.

Parameter	Free IM-Passive	Free IM-Iontophoresis	IM loaded LbL-AuNP-Passive	IM loaded LbL-AuNP-Iontophoresis
4 h				
Flux (µg/cm^2/h)	0.94±0.18	1.64±0.21	1.1±0.30	6.37±0.66 *
Lag time (h)	3.38±0.45	0.82±0.17	2.20±0.04	0.96±0.51
Q_4 (µg/cm^2)	6.90±1.12	10.10±0.71	5.47±0.65	31.68±4.80 *
Permeability coefficient (cm^2/h)	0.002±0.0004	0.004±0.0005	0.003±0.001	0.017±0.002 *
48 h				
Flux (µg/cm^2/h)	1.03±0.19	NA	1.2±0.28	NA
Lag time (h)	3.22±1.08		3.15±0.35	
Q_{48} (µg/cm^2)	267.6±64.6		129.83±6.55	
Permeability coefficient (cm^2/h)	0.0026±0.0005		0.003±0.001	

Q4 and Q48 represents cumulative amount of IM permeated across skin after 4 h and 48 h respectively. Data was presented as mean (n=4) ± standard deviation. * Represents that the values are significantly ($p<0.05$) different compared with all other values within the parameter.

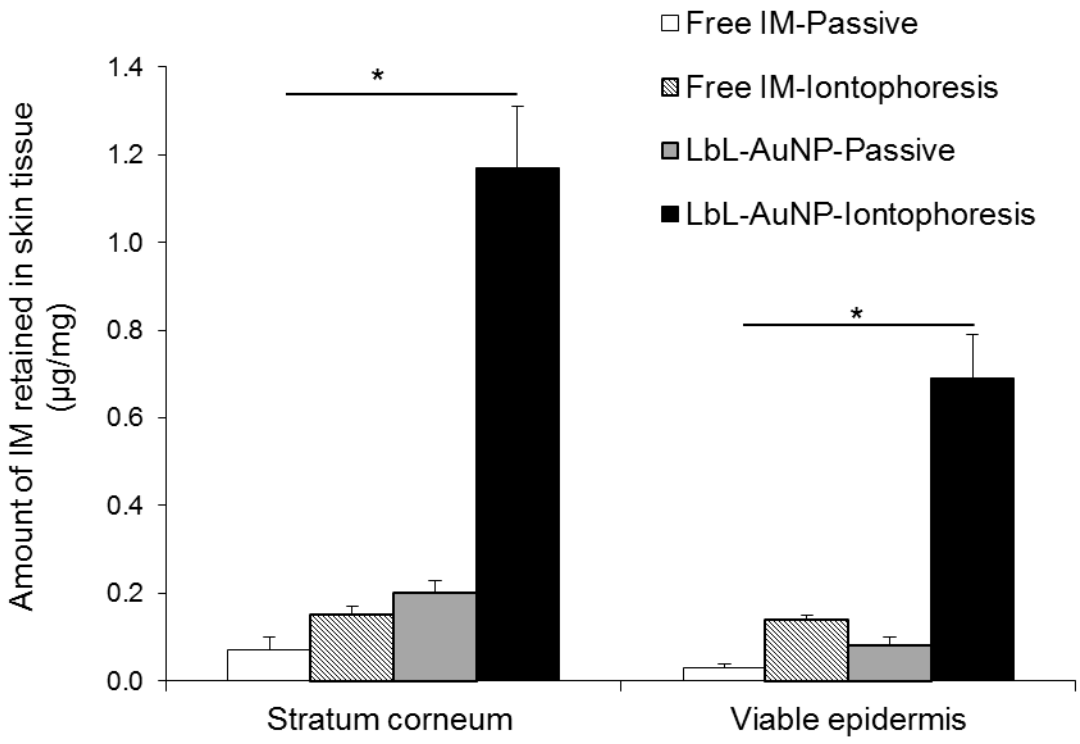

Fig. 2.11. Skin disposition of IM after passive and iontophoretic application of free IM and IM loaded LbL-AuNP. Skin samples were treated for 4 h. Data were presented as mean (n=4) ± SD. * Represents that the values were significantly ($p<0.05$) different compared to all other treatments.

2.3.4. Cell uptake and inhibition of cancer cell growth by IM loaded LbL-AuNP

FITC labeling of PEI was confirmed by thin layer chromatography (Fig. 2.12). FITC conjugation of PEI resulted in shift in absorption maxima of FITC from 492 nm to 498 nm. Fluorescence spectrum showed emission wavelength at 519 nm and 522 nm for FITC and FITC-labeled PEI respectively. Fig. 2.13 shows FTIR spectra of free FITC and FITC-PEI conjugate.

Fig. 2.12. Characterization of free FITC (a), PEI (b) and FITC-PEI conjugate (c) by thin layer chromatography.

Free FITC showed absorbance peak at 2039 cm^{-1} wavenumber characteristic of isothiocyanate (N=C=S). On the other hand, FITC-PEI conjugate showed characteristic absorbance peak at 1100 cm^{-1} wavenumber corresponding to thiourea (N-CS-N) bond between isothiocyanate group of FITC and amine group of PEI. UV-visible spectroscopic analysis showed 0.93 moles of FITC conjugated to one mole of PEI. FITC labeled PEI was used to adsorb as the outer layer of LbL-AuNP.

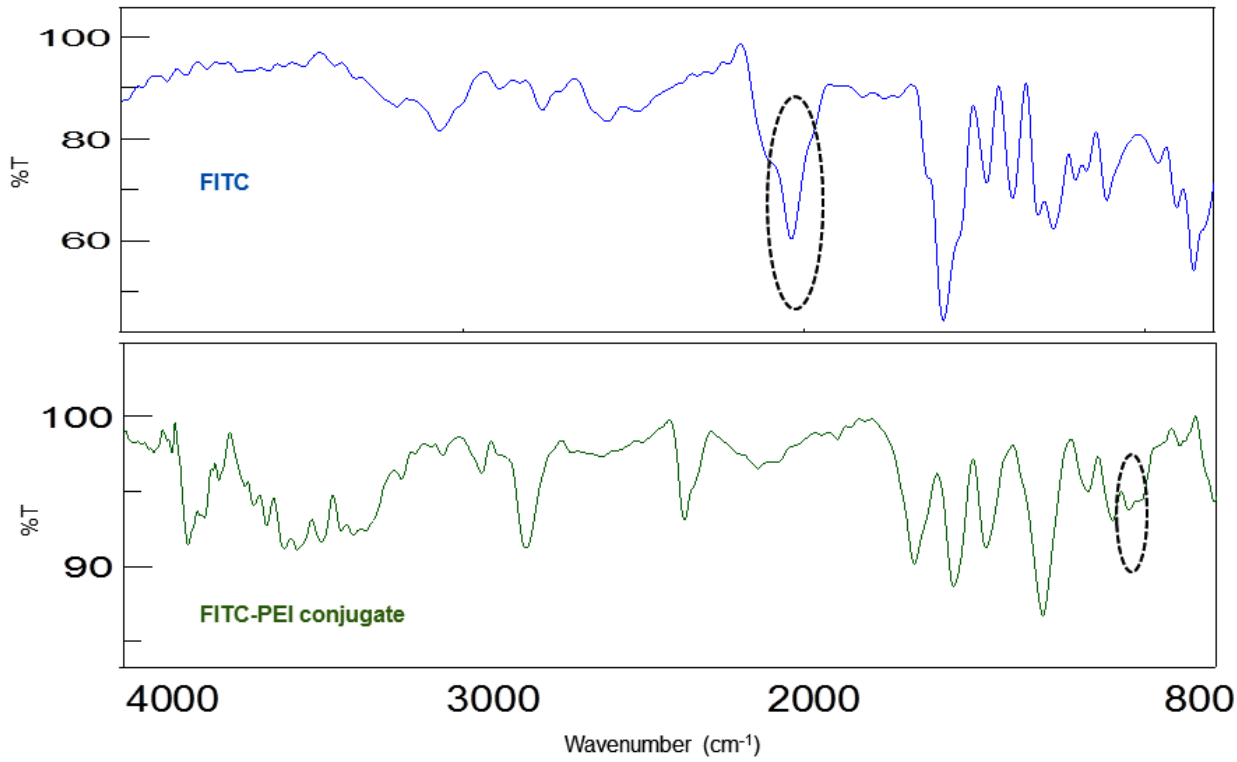

Fig. 2.13. FTIR spectra of free FITC and FITC-PEI conjugate.

Fig. 2.14a shows the microscopic images B16F10 cells after incubation with LbL-AuNP for 5, 15, 30 and 60 min. Images show that within 5 min of incubation, LbL-AuNP adsorbed onto B16F10 cells. Increase in incubation time increased cell associated fluorescence. Background corrected fluorescence image analysis showed gradual increase in cell associated fluorescence and thus cell uptake of LbL-AuNP with the increase in incubation time from 5 min to 60 min (Fig. 2.14b). After 60 min incubation, images showed that LbL-AuNP localized in nucleus of cells as observed from change in color after merging the green and blue filter images.

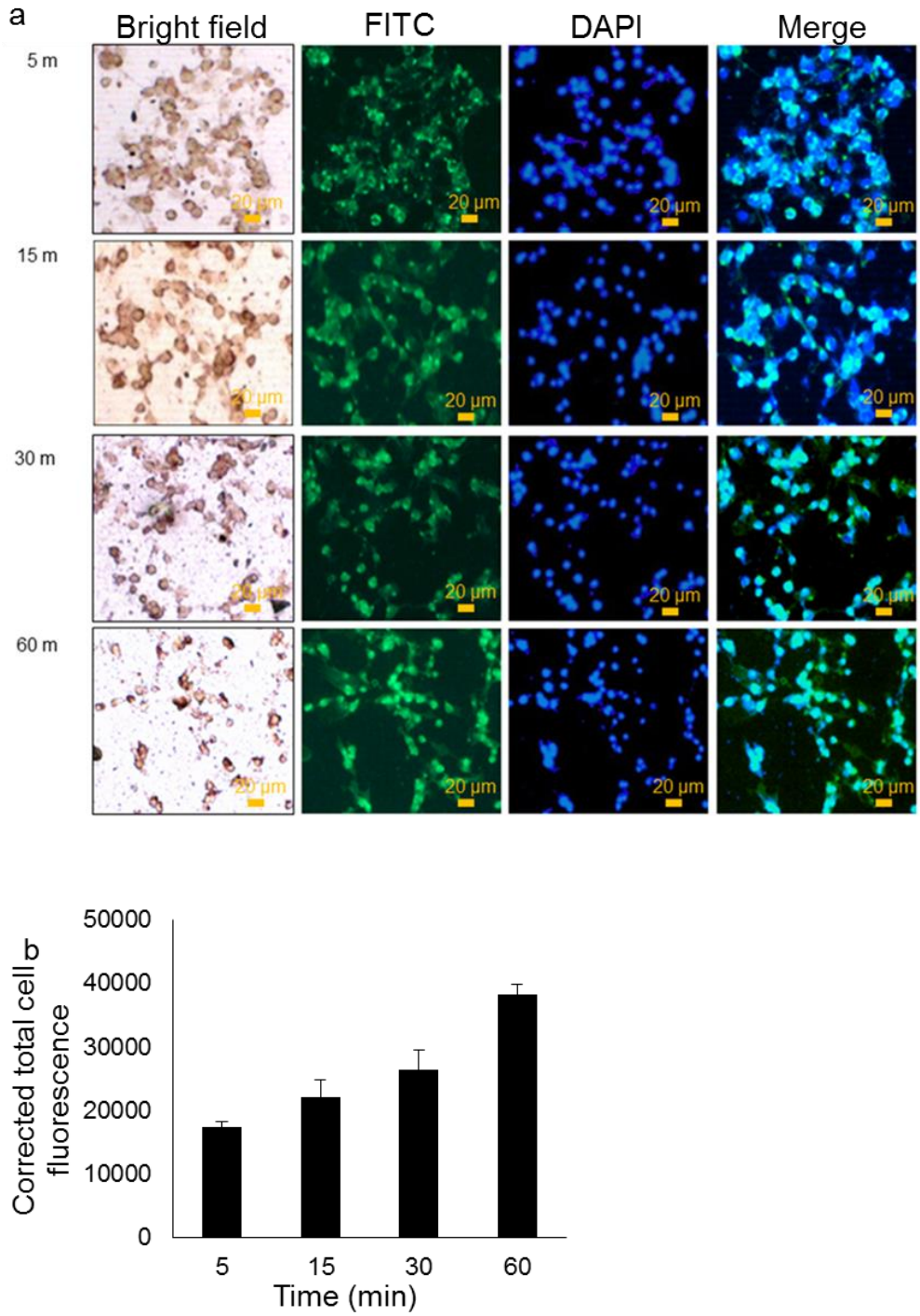

Fig 2.14. a, Cell uptake of FITC labeled LbL-AuNP in B16F10 cancer cells after incubation for 5, 15, 30 and 60 min. Micrographs were presented in bright field, FITC filter, DAPI filter, merge of FITC and DAPI filter images. Images were representative of at least three experiments; **b**. Corrected total cell fluorescence calculated for FITC labeled LbL-AuNP cell uptake studies. Images were analyzed using Image J software. At least 3 images from three different experiments were analyzed. Within each image ten random regions of interest were selected.

Fig. 2.15 shows the inhibition of B16F10 murine melanoma cell growth after treatment with AuNP, LbL-AuNP, free IM and IM loaded LbL-AuNP. It was found that increase in concentration of AuNP concentration from 1 to 250 µM increased growth inhibition from 10.8 ± 0.06 to 31.2 ± 0.12 %. Blank LbL-AuNP showed 62.9 ± 0.06 % growth inhibition at 250 µM, while IM loaded LbL-AuNP (77.5 µM of IM) showed significantly ($p<0.001$) greater growth inhibition (81.5 ± 0.06 %). On the other hand, free IM only showed 58.6 ± 0.13 % growth inhibition at 77.5 µM.

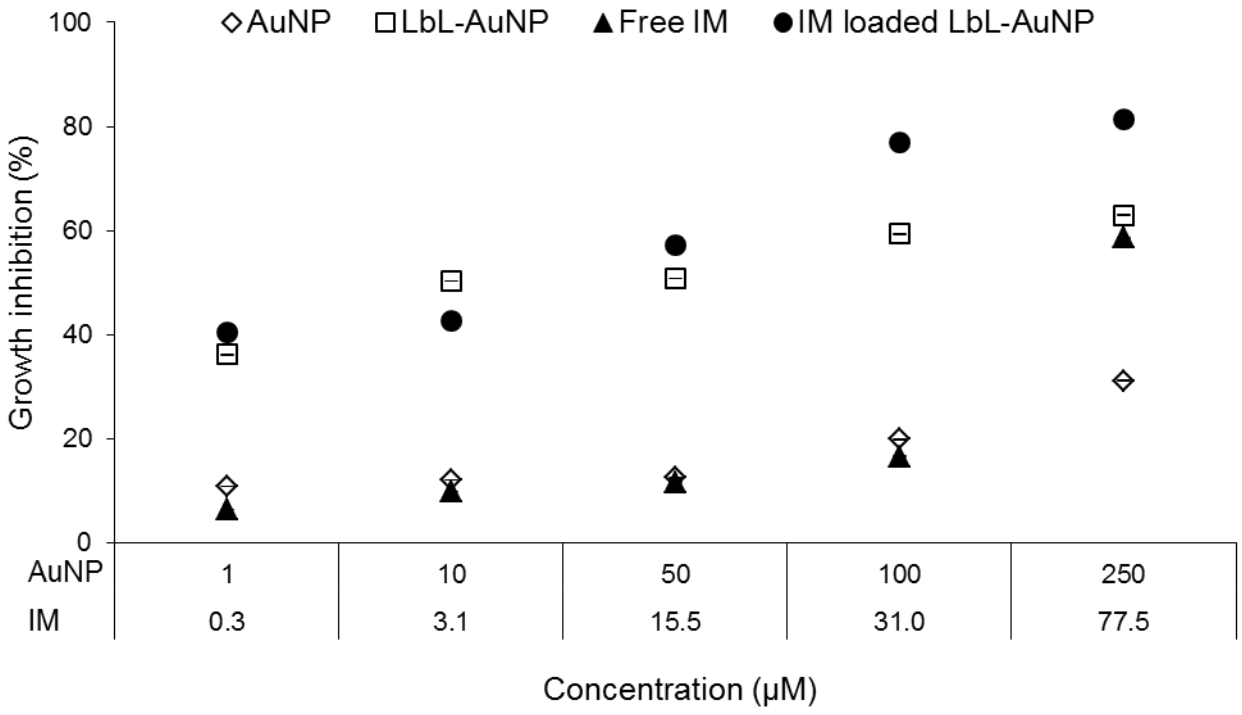

Fig. 2.15. Inhibition of B16F10 cancer cell growth after treatment with AuNP, LbL-AuNP, free IM and IM loaded LbL-AuNP. Data were presented as mean (n=8) ± SD.

2.4. DISCUSSION

Gold has been utilized in the form of nanoparticles since prehistoric period (Wyman et al., 2011). Metallic gold was found to be much stable compared to other metals such as silver and bronz (Ghosh et al., 2007). On the other hand, gold at nano-scale is more reactive and tend to aggregate (Dreaden et al., 2012). Traditionally AuNP were stabilized by thiol exchange of citrate ligand with mercaptoundecenoic acid and similar molecules (Auffan et al., 2009; Kaufman et al., 2007). This strategy has also been applied to ligate a therapeutic moiety to AuNP either directly or through a linker (Auffan et al., 2009). The drawback of thiol-based linkage is that in the presence of ionic medium such as culture medium, AuNP are not stable (Zhu et al., 2003; Zhang et al., 2008). Furthermore only a few small or macromolecules can be ligated to the surface of AuNP (Mei et al., 2009). To overcome these limitations without significant increase in particle size, we have coated AuNP with charged polymers in a layer-by-layer strategy. Stability studies indicated that LbL-AuNP were stable in cell culture medium with 2 % fetal bovine serum, up to 0.5 M NaCl, phosphate buffer saline and at a pH range of 4 to 8. LbL coating of AuNP enabled IM encapsulation.

Our previous studies on layer-by-layer microcapsules prepared using PEI and PSS polymers showed greater encapsulation efficiency for charged small molecules including IM (Baptista et al., 2008). Encapsulation efficiency of small molecules in microcapsules increased with the presence of charge, hydrogen bond acceptors and donors or potential for hydrophobic interactions (Mandapalli et al., 2014). In this study, loading efficiency of IM in LbL-AuNP was 28%, which is to our knowledge the highest reported loading of a small molecule in AuNP. Other studies using doxorubicin, paclitaxel and curcumin reported 17 %, 3.52 % and 26 % as greatest loading efficiency in AuNP (Kim et al., 2008; Oh et al., 2008; Gangwar et al., 2012). Furthermore, increase in surface conjugation of doxorubicin decreased the stability of AuNP (de Oliveira et al., 2013). Release of small molecules conjugated to

AuNP through linkers is dependent on the degradation kinetics of the linker, enzyme expression or pH of the medium (Venkatesan et al., 2013; Venkatpurwar et al., 2011). While it is advantageous to have spatial control, drug release could be unpredictable. Entrapment of molecule through weaker interactions in LbL matrix shows diffusion controlled or erosion controlled release mechanism (Baptista et al., 2008).

LbL polyelectrolyte coated AuNP had high surface charge density for effective iontophoretic delivery. Nanoparticles including AuNP have been shown to get transported across stratum corneum through paracellular and/or appendageal pathways (Arruebo et al., 2011). Further application of iontophoresis increases the pore size of hydrophilic channels within stratum corneum (Wang et al., 2011). The penetration enhancement showed by LbL-AuNP in the presence of electric current is attributed to small particle size, high charge density and positive charge. It was showed that particles of size <100 nm can penetrate skin membrane up to stratum corneum (Naik et al., 2000; Baroli et al., 2007). In general nanocarriers with positively charged surface interact with negatively charged skin enhancing skin penetration of small molecules (Venuganti et al., 2011).

IM has been clinically studied for its efficacy against melanoma. In clinical trials, IM is being administered as solid dosage form through oral administration (Tournebize et al., 2012). To the best of our knowledge there are no studies investigating the topical application of IM. Passive application of IM for topical delivery is limited as reported here. The enhancement in skin retention of IM was greater compared with enhancement in cumulative amount of IM permeated across skin after iontophoresis of LbL-AuNP.

Anti-cancer activity of IM is attributed to its inhibitory effect on c-kit tyrosine kinase receptor signaling pathway. This is also found to be over-expressed in melanoma of skin (Kim et al., 2008). Therefore, we have studied the cell uptake and cytotoxicity of IM loaded LbL-AuNP in murine melanoma B16F10 cells. Nano-size and high positive surface charge

has been important attributes for cell uptake of particles. Interestingly we have also found that LbL-AuNP showed nuclear localization within 60 min of incubation. AuNP are reported to be taken up by cells through endocytosis pathways (Guo et al., 2011). LbL polymer coating of AuNP decreased the cancer cell viability compared with free AuNP. This is because of greater cell interaction of charged polymers on LbL-AuNP. The outer layer of LbL-AuNP was PEI which is known to inhibit cancer cell growth (Shukla et al., 2005; Moghimi et al., 2005). However further studies are required to investigate the cancer cell selectivity of LbL-AuNP for cancer cells. IM loading in LbL-AuNP further inhibited the cancer cell growth. Overall we have significantly improved the small molecule loading efficiency in AuNP by LbL polymer coating and enhanced the skin permeation of IM using a combination of LbL-AuNP and iontophoresis.

2.5. CONCLUSIONS

The results show that layer-by-layer polymer coated gold nanoparticles can be developed for topical delivery of small molecule drugs. The loading efficiency of small molecules in gold nanoparticles can be enhanced by their layer-by-layer polymer coating. Iontophoresis application significantly enhances skin penetration of polymer coated gold nanoparticles further enhancing the viable skin penetration of imatinib. Moreover, LbL coated gold nanoparticles are rapidly taken up by murine melanoma cells and significantly decreases the cancer cell growth. Overall the findings in this study can be applied to develop gold nanoparticles for topical delivery of small molecules.

Chapter 3

LbL-AuNP for topical iontophoretic delivery of STAT3 siRNA to treat melanoma

Graphical abstract

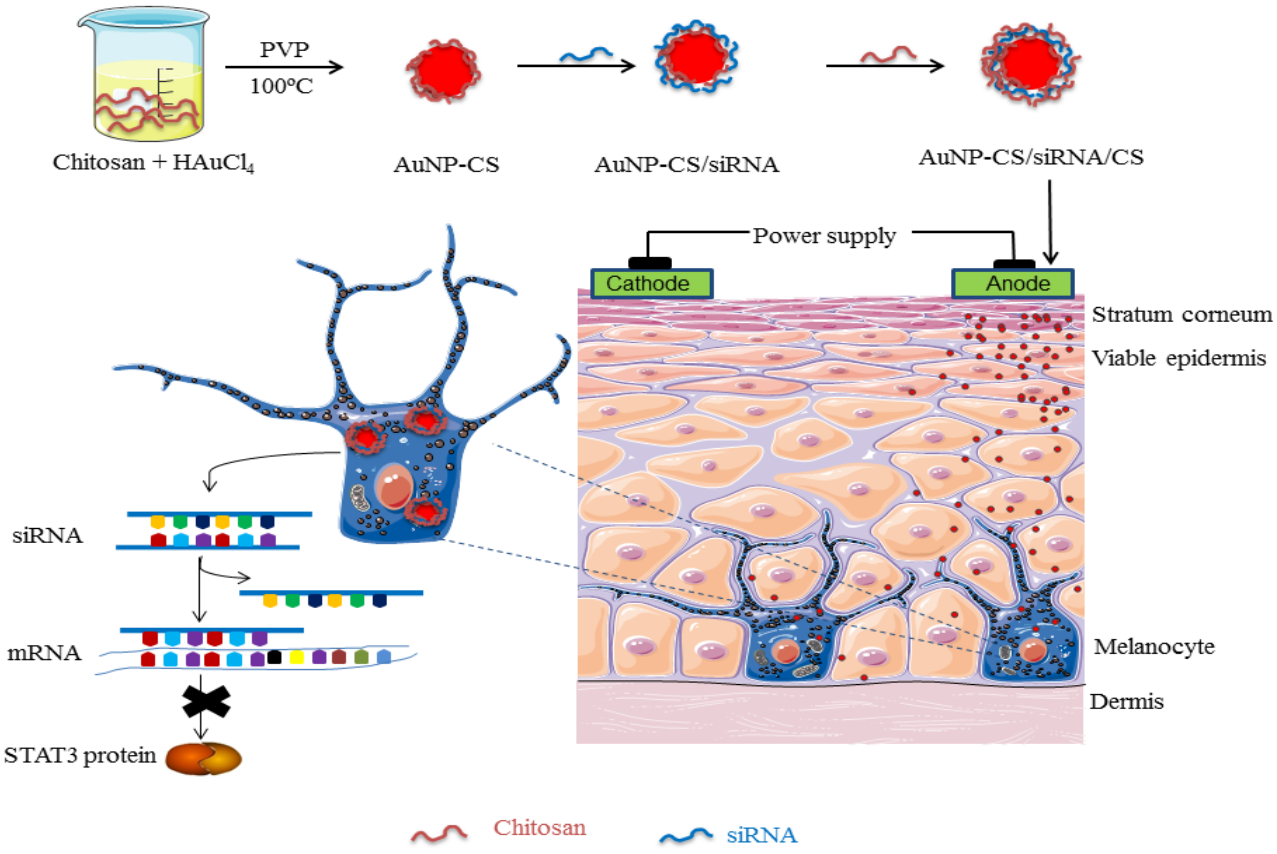

3.1. INTRODUCTION

Melanoma is a malignant skin cancer characterized by the excess proliferation of melanocytes present within the epidermis. A worldwide melanoma incidence in 2012 included 232,000 new cases and 55,000 deaths (Ferlay et al., 2015). The current treatment options available against melanoma include surgical resection of the tumor, followed by chemotherapy. Small molecule chemotherapeutic agents clinically available against melanoma include dacarbazine, cisplatin, and more recently approved ipilimumab and dabrafenib (Maverakis et al., 2015). Furthermore, multiple treatment options including monoclonal antibodies, immunomodulators are being investigated in various clinical trials (Larkin et al., 2015). A serine-threonine protein kinase, BRAF has been one of the key targets that have been investigated to control the melanoma progression (Seremet et al., 2015). Multiple chemotherapeutic agents including the recently approved vemurafenib and dabrafenib targets mutated form of BRAF i.e. BRAFV600E (Seremet et al., 2015; Chapman et al., 2011). However, it has been identified that inhibition of BRAF did not completely regress the tumor and the cancer cells developed resistance towards the BRAF inhibitors (Yadav et al., 2012). Meanwhile, signal transducer and activator of transcription 3 (STAT3) is an intracellular signaling molecule implicated in the survival, proliferation, angiogenesis, metastasis and immune evasion of cancer cells (Kortylewski et al., 2005). STAT3 has been reported to be over expressed in multiple cancer types including melanoma (Kortylewski et al., 2005; Xie et al., 2006). It has been shown that inhibition of STAT3 down regulates genes involved in angiogenesis and metastasis and promotes apoptosis of cancer cells (Alshamsan et al., 2011). However, there have been no small molecule inhibitors of STAT3 protein. To that end, the STAT3 protein suppression using RNA interference holds promise (Alshamsan

et al., 2011). In the present study we used anti-STAT3 small interfering RNA (siRNA) for treatment of melanoma.

siRNA suppresses unwanted protein production by binding to target mRNA in a sequence specific manner and prevents the mRNA translation to protein (Wittrup et al., 2015). However, the clinical application of therapeutic siRNA is limited by its poor deliverability. siRNA is highly prone to degradation by nucleases resulting in short half-life. Furthermore, siRNA show poor penetration across the biological barriers including epithelial, endosomal, and cell membrane barrier (Wang et al., 2010). To overcome the siRNA delivery challenges, non-viral nucleic acid carriers have been developed (Zhang et al., 2007). These include liposomes and polymeric nanoparticles among others. In general, cationic polymers or lipidic systems are complexed to negatively charged siRNA through electrostatic interactions. The overall positive charge and nanoscale particle size of the carrier-siRNA complex helps in translocation across bio membranes to reach intracellular compartments (Davis et al., 2010; Mao et al., 2010).

Recently, metal-based nanoparticles such as gold nanoparticles have shown potential in biomedical applications including imaging, drug delivery and photothermal therapy (Alkilany et al., 2012). This is attributed to their biocompatibility, chemically inert property, nanosize, ability to attach various ligands for targeting and longer plasma circulation (Tan et al., 2005; Bednarski et al., 2015). In the previous chapter, we observed that layer-by-layer gold nanoparticles prepared by alternative adsorption of polyethylenimine and polystyrene sulfonate were found to show greater cytotoxicity in B16F10 murine melanoma cells. The cytotoxicity was attributed to the outer layer of polyethylenimine (Brunot et al., 2007). In this study, we replaced the polyethylenimine with low molecular weight chitosan to reduce the toxicity of blank layer-by-layer gold nanoparticles. Chitosan is a naturally occurring biodegradable polysaccharide obtained through deacetylation of chitin (Younes et al., 2015).

The low molecular weight chitosan has been found to show minimal cytotoxicity compared to high molecular weight chitosan (Kean et al., 2010). Here, we have constructed layer-by-layer gold nanoparticles as carrier for siRNA by sequential adsorption of chitosan and siRNA.

To deliver the STAT3 siRNA against melanoma in a non-invasive fashion, the siRNA loaded gold nanoparticles were topically applied. To improve the skin penetration of gold nanoparticles, a physical penetration enhancement technique, iontophoresis was employed. We hypothesize that iontophoresis would enhance the skin penetration of siRNA entrapped nanoparticles, and cationic nanoparticles themselves would be rapidly taken up by the cancer cells through endocytosis mechanisms. The cell uptake mechanism was studied by inhibiting clathrin and caveolae mediated endocytosis pathways.

3.2. MATERIALS AND METHODS

Tetrachloroaurate trihydrate ($HAuCl_4$ $3H_2O$), sodium alginate (SA, MW: 80 kDa), poly(N-vinyl pyrrolidone) (PVP K-30, MW: 40 kDa), fluorescein isothiocyanate (FITC), Triton X-100, DAPI, phenylmethylsulfonyl fluoride (PMSF), sodium fluoride, sodium deoxycholate, leupeptin, pepstatin, and nitrocellulose membrane were purchased from Sigma Aldrich Chemical Company (Bengaluru, India). Chitosan (CS, MW: 15 kDa, degree of deacetylation: 85%) was purchased from Polysciences, Inc.,USA.

STAT3 siRNA (sense: 5′AAAUGAAGGUGGUGGAGAAUU3′; antisense: 5′UUCU CCACCACCUUCAUUUUU3′) was purchased from Dharmacon Inc., USA. Scrambled sequence siRNA, STAT3 monoclonal antibody, β-actin primary antibody and horseradish peroxidase-conjugated secondary antibodies were purchased from Santa Cruz Biotechnology Inc., USA. Silencer® Cy™3 labeled siRNA was purchased from Life Technologies Inc., USA. Bovine serum albumin (BSA), nonfat milk powder, sodium dodecyl sulfate (SDS), Tris

base, boric acid, ethylenediaminetetraacetic acid dihydrate (EDTA), ethidium bromide, polyacrylamide, agarose, Dulbecco's modified Eagle's medium (DMEM), Dulbecco's phosphate buffered saline, fetal bovine serum (FBS), bromophenol blue, mercaptoethanol and thiazolyl blue tetrazolium bromide (MTT) were purchased from Himedia Laboratories (Mumbai, India). All the chemicals were used without further purification. Milli-Q (Millipore Corporation, USA) water with resistivity of 18.2 $M\Omega.cm^{-1}$ was used for all the experiments.

3.2.1. Preparation of chitosan capped gold nanoparticles (AuNP-CS)

Chitosan capped gold nanoparticles (AuNP-CS) were prepared by direct reduction of $HAuCl_4$ using chitosan. $HAuCl_4$ (0.25 mM) was mixed with chitosan solution and heated at 100 ºC. This reaction mixture was allowed to boil under continuous agitation until the color turns deep red indicating formation of AuNP (Boca et al., 2011). To optimize the $HAuCl_4$ reduction, different concentrations of chitosan (0.1 to 0.5 % w/w) were studied. Later, PVP was added as a stabilizing agent at 60:1 molar ratio (PVP monomer / $HAuCl_4$). For this, aqueous solution of PVP was added drop wise to AuNP-CS solution and the reaction mixture was allowed to stir at 1200 rpm for 24 h. The AuNP-CS particles were further used for adsorption of siRNA.

3.2.2. Layer-by-layer adsorption of siRNA and CS on AuNP-CS

The optimal nitrogen to phosphate (N/P) ratio of AuNP-CS and siRNA for complexation was determined by gel retardation assay. siRNA (1 nM) in HEPES buffer (10 mM) was mixed with AuNP-CS at 5:1 and 10:1 w/w ratio and incubated for 2 h. Later, the sample was centrifuged at 15000 rpm for 30 min to remove unadsorbed siRNA. The supernatant(10 µl) was mixed with 2 µl of 6X loading buffer (10 mM Tris-HCl, 0.03 %

bromophenol blue, 0.03 % xylene cyanol FF, 60 % glycerol, 60 mM EDTA). Electrophoresis was performed using 2 % agarose gel in a horizontal gel electrophoresis unit (Bio-Rad Laboratories, USA) ran at 50 V for 2 h. Then the bands were stained with 0.5 µg/mL ethidium bromide for 10 min and visualized using gel documentation system (Gel Doc XR$^+$ Imaging system, Bio-Rad Laboratories, USA). The gel retardation assay showed that 10:1 (AuNP/siRNA) results in greater complexation. Then the AuNP-CS/siRNA particles were coated with CS. For this, the AuNP-CS/siRNA particles were incubated with chitosan solution (1 mg/mL) for 1 h under continuous stirring at 1200 rpm to form AuNP-CS/siRNA/CS nanoparticles. The encapsulation efficiency (EE) of siRNA was determined by measuring the absorbance of the supernatant collected during deposition and washing steps at 260 nm wavelength using biospectrometer® (Eppendorf , Hamburg, Germany). The EE of siRNA was calculated by using Equation (1)

$$\text{Encapsulation efficiency (\%)} = \frac{Total\ amount\ of\ siRNA - amount\ of\ siRNA\ in\ supernatant}{Total\ amount\ of\ siRNA} \times 100 \quad (1)$$

As control nanoparticle formulations, LbL-AuNP were prepared by replacing STAT3 siRNA with scrambled siRNA or sodium alginate. In-vitro release of siRNA was performed in PBS using LbL-AuNP prepared by cy3 labeled siRNA.

3.2.3. Characterization of the AuNP-CS/siRNA/CS

The particle size and zeta-potential of nanoparticles after sequential adsorption of CS and siRNA were determined using Zetasizer (Nano ZS, Malvern Instruments Inc., UK). For particle size analyses, samples were dispersed in deionized water. For zeta-potential measurement, samples were dispersed in deionized water, and 0.75 mL of sample solution was injected into clear folded capillary cell (DTS1060). Zeta-potential measurement was carried out at 25 ºC using Smoluchowski model in automatic mode.

AuNP-CS shows strong optical absorption and scattering of UV-visible radiation due to the excitation of localized surface plasmon resonance (SPR). The UV-visible absorption spectra of free AuNP-CS and after adsorption of siRNA/SA and CS were recorded using UV-visible spectrophotometer (SpectraMax M4, Molecular Devices Inc., USA).

3.2.4. Effect of STAT3 siRNA on melanocyte cell viability

B16F10 murine melanoma cells were cultured in growth medium containing Dulbecco's modified Eagle's medium (DMEM) supplemented with 10 % fetal bovine serum (FBS) and 1 % penicillin/streptomycin solution. Cells were incubated at 37 ºC and 5 % CO_2. For cell viability study; cells (1 x 10^4) were seeded in 96-well plates 24 h before incubation with formulations. Cell viability was studied at different concentrations of AuNP-CS and AuNP-CS/STAT3 siRNA/CS. Nanoparticles loaded with scrambled siRNA or SA were used as negative control and size control, respectively.

Formulations were prepared in DMEM at siRNA concentration of 0.25 nM and 0.5 nM. Free STAT3 siRNA was used at 0.5 nM concentration. AuNP-CS and AuNP-CS/SA/CS were studied at Au concentration of 338 µM and 675 µM. The cells were incubated with formulations for 8 h at 37 °C. Later, the culture medium was replaced with fresh medium and cells were further incubated for 48 h. Then the cell viability was determined using thiazolyl blue tetrazolium bromide (MTT) assay, where the absorbance of DMSO solubilized formazan crystals was measured at 572 nm wavelength.

3.2.5. Cell uptake studies

Cell uptake studies were performed using size control particles of AuNP-CS/SA/CS in B16F10 cells. To visualize nanoparticles using fluorescence microscope, CS was labeled with FITC. For FITC labeling of chitosan, 10 mol excess of FITC was dissolved in methanol and added drop wise to chitosan solution in 1 % acetic acid. The reaction mixture was incubated for 8 h in dark at room temperature. Later, FITC-labeled chitosan (FITC-CS) was precipitated by adjusting the pH to 10 with 0.5 M NaOH. The unreacted FITC was washed with distilled water and separated by centrifugation until no fluorescence was detected in the supernatant. Later, the FITC-CS dissolved in 10 ml 1 % acetic acid was then dialyzed (pre-wetted regenerated cellulose, molecular weight cut-off of 2 kDa, SpectraPor Inc., CA, USA) to further remove any unconjugated FITC. Complete removal of free FITC was confirmed by thin layer chromatography using 5:4:1 of chloroform: methanol: water as mobile phase. The FITC-CS conjugate was characterized using UV-visible spectroscopy, fluorescence spectroscopy and fourier transform infrared spectroscopy (FTIR).

B16F10 cells (1×10^5) were seeded in 12-well plates and incubated at 37 °C. After 24 h, cells were treated with FITC labeled AuNP-CS/SA/CS for 15, 30, 60 and 120 min. Later, cells were washed with ice cold PBS and fixed using 4 % paraformaldehyde. Cells were permeabilized using 0.1 % Triton X-100 and were incubated with DAPI (1 µg/mL) for 5 min. Fluorescence images were acquired after excitation of FITC and DAPI at 488 and 358 nm wavelength, respectively using 20X objective lens (Olympus IX53, Olympus Corporation, Japan). Image analyses were performed using Image J software (version 1.47 V, National Institutes of Health, USA).

3.2.6. Determination of cell uptake mechanism

Cell uptake of FITC labeled AuNP-CS/SA/CS was evaluated using endocytosis uptake inhibitors including chlorpromazine hydrochloride and methyl-β-cyclodextrin for selective inhibition of clathrin-mediated endocytosis and caveolae-mediated endocytosis, respectively. B16F10 cells (2×10^5) were seeded in a 6-well plate and incubated for 24 h at 37 °C and 5 % CO_2. Cells were pre-treated for 1 h with chlorpromazine hydrochloride or methyl-β-cyclodextrin at 0.028 mM, 5 mM concentration, respectively. Later, cells were washed with PBS and incubated with FITC labeled AuNP-CS/SA/CS for 2 h. Then, cells were washed with PBS and analyzed using fluorescence microscope and flow cytometer. For fluorescence microscopy, cells were stained with DAPI as described above. For flow cytometry, the cells were trypsinized and centrifuged at 1200 rpm for 10 min. The cell pellet was resuspended in PBS and analyzed using flow cytometer (Flow Sight, Amnis, Millipore Inc., Germany).

3.2.7. In-vitro gene silencing

In-vitro gene silencing of STAT3 siRNA delivered using LbL-AuNP was performed by Western blot analysis. B16F10 cells (2×10^5) were seeded in 6-well plate and treated for 8 h with AuNP-CS/STAT3 siRNA/CS, AuNP-CS/scrambled siRNA/CS containing 0.25 or 0.5 nM siRNA. AuNP-CS/SA/CS was used as size control at Au concentration of 338 µM and 675µM. After incubation, the unentrapped formulation was removed and replaced with cell culture medium containing DMEM supplemented with 10 % FBS and further incubated for 48 h at 37 ºC. Later, the cells were harvested and total protein was extracted using lysis buffer (50 mM Tris-HCl, 150 mM NaCl, 0.1 % Triton X-100, 0.5 % sodium deoxy cholate, 1 mM sodium orthovanadate, 1 mM sodium floride, 1 µg/mL pepstatin and 1 µg/mL leupeptin). The total protein was estimated by Bradford's assay using BSA as reference

standard. BSA and protein samples (5 µl) were mixed with 250 µl of the Bradford reagent and incubated at room temperature for 30 min. Then, the absorbance of protein-dye complex was measured at 595 nm wavelength. The protein concentration was determined using BSA standard calibration curve (0.1-1.4 mg/mL) with correlation coefficient of 0.99.

Total protein (40 µg) was separated using sodium dodecyl sulfate-poly acrylamide gel electrophoresis (SDS-PAGE) (Hoefer Inc., USA) containing 5 % stacking gel and 10 % resolving gel and electrophoresed at 50 V for 2 h. Later, proteins were transferred to nitrocellulose membrane after application of 100 V for 1 h. STAT3 protein was probed by incubating the nitrocellulose membrane in STAT3 primary antibody (dilution range is 1:100) at 4 ºC. Later, the membrane was incubated with HRP-conjugated secondary antibody for 2 h. The protein bands were visualized after incubation in enhanced chemiluminiscent substrate solution (ECL reagent, Super signal Pro, Thermo scientific, USA). The membrane was exposed to X-ray film for 2 min and then sequentially incubated in developer solution, stopper solution (1 % acetic acid) and fixer solution (Sigma Aldrich, USA) for 1 min and finally washed with water. Band densities were determined using Image J software (version 1.47 V, National Institutes of Health, USA).

3.2.8. Apoptosis Assay

Induction of apoptosis by siRNA loaded AuNP was studied using FITC-Annexin V/PI apoptosis assay (Molecular Probes, Inc, USA). B16F10 cells (2×10^5) were seeded in 6-well plates and treated for 8h with AuNP-CS/STAT3 siRNA/CS, AuNP-CS/scrambled siRNA/CS at 0.25 and 0.5 nM siRNA concentration. AuNP-CS/SA/CS was used as size control at Au concentration of 338 µM and 675 µM.

For flow cytometric analysis, the cells were harvested using trypsin and suspended in ice cold PBS. The cell count was determined by trypan blue exclusion assay. The cells were centrifuged at 1200 rpm for 5 min and cell pellet was resuspended in 1X annexin binding buffer (5 mM HEPES, 140 mM NaCl, 2.5 mM $CaCl_2$, pH 7.4). FITC-Annexin V (5 µl) and 1µl of 100 µg/mL propidium iodide solutions were added to each of 100 µl cell suspension and incubated for 15 min at room temperature. After the incubation period, 400 µl of 1X annexin binding buffer was added. The fluorescence intensity of FITC and PI were measured at 530 nm and 575 nm emission wavelength, respectively. The cell population (%) was separated into four groups; live cells (no fluorescence, Annexin V -/ PI -); early apoptotic cells (green fluorescence, Annexin V +/ PI -); late apoptotic cells (both green and red fluorescence, Annexin V +/ PI +) and dead cells (red fluorescence, Annexin V -/ PI +).

3.2.9. Skin penetration of siRNA

Skin penetration of Cy3 labeled siRNA was performed using excised porcine ear skin. Porcine ears were procured immediately after kill from local abattoir. Ears were cleaned under tap water and hair on the dorsal side was removed using a hair clipper (HC70, Remington Inc., Germany). Then the full thickness skin was carefully excised using scalpel and forceps. Later, the underlying fat tissue was scrapped off using a blunt scalpel. The skin thickness was measured using digital micrometer (Baker gauges India Pvt. Ltd. Mumbai, India). The skin resistance (R) was measured by applying current (I, 1 mA) across the skin using DC power supply unit (V-care Meditech Pvt. Ltd., Bangalore, India) and voltage drop (V) was determined using digital multimeter (17B, Fluke Corporation, USA). The resistance (R) was calculated using Ohm's law (V=IR). Skin sample was mounted between receptor and donor compartments of a Franz diffusion cell (Permegear Inc., USA) with stratum corneum (SC) facing the donor compartment. The effective diffusional area was 0.637 cm^2 and the

volume of receptor compartment was 5 mL. PBS (pH 7.4) was used as receptor medium and maintained at 37±0.5ºC.

Cy3 labeled siRNA and FITC labeled CS were used to construct AuNP-CS/siRNA/CS. Donor compartment was charged with AuNP-CS/siRNA/CS dispersed in 0.2 mL of PBS (pH 7.4). For anodal iontophoresis application, a current density of 0.47 mA/cm^2 was applied for 4 h using silver electrode placed in the donor and silver chloride electrode placed in the receptor compartment. A salt bridge (1 % agarose containing 2 mM NaCl) was used to avoid direct contact of silver wire with formulation. After 4 h passive or iontophoretic treatment of the skin, the samples were washed with PBS thrice and frozen after embedding in optimum cutting temperature (OCT) medium for cryo sectioning. Skin samples were cryo sectioned at a thickness of 10 µm using a cryotome (Leica CM 1520, Leica biosciences, Germany). The skin samples were then mounted on a glass slide. Fluorescence images were acquired after excitation of FITC and Cy3 using 488 nm and 547 nm laser under 10X objective lens. Bright field images were acquired after staining with hematoxylin.

Confocal laser scanning microscope (Leica TCS SP8, Leica Microsystems CMS, Germany) was also used to study the skin penetration of LbL-AuNP. After passive or iontophoretic treatment with FITC labeled LbL-AuNP, skin was washed to remove adsorbed nanoparticles and mounted on a microscope glass slide. FITC was excited using Argon laser at an excitation wavelength of 488 nm. The images were acquired using 40X/0.30 oil (HCPL APO CS2) objective lens. To analyze the skin distribution and depth of penetration of LbL-AuNP, skin was optically sectioned from 0-100 µm depth at a step size of 1 µm/scan. The gain and offset were kept constant for all the images acquired. Mean fluorescence intensity of images was analyzed using Leica LAS X software.

3.2.10. Statistical Analysis

All the results were presented as mean ± standard deviation. The results were compared by performing analysis of variance (Version 6, Graph Pad Prism, USA), and the results were considered to be significant at $p<0.05$.

3.3. RESULTS

3.3.1. Characterization of the layer-by-layer AuNP

The optimal chitosan concentration required for reduction of $HAuCl_4$ was found to be 0.2 %. The average particle size of AuNP-CS was found to be 68.1±6.6 nm (PDI: 0.29±0.05), 62.5±3.4 nm (PDI: 0.27±0.04) and 158.6±14.9 nm (PDI: 0.55±0.02) after reduction of $HAuCl_4$ using 0.1, 0.2 and 0.5 % of chitosan, respectively. Fig. 3.1a shows the particle size distribution of AuNP-CS at 0.2 % chitosan concentration. The zeta-potential of AuNP-CS was found to be 54.3±2.5, 52.1±1.7 and 47.9±2.4 mV at chitosan concentration of 0.1, 0.2 and 0.5 %, respectively. The surface plasmon resonance (SPR) wavelength of AuNP-CS was found to be 520 nm and the wavelength did not change with different chitosan concentrations (Fig. 3.1c). The weight ratio of AuNP-CS to siRNA (10:1) was optimized based on agarose gel retardation assay and found that 10:1 (siRNA/AuNP-CS) is required for complete complexation (Fig. 3.1d). Fig. 3.1a shows that the particle size increased from 62.5±3.4 nm (PDI: 0.27±0.04) to 83.1±7.4 nm (PDI: 0.27±0.08) and 150.4±10.1 nm (PDI: 0.41±0.06) after LbL adsorption of STAT3 siRNA and CS, respectively. The zeta-potential was found to be (-) 32.7±3.1 mV and +35.1±5.8 mV after adsorption of STAT3 siRNA and CS, respectively (Fig. 3.1b). LbL adsorption of STAT3 siRNA and CS onto CS-AuNP showed bathochromic shifts in SPR wavelength at 524 nm and 530 nm, respectively (Fig. 3.1c).

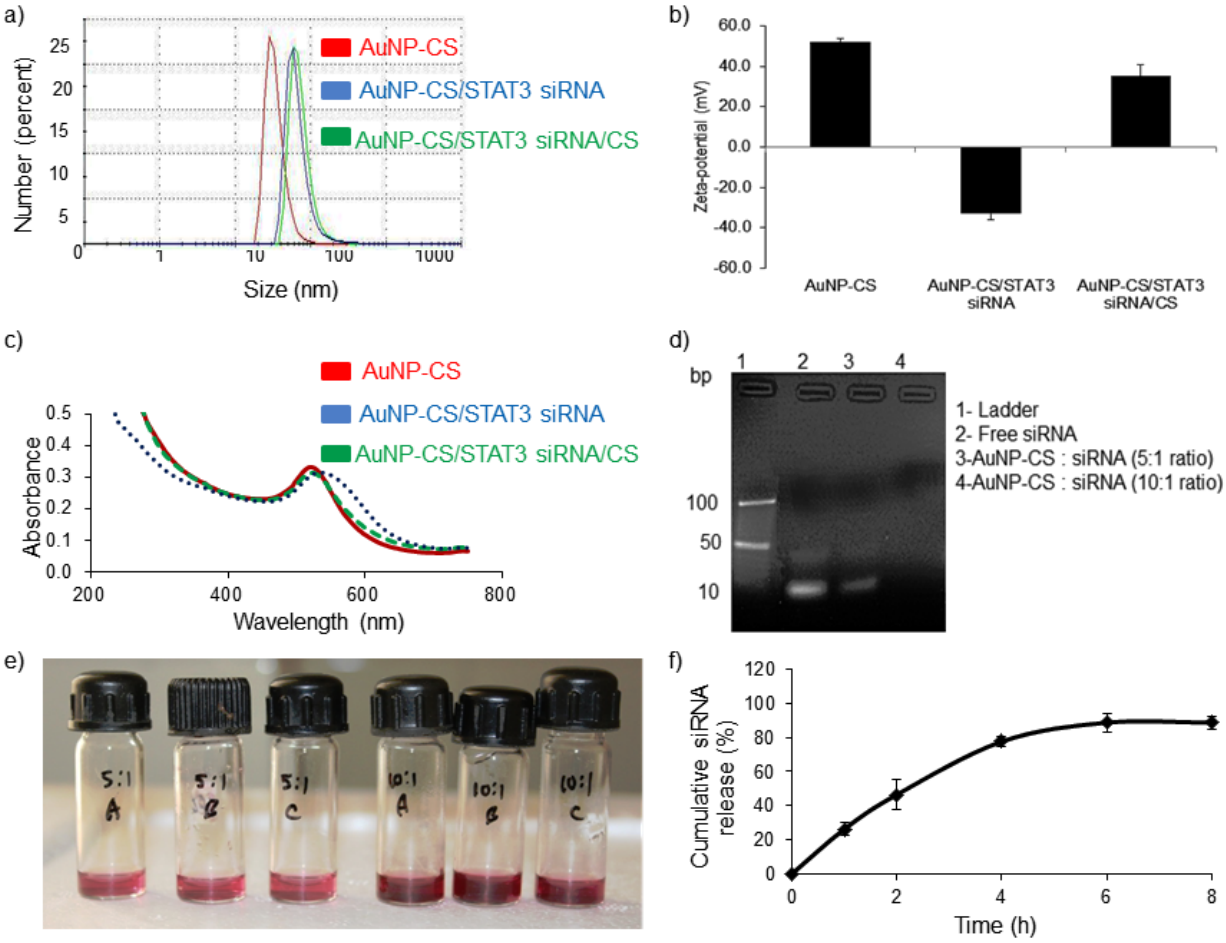

Fig. 3.1. Characterization of chitosan functionalized gold nanoparticles. **a**, Representative number weighted particle size distribution after sequential adsorption of siRNA and chitosan on AuNP-CS; **b**, zeta-potential measured after sequential adsorption of siRNA and chitosan on AuNP-CS; **c**, surface plasmon resonance upon sequential adsorption of chitosan, siRNA and chitosan up on AuNP; **d**, optimization of the CS-AuNP and siRNA complex weight ratio (w/w) using agarose gel retardation assay; **e**, digital photograph of LbL-AuNP-CS/siRNA/CS prepared at 5:1 and 10:1 (N/P) ratios; **f**, cumulative percentage of siRNA released from LbL-AuNP with time. Data in **b** and **f** was presented as mean (n = 3) ± standard deviation.

Table 3.1 shows the average particle size, zeta-potential and SPR after sequential adsorption of CS and siRNA. There was no significant difference in the particle size, zeta-potential and SPR wavelength among the nanoparticles prepared using STAT3 siRNA or scrambled siRNA (Table 3.1). On the other hand, when siRNA is replaced with SA, the particle size increased to 162.6±3.6 nm (PDI: 0.28±0.02) and further adsorption of CS, the particle size increased to 172.7±8.8 nm (PDI: 0.35±0.03). Similarly, the zeta-potential was found to be (-)76.6±3.3 mV and +41.1±1.1 mV after adsorption SA and CS on AuNP-CS. Fig. 3.1e shows the digital photograph of AuNP-CS/siRNA/CS prepared at 5:1 and 10:1 (N/P) ratio. UV-spectrometer analysis showed that the encapsulation efficiency of siRNA was 21.6±5.7 % and 58.3±7.5 % at AuNP-CS to siRNA ratio of 5:1 and 10:1, respectively. This translates to approximately 3×10^3 and 8×10^3 molecules of siRNA adsorbed to one AuNP-CS nanoparticle at 5:1 and 10:1 w/w ratio, respectively. In-vitro release studies showed that siRNA release from LbL-AuNP was controlled up to 6 h in PBS (Fig. 3.1f).

Table 3.2 shows the stability of AuNP-CS after incubation in PBS and cell culture medium at different time points. The particle size of AuNP-CS increased from 62.5±3.4 nm (PDI: 0.27±0.04 to 162.0±4.8 nm (PDI: 0.20±0.02) and 228.8±11.8 nm (PDI: 0.23±0.02) after incubation in PBS and DMEM for 48 h, respectively. The zeta-potential was neutralized and non-significant increase in SPR wavelength was observed.

Table 3.3 shows the stability of AuNP-CS/siRNA/CS incubated in PBS or DMEM up to 72 h. The AuNP-CS/siRNA/CS particles were stable without significant change in particle size, zeta-potential and SPR wavelength for up to 48 h. Further incubation up to 72 h increased the particle size to 203.6±16.3 nm (PDI: 0.38±0.01), decreased the zeta-potential to -2.9±1.0 mV.

Table 3.1. Particle size, zeta-potential and surface plasmon resonance (SPR) wavelength of siRNA loaded LbL-AuNP.

Nanoparticle	Particle size (nm)*	Zeta-potential (mV)	SPR (nm)
STAT3 siRNA			
AuNP-CS	62.5±3.4 (0.27±0.04)	52.1±1.7	520
AuNP-CS/STAT3 siRNA	83.1±7.4 (0.27±0.08)	-32.7±3.1	524
AuNP-CS/STAT3 siRNA/CS	150.4±10.1 (0.41±0.06)	35.1±5.8	530
Scrambled siRNA			
AuNP-CS	62.5±3.4 (0.27±0.04)	52.1±1.7	520
AuNP-CS/Scrambled siRNA	79.7±8.5 (0.35±.0.12)	-28.5±0.6	524
AuNP-CS/Scrambled siRNA/CS	157.3±19.1 (0.28±0.04)	31.9±0.5	530
Sodium alginate (SA)			
AuNP-CS	62.5±3.4 (0.27±0.04)	52.1±1.7	520
AuNP-CS/SA	162.6±3.6 (0.28±.0.02)	-76.6±3.3	526
AuNP-CS/SA/CS	172.7±8.8 (0.35±0.03)	41.1±1.1	532

Data were presented as mean ± standard deviation (n=3). * Values in parentheses represent polydispersity index (PDI) ± standard deviation.

Table 3.2. Stability of AuNP-CS in the presence of phosphate buffered saline and DMEM medium containing 2 % FBS.

Incubation time	Size (nm)*	Zeta-potential (mV)	SPR (nm)
PBS			
0	62.5±3.4 (0.27±0.04)	52.1±1.7	520
6h	131.0±11.6 (0.20±0.004)	6.06±0.7	522
24h	135.1±12.5 (0.15±0.01)	4.97±2.1	524
48h	162.0±4.8 (0.20±0.02)	2.46±0.8	524
DMEM medium with 2% FBS			
0	62.5±3.4 (0.27±0.04)	52.1±1.7	NA#
6h	97.89±14.8 (0.75±0.01)	-8.7±1.4	NA
24h	131.24±4.8 (0.24±0.02)	-9.18±2.1	NA
48h	228.8±11.8 (0.23±0.02)	-3.7±0.8	NA

Data were presented as mean ± standard deviation (n=3). * Values in parentheses represent polydispersity index (PDI) ± standard deviation. # Not applicable.

Table 3.3. Stability of AuNP-CS/siRNA/CS in the presence of phosphate buffered saline (PBS) and DMEM medium containing 2% FBS.

Time (h)	Particle size (nm)*	Zeta-potential (mV)	SPR (nm)
PBS			
0	157.3±19.1 (0.28±0.00)	31.9±0.5	530
12	161.9±5.9 (0.39±0.15)	0.8±1.1	530
24	171.9±23.8 (0.26±0.07)	-0.4±0.3	532
48	154.3±21.9 (0.32±0.19)	-2.8±1.1	532
72	203.6±16.3 (0.38±0.01)	-2.9±1.0	534
DMEM with 2% FBS			
0	157.3±19.1 (0.28±0.00)	31.9±0.5	530
12	131.4±26.8 (0.29±0.07)	0.41±0.17	NA#
24	184.8±19.9 (0.31±0.03)	0.25±0.05	NA
48	151.3±27.8 (0.40±0.14)	0.32±0.06	NA
72	205.9±15.3 (0.27±0.02)	-8.09±1.70	NA

Data were presented as mean ± standard deviation (n=3). * Values in parentheses represent polydispersity index (PDI) ± standard deviation. # Not applicable.

3.3.2. Effect of STAT3 siRNA on cell viability

Fig. 3.2a shows the B16F10 cell growth inhibition after treatment with free and AuNP loaded siRNA. The free siRNA at 0.5 nM did not show significant growth inhibition (2.1±0.1 %). The AuNP-CS/STAT3siRNA/CS treatment resulted in 49.4±0.6 % and 66.2±0.2 % growth inhibition at 0.25 nM and 0.5 nM STAT3 siRNA concentration, respectively. The control treatment of AuNP-CS/scrambled siRNA/CS showed an inhibition of 33.0±0.4 % and 46.0±0.1 % at 0.25 nM and 0.5 nM concentration, respectively. The size control particles of AuNP-CS/SA/CS showed growth inhibition of 29.9±0.9 % and 37.2±0.4 % at 338 µM and

675 µM of Au concentration, respectively. Blank AuNP-CS showed growth inhibition of 27.8±0.2 and 39.3±0.6 % at 338 µM and 675 µM of Au, respectively (Fig. 3.2b).

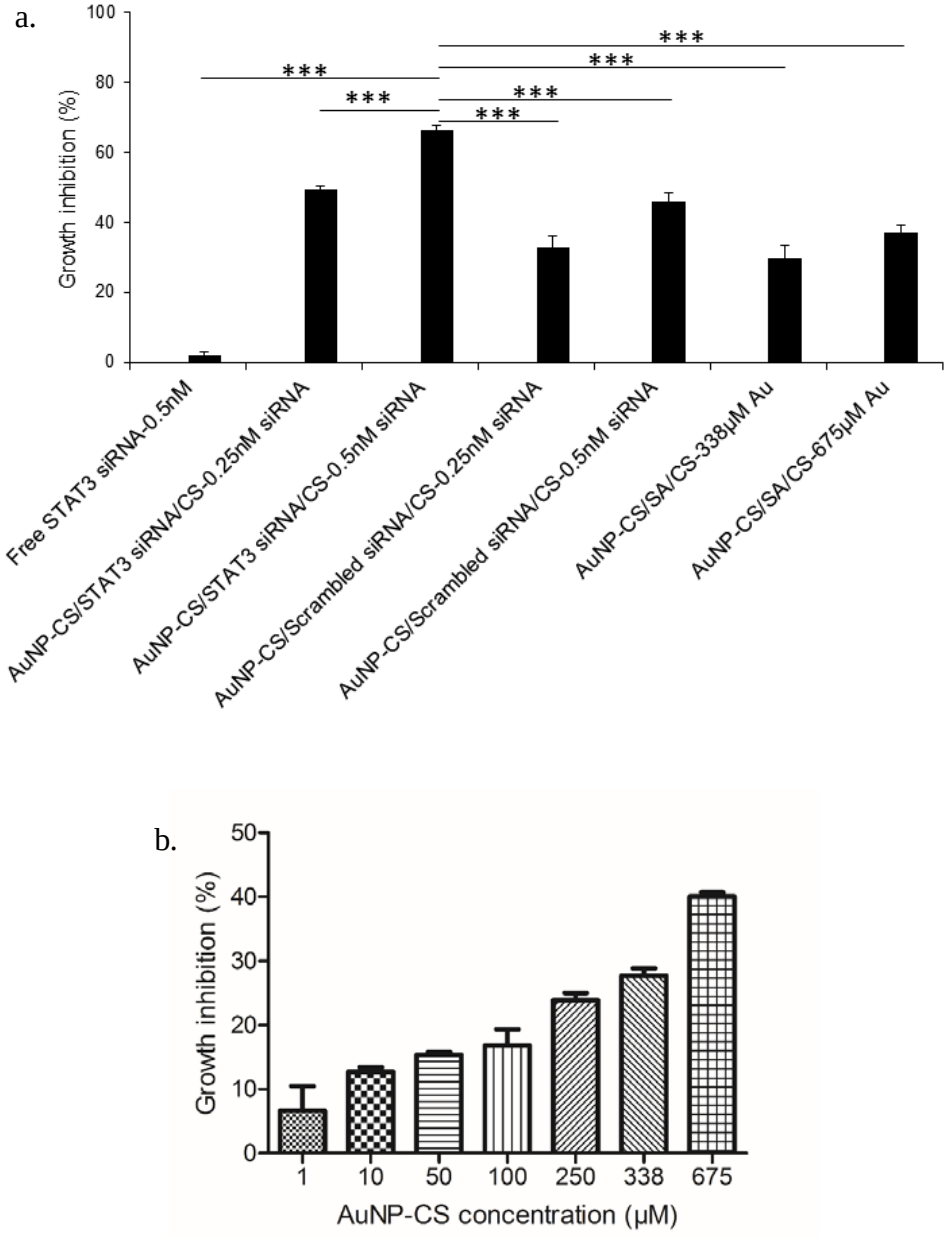

Fig 3.2. a, Inhibition of B16F10 cancer cell growth after treatment with different concentration of free siRNA and siRNA loaded AuNP. Data represents mean ± standard deviation (n =3); **b**, Inhibition of B16F10 cancer cell growth after treatment with free AuNP-CS at Au concentration from 1-675 µM. Data represented as mean ± standard deviation (n=6).

3.3.3. Cell uptake studies

Cell uptake studies were performed using FITC labeled AuNP-CS/SA/CS.FITC labeling of chitosan was confirmed by thin layer chromatography. FITC conjugation of chitosan resulted in shift in absorption maxima of FITC from 491 nm to 495 nm wavelength. Spectro fluorimetry showed peak emission wavelength at 519 nm and 522 nm for free FITC and FITC-chitosan, respectively. Fig 3.3 shows FTIR spectra of free FITC and FITC-chitosan conjugate. Free FITC showed absorbance peak at 2039 cm^{-1} wavenumber characteristic of isothiocyanate (N=C=S). On the other hand, FITC-chitosan conjugate showed characteristic absorbance peak at 1109 cm^{-1} wavenumber corresponding to the thiourea (N-CS-N) bond between isothiocyanate group of FITC and amine group of chitosan. UV-visible spectroscopic analysis showed 0.28 moles of FITC conjugated to one mole of chitosan.

Fig. 3.4a shows the fluorescence images of B16F10 cells after incubation with FITC labeled AuNP-CS/SA/CS for 15, 30, 60 and 120 min. After 15 min of incubation, LbL-AuNP were taken up in B16F10 cells. Background corrected fluorescence image analysis showed gradual increase in cell associated fluorescence with the increase in incubation time from 15 min to 120 min (Fig. 3.4b). After 60 min incubation, FITC labeled LbL-AuNP were completely localized in B16F10 cells as observed from merged images.

Flow cytometric analysis showed increase in fluorescence intensity of B16F10 cells after incubation with FITC labeled LbL-AuNP (Fig. 3.4c). The geometrical mean fluorescence intensity significantly ($p<0.05$) increased with the increase in incubation time from 15 min to 120 min (Fig. 3.4d).

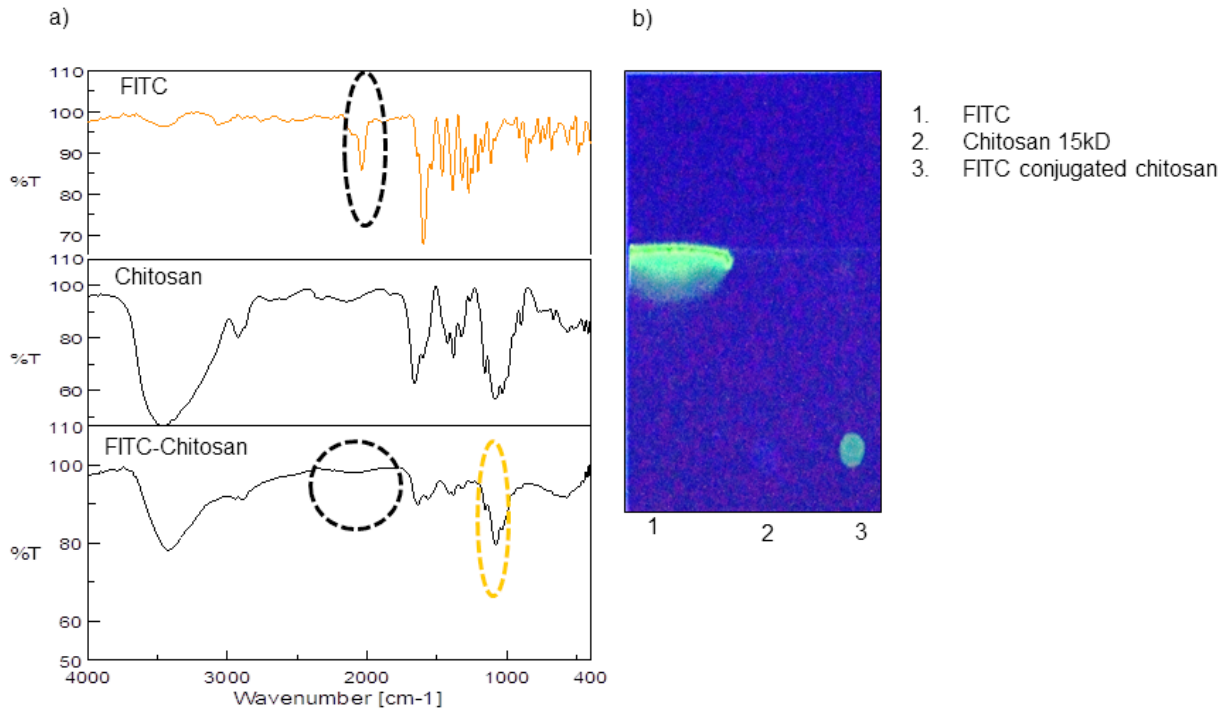

Fig 3.3. Characterization of FITC-Chitosan conjugate **a**, FTIR spectra of free FITC, chitosan and FITC-Chitosan conjugate; **b**, representative photograph of thin layer chromatographic plate showing free FITC (lane 1), free chitosan (lane 2) and FITC-Chitosan conjugate (lane 3). Images were representative of at least three experiments.

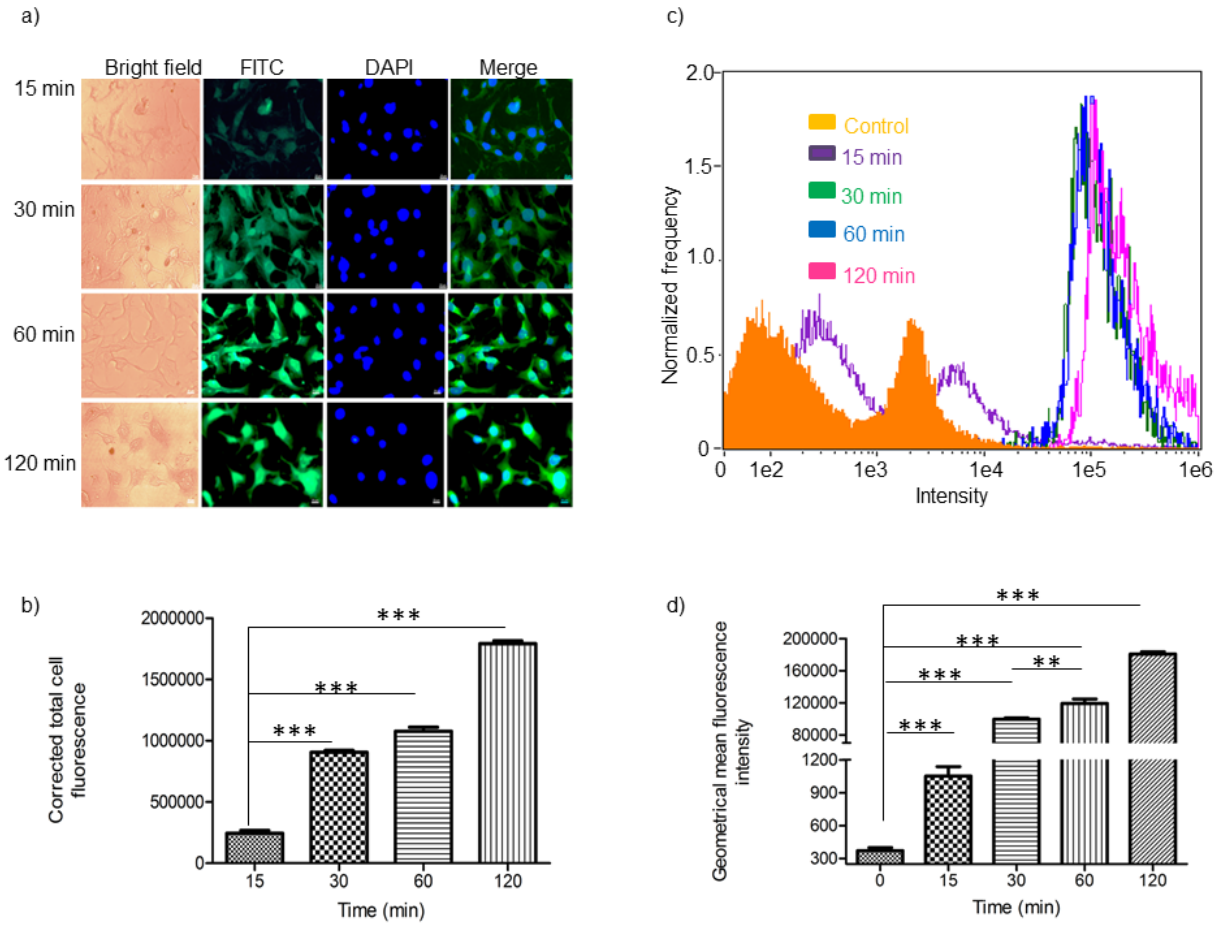

Fig 3.4. **a**, Cell uptake of FITC labeled AuNP-CS/SA/CS in B16F10 cancer cells after incubation for 15, 30, 60 and 120 min. Micrographs were presented in bright field, FITC filter, DAPI filter, merge of FITC and DAPI filter images. Images were representative of at least three experiments. **b**, Corrected total cell fluorescence calculated through image analysis using Image J software. **c**, FACS analysis of time dependent B16F10 cell uptake of AuNP-CS/SA/CS. **d**, The geometric mean of fluorescence obtained using Ideas software. Geometric means of the fluorescence obtained from three separate experiments were plotted. Data represents mean ± standard deviation (n=3). Scale bar represents 20 µm.

3.3.4. Cell uptake mechanism

To understand the LbL-AuNP cell uptake mechanism, specific endocytosis inhibitors for clathrin and caveolae mediated pathways were utilized. There was a reduced uptake of FITC labeled LbL-AuNP after pre-treatment with chlorpromazine than after treatment with methyl-β-cyclodextrin compared with control cells (without inhibitor pretreatment) (Fig. 3.5a). The background corrected fluorescence image analysis showed a significant ($p<0.0.5$) decrease in cell associated fluorescence compared to control cells (Fig. 3.5b). It was observed that the morphology of B16F10 cells slightly altered after pretreatment with inhibitors. Similarly, flow cytometry showed 43% and 2% reduction in fluorescence intensity of B16F10 cells after pretreatment with chlorpromazine and methyl-β-cyclodextrin, respectively (Fig. 3.5c &3.5d).

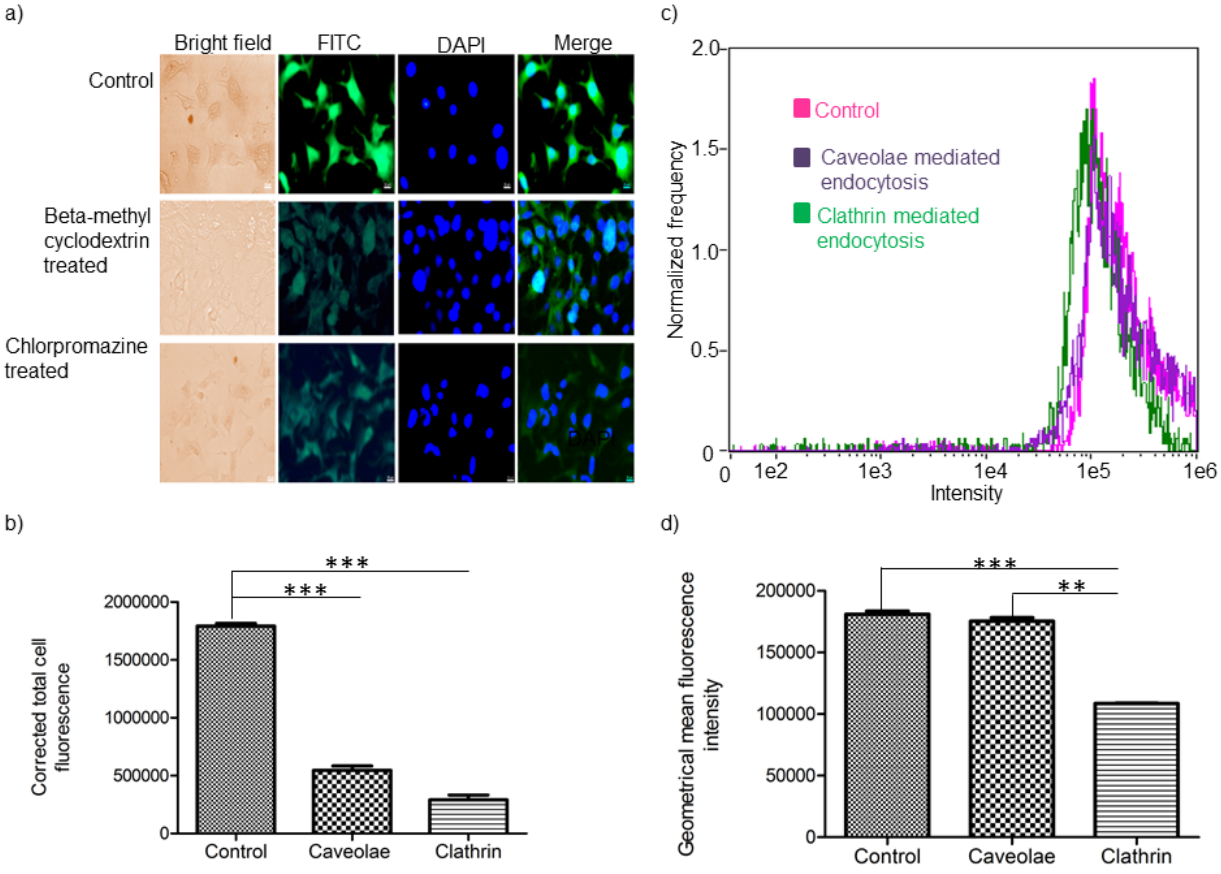

Fig. 3.5. a, B16F10 cell uptake of AuNP after treatment with endocytosis inhibitors. Images were representative of at least three experiments. **b**, Corrected total cell fluorescence calculated through image analysis using Image J software. **c**, FACS analysis of time dependent B16F10 cell uptake of AuNP-CS/SA/CS. **d**, The geometric mean of fluorescence obtained using Ideas software. Geometric means of the fluorescence obtained from three separate experiments were plotted. Data represents mean ± standard deviation (n =3). Scale bar represents 20 µm.

3.3.5. In-vitro gene silencing

Results from Western blot analysis showed that the STAT3 expression decreased by 44.7 % and 47.3 % after treatment with AuNP-CS/STAT3 siRNA/CS containing 0.25 nM and 0.5 nM siRNA, respectively (Fig. 3.6). There was no suppression of STAT3 protein after treatment with 0.25 nM and 0.5 nM of AuNP-CS/scrambled siRNA/CS. Similarly, there was no inhibition of STAT3 protein after treatment with AuNP-CS/SA/CS containing Au concentration of 338 μM and 675 μM.

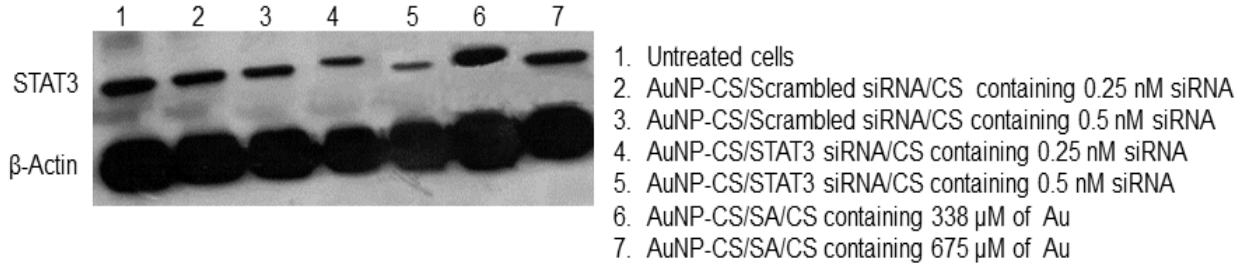

Fig. 3.6. Expression of STAT3 protein in B16F10 cells after treatment with STAT3 siRNA. β-actin was used as loading control.

3.3.6. Apoptosis Assay

Fig. 3.7 shows representative images of apoptotic cells captured using imaging flow cytometer. Fig. 3.8 shows percentage of cells at different stages of cell death after treatment with free and AuNP loaded siRNA. The gated cell population (10000 cells) was divided into four quadrants as live cells, early apoptotic cells, late apoptotic cells and dead cells. It is observed that there was a significant difference in the percentage of early and late apoptotic events after treatment with formulations containing STAT3 siRNA and scrambled siRNA compared to untreated cells.

It is observed that 41.90±2.12 % and 43.95±0.21 % of annexin V+/ PI+ cells indicating late apoptosis was observed after treatment with AuNP-CS/STAT3 siRNA/CS containing 0.25 nM and 0.5 nM of STAT3 siRNA. Whereas treatment with 0.25 nM and 0.5 nM of AuNP-CS/scrambled siRNA/CS showed 1.87±0.06 and 2.87±0.08 %, respectively. Free siRNA at 0.5 nM did not show any apoptotic events. The percentage of Annexin V+/PI+ cells after treatment with AuNP-CS/SA/CS containing 338 μM and 675 μM of Au were 6.65±0.71 % and 13.25±0.21 %, respectively.

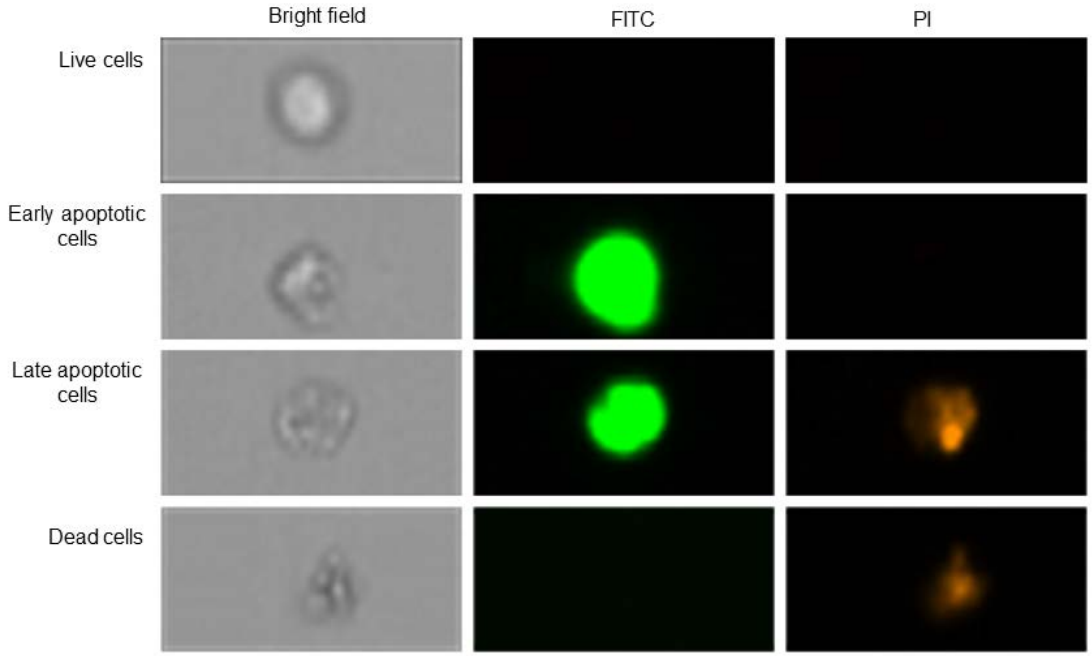

Fig. 3.7. B16F10 cells stained with FITC-Annexin V and propidium iodide (PI) captured using Amnis® Imaging flow cytometer (EMD Millipore, USA).

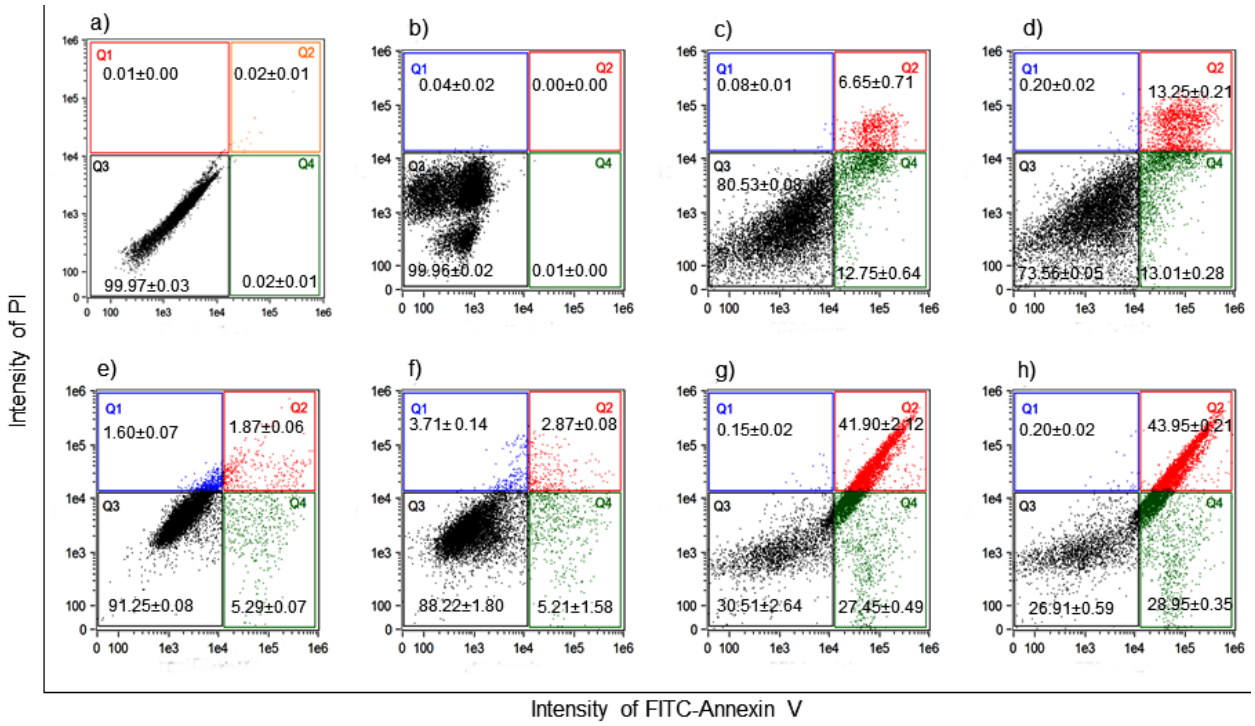

Fig. 3.8. Apoptosis events observed in B16F10 cells after treatment with formulations. a, untreated cells; b, free STAT3 siRNA; c & d, AuNP-CS/SA/CS containing 338 µM and 675 µM of AuNP; e & f, AuNP-CS/Scrambled-siRNA/CS at 0.25 nM and 0.5 nM; g & h, AuNP-CS/STAT3-siRNA/CS at 0.25 nM and 0.5 nM, respectively. Dot plots are representative of three independent experiments.

3.3.7. Skin permeation of LbL-AuNP

Skin permeation of AuNP-CS/siRNA/CS was studied on excised porcine ear skin having thickness of 0.96±0.5 mm and electrical resistance of 4.34±0.15 kΩ. After 4 h passive and iontophoresis application of LbL-AuNP, skin resistance decreased to 3.29±0.21 kΩ and 2.03±0.5 kΩ, respectively. The stability of AuNP-CS/siRNA/CS in PBS was determined for the experimental duration of 4h by dynamic light scattering and zeta-potential measurements. The particle size increased to 157.5±14.1 (PDI: 0.44±0.08) and 229.1±6.4 (PDI: 0.36±0.04) from 151.8±4.9 nm (PDI; 0.43±0.01) after passive and anodal iontophoresis application, respectively. Whereas, zeta-potential decreased to 28.1±1.2 mV and 24.7±0.3 mV from

48.1±1.4 mV after passive and anodal iontophoresis application. Fig. 3.9 shows the skin penetration of AuNP-CS/siRNA/CS after passive and iontophoresis application. Passive application of AuNP-CS/siRNA/CS did not penetrate the skin and nanoparticles were retained within the stratum corneum. It is evident that AuNP-CS/siRNA/CS were able to penetrate the stratum corneum (SC) and viable epidermis (VE) after anodal iontophoresis (Fig. 3.9). Iontophoretic application promoted the skin penetration of AuNP-CS/siRNA/CS mainly through intercellular and follicular pathways (Fig. 3.10).

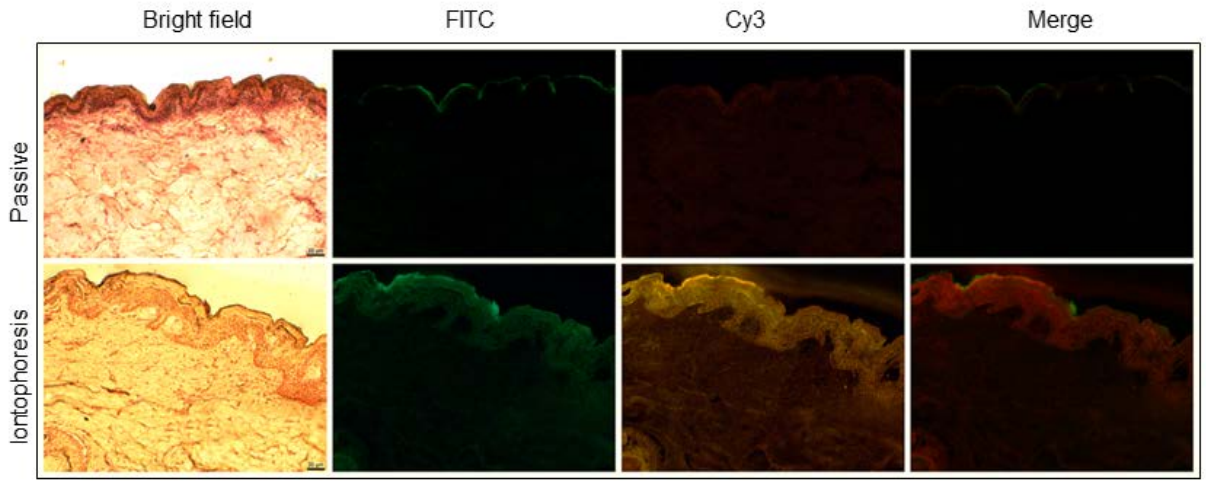

Fig. 3.9. Skin permeation of AuNP-CS/siRNA/CS after passive and anodal iontophoresis application. Cy3 labeled siRNA and FITC labeled CS were used to construct AuNP-CS/siRNA/CS. Micrographs were presented in bright field after hematoxylin staining, FITC filter, Cy3 filter, and merge of FITC and Cy3 filter images. All the images were representative of at least three experiments. Scale bar represents 20 µm.

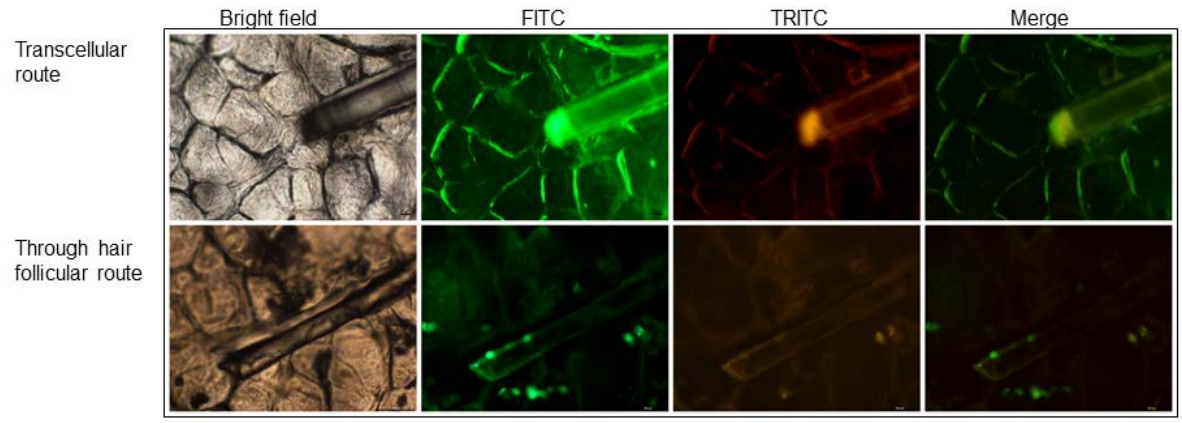

Fig. 3.10. Skin permeation studies of FITC labeled AuNP-CS/Cy 3 siRNA/CS using anodal iontophoresis showing penetration of FITC labeled AuNP-CS/Cy 3 siRNA/CS through transcellular and appendageal route (mainly hair follicular route). Micrographs were presented in bright field after hematoxylin, FITC filter, DAPI filter, merge of FITC and TRITC filter images. Images were representative of at least three experiments.

Similarly, Fig. 3.11 shows the confocal images of skin after passive and iontophoresis application of LbL-AuNP. It is observed that iontophoresis improved penetration of LbL-AuNP up to 70 µm compared to 30 µm after passive application. Fig. 3.12 shows greater average fluorescence intensity within skin after iontophoresis application compared with passive delivery.

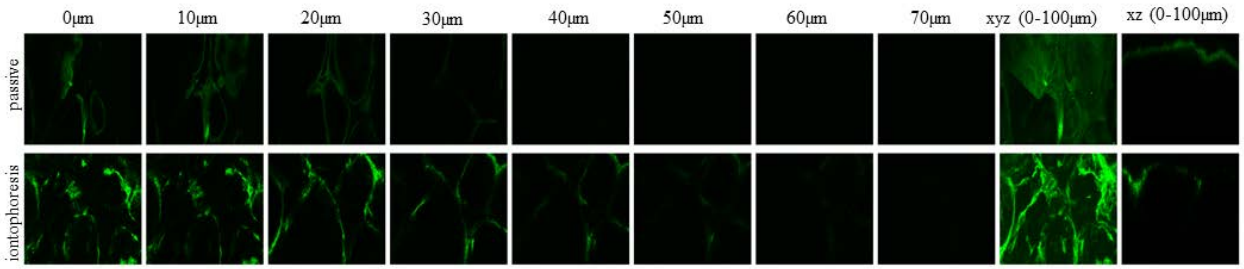

Fig. 3.11. Confocal microscopic images of skin samples after treatment with AuNP-CS/siRNA/CS for 2 h. Images were shown from surface to 100 µm depth inside skin in XYZ and XZ sections. All the images were representative of at least three experiments.

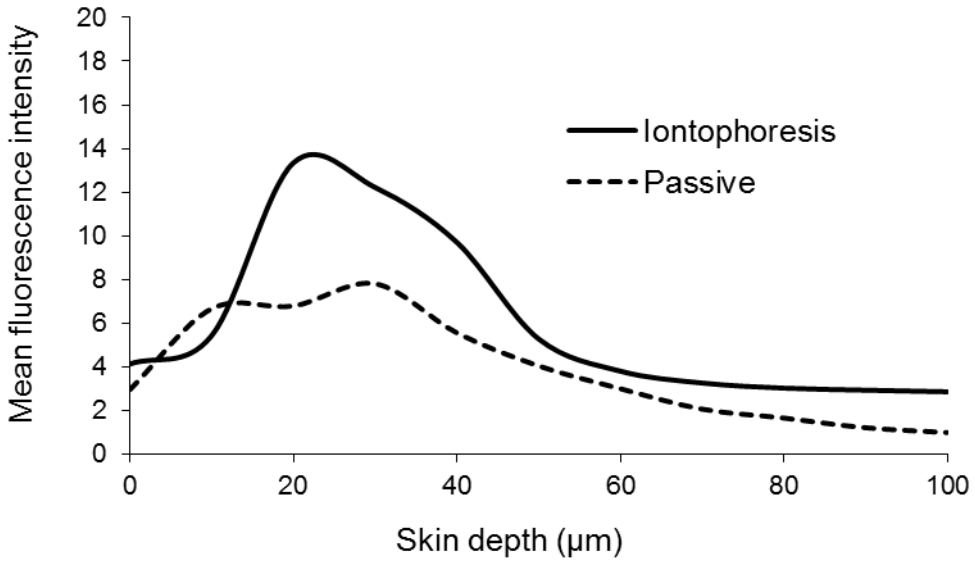

Fig. 3.12. Mean fluorescence intensity of images acquired from surface to 100 μm inside skin using confocal laser scanning microscope.

3.4. DISCUSSION

Localized delivery is expected to provide greater concentration of chemotherapeutic agents at the tumor site and avoid unwanted adverse effects (Byrne et al., 2015). Non-invasive topical delivery of anti-cancer agents show potential in treating easily accessible skin malignancies including melanoma (Venuganti et al., 2015; Kigasawa et al., 2010). However, skin is a formidable barrier which limits the transport of active molecules. Especially, macromolecules such as siRNA with high molecular weight (13 kDa) and greater negative charge density show poor skin penetration (Aldawsari et al., 2015). Furthermore, naked siRNA is prone to rapid degradation in biological systems. Therefore, to improve the stability and cell uptake, siRNA was entrapped in LbL-AuNP; and iontophoresis was employed to promote the skin penetration.

Confocal laser scanning microscope has been utilized to optically section the skin and determine the depth of penetration of fluorescent dye tagged LbL-AuNP. Similar to the earlier reports, the depth of skin penetration of nanoparticles was found to be between 50-100

µm in the presence of iontophoresis (Venuganti et al., 2015). In other words, LbL-AuNP reached the target site of viable epidermis where melanocytes are located. The optical sectioning using confocal microscope is supported by the depth of penetration shown in skin cryosections. It was observed from the images that the primary mechanism of skin penetration is through intercellular pathways within stratum corneum (Venuganti et al., 2011). Furthermore, greater fluorescence intensity was also observed near the hair follicles. Nanoparticles of particle size range between 50-200 nm have been shown to penetrate skin through follicular pathways (Prow et al., 2011). In our previous chapter, we have also showed that iontophoretic application of LbL-AuNP significantly improved the deposition of imatinib mesylate in viable epidermis (Labala et al., 2015). The LbL-AuNP and siRNA did not permeate across the skin to reach the receptor medium. Therefore, the nanoparticles were found to be localized within the skin tissue.

The ability of siRNA to silence target gene depends on its efficient cell uptake and cytoplasmic translocation (Sun et al., 2015). In general, nanoparticles are taken-up by cells through endocytosis pathways (Shan et al., 2011). Clathrin, caveolae and non-clathrin and non-caveolae dependent cell uptake are the predominant endocytosis mechanisms (Zhang et al., 2015). While there have been no reports on mechanism of cell-uptake of LbL-AuNP, the metallic AuNP have been shown to be taken-up through clathrin-mediated endocytosis (Klingberg et al., 2015). In general, the nanoparticles of size <200 nm are expected to be endocytosed through clathrin-mediated pathways, while the nanoparticles >200 nm particle size are endocytosed through caveolae-mediated pathways (Rejman et al., 2004). Furthermore, upon endocytosis, the cargo has to be released within the cytoplasm to bind to target mRNA and escape the lysosomal degradation (Shim et al., 2012). Polyethyleneimine (PEI) has been the widely used non-viral carrier for nucleic acid delivery (Kircheis et al., 2001). One of the advantages of nucleic acid complexation with PEI is rapid endosomolysis

upon cell uptake attributed to proton-sponge effect. However, PEI is known to be cytotoxic (Brunot et al., 2007). In our previous chapter, blank LbL-AuNP made of PEI, decreased cell viability by 60% compared to control at 250 µM Au concentration (Labala et al., 2015). On the other hand, chitosan is a natural polysaccharide synthesized by deacetalyzation of chitin and found to be biocompatible and biodegradable (Rudzinski et al., 2010). Multiple studies have compared the transfection efficiency of chitosan with that of PEI. It can be said that, while the buffering capacity and endosomolysis is weaker for chitosan based nanoparticles, the transfection efficiency is not significantly different with that of PEI (Mao et al., 2001; Köpping et al., 2001). Chitosan-plasmid DNA complexes have been shown to be released from endosomes due to swelling of chitosan and endosomal rupture (Ishii et al., 2001). However, it should be noted that most of the studies where chitosan is used to deliver siRNA, chitosan is electrostatically complexed to nucleic acids through ionic gelation method. Therefore, the physical and chemical characteristics could be different from siRNA entrapped LbL-AuNP. In this study, chitosan coated AuNP showed 48 % STAT3 protein suppression, and 44 % and 29 % of late and early apoptotic cells, respectively. Chitosan coated blank LbL-AuNP showed significantly lower cytotoxicity compared to PEI surfaced LbL-AuNP shown in our earlier chapter (Labala et al., 2015).

Many of the oncogenic signaling pathways including receptor and non-receptor tyrosine kinases converge and transmit through STAT3 mediated pathway (Niu et al., 2002; Yu et al., 2009). STAT3 has been identified to be activated in multiple cancers types including melanoma. This activated STAT3 would enhance the cell growth and proliferation through regulation of anti-apoptotic genes Bcl-X_L, c-Myc and cyclin D1 (Kortylewski et al., 2005). The B16F10 murine melanoma cells and in-vivo tumor specimens were reported to show enhanced STAT3 expression. Melanoma cells have been shown to undergo cell death through apoptosis upon inhibition of STAT3 signaling pathway (Alshamsan et al., 2011).

Specifically, suppression of STAT3 expression resulted in significant increase in IL-6 and caspase 3 expression, and significant decrease in VEGF level causing cell death. The STAT3 protein inhibition has been shown using non-specific small molecules such as curcumin (Bill et al., 2012). To that end, siRNA mediated STAT3 gene silencing is more specific and effective. To the best of our knowledge, this is the first time LbL-AuNP have been utilized to deliver siRNA through skin with the application of iontophoresis.

3.5. CONCLUSIONS

AuNP can be prepared by direct reduction of $HAuCl_4$ using chitosan. The LbL-AuNP are stable in PBS and cell culture medium for up to 48 h. siRNA can be layered on chitosan coated AuNP. Murine melanoma cells take up the siRNA loaded LbL-AuNP within 1 h predominantly through clathrin mediated pathway. The STAT3 siRNA loaded LbL-AuNP decrease the cancer cell viability through apoptosis mechanism. Furthermore, iontophoresis application enhances the skin penetration of siRNA loaded LbL-AuNP to reach viable epidermis. The LbL-AuNP penetrates the skin mainly through intercellular and follicular pathways.

Chapter 4

LbL-AuNP for topical iontophoretic co-delivery of STAT3 siRNA and imatinib mesylate to treat melanoma

Graphical abstract

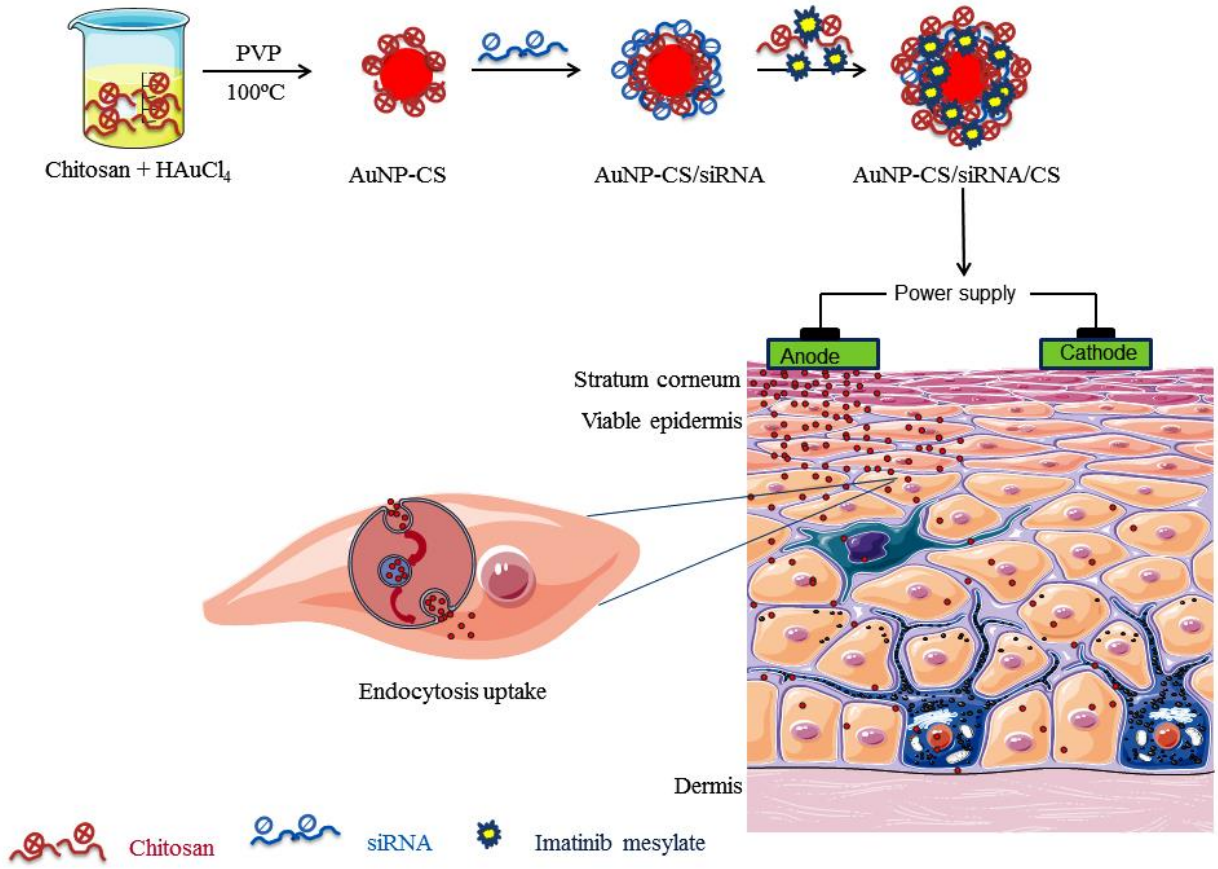

4.1. INTRODUCTION

In the previous chapter, we used STAT3 siRNA delivered using layer by layer chitosan coated gold nanoparticles (LbL-AuNP-CS) for treatment of melanoma, it was observed that delivery of STAT3 siRNA by LbL-AuNP in murine melanoma cells reduced STAT3 gene expression by ~48 % and also reduced cell viability by 66 %. We also observed that delivery of STAT3 siRNA by LbL-AuNP induced apoptosis of murine melanoma cells (Labala et al., 2016; Niu et al., 1999). Recent studies show that melanoma acquired resistance to chemotherapeutic agents and mono therapy based on specific target protein (Villanueva et al., 2010; Wagle et al., 2014). Targeting multiple cell signaling pathways which are important to malignant transformation and progression is an attractive approach for treatment of melanoma (Smalley et al., 2006; Bild et al., 2006).

In addition to STAT3 signaling, there are various other signaling factors also contribute for melanoma progression. Among those, c-kit protein (CD117) is a membrane-bound tyrosine kinase receptor and its overexpression has been observed in melanoma cases (Smalley et al., 2009). Micropthalmia-associated transcription factor expression is also induced by stimulation of the c-kit receptor and subsequently linked downstream to expression of the antiapoptotic protein BCL2 (Wyman et al., 2006). Therefore in continuation to previous work (Labala et al., 2016), we have used imatinib mesylate (IM), a selective cKIT receptor inhibitor for co-delivery with STAT3 siRNA for effective management of melanoma. We studied, cell viability, apoptotic potential, in-vitro gene silencing effects of STAT3 siRNA and IM co-delivered using LbL-AuNP in B16F10 murine melanoma cells.

Non-invasive topical application of chemotherapeutic agents is an approach for avoiding systemic toxicity associated with higher doses. As the systemic delivery of siRNA is impossible due to its extensive degradation by nucleases, the topical application of siRNA

offers many therapeutic advantages for silencing genes in the skin (Chen et al., 2014). Recent studies showed that topical delivery of siRNA using spherical gold nanoparticle conjugates delivered siRNA into skin layers without using transfection agents or barrier disruption agents (Zheng et al., 2012; Labouta et al., 2013).

Our previous studies showed that iontophoresis application of siRNA delivered using LbL-AuNP enhanced its skin penetration to a depth of ~70 µm and also improved bioavailability of siRNA in viable epidermis (Labala et al., 2016). In continuation, we also investigated the feasibility of LbL-AuNP for in-vivo iontophoretic application of IM and STAT3 siRNA in mouse melanoma tumor models. We hypothesized that iontophoretic delivery of siRNA in combination with IM could be effective in melanoma treatment.

4.2. MATERIALS AND METHODS

Tetrachloroaurate trihydrate ($HAuCl_4$ $3H_2O$), sodium alginate (SA, MW: 80 kDa), poly(N-vinyl pyrrolidone) (PVP K-30, MW: 40 kDa), imatinib mesylate (IM), fluorescein isothiocyanate (FITC), Triton X-100, DAPI, phenyl methyl sulfonyl fluoride (PMSF), sodium fluoride, sodium deoxycholate, leupeptin, pepstatin, Potassium bromide (KBr) and nitrocellulose membrane were purchased from Sigma Aldrich Chemical Company (Bengaluru, India). Chitosan (CS, MW: 15 kDa, degree of deacetylation: 85%) was purchased from Polysciences, Inc., USA.

STAT3 siRNA (sense: 5′AAAUGAAGGUGGUGGAGAAUU3′; antisense: 5′UUCUCCACC ACCUUCAUUUUU-3′) was purchased from Dharmacon Inc., USA. Scrambled sequence siRNA, STAT3 monoclonal antibody, β-actin primary antibody and horseradish peroxidase-conjugated secondary antibodies were purchased from Santa Cruz Biotechnology Inc., USA. Silencer® Cy™3 labeled siRNA was purchased from Life Technologies Inc., USA. Bovine serum albumin (BSA), nonfat milk powder, sodium dodecyl sulfate (SDS), Tris base, boric acid, ethylenediamine tetraaceticacid dihydrate (EDTA), ethidium bromide, polyacrylamide, agarose, Dulbecco's modified Eagle's medium (DMEM), Dulbecco's phosphate buffered saline, fetal bovine serum (FBS), bromophenol blue, mercaptoethanol and thiazolyl blue tetrazolium bromide (MTT) were purchased from Himedia Laboratories (Mumbai, India).

4.2.1. Preparation of LbL-AuNP for co-delivery of siRNA and IM

LbL-AuNP were prepared as described in our earlier chapter (Labala et al., 2016). For co-delivery application AuNP-CS/siRNA particles were incubated in chitosan solution (1 mg/mL) containing 20 mg/ml of imatinib mesylate for 1 h under continuous stirring at 1000 rpm. After incubation, IM loaded AuNP-CS/siRNA/CS particles were centrifuged at 15000 rpm for 35 min to remove unbound chitosan and IM. The supernatant was analyzed by RP-HPLC method for determination of loading efficiency. The loading efficiency of IM was calculated by using Equation (1). STAT3 siRNA replaced by Scrambled siRNA and sodium alginate (SA) were used as controls.

$$\text{Loading efficiency (\%)} = \frac{\text{Concentration of IM in LbL}-\text{AuNP}}{\text{Concentration of LbL}-\text{AuNP}} \times 100 \qquad (1)$$

4.2.2. Characterization of IM loaded LbL-AuNP

The particle size and zeta-potential of nanoparticles were determined using Zetasizer (Nano ZS, Malvern Instruments Inc., UK) as per the method described earlier (Labala et al., 2016). Sequential adsorption of polymers on to AuNP-CS was studied using Fourier transform infrared (FTIR) spectrometer (FT/IR-4200, Jasco Inc, USA). Furthermore, FTIR was also used to characterize the encapsulation of IM in AuNP-CS/SA/CS. Samples (1 mg) were mixed with potassium bromide at 1:100 ratio and a pellet was prepared using high pressure hydraulic press (Riken Seiki, Tokyo, Japan) after application of 20 MPa pressure. Spectra were recorded within the range of 4000–400 cm^{-1} at a spectral resolution of 2 cm^{-1}.

Differential scanning calorimeter (DSC-60, Shimadzu, Japan) was used to study the thermal transitions of free AuNP-CS and LbL-AuNP-CS. Furthermore, DSC was also used to study the encapsulation of IM in LbL-AuNP-CS. Sample (3 mg) was placed in an aluminum

pan and sealed with a lid using a press. Thermograms were recorded at a heating rate of 10 ^{o}C per min from ambient temperature up to 450 ^{o}C.

4.2.3. In-vitro release of IM from LbL-AuNP

In-vitro release of IM from AuNP-CS/SA/CS were performed using dialysis membrane (molecular weight cut-off of 12–14 kDa, Spectrum Labs, Houston, USA) in Franz diffusion cell apparatus. Phosphate buffered saline (PBS) (pH 7.4) was used as receptor medium. Samples (0.3 mL) were withdrawn from receptor compartment at predetermined time intervals and replaced with fresh PBS maintained at 37 ^{o}C. In-vitro diffusion of equivalent concentrations of free IM across dialysis membrane was also performed. IM release was analyzed using RP-HPLC method as described in the previous chapter (Labala et al., 2015).

4.2.4. Effect of co-delivery of STAT3 siRNA and IM on melanocyte cell viability

B16F10 murine melanoma cells were cultured in growth medium containing Dulbecco's modified Eagle's medium (DMEM) supplemented with 10 % fetal bovine serum (FBS) and 1% penicillin/streptomycin solution. Cells were incubated at 37 ºC and 5 % CO_2. For cell viability study, cells (1 x 10^4) were seeded in 96-well plates 24 h before incubation with formulations. Cell viability was studied using imatinib loaded AuNP-CS/STAT3 siRNA/CS, AuNP-CS/Scrambled siRNA/CS containing 0.5 nM siRNA and 130 µM of IM respectively. Whereas IM loaded AuNP-CS/SA/CS containing 167 µM of IM and Free IM at 130 µM, 167 µM were used as controls. Formulations and free IM were prepared in DMEM medium and incubated with cells for 8 h at 37 °C. Later, the culture medium was replaced

with fresh medium and cells were further incubated for 48 h. Then the cell viability was determined using thiazolyl blue tetrazolium bromide (MTT) assay.

4.2.5. Apoptosis Assay

B16F10 cells (2 x 10^5) were seeded in 6-well plates and incubated for overnight for adhesion. Later, cells were treated for 8 h with IM loaded AuNP-CS/STAT3 siRNA/CS, AuNP-CS/scrambled siRNA/CS containing 0.5 nM siRNA and 130 µM of IM respectively. Whereas IM loaded AuNP-CS/SA/CS was used as size control and it contains 167 µM of IM. Effect of free IM at 130 µM, 167 µM was also studied. IM loaded AuNP-CS/SA/CS containing 167µM of IM was used as size control. After, incubation the unentrapped formulation was removed and replaced with complete medium. The cells were further incubated for 48 h and apoptosis assay was performed using FITC-Annexin V/PI apoptosis assay (Labala et al, 2016).

4.2.6. Protein analysis

B16F10 cells (2 x 10^5) were seeded in 6-well plate and treated for 8 h with IM loaded AuNP-CS/STAT3 siRNA/CS, AuNP-CS/scrambled siRNA/CS, AuNP-CS/SA/CS. After incubation, the unentrapped formulation was removed and replaced with cell culture medium containing DMEM supplemented with 10 % FBS and further incubated for 48 h at 37 ºC. Later, the cells were harvested and total protein was extracted, analyzed for STAT3 content using Western blot assay as described in our previous report (Labala et al, 2016).

4.2.7. In-vivo gene silencing using tumor bearing C57BL/6 mice

Female C57BL/6 mice (4-6 week old) were purchased from the National institute of nutrition (NIN), (Hyderabad, India). For tumor establishment, 1 X 10^6 B16F10 cells were suspended in Hank's balanced salt solution and injected subcutaneously in the upper left flank of female C57BL/6 mice. Tumor volume was calculated using Equation (2).

$$\text{Tumor volume } (mm^3) = \frac{Longitudinal\ diameter\ (mm) \times (transverse\ diameter\ (mm))^2}{2} \quad (2)$$

Treatment with formulations was started after reaching tumor volume of 150 mm^3. Tumor bearing mice were treated with LbL-AuNP containing final siRNA concentration of 0.6 mg/kg body weight. The formulations were applied by passive, iontophoresis application and intratumoral injection. For, passive application the formulations (50 µl) were applied to tumor surface, after hair is removed with hair clipper (Philips, India). Iontophoresis application was performed after formulations were embedded in 0.4 % agarose gel containing 2 mM NaCl. Anodal iontophoresis (current density of 0.5 mA/cm^2) was applied for 2 h while animal is under isoflurane anesthesia. For intratumoral injection the formulation was injected in various regions of tumor.

Tumor bearing mice were treated with IM loaded AuNP-CS/STAT3 siRNA/CS, AuNP-CS/scrambled siRNA/CS, AuNP-CS/SA/CS. Each mice in group (5 mice per group) received passive, iontophoresis and intratumoral injection treatment for every 3 days and treatment was carried out for 4 times. Thereafter, mice were euthanized 3 day after the final treatment dose and tumor samples were immediately isolated and weighed. Total protein was isolated from the excised tumor using Trizol® reagent and STAT3 expression was analyzed using western blot analysis.

4.2.8. Statistical Analysis

All the results were presented as mean ± standard deviation. The results were compared by performing analysis of variance (Version 6, Graph Pad Prism, USA), and the results were considered to be significant at $p<0.05$.

4.3. RESULTS

4.3.1. Characterization of the LbL-AuNP

The average particle size and zeta-potential of AuNP-CS were found to be 62.5±3.4 nm (PDI: 0.27±0.04), 52.1±1.7 mV respectively. Layer-by-layer adsorption of siRNA on AuNP-CS increased particle size to 150.4±10.1 nm (PDI 0.41±0.06), 157.3±19.1 nm (PDI 0.28±0.04) and 172.7±8.8 nm (PDI 0.35±0.03) respectively, with STAT3 siRNA, scrambled siRNA and SA (Fig.4.1a). The zeta-potential was found to be -32.7±3.1, -28.5±0.6 and -76.6±3.3 mV respectively, after adsorption with STAT3 siRNA, scrambled siRNA and SA. Adsorption of final CS layer containing IM on to AuNP-CS/STAT3 siRNA, AuNP-CS/scrambled siRNA and AuNP-CS/SA showed increased particle size to 197.8±18.7 nm (PDI 0.22±0.10), 214.7±21.9 nm (PDI 0.24±0.16) and 232.5±18.1 nm (PDI 0.33±0.02), respectively. Whereas zeta-potential was observed to be 46.8±2.7, 47.0±0.6 and 44.4±0.5 mV respectively with IM loaded LbL-AuNP containing STAT3 siRNA, scrambled siRNA and SA (Fig. 4.1b).

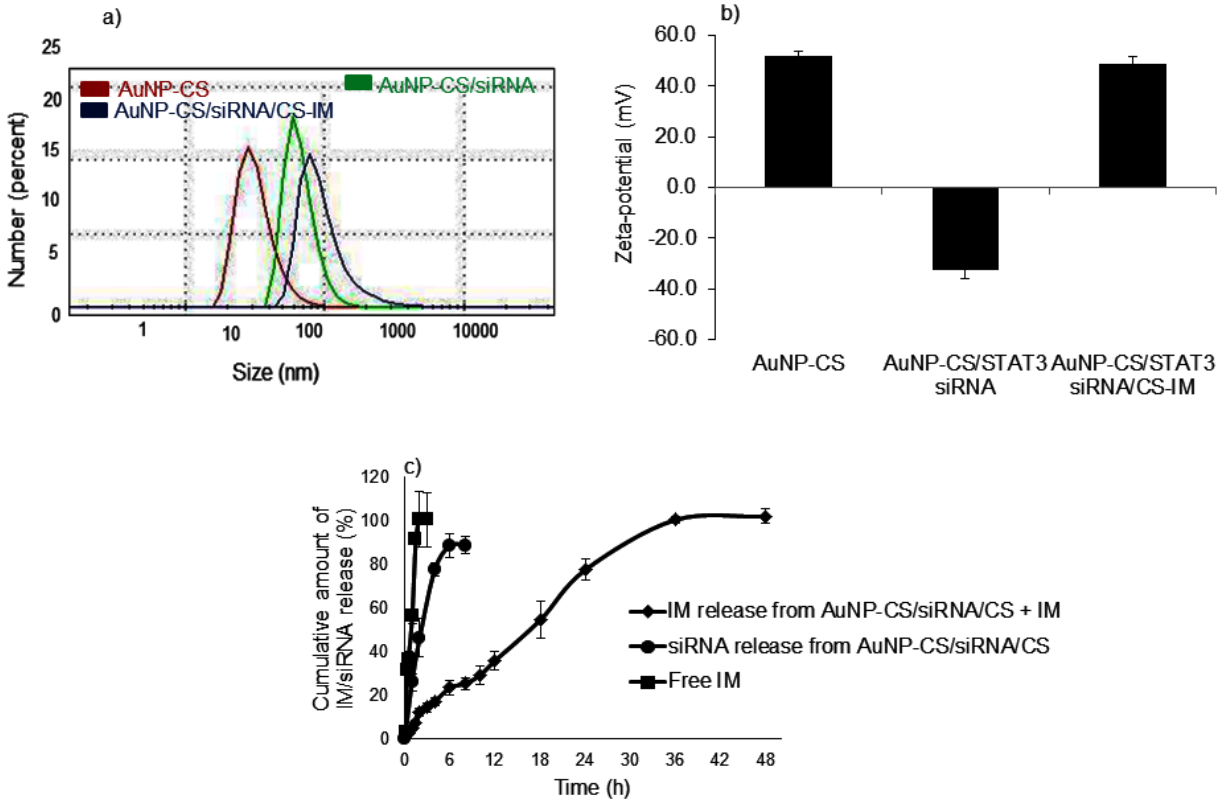

Fig. 4.1. Characterization of LbL-AuNP. **a**, representative number weighted particle size distribution after sequential adsorption of siRNA, chitosan and IM on AuNP-CS; **b**, zeta-potential measured after sequential adsorption of siRNA, chitosan and IM on AuNP-CS; **c**, In-vitro release of IM and siRNA from LbL-AuNP and diffusion of free IM. Data was presented as mean (n=3) ± SD.

FTIR analysis showed characteristic broad band for chitosan at 3373 cm^{-1} is due to overlapped -OH and -NH groups. The absorption peaks at 1076 cm^{-1} is due to skeletal vibration involving C-O-C bridge stretching of the glucosamine residue in chitosan (Salehizadeh et al., 2012). Alginic acid showed characteristic band at 3405 cm^{-1} and 1654 cm^{-1} corresponds to O-H stretch and C=O stretch. PVP showed characteristic band at 1687 cm^{-1} (C=O stretch) and 1285 cm^{-1} (C-N stretch) wave numbers respectively (Fig.4.2). FTIR spectrum of AuNP-CS showed characteristic band for interaction with chitosan at 3355 cm^{-1} and stabilization of AuNP-CS by PVP was confirmed by presence of characteristic band at 1379 cm^{-1}, 1651 cm^{-1} respectively due to the ring vibration of pyridine and C=O stretching.

LbL adsorption of polymers on to AuNP-CS surface showed shift in characteristic peaks of chitosan and SA polymers. In case of CS, 3373 cm^{-1} (N-H stretch) and 1076 cm^{-1} (C-O-C bridge stretching) were shifted to 3291 cm^{-1} and 1037 cm^{-1} respectively. In case of SA, wave numbers of 3405 cm^{-1}, 1654 cm^{-1} were shifted to 3419 cm^{-1} and 1612 cm^{-1} respectively (Fig.4.2).

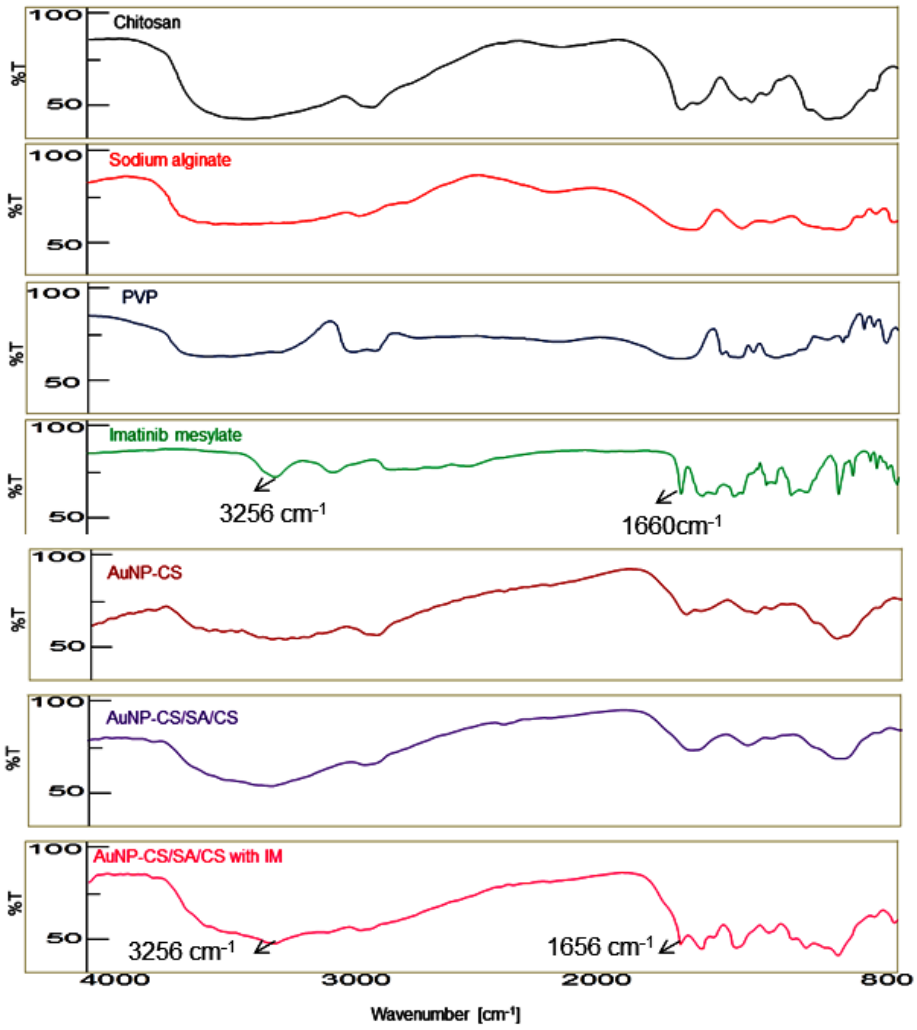

Fig. 4.2. FTIR Characterization of neat chitosan, neat SA, neat PVP, IM, AuNP-CS, AuNP-CS/SA/CS and IM loaded AuNP-CS/SA/CS. Spectra were representative of at least three different experiments.

The DSC thermogram of chitosan showed glass transition temperature (T_g) and melting temperature (T_m) respectively, at 77.2 ^oC and 238.6 ^oC. Sodium alginate showed the thermal transitions for dehydration at 96.7 °C, decomposition of biopolymer at 249.7 °C and decomposition of carbonaceous material at 345.2 °C. AuNP-CS showed Tg and Tm, respectively at 62.5 °C and 214.4 °C due to presence of CS. AuNP-CS/SA/CS showed Tg at 82.5 °C and two exothermic peaks respectively, at 225.2 °C and 325.1 °C (Fig. 4.3).

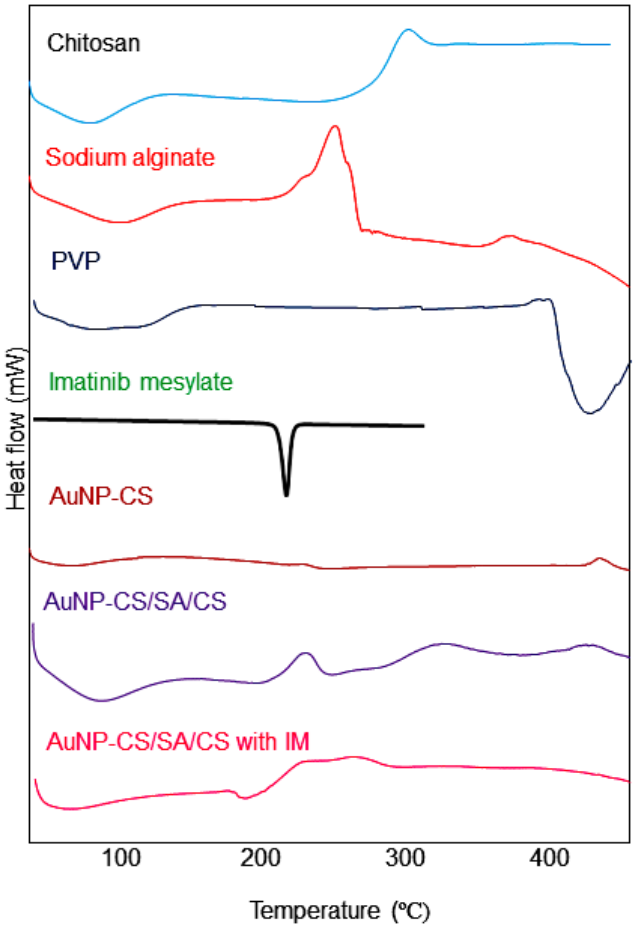

Fig. 4.3. DSC thermograms of neat chitosan, neat SA, neat PVP, IM, AuNP-CS, AuNP-CS/SA/CS and IM loaded AuNP-CS/SA/CS. Thermograms were representative of at least three different experiments.

4.3.2. Encapsulation of siRNA and IM in LbL-AuNP

UV-spectrometer analysis showed that the encapsulation efficiency of siRNA was 58.3±7.5 %. This translates to approximately 8×10^3 molecules of siRNA adsorbed to one AuNP-CS nanoparticle. Loading efficiency of IM in AuNP-CS/SA/CS and AuNP-CS/siRNA/CS was found to be 24.5±2.5 % and 19.2±3.0 % respectively. Further, encapsulation of IM in AuNP-CS/SA/CS was characterized by FTIR and DSC. FTIR studies showed shift in absorbance peak of IM after encapsulation, where 1660 cm^{-1} (C=O stretch) shifted to 1656 cm^{-1} and 3256 cm^{-1} (N-H stretch) shifted to 3265 cm^{-1} (Fig.4.2). Similarly, DSC thermograms showed shift in melting temperature (T_m) of free IM from 226.5 ^oC to 263.8 ^oC after encapsulation (Fig.4.3).

4.3.3. In-vitro release of IM and siRNA from LbL-AuNP

Fig. 4.1c shows in-vitro release profiles of IM from LbL-AuNP and diffusion of free IM across dialysis membrane. IM release from LbL-AuNP was controlled up to 36 h, while 100 % free IM diffused across membrane within 2 h. The in-vitro release profiles were fitted into kinetic models of zero-order, first-order, Hixon-Crowell and Korsmeyer-Peppas. Correlation coefficients of regression analyses were found to be 0.990, 0.925, 0.945 and 0.957 for zero-order, first-order, Higuchi, Hixon-Crowell and Korsmeyer-Peppas models, respectively. The release exponent “n” obtained from Korsmeyer-Peppas model was found to be 0.742.

4.3.4. Effect of co-delivery of STAT3 siRNA and IM on cell viability

Fig.4.4 shows the B16F10 cell growth inhibitions after treatment with IM loaded AuNP-CS/STAT3 siRNA/CS, AuNP-CS/Scrambled siRNA/CS, AuNP-CS/SA/CS and free IM. It is observed that IM loaded AuNP-CS/STAT3 siRNA/CS showed 82.02±2.93 %

growth inhibition compared to 68.76±3.22 % and 71.86±4.13 % respectively with IM loaded AuNP-CS/Scrambled siRNA/CS, AuNP-CS/SA/CS. In our previous chapter we observed that AuNP-CS/STAT3siRNA/CS treatment resulted in 66.2±0.2 % growth inhibition (Labala et al., 2016). Free IM showed 65.18±3.83 % and 59.06±3.43 % growth inhibition respectively, at 167µM and 130µM concentration. Whereas blank AuNP-CS/SA/CS and free STAT3 siRNA showed 37.16±0.40 % and 2.08±0.12 %.

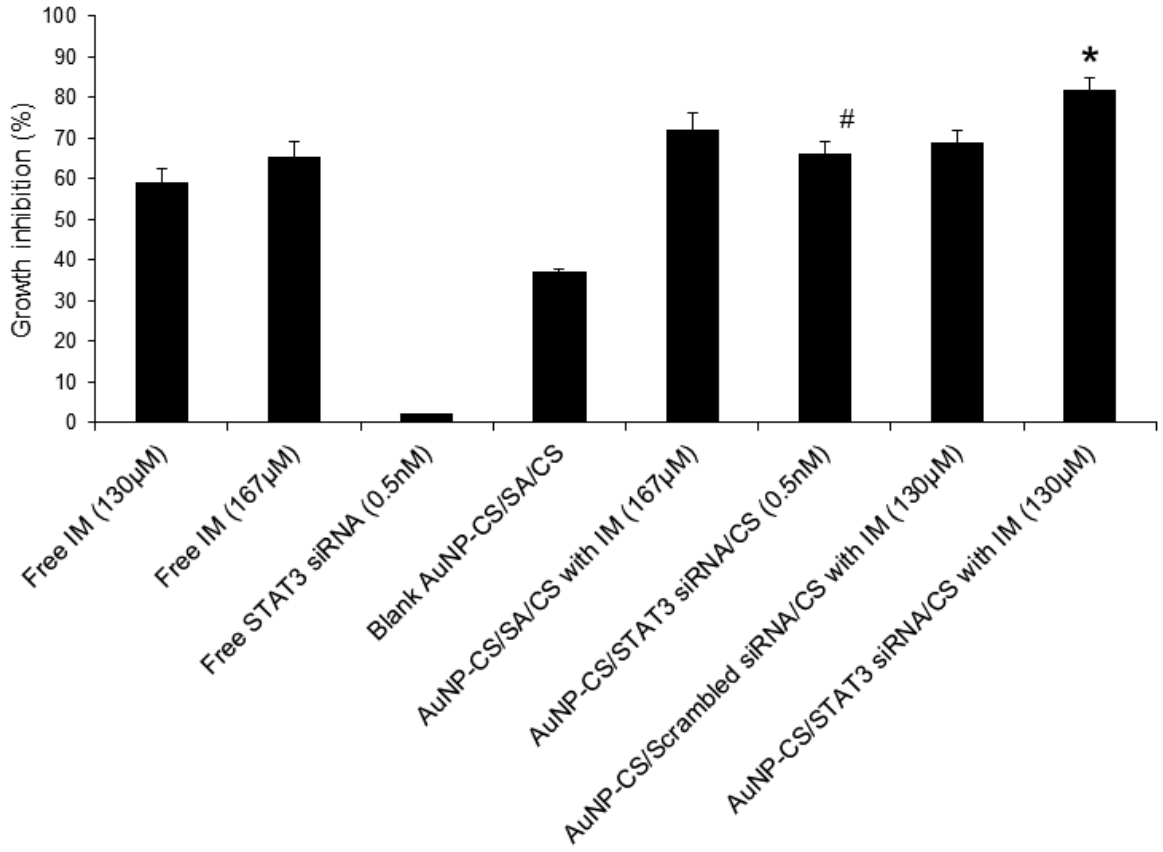

Fig. 4.4. Inhibition of B16F10 murine melanoma cancer cell growth after treatment with LbL-AuNP formulations containing IM and siRNA. Data represents mean (n =3) ± standard deviation. * represents that the values are significantly different at $p< 0.05$.[#] Reproduced from our previous work (Labala et al., 2016).

4.3.5. In-vitro gene silencing

Results from Western blot analysis showed that the STAT3 expression decreased by 47.2±5.9 % after treatment with IM loaded AuNP-CS/STAT3 siRNA/CS (Fig. 4.5). Whereas IM loaded AuNP-CS/SA/CS showed nonspecific inhibition of 18.8±4.9 %. There was no suppression of STAT3 protein after treatment with IM loaded AuNP-CS/scrambled siRNA/CS. Similarly, there was no suppression of STAT3 protein after treatment with free IM and blank AuNP-CS/SA/CS (Labala et al., 2016).

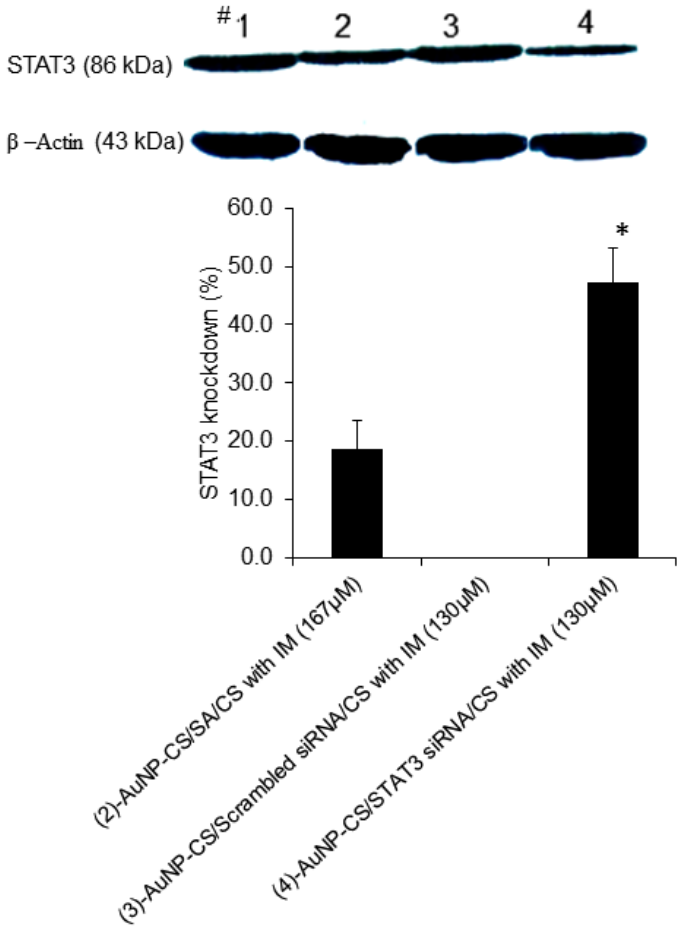

Fig. 4.5. Expression of STAT3 protein in B16F10 murine melanoma cells after treatment with LbL-AuNP formulations. β-actin was used as loading control. Images were analyzed using ImageJ software. Data represents mean (n =3) ± standard deviation. * represents that the values are significantly different at $p < 0.05$.

4.3.6. Apoptosis Assay

Fig.4.6 shows percentage of cells at different stages of cell death after treatment with formulations. The gated cell population (10000 cells) was divided into four quadrants as live cells, early apoptotic cells, late apoptotic cells and dead cells. It is observed that there was a significant difference in the percentage of early and late apoptotic events after treatment with IM loaded AuNP-CS/STAT3 siRNA/CS compared to other groups. It is observed that 49.3±3.45 % and 14.1±1.61 % of annexin V+/ PI+ cells indicating late apoptosis was observed after treatment with IM loaded AuNP-CS/STAT3 siRNA/CS, AuNP-CS/Scrambled siRNA/CS. Whereas treatment with IM loaded AuNP-CS/SA/CS showed 28.5±0.11 % late apoptosis. Free IM at 130µM and 167µM showed 8.06±0.56 % and 11.30±1.48 % late apoptotic events respectively. There was no induction of apoptotic events after treatment with free STAT3 siRNA; however blank AuNP-CS/SA/CS showed 13.25±0.21 % late apoptotic events (Labala et al., 2016).

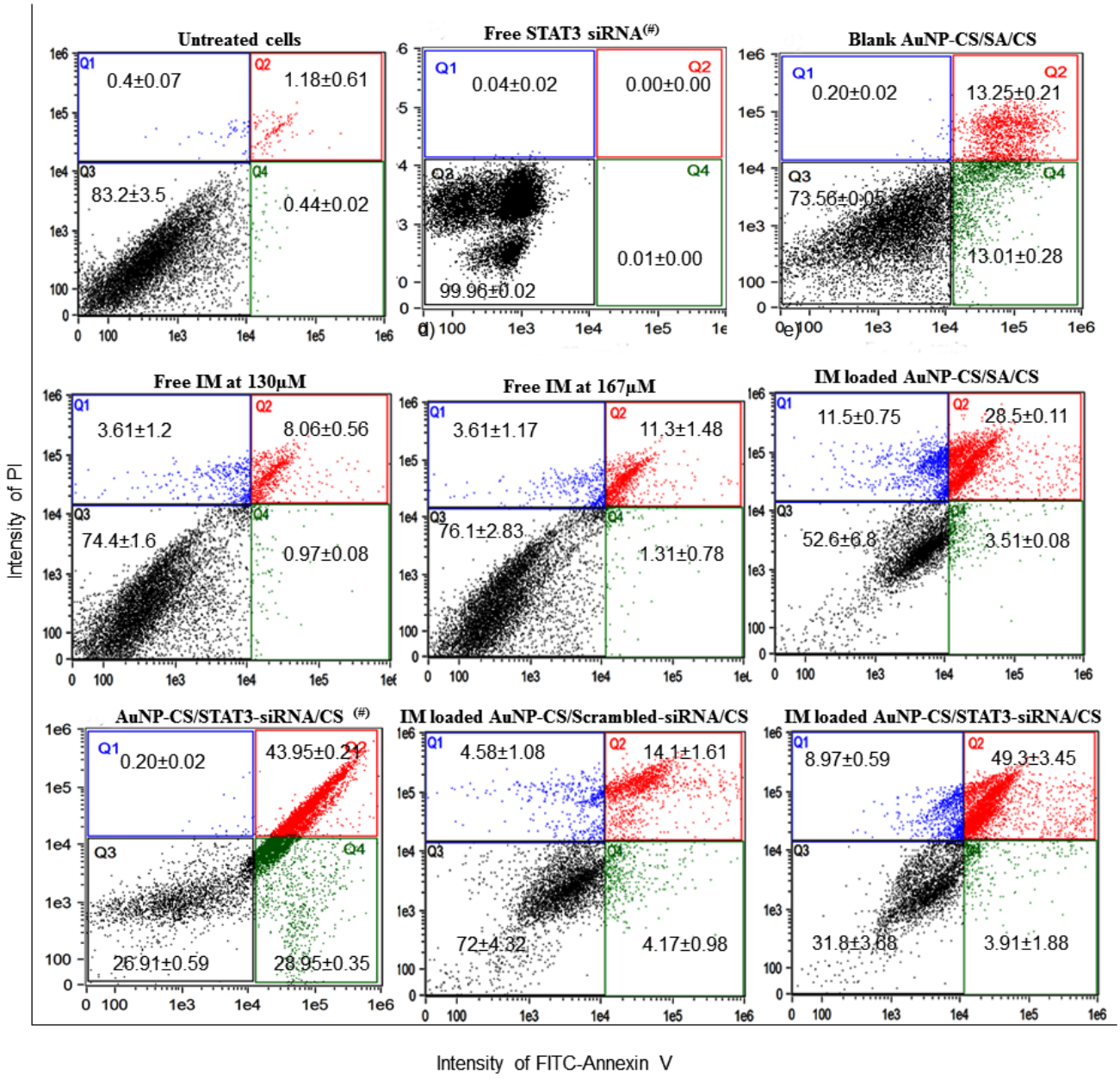

Fig. 4.6. Apoptosis events observed in B16F10 cells after treatment with LbL-AuNP formulations. Dot plots are representative of three independent experiments. [#] reproduced from our previous work (Labala et al., 2016).

4.3.7. In-vivo gene silencing

Fig.4.7a shows the photograph of isolated tumors after treatment with formulations. It is observed that intratumoral injection of IM loaded AuNP-CS/STAT3 siRNA/CS showed tumor weight and tumor volume of 1.07±0.19 g and 477±59 mm^3, respectively compared with 4.98±1.58 g and 3540±726 mm^3 in case of untreated control. Passive application of IM loaded AuNP-CS/STAT3 siRNA/CS did not show reduction in tumor volume, whereas iontophoretic application of the same showed tumor volume and tumor weight of 773±162 mm3 and 1.36±0.51 g, respectively (Fig. 4.7b, Fig. 4.8). Intratumoral injection of AuNP-CS/STAT3 siRNA/CS showed 1.59±0.79 g and 1321±674 mm^3, whereas iontophoretic application showed 2.16±0.27 g and 2073±306 mm^3 respectively. Iontophoretic application of AuNP-CS/ scrambled siRNA /CS, AuNP-CS/ SA /CS and intratumoral injection of free IM did not show reduction in tumor volume.

The in-vivo STAT3 expression showed in Fig. 4.9. It is observed that intratumoral injection of AuNP-CS/STAT3 siRNA/CS alone and in combination with IM showed 11.37±0.09 %, 18.33±0.25 % reduction in STAT3 expression. The iontophoretic application of AuNP-CS/STAT3 siRNA/CS alone and in combination with IM showed 7.97±0.02 % and 15.73±0.16 % reduction in STAT3 expression. The iontophoresis application of AuNP-CS/ scrambled siRNA /CS, AuNP-CS/ SA /CS did not show reduction in STAT3 expression.

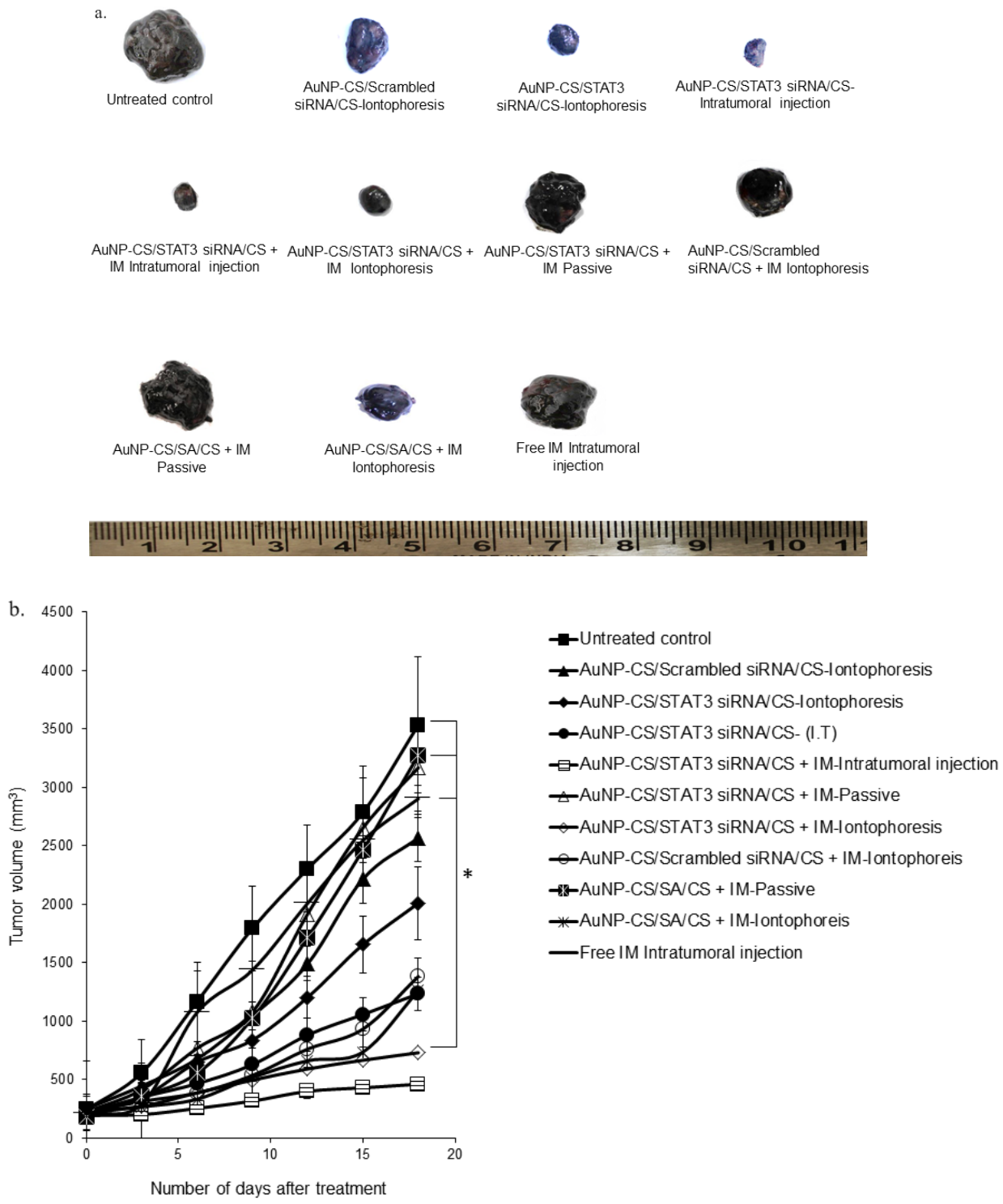

Fig. 4.7. a. Photograph of tumors isolated from tumor bearing C57BL/6 mice after treatment with formulations; **b**. measurement of tumor volume after initiation of treatment with formulations. Data represents mean (n =5) ± standard deviation. * represents that the values are significantly different at $p < 0.05$. I.T is the abbreviation for intratumoral injection.

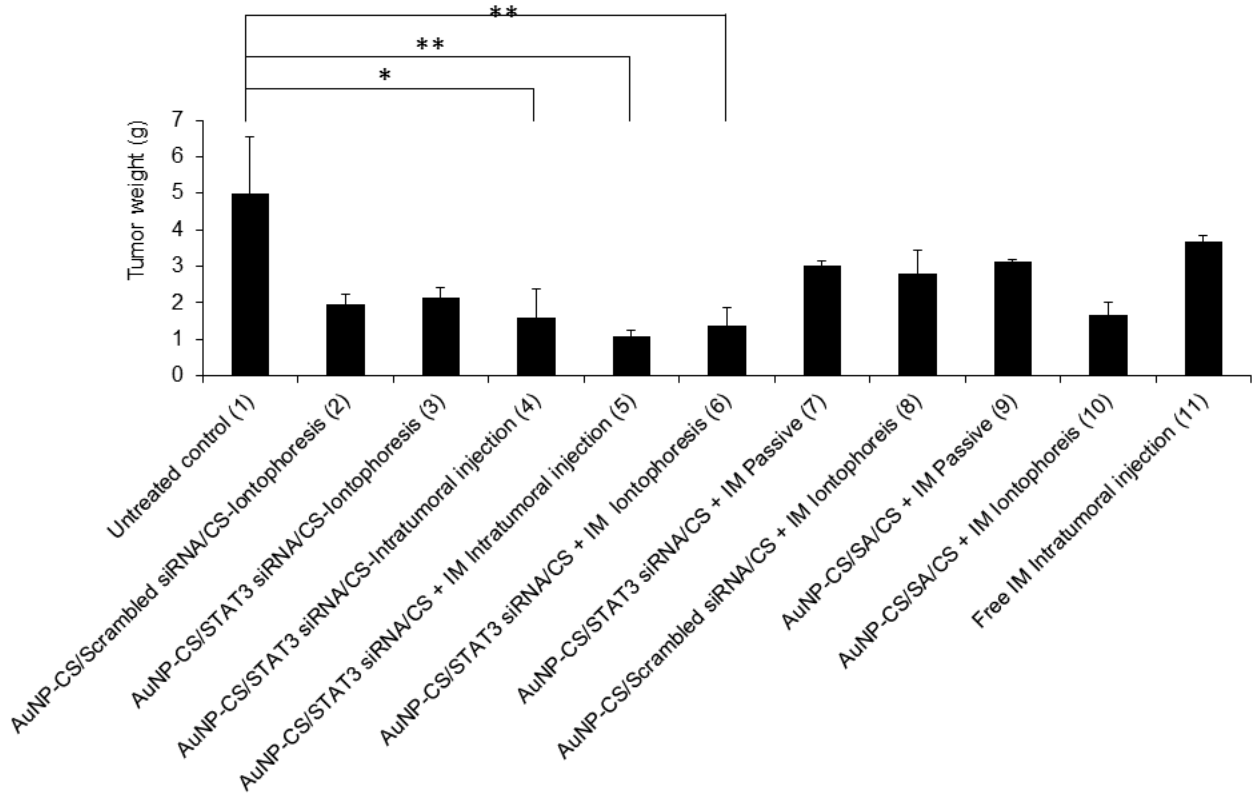

Fig. 4.8. Weight of tumors isolated from C57BL/6 tumor bearing mice after treatment with final dose of formulations. Data represents mean (n =5) ± standard deviation. * and ** represents that the values are significantly different at $p < 0.05$ and $p < 0.01$, respectively.

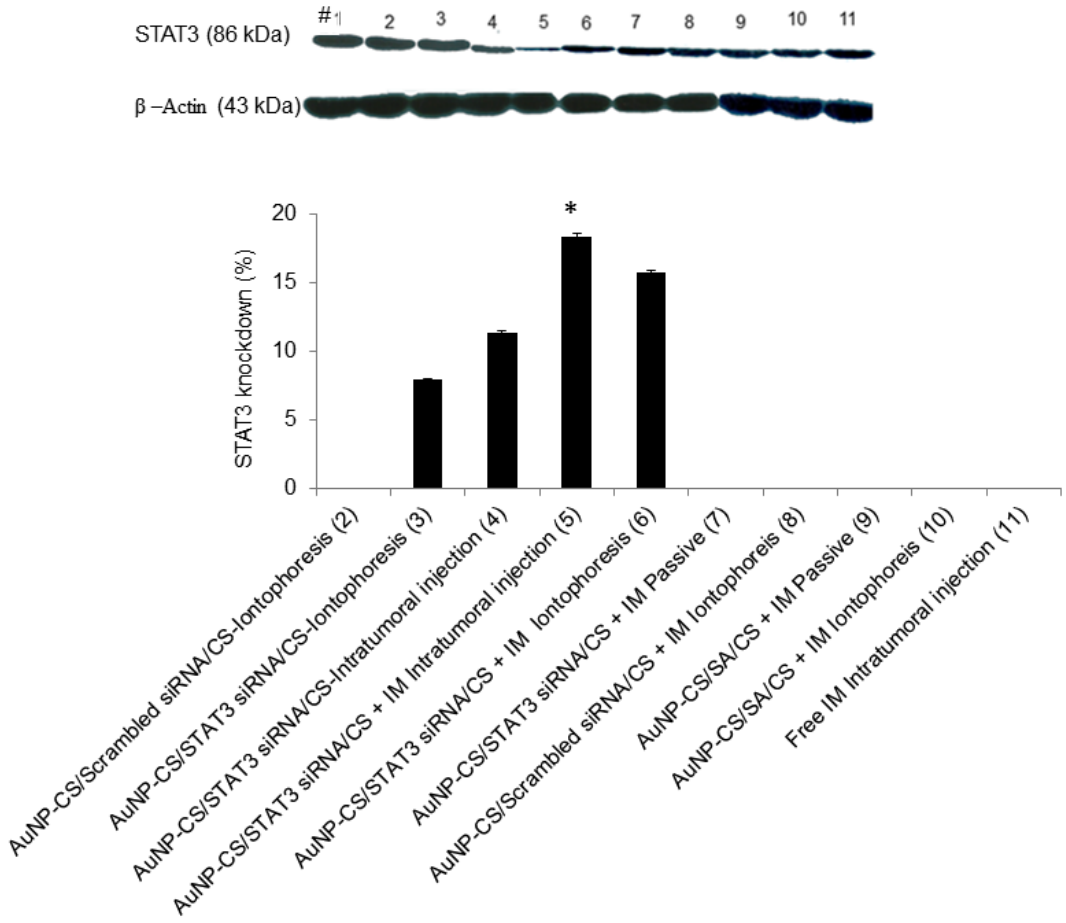

Fig. 4.9. Expression of STAT3 protein in tumor bearing C57BL/6 mouse after treatment with formulations. β-actin was used as loading control. Images were analyzed using ImageJ software. Data represents mean (n =5) ± standard deviation. * represents that the values are significantly different at $p < 0.05$.

4.4. DISCUSSION

Development of multidrug resistance in cancer cells and adverse side effects are major obstacles for effective cancer chemotherapy (Chen et al., 2009; Thomas et al., 2003). Long term treatment of small molecule anticancer agents induce proteins associated with multi-drug resistance (MDR), there by decrease the cellular concentration of chemotherapeutic agents (Baguley et al., 2010; Ling et al.,1997). Several studies have been carried out during the past few years to enhance the efficacy of chemotherapy by reducing the drug efflux mechanism via the co-delivery of MDR modulators with anti-cancer agents (Szakács et al., 2006). Co-delivery of siRNA and anticancer drugs is one of the novel approaches to avoid drug resistance (Taratula et al., 2013; Meng et al., 2013; He et al., 2014). The siRNA can be used to down-regulate the proteins associated with multi drug resistance, cell proliferation and apoptosis (Kanasty et al., 2013). Co-delivery of doxorubicin with bcl-2 siRNA down regulates proteins associated with multidrug resistance and also potentiates the action of doxorubicin, there by reduces the dose frequency by 50% (Chen et al., 2009). It is reported that co-delivery of p53 targeting siRNA (sip53) and cisplatin in human bladder cancer cell lines showed 72.3 % reduction in viability compared to only sip53 (38.7 %) or cisplatin (44.9 %) (Zhu et al., 2013).

The co-delivery of siRNA with small molecule chemotherapeutic agents reduces dose required to elicit therapeutic response and also systemic toxicity (Kemp et al., 2016; Dong et al 2016). The siRNA and small molecule chemo therapeutic agents will have very different physico-chemical, and biological characteristics, thus designing an effective siRNA/drug co-delivery system can be challenging (Conde et al., 2015). In general, siRNA and drug nanocarriers should be nontoxic and non-immunogenic. The siRNA nanocarriers should be able to condense siRNA effectively via electrostatic interaction or chemical conjugation,

while drug nanocarriers should encapsulate anticancer drugs effectively via physical encapsulation or direct chemical conjugation (Taratula et al., 2016; Kesharwani et al., 2016).

Recently, chitosan and chitosan derivatives have been developed for DNA and siRNA delivery because of their cationic charge, biodegradability and biocompatibility. However, the transfection efficiency of chitosan depends on MW of chitosan, its degree of deacetylation (Ragelle et al., 2013; Ragelle et al., 2016; Mao et al., 2010). In the present study the chitosan (15kDa) was used with deacetylation degree above 85%. Recently gold-chitosan nano conjugates were developed for delivery carriers for siRNA (Han et al., 2012), It is observed that chitosan is also having same potential as lipofectamine for delivery of siRNA and showed comparable gene silencing effect (Ji et al., 2009). As the systemic delivery of siRNA is impossible, there is a need to explore alternatives routes for siRNA delivery (Wittrup et al., 2015). Topical application of siRNA is an attractive method for treating skin disorders; however, transdermal permeation of macromolecules such as siRNA or proteins has remained a major challenge due to barrier properties of skin. Recent studies showed that topical delivery of siRNA using gold nanoparticle conjugates delivered siRNA into skin layers without using transfection agents or barrier disruption agents (Zheng et al., 2012; Huang et al., 2010).

In our previous studies we used LbL-AuNP for delivery of STAT3 siRNA alone, it is observed that LbL-AuNP were rapidly up taken by murine melanoma cells and also showed growth inhibition of 66.2±0.2 %. Recently, iontophoresis is utilized for delivery of macromolecules through skin (Kigasawa et al., 2010; Venuganti et al., 2015). In our previous studies we also observed that anodal iontophoresis application of LbL-AuNP significantly improved the skin bio-availability of siRNA and able to deliver the siRNA till viable epidermis (Labala et al., 2016). STAT3 siRNA alone delivered by LbL-AuNP showed 48%

STAT3 protein suppression and induced apoptosis of murine melanoma cells. In the present study we reported co-delivery of STAT3 siRNA and IM using LbL-AuNP. Co-delivery of STAT3 siRNA and IM significantly reduced B16F10 cell growth. In the present study sodium alginate was used as size control and in-vitro gene silencing studies showed 18.8±4.9 % reduction in STAT3 expression. This non-specific STAT3 silencing of alginic acid is hypothesized due to its origin. Alginic acid from brown algae showed anti-cancer, anti-oxidant and anti-inflammatory actions. Recent studies also reported the growth inhibition of alginic acid on B16F10 mouse murine melanoma cells, monkey kidney cell line (vero) and human promyelocytic leukemia cell line (HL-60) (Lakmal et al., 2014; Namvar et al., 2015). However SA did not show inhibition on STAT3 expression in-vivo. The in-vivo iontophoretic application of AuNP-CS/STAT3 siRNA/CS alone and in combination with IM showed 7.97±0.02 % and 15.73±0.16 % reduction in STAT3 expression respectively. Co-delivery of STAT3 siRNA and IM reduced tumor growth compared to stand alone treatment. The passive application of STAT3 and IM in combination did not show reduction in tumor volume. It is hypothesized that altering current density and use of chemical enhancers would further increase the deliverability of siRNA for topical application.

4.5. CONCLUSIONS

The present study demonstrated co-delivery of STAT3 siRNA and IM using LbL-AuNP. Co-delivery of therapeutic molecules targeting different signal transduction pathways would be helpful to avoid resistance in multiple cancers. In-vitro studies showed that co-delivery of STAT3 siRNA and IM significantly reduced cell viability. In-vivo iontophoretic application showed greater reduction in tumor volume and tumor weight. It is observed that STAT3 expression was reduced after iontophoretic delivery of IM loaded AuNP-CS/STAT3

siRNA/CS. whereas passive application of STAT3 and IM using LbL-AuNP did not show reduction in tumor volume, weight and STAT3 expression. It is observed that alteration of current density and incorporation of penetration enhancers would further increase therapeutic efficacy of siRNA for in-vivo applications.

Chapter 5

Summary and Conclusions

5. SUMMARY AND CONCLUSIONS

Layer-by-layer assembled nanoparticles provide a robust platform for delivery of small and macromolecule. Due to its technological ease, low manufacturing cost, stability, protection of encapsulated therapeutic agent, this technique shows potential to be a leading drug delivery technology in future.

The present investigation demonstrated the feasibility of layer-by-layer assembled gold nanoparticles (LbL-AuNP) for encapsulation of small and macro molecule therapeutics. The loading efficiency of therapeutic molecules in AuNP can be improved by layer-by-layer polymer coating. This study shows that iontophoresis application significantly enhances skin penetration of polymer coated gold nanoparticles, further enhancing the viable skin penetration of imatinib mesylate. Moreover, LbL coated gold nanoparticles are rapidly taken up by murine melanoma cells and significantly decreases the cancer cell growth. The nano-size and high positive surface charge has been important attributes for cell uptake of particles.

To reduce the toxicity associated with PEI on normal cells, we demonstrated the use of chitosan for fabrication of LbL-AuNP. The use of chitosan in preparation of LbL-AuNP significantly reduced the toxicity of AuNP. Encapsulation of siRNA was optimized by increasing complexation ratio of AuNP-CS to siRNA. It is observed that LbL-AuNP are stable in PBS and cell culture medium for up to 48 h. It is observed that murine melanoma cells take up the siRNA loaded LbL-AuNP within 1 h predominantly through clathrin mediated pathway. The STAT3 siRNA loaded LbL-AuNP decrease the cancer cell viability through apoptosis mechanism. Furthermore, iontophoresis application enhances the skin penetration of siRNA loaded LbL-AuNP to reach viable epidermis. The LbL-AuNP penetrates the skin mainly through intercellular and follicular pathways.

The present investigation also showed that LbL-AuNP can be used for co-delivery of charged molecules. In this study STAT3 siRNA and IM were co-delivered and these molecules are having inhibitory role on key signaling pathways of melanoma progression, survival and invasion. The in-vitro and in-vivo silencing of STAT3 demonstrated safe delivery of siRNA upon iontophoresis application. Co-delivery of STAT3 siRNA and IM showed significant reduction in cancer cell growth by promoting apoptosis. In-vivo iontophoresis application of co-delivered LbL-AuNP showed significant reduction in tumor volume and tumor weight. Intratumoral injection of free IM did not show reduction in tumor volume due to rapid clearance, whereas LbL-AuNP retained sufficiently longer time in the tumor environment and released the IM in controlled manner for longer duration. The in-vivo gene silencing effect of siRNA delivered by LbL-AuNP can be further enhanced by altering current density and also by incorporation of penetration enhancers.

Overall, this study demonstrated that layer-by-layer assembled gold nanoparticles can be utilized for topical iontophoretic delivery of small and macromolecules for treatment of melanoma and various other skin conditions.

FUTURE SCOPE AND DIRECTIONS

Since last decade, layer-by-layer technology drawing much attention for drug delivery applications. Due to the robust nature of self-assembly process, high encapsulation efficiency, surface functionalization and biocompatibility of LbL self-assembled systems holds great potential in controlled and targeted release of various therapeutic agents.

The direct outcome of the present study led to development of potential drug delivery carrier for topical iontophoretic delivery of small and macromolecule therapeutics. To this end, the iontophoretic co-delivery of IM and STAT3 siRNA using LbL-AuNP showed enhanced tumor suppression and target gene silencing.

Future studies based on this dissertation could include the investigation of photothermal effect of AuNP along with surface functionalization of LbL-AuNP with tumor specific bio-markers for effective management of skin cancer.

This technique can be used for delivery of any charged therapeutic molecule, hence there will be broad scope for LbL technology in drug delivery. The long term focus of our research would be to investigate new methods to deliver small and macromolecule therapeutics through the skin in a non-invasive fashion.

REFERENCES

Albanese, A., Tang, P.S. and Chan, W.C., 2012.The effect of nanoparticle size, shape, and surface chemistry on biological systems. *Annual review of biomedical engineering*, *14*, pp.1-16.

Aldawsari, M., B Chougule, M. and Jayachandra Babu, R., 2015.Progress in topical siRNA delivery approaches for skin disorders. *Current pharmaceutical design*, *21*(31), pp.4594-4605.

Alegre, M.L., Frauwirth, K.A. and Thompson, C.B., 2001. T-cell regulation by CD28 and CTLA-4. *Nature Reviews Immunology*, *1*(3), pp.220-228.

Alkilani, A.Z., McCrudden, M.T. and Donnelly, R.F., 2015. Transdermal Drug Delivery: Innovative Pharmaceutical Developments Based on Disruption of the Barrier Properties of the stratum corneum. *Pharmaceutics*, *7*(4), pp.438-470.

Alkilany, A.M., Thompson, L.B., Boulos, S.P., Sisco, P.N. and Murphy, C.J., 2012. Gold nanorods: their potential for photothermal therapeutics and drug delivery, tempered by the complexity of their biological interactions. *Advanced drug delivery reviews*, *64*(2), pp.190-199.

Allen, T.M. and Cullis, P.R., 2004. Drug delivery systems: entering the mainstream. *Science*, *303*(5665), pp.1818-1822.

Alshamsan, A., Hamdy, S., Haddadi, A., Samuel, J., El-Kadi, A.O., Uludağ, H. and Lavasanifar, A., 2011. STAT3 knockdown in B16 melanoma by siRNA lipopolyplexes induces bystander immune response in vitro and in vivo. *Translational oncology*, *4*(3), pp.178-188.

Alshamsan, A., Hamdy, S., Samuel, J., El-Kadi, A.O., Lavasanifar, A. and Uludağ, H., 2010.The induction of tumor apoptosis in B16 melanoma following STAT3 siRNA delivery with a lipid-substituted polyethylenimine. *Biomaterials*, *31*(6), pp.1420-1428.

Andrews SN, Jeong E, Prausnitz MR., 2013. Transdermal delivery of molecules is limited by full epidermis, not just stratum corneum. *Pharmaceutical research*, *30*(4), pp. 1099-109.

Antonova, E., Raimundo, K. and Zazzali, J., 2015. My Hives Diary: An Ios App to Track Urticaria Symptoms. *Journal of Allergy and Clinical Immunology*, *135*(2), pp.131.

Antony, J. and Celine, T.M., 2014. A study on pattern of diseases of skin and subcutaneous tissue. *African Journal of Medical and Health Sciences*,*13*(1), p.34.

Arora, A., Prausnitz, M.R. and Mitragotri, S., 2008. Micro-scale devices for transdermal drug delivery. *International Journal of pharmaceutics*, *364*(2), pp.227-236.

Arruebo, M., Vilaboa, N., Sáez-Gutierrez, B., Lambea, J., Tres, A., Valladares, M. and González-Fernández, Á., 2011. Assessment of the evolution of cancer treatment therapies. *Cancers*, *3*(3), pp.3279-3330.

Asadishad, B., Vossoughi, M. and Alamzadeh, I., 2010. In vitro release behavior and cytotoxicity of doxorubicin-loaded gold nanoparticles in cancerous cells. *Biotechnology letters*, *32*(5), pp.649-654.

Ascenso, A., Raposo, S., Batista, C., Cardoso, P., Mendes, T., Praça, F.G., Bentley, M.V.L.B. and Simões, S., 2015. Development, characterization, and skin delivery studies of related ultradeformable vesicles: transfersomes, ethosomes, and transethosomes. *International journal of nanomedicine, 10*, pp.5837-5839.

Asero, R., Tedeschi, A. and Cugno, M., 2014. Treatment of chronic urticaria. *Immunology and allergy clinics of North America, 34*(1), pp.105-116.

Auffan, M., Rose, J., Wiesner, M.R. and Bottero, J.Y., 2009. Chemical stability of metallic nanoparticles: a parameter controlling their potential cellular toxicity in vitro. *Environmental Pollution*, *157*(4), pp.1127-1133.

Azagury, A., Khoury, L., Enden, G. and Kost, J., 2014. Ultrasound mediated transdermal drug delivery. *Advanced drug delivery reviews, 72*, pp.127-143.

Baguley, B.C., 2010. Multiple drug resistance mechanisms in cancer.*Molecular biotechnology*, *46*(3), pp.308-316.

Bahner, J.D. and Bordeaux, J.S., 2013. Non-melanoma skin cancers: photodynamic therapy, cryotherapy, 5-fluorouracil, imiquimod, diclofenac, or what? Facts and controversies. *Clinics in dermatology*, *31*(6), pp.792-798.

Bandarchi, B., Jabbari, C.A., Vedadi, A. and Navab, R., 2013. Molecular biology of normal melanocytes and melanoma cells. *Journal of clinical pathology*, *66*(8), pp.644-648.

Baptista, P., Pereira, E., Eaton, P., Doria, G., Miranda, A., Gomes, I., Quaresma, P. and Franco, R., 2008. Gold nanoparticles for the development of clinical diagnosis methods. *Analytical and bioanalytical chemistry*, *391*(3), pp.943-950.

Barckhausen, C., Roos, W.P., Naumann, S.C. and Kaina, B., 2014. Malignant melanoma cells acquire resistance to DNA interstrand cross-linking chemotherapeutics by p53-triggered upregulation of DDB2/XPC-mediated DNA repair. *Oncogene*, *33*(15), pp.1964-1974.

Baroli, B., Ennas, M.G., Loffredo, F., Isola, M., Pinna, R. and López-Quintela, M.A., 2007. Penetration of metallic nanoparticles in human full-thickness skin. *Journal of Investigative Dermatology*, *127*(7), pp.1701-1712.

Barry, B.W., 2001. Novel mechanisms and devices to enable successful transdermal drug delivery. *European journal of pharmaceutical sciences*, *14*(2), pp.101-114.

Bartlett, D.W. and Davis, M.E., 2007. Effect of siRNA nuclease stability on the in vitro and in vivo kinetics of siRNA-mediated gene silencing. *Biotechnology and bioengineering*, *97*(4), pp.909-921.

Bashir, S.J., Chew, A.L., Anigbogu, A., Dreher, F. and Maibach, H.I., 2001. Physical and physiological effects of stratum corneum tape stripping. *Skin Research and Technology*, *7*(1), pp.40-48.

Becker, S., Zorec, B., Miklavčič, D. and Pavšelj, N., 2014. Transdermal transport pathway creation: Electroporation pulse order. *Mathematical biosciences*, *257*, pp.60-68.

Bednarski, M., Dudek, M., Knutelska, J., Nowiński, L., Sapa, J., Zygmunt, M., Nowak, G., Luty-Błocho, M., Wojnicki, M., Fitzner, K. and Tęsiorowski, M., 2015. The influence of the route of administration of gold nanoparticles on their tissue distribution and basic biochemical parameters: In vivo studies. *Pharmacological Reports*, *67*(3), pp.405-409.

Benson, H.A. and Watkinson, A.C., 2012. Skin structure, function, and permeation. *Topical and Transdermal Drug Delivery and Development*, *9*(3), pp.3-22.

Benson, H.A., 2005. Transdermal drug delivery: penetration enhancement techniques. *Current drug delivery*, *2*(1), pp.23-33.

Berrocal, A., Cabañas, L., Espinosa, E., Fernández-de-Misa, R., Martín-Algarra, S., Martínez-Cedres, J.C., Ríos-Buceta, L. and Rodríguez-Peralto, J.L., 2014. Melanoma: diagnosis, staging, and treatment. Consensus group recommendations. *Advances in therapy*, *31*(9), pp.945-960.

Bhosle, M., Klingman, D., Aagren, M., Wisniewski, T. and Lee, W.C., 2011. Human growth hormone treatment: Synthesis of literature on product delivery systems and administration practices. *Journal for Specialists in Pediatric Nursing*, *16*(1), pp.50-63.

Bild, A.H., Yao, G., Chang, J.T., Wang, Q., Potti, A., Chasse, D., Joshi, M.B., Harpole, D., Lancaster, J.M., Berchuck, A. and Olson, J.A., 2006. Oncogenic pathway signatures in human cancers as a guide to targeted therapies. *Nature*, *439*(7074), pp.353-357.

Bill, M.A., Nicholas, C., Mace, T.A., Etter, J.P., Li, C., Schwartz, E.B., Fuchs, J.R., Young, G.S., Lin, L., Lin, J. and He, L., 2012. Structurally modified curcumin analogs inhibit STAT3 phosphorylation and promote apoptosis of human renal cell carcinoma and melanoma cell lines. *PLoS One*, *7*(8), p.40724.

Blume-Jensen, P. and Hunter, T., 2001. Oncogenic kinase signalling. *Nature*, *411*(6835), pp.355-365.

Boca, S.C., Potara, M., Toderas, F., Stephan, O., Baldeck, P.L. and Astilean, S., 2011. Uptake and biological effects of chitosan-capped gold nanoparticles on Chinese Hamster Ovary cells. *Materials Science and Engineering: C*, *31*(2), pp.184-189.

Bolzinger, M.A., Briançon, S., Pelletier, J. and Chevalier, Y., 2012. Penetration of drugs through skin, a complex rate-controlling membrane. *Current Opinion in Colloid & Interface Science*, *17*(3), pp.156-165.

Borges, O. and Borchard, G., 2013. Mucosal vaccination: opportunities and challenges. *Novel Immune Potentiators and Delivery Technologies for Next Generation Vaccines*, pp.65-80. Springer US.

Brown, S.D., Nativo, P., Smith, J.A., Stirling, D., Edwards, P.R., Venugopal, B., Flint, D.J., Plumb, J.A., Graham, D. and Wheate, N.J., 2010. Gold nanoparticles for the improved anticancer drug delivery of the active component of oxaliplatin. *Journal of the American Chemical Society*, *132*(13), pp.4678-4684.

Brunot, C., Ponsonnet, L., Lagneau, C., Farge, P., Picart, C. and Grosgogeat, B., 2007. Cytotoxicity of polyethyleneimine (PEI), precursor base layer of polyelectrolyte multilayer films. *Biomaterials*, *28*(4), pp.632-640.

Burdelya, L., Kujawski, M., Niu, G., Zhong, B., Wang, T., Zhang, S., Kortylewski, M., Shain, K., Kay, H., Djeu, J. and Dalton, W., 2005. Stat3 activity in melanoma cells affects migration of immune effector cells and nitric oxide-mediated antitumor effects. *The Journal of Immunology*, *174*(7), pp.3925-3931.

Byrne, J.D., Jajja, M.N., O'Neill, A.T., Bickford, L.R., Keeler, A.W., Hyder, N., Wagner, K., Deal, A., Little, R.E., Moffitt, R.A. and Stack, C., 2015. Local iontophoretic administration of cytotoxic therapies to solid tumors. *Science translational medicine*, *7*(273), pp.273-284.

Caminade, A.M., Yan, D. and Smith, D.K., 2015. Dendrimers and hyperbranched polymers. *Chemical Society Reviews*, *44*(12), pp.3870-3873.

Campbell, C.S., Contreras-Rojas, L.R., Delgado-Charro, M.B. and Guy, R.H., 2012. Objective assessment of nanoparticle disposition in mammalian skin after topical exposure. *Journal of Controlled Release*, *162*(1), pp.201-207.

Cázares-Delgadillo, J., Naik, A., Ganem-Rondero, A., Quintanar-Guerrero, D. and Kalia, Y.N., 2007. Transdermal Delivery of Cytochrome C—A 12.4 kDa protein—across Intact Skin by constant–current Iontophoresis. *Pharmaceutical research*, *24*(7), pp.1360-1368.

Cevc, G., 1996. Transfersomes, liposomes and other lipid suspensions on the skin: permeation enhancement, vesicle penetration, and transdermal drug delivery. *Critical Reviews™ in Therapeutic Drug Carrier Systems*, *13*, pp.3-4.

Cevc, G., 1997. Drug delivery across the skin. *Expert opinion on investigational drugs*, *6*(12), pp.1887-1937.

Chapman, P.B., Hauschild, A., Robert, C., Haanen, J.B., Ascierto, P., Larkin, J., Dummer, R., Garbe, C., Testori, A., Maio, M. and Hogg, D., 2011. Improved survival with vemurafenib in melanoma with BRAF V600E mutation. *New England Journal of Medicine*, *364*(26), pp.2507-2516.

Chen, A.M., Zhang, M., Wei, D., Stueber, D., Taratula, O., Minko, T. and He, H., 2009. Co-delivery of doxorubicin and Bcl-2 siRNA by mesoporous silica nanoparticles enhances the efficacy of chemotherapy in multidrug-resistant cancer cells. *Small*, *5*(23), pp.2673-2677.

Chen, M., Zakrewsky, M., Gupta, V., Anselmo, A.C., Slee, D.H., Muraski, J.A. and Mitragotri, S., 2014. Topical delivery of siRNA into skin using SPACE-peptide carriers. *Journal of Controlled Release*, *179*, pp.33-41.

Cheng, Y., C. Samia, A., Meyers, J.D., Panagopoulos, I., Fei, B. and Burda, C., 2008. Highly efficient drug delivery with gold nanoparticle vectors for in vivo photodynamic therapy of cancer. *Journal of the American Chemical Society*, *130*(32), pp.10643-10647.

Conde, J., Ambrosone, A., Hernandez, Y., Tian, F., McCully, M., Berry, C.C., Baptista, P.V., Tortiglione, C. and Jesus, M., 2015. 15 years on siRNA delivery: Beyond the State-of-the-Art on inorganic nanoparticles for RNAi therapeutics. *Nano Today*, *10*(4), pp.421-450.

Dai, D.L., Martinka, M. and Li, G., 2005. Prognostic significance of activated Akt expression in melanoma: a clinicopathologic study of 292 cases. *Journal of clinical oncology*, *23*(7), pp.1473-1482.

Davies, H., Bignell, G.R., Cox, C., Stephens, P., Edkins, S., Clegg, S., Teague, J., Woffendin, H., Garnett, M.J., Bottomley, W. and Davis, N., 2002. Mutations of the BRAF gene in human cancer. *Nature*, *417*(6892), pp.949-954.

Davis, J.E., Anderson, J.E. and Kim, K.B., 2014. Dabrafenib therapy for advanced melanoma. *Annals of Pharmacotherapy*, *48*(4), pp.519-529.

Davis, M.E., 2009. The first targeted delivery of siRNA in humans via a self-assembling, cyclodextrin polymer-based nanoparticle: from concept to clinic. *Molecular pharmaceutics*, *6*(3), pp.659-668.

Davis, M.E., Zuckerman, J.E., Choi, C.H.J., Seligson, D., Tolcher, A., Alabi, C.A., Yen, Y., Heidel, J.D. and Ribas, A., 2010. Evidence of RNAi in humans from systemically administered siRNA via targeted nanoparticles. *Nature*, *464*(7291), pp.1067-1070.

De Oliveira, R., Zhao, P., Li, N., de Santa Maria, L.C., Vergnaud, J., Ruiz, J., Astruc, D. and Barratt, G., 2013. Synthesis and in vitro studies of gold nanoparticles loaded with docetaxel. *International journal of pharmaceutics*, *454*(2), pp.703-711.

De Volder, M.F., Tawfick, S.H., Baughman, R.H. and Hart, A.J., 2013. Carbon nanotubes: present and future commercial applications. *Science*,*339*(6119), pp.535-539.

Deeks, E.D., 2014. Nivolumab: a review of its use in patients with malignant melanoma. *Drugs*, *74*(11), pp.1233-1239.

Denet, A.R., Vanbever, R. and Préat, V., 2004. Skin electroporation for transdermal and topical delivery. *Advanced drug delivery reviews*, *56*(5), pp.659-674.

Deroose, J.P., Eggermont, A.M., van Geel, A.N., de Wilt, J.H., Burger, J.W. and Verhoef, C., 2012. 20 years experience of TNF-based isolated limb perfusion for in-transit melanoma metastases: TNF dose matters. *Annals of surgical oncology*, *19*(2), pp.627-635.

Dolcet, X., Llobet, D., Pallares, J. and Matias-Guiu, X., 2005. NF-kB in development and progression of human cancer. *Virchows archiv*, *446*(5), pp.475-482.

Dong, D., Gao, W., Liu, Y. and Qi, X.R., 2015. Therapeutic potential of targeted multifunctional nanocomplex co-delivery of siRNA and low-dose doxorubicin in breast cancer. *Cancer letters*, *359*(2), pp.178-186.

Donnelly, R.F., Singh, T.R.R., Tunney, M.M., Morrow, D.I., McCarron, P.A., O'Mahony, C. and Woolfson, A.D., 2009. Microneedle arrays allow lower microbial penetration than hypodermic needles in vitro. *Pharmaceutical research*, *26*(11), pp.2513-2522.

D'Orazio, J., Jarrett, S., Amaro-Ortiz, A. and Scott, T., 2013. UV radiation and the skin. *International journal of molecular sciences*, *14*(6), pp.12222-12248.

Downward, J., 2003. Targeting RAS signalling pathways in cancer therapy. *Nature Reviews Cancer*, *3*(1), pp.11-22.

Dreaden, E.C., Alkilany, A.M., Huang, X., Murphy, C.J. and El-Sayed, M.A., 2012. The golden age: gold nanoparticles for biomedicine. *Chemical Society Reviews*, *41*(7), pp.2740-2779.

Dubey, S. and Kalia, Y.N., 2010. Non-invasive iontophoretic delivery of enzymatically active ribonuclease A (13.6 kDa) across intact porcine and human skins. *Journal of controlled release*, *145*(3), pp.203-209.

Dykman, L. and Khlebtsov, N., 2012. Gold nanoparticles in biomedical applications: recent advances and perspectives. *Chemical Society Reviews*, *41*(6), pp.2256-2282.

Egan, D.N., Yang, Z., Phillips, J. and Abkowitz, J.L., 2015. Inducing iron deficiency improves erythropoiesis and photosensitivity in congenital erythropoietic porphyria. *Blood*, *126*(2), pp.257-261.

Elias, P.M. and Friend, D.S., 1975. The permeability barrier in mammalian epidermis. *The Journal of cell biology*, *65*(1), pp.180-191.

Elsabahy, M. and Wooley, K.L., 2012. Design of polymeric nanoparticles for biomedical delivery applications. *Chemical Society Reviews*, *41*(7), pp.2545-2561.

Erkinjuntti, T., Benavente, O., Eliasziw, M., Munoz, D.G., Sulkava, R., Haltia, M. and Hachinski, V., 1996. Diffuse vacuolization (spongiosis) and arteriolosclerosis in the frontal white matter occurs in vascular dementia. *Archives of neurology*, *53*(4), pp.325-332.

Escobar-Chávez, J.J., 2012. Nanocarriers for transdermal drug delivery. *skin*, *19*, p.22.

Escobar-Chávez, J.J., Revilla-Vázquez, A.L., Domínguez-Delgado, C.L., Rodríguez-Cruz, I.M., Aléncaster, N.C. and Díaz-Torres, R., 2012. *Nanocarrier systems for transdermal drug delivery*. INTECH Open Access Publisher.

Fathi-Azarbayjani, A., Qun, L., Chan, Y.W. and Chan, S.Y., 2010. Novel vitamin and gold-loaded nanofiber facial mask for topical delivery. *Aaps Pharmscitech*, *11*(3), pp.1164-1170.

Feldman, S.R., Horn, E.J., Balkrishnan, R., Basra, M.K., Finlay, A.Y., McCoy, D., Menter, A., van de Kerkhof, P.C. and Council, I.P., 2008. Psoriasis: improving adherence to topical therapy. *Journal of the American Academy of Dermatology*, *59*(6), pp.1009-1016.

Fellner, C., 2012. Ipilimumab (yervoy) prolongs survival in advanced melanoma: serious side effects and a hefty price tag may limit its use. *Pharmacy and Therapeutics*, *37*(9), p.503.

Ferlay, J., Soerjomataram, I., Dikshit, R., Eser, S., Mathers, C., Rebelo, M., Parkin, D.M., Forman, D. and Bray, F., 2015. Cancer incidence and mortality worldwide: sources, methods and major patterns in GLOBOCAN 2012. *International journal of cancer*, *136*(5), pp.359-386.

Filip, G.A., Postescu, I.D., Bolfa, P., Catoi, C., Muresan, A. and Clichici, S., 2013. Inhibition of UVB-induced skin phototoxicity by a grape seed extract as modulator of nitrosative stress, ERK/NF-kB signaling pathway and apoptosis, in SKH-1 mice. *Food and Chemical Toxicology*, *57*, pp.296-306.

Foldvari, M., 2000. Non-invasive administration of drugs through the skin: challenges in delivery system design. *Pharmaceutical science & technology today*, *3*(12), pp.417-425.

Fraker, D.L., Alexander, H.R., Andrich, M. and Rosenberg, S.A., 1996. Treatment of patients with melanoma of the extremity using hyperthermic isolated limb perfusion with melphalan, tumor necrosis factor, and interferon gamma: results of a tumor necrosis factor dose-escalation study. *Journal of clinical oncology*, *14*(2), pp.479-489.

Gangwar, R.K., Dhumale, V.A., Kumari, D., Nakate, U.T., Gosavi, S.W., Sharma, R.B., Kale, S.N. and Datar, S., 2012. Conjugation of curcumin with PVP capped gold nanoparticles for improving bioavailability. *Materials Science and Engineering: C*, *32*(8), pp.2659-2663.

Gauglitz GG, Schauber J., 2013. Skin: architecture and Function. *Dermal Replacements in General, Burn, and Plastic Surgery*, (pp. 1-11). Springer Vienna.

Geluk, A., van Meijgaarden, K.E., Wilson, L., Bobosha, K., van der Ploeg-van, J.J., van den Eeden, S.J., Quinten, E., Dijkman, K., Franken, K.L., Haisma, E.M. and Haks, M.C., 2014. Longitudinal immune responses and gene expression profiles in type 1 leprosy reactions. *Journal of clinical immunology*, *34*(2), pp.245-255.

Ghosh, S.K. and Pal, T., 2007. Interparticle coupling effect on the surface plasmon resonance of gold nanoparticles: from theory to applications. *Chemical Reviews*, *107*(11), pp.4797-4862.

Goding, C.R., 2000. Mitf from neural crest to melanoma: signal transduction and transcription in the melanocyte lineage. *Genes & Development*, *14*(14), pp.1712-1728.

Goldberg, S.N., Gazelle, G.S. and Mueller, P.R., 2000. Thermal ablation therapy for focal malignancy: a unified approach to underlying principles, techniques, and diagnostic imaging guidance. *American journal of roentgenology*, *174*(2), pp.323-331.

Gómez, C., Costela, Á., García-Moreno, I., Llanes, F., Teijón, J.M. and Blanco, M.D., 2011. Skin laser treatments enhancing transdermal delivery of ALA. *Journal of pharmaceutical sciences*, *100*(1), pp.223-231.

Gönüllü, Ü., Üner, M., Yener, G., Karaman, E.F. and Aydoğmuş, Z., 2015. Formulation and characterization of solid lipid nanoparticles, nanostructured lipid carriers and nanoemulsion of lornoxicam for transdermal delivery. *Acta Pharmaceutica*, *65*(1), pp.1-13.

Gratieri, T. and Kalia, Y.N., 2014. Topical iontophoresis for targeted local drug delivery to the eye and skin. *Focal Controlled Drug Delivery* (pp. 263-284). Springer US.

Gratieri, T., Kalaria, D. and Kalia, Y.N., 2011. Non-invasive iontophoretic delivery of peptides and proteins across the skin. *Expert opinion on drug delivery*, *8*(5), pp.645-663.

Gray-Schopfer, V., Wellbrock, C. and Marais, R., 2007. Melanoma biology and new targeted therapy. *Nature*, *445*(7130), pp.851-857.

Günther, S., Weiser, A.A., Ahmed, J. and Preissner, R., 2007.Superhaptens and their potential role in contact dermatitis. *Drug Discovery Today: Therapeutic Strategies*, *4*(1), pp.11-17.

Guo, J., Si, L., Kong, Y., Flaherty, K.T., Xu, X., Zhu, Y., Corless, C.L., Li, L., Li, H., Sheng, X. and Cui, C., 2011. Phase II, open-label, single-arm trial of imatinib mesylate in patients with metastatic melanoma harboring c-Kit mutation or amplification. *Journal of Clinical Oncology*, *29*(21), pp.2904-2909.

Haake, A., Scott, G.A. and Holbrook, K.A., 2001. Structure and function of the skin: overview of the epidermis and dermis. *The biology of the skin*, *2001*, pp.19-45.

Han, L., Zhao, J., Zhang, X., Cao, W., Hu, X., Zou, G., Duan, X. and Liang, X.J., 2012. Enhanced siRNA delivery and silencing gold–chitosan nanosystem with surface charge-reversal polymer assembly and good biocompatibility. *ACS nano*, *6*(8), pp.7340-7351.

Harding, C.R., 2004. The stratum corneum: structure and function in health and disease. *Dermatologic therapy*, *17*(s1), pp.6-15.

Hauschild, A., Grob, J.J., Demidov, L.V., Jouary, T., Gutzmer, R., Millward, M., Rutkowski, P., Blank, C.U., Miller, W.H., Kaempgen, E. and Martín-Algarra, S., 2012. Dabrafenib in BRAF-mutated metastatic melanoma: a multicentre, open-label, phase 3 randomised controlled trial. *The Lancet*, *380*(9839), pp.358-365.

Hawrot, A., Alam, M. and Ratner, D., 2003. Squamous cell carcinoma. *Current Problems in Dermatology*, *15*(3), pp.91-133.

Hayat, S. and Nawaz, R., 2014. A descriptive review on transdermal patches. *World J. Pharm. Pharm. Sci*, *3*(12), pp.124-137.

He, C., Lu, K., Liu, D. and Lin, W., 2014. Nanoscale metal–organic frameworks for the co-delivery of cisplatin and pooled siRNAs to enhance therapeutic efficacy in drug-resistant ovarian cancer cells. *Journal of the American Chemical Society*, *136*(14), pp.5181-5184.

He, H., Pham-Huy, L.A., Dramou, P., Xiao, D., Zuo, P. and Pham-Huy, C., 2013. Carbon nanotubes: applications in pharmacy and medicine. *BioMed research international*.

Hejazi, R. and Amiji, M., 2003. Chitosan-based gastrointestinal delivery systems. *Journal of controlled release*, *89*(2), pp.151-165.

Helliwell, P.S., 2015. Screening for Psoriatic Arthritis in People with Psoriasis. *The Journal of rheumatology*, *42*(5), pp.736-738.

Herwadkar, A., Sachdeva, V., Taylor, L.F., Silver, H. and Banga, A.K., 2012. Low frequency sonophoresis mediated transdermal and intradermal delivery of ketoprofen. *International journal of pharmaceutics*, *423*(2), pp.289-296.

Hoare, C., Po, A.L.W. and Williams, H., 2000. Systematic review of treatments for atopic eczema. *Health Technol Assess*, *4*(37), pp.1-191.

Housman, T.S., Feldman, S.R., Williford, P.M., Fleischer, A.B., Goldman, N.D., Acostamadiedo, J.M. and Chen, G.J., 2003. Skin cancer is among the most costly of all cancers to treat for the Medicare population. *Journal of the American Academy of Dermatology*, *48*(3), pp.425-429.

Huang, Y., Yu, F., Park, Y.S., Wang, J., Shin, M.C., Chung, H.S. and Yang, V.C., 2010. Co-administration of protein drugs with gold nanoparticles to enable percutaneous delivery. *Biomaterials*, *31*(34), pp.9086-9091.

Ibeto, L.K. and Love, P.B., 2016. Squamous Cell Carcinoma. *Clinical Cases in Skin of Color* (pp. 89-97). Springer International Publishing.

Iqbal, N. and Iqbal, N., 2014. Imatinib: a breakthrough of targeted therapy in cancer. *Chemotherapy research and practice*.

Ishii, T., Okahata, Y. and Sato, T., 2001. Mechanism of cell transfection with plasmid/chitosan complexes. *Biochimica et Biophysica Acta (BBA)-Biomembranes*, *1514*(1), pp.51-64.

Jemal, A., Bray, F., Center, M.M., Ferlay, J., Ward, E. and Forman, D., 2011. Global cancer statistics. *CA: a cancer journal for clinicians*, *61*(2), pp.69-90.

Ji, A.M., Su, D., Che, O., Li, W.S., Sun, L., Zhang, Z.Y., Yang, B. and Xu, F., 2009. Functional gene silencing mediated by chitosan/siRNA nanocomplexes. *Nanotechnology*, *20*(40), p.405103.

Junginger, H.E., Hoogstraate, J.A. and Verhoef, J.C., 1999. Recent advances in buccal drug delivery and absorption—in vitro and in vivo studies. *Journal of controlled release*, *62*(1), pp.149-159.

Kalaria, D.R., Dubey, S. and Kalia, Y.N., 2012. Clinical applications of transdermal iontophoresis. *Topical and Transdermal Drug Delivery and Development*, pp.67-83.

Kanasty, R., Dorkin, J.R., Vegas, A. and Anderson, D., 2013. Delivery materials for siRNA therapeutics. *Nature materials*, *12*(11), pp.967-977.

Kasper, M., Jaks, V., Hohl, D. and Toftgård, R., 2012. Basal cell carcinoma—molecular biology and potential new therapies. *The Journal of clinical investigation*, *122*(2), pp.455-463.

Kaufman, E.D., Belyea, J., Johnson, M.C., Nicholson, Z.M., Ricks, J.L., Shah, P.K., Bayless, M., Pettersson, T., Feldotö, Z., Blomberg, E. and Claesson, P., 2007. Probing protein adsorption onto mercaptoundecanoic acid stabilized gold nanoparticles and surfaces by quartz crystal microbalance and ζ-potential measurements. *Langmuir*, *23*(11), pp.6053-6062.

Kean, T. and Thanou, M., 2010. Biodegradation, biodistribution and toxicity of chitosan. *Advanced drug delivery reviews*, *62*(1), pp.3-11.

Kemp, J.A., Shim, M.S., Heo, C.Y. and Kwon, Y.J., 2016. "Combo" nanomedicine: Co-delivery of multi-modal therapeutics for efficient, targeted, and safe cancer therapy. *Advanced drug delivery reviews*, *98*, pp.3-18.

Kesharwani, P., Banerjee, S., Gupta, U., Amin, M.C.I.M., Padhye, S., Sarkar, F.H. and Iyer, A.K., 2015. PAMAM dendrimers as promising nanocarriers for RNAi therapeutics. *Materials Today*, *18*(10), pp.565-572.

Khavkin, J. and Ellis, D.A., 2011. Aging skin: histology, physiology, and pathology. *Facial plastic surgery clinics of North America*, *19*(2), pp.229-234.

Kigasawa, K., Kajimoto, K., Hama, S., Saito, A., Kanamura, K. and Kogure, K., 2010. Noninvasive delivery of siRNA into the epidermis by iontophoresis using an atopic dermatitis-like model rat. *International journal of pharmaceutics*, *383*(1), pp.157-160.

Kim, B., Han, G., Toley, B.J., Kim, C.K., Rotello, V.M. and Forbes, N.S., 2010. Tuning payload delivery in tumour cylindroids using gold nanoparticles. *Nature nanotechnology*, *5*(6), pp.465-472.

Kim, B.S., Park, S.W. and Hammond, P.T., 2008. Hydrogen-bonding layer-by-layer-assembled biodegradable polymeric micelles as drug delivery vehicles from surfaces. *Acs Nano*, *2*(2), pp.386-392.

Kim, D.K., Choi, S.W. and Kwak, Y.H., 2012. The effect of SonoPrep® on EMLA® cream application for pain relief prior to intravenous cannulation. *European journal of pediatrics*, *171*(6), pp.985-988.

Kim, K.B., Eton, O., Davis, D.W., Frazier, M.L., McConkey, D.J., Diwan, A.H., Papadopoulos, N.E., Bedikian, A.Y., Camacho, L.H., Ross, M.I. and Cormier, J.N., 2008. Phase II trial of imatinib mesylate in patients with metastatic melanoma. *British journal of cancer*, *99*(5), pp.734-740.

Kimber, I., Basketter, D.A., Gerberick, G.F. and Dearman, R.J., 2002. Allergic contact dermatitis. *International immunopharmacology*, *2*(2), pp.201-211.

Kircheis, R., Wightman, L. and Wagner, E., 2001. Design and gene delivery activity of modified polyethylenimines. *Advanced drug delivery reviews*, *53*(3), pp.341-358.

Kirkwood, J.M., Bastholt, L., Robert, C., Sosman, J., Larkin, J., Hersey, P., Middleton, M., Cantarini, M., Zazulina, V., Kemsley, K. and Dummer, R., 2012. Phase II, open-label, randomized trial of the MEK1/2 inhibitor selumetinib as monotherapy versus temozolomide in patients with advanced melanoma. *Clinical Cancer Research*, *18*(2), pp.555-567.

Kis, E.E., Winter, G. and Myschik, J., 2012. Devices for intradermal vaccination. *Vaccine*, *30*(3), pp.523-538.

Klinac, D., Gray, E.S., Freeman, J.B., Reid, A., Bowyer, S., Millward, M. and Ziman, M., 2014. Monitoring changes in circulating tumour cells as a prognostic indicator of overall survival and treatment response in patients with metastatic melanoma. *BMC cancer*, *14*(1), p.423.

Klingberg, H., Oddershede, L.B., Loeschner, K., Larsen, E.H., Loft, S. and Møller, P., 2015. Uptake of gold nanoparticles in primary human endothelial cells. *Toxicology Research*, *4*(3), pp.655-666.

Kong, M., Hou, L., Wang, J., Feng, C., Liu, Y., Cheng, X. and Chen, X., 2015. Enhanced transdermal lymphatic drug delivery of hyaluronic acid modified transfersomes for tumor metastasis therapy. *Chemical Communications*, *51*(8), pp.1453-1456.

Köpping-Höggård, M., Tubulekas, I., Guan, H., Edwards, K., Nilsson, M., Varum, K. and Artursson, P., 2001. Chitosan as a nonviral gene delivery system. Structure-property relationships and characteristics compared with polyethyleneimine in vitro and after lung administration in vivo. *Gene Ther, 8*, pp.1108-1121.

Kortylewski, M., Jove, R. and Yu, H., 2005. Targeting STAT3 affects melanoma on multiple fronts. *Cancer and Metastasis Reviews, 24*(2), pp.315-327.

Koutsonanos, D.G., del Pilar Martin, M., Zarnitsyn, V.G., Sullivan, S.P., Compans, R.W., Prausnitz, M.R. and Skountzou, I., 2009. Transdermal influenza immunization with vaccine-coated microneedle arrays. *PloS one*, *4*(3), pp.4773-4778.

Kraemer, K.H., Lee, M.M. and Scotto, J., 1987. Xeroderma pigmentosum: cutaneous, ocular, and neurologic abnormalities in 830 published cases. *Archives of dermatology, 123*(2), pp.241-242.

Kuschal, C., DiGiovanna, J.J., Khan, S.G., Gatti, R.A. and Kraemer, K.H., 2013. Repair of UV photolesions in xeroderma pigmentosum group C cells induced by translational readthrough of premature termination codons. *Proceedings of the National Academy of Sciences*, *110*(48), pp.19483-19488.

Labala, S., Jose, A. and Venuganti, V.V.K., 2016. Transcutaneous iontophoretic delivery of STAT3 siRNA using layer-by-layer chitosan coated gold nanoparticles to treat melanoma. *Colloids and Surfaces B: Biointerfaces*, 146, pp.188-197.

Labala, S., Mandapalli, P.K., Kurumaddali, A. and Venuganti, V.V.K., 2015. Layer-by-Layer Polymer Coated Gold Nanoparticles for Topical Delivery of Imatinib Mesylate To Treat Melanoma. *Molecular pharmaceutics*, *12*(3), pp.878-888.

Labouta, H.I. and Schneider, M., 2013. Interaction of inorganic nanoparticles with the skin barrier: current status and critical review.*Nanomedicine: Nanotechnology, Biology and Medicine*, *9*(1), pp.39-54.

Lakmal, H.C., Samarakoon, K.W., Lee, W., Lee, J.H., Abeytunga, D.T.U., Lee, H.S. and Jeon, Y.J., 2014. Anticancer and antioxidant effects of selected Sri Lankan marine algae. *Journal of the National Science Foundation of Sri Lanka*, *42*(4), pp.315-323.

Lane, M.E., 2013. Skin penetration enhancers. *International journal of pharmaceutics*, *447*(1), pp.12-21.

Langer, R., 1990. New methods of drug delivery. *Science*, *249*(4976), pp.1527-1533.

Lapointe, R., Bellemare-Pelletier, A., Housseau, F., Thibodeau, J. and Hwu, P., 2003. CD40-stimulated B lymphocytes pulsed with tumor antigens are effective antigen-presenting cells that can generate specific T cells. *Cancer research*, *63*(11), pp.2836-2843.

Larese Filon, F., Crosera, M., Adami, G., Bovenzi, M., Rossi, F. and Maina, G., 2011. Human skin penetration of gold nanoparticles through intact and damaged skin. *Nanotoxicology*, *5*(4), pp.493-501.

Larkin, J., Chiarion-Sileni, V., Gonzalez, R., Grob, J.J., Cowey, C.L., Lao, C.D., Schadendorf, D., Dummer, R., Smylie, M., Rutkowski, P. and Ferrucci, P.F., 2015. Combined nivolumab and

ipilimumab or monotherapy in untreated melanoma. *New England Journal of Medicine*, *373*(1), pp.23-34.

Ledger, P.W., Cormier, M.J. and Amkraut, A., Alza Corporation, 1992. *Sensitizing drug and antigen processing-inhibiting agent*. U.S. Patent 5,120,545.

Lee, J., Kim, J., Go, J., Lee, J.H., Han, D.W., Hwang, D. and Lee, J., 2015. Transdermal treatment of the surgical and burned wound skin via phytochemical-capped gold nanoparticles. *Colloids and Surfaces B: Biointerfaces*, *135*, pp.166-174.

Leung, D.Y., Boguniewicz, M., Howell, M.D., Nomura, I. and Hamid, Q.A., 2004. New insights into atopic dermatitis. *The Journal of clinical investigation*, *113*(5), pp.651-657.

Levy, C., Khaled, M. and Fisher, D.E., 2006. MITF: master regulator of melanocyte development and melanoma oncogene. *Trends in molecular medicine*, *12*(9), pp.406-414.

Ling, V., 1997. Multidrug resistance: molecular mechanisms and clinical relevance. *Cancer chemotherapy and pharmacology*, *40*(1), pp.3-8.

Litvin, O., Schwartz, S., Wan, Z., Schild, T., Rocco, M., Oh, N.L., Chen, B.J., Goddard, N., Pratilas, C. and Pe'er, D., 2015. Interferon α/β Enhances the Cytotoxic Response of MEK Inhibition in Melanoma. *Molecular cell*, *57*(5), pp.784-796.

Liu, Y.J., 2001. Dendritic cell subsets and lineages, and their functions in innate and adaptive immunity. *Cell*, *106*(3), pp.259-262.

Lobovkina, T., Jacobson, G.B., Zare, R.N., Neofytou, E., Beygui, R.E. and Russo, M., The Board Of Trustees Of The Leland Stanford Junior University, 2013. *Nanoparticles, nanoparticle delivery methods, and systems of delivery*. U.S. Patent Application 13/799,883.

Lowman, A.M., Morishita, M., Kajita, M., Nagai, T. and Peppas, N.A., 1999. Oral delivery of insulin using pH-responsive complexation gels. *Journal of pharmaceutical sciences*, *88*(9), pp.933-937.

Lv, H., Zhang, S., Wang, B., Cui, S. and Yan, J., 2006. Toxicity of cationic lipids and cationic polymers in gene delivery. *Journal of Controlled Release*, *114*(1), pp.100-109.

Ma, Y.Q., 2013. Theoretical and computational studies of dendrimers as delivery vectors. *Chemical Society Reviews*, *42*(2), pp.705-727.

Madonna, G., Ullman, C.D., Gentilcore, G., Palmieri, G. and Ascierto, P.A., 2012. NF-κB as potential target in the treatment of melanoma. *Journal of translational medicine*, *10*(1), p.1.

Mandapalli, P.K., Labala, S., Vanamala, D., Koranglekar, M.P., Sakimalla, L.A. and Venuganti, V.V.K., 2014. Influence of charge on encapsulation and release behavior of small molecules in self-assembled layer-by-layer microcapsules. *Drug delivery*, *21*(8), pp.605-614.

Mansouri, Y. and Berth-Jones, J., 2011. GP guide to the diagnosis and management of eczema. *Prescriber*, *22*(4), pp.32-39.

Mao, H.Q., Roy, K., Troung-Le, V.L., Janes, K.A., Lin, K.Y., Wang, Y., August, J.T. and Leong, K.W., 2001. Chitosan-DNA nanoparticles as gene carriers: synthesis, characterization and transfection efficiency. *Journal of controlled release*, *70*(3), pp.399-421.

Mao, S., Sun, W. and Kissel, T., 2010. Chitosan-based formulations for delivery of DNA and siRNA. *Advanced drug delivery reviews*, *62*(1), pp.12-27.

Marro, D., Kalia, Y.N., Delgado-Charro, M.B. and Guy, R.H., 2001. Contributions of electromigration and electroosmosis to iontophoretic drug delivery. *Pharmaceutical research*, *18*(12), pp.1701-1708.

Masterpol, K.S., Primiani, A. and Duncan, L.M., 2013. Invasive Primary Cutaneous Melanoma. In *Atlas of Essential Dermatopathology* (pp. 102-103).Springer London.

Maverakis, E., Cornelius, L.A., Bowen, G.M., Phan, T., Patel, F.B., Fitzmaurice, S., He, Y., Burrall, B., Duong, C., Kloxin, A.M. and Sultani, H., 2015. Metastatic melanoma–a review of current and future treatment options. *Acta dermato-venereologica*, *95*(5), pp.516-527.

McArthur, G.A., Chapman, P.B., Robert, C., Larkin, J., Haanen, J.B., Dummer, R., Ribas, A., Hogg, D., Hamid, O., Ascierto, P.A. and Garbe, C., 2014. Safety and efficacy of vemurafenib in BRAF V600E and BRAF V600K mutation-positive melanoma (BRIM-3): extended follow-up of a phase 3, randomised, open-label study. *The lancet oncology*, *15*(3), pp.323-332.

Means, A.D., Prieto, V.G., Reed, J.A. and Shea, C.R., 2015. Recurrent Melanocytic Nevus Versus Melanoma. In *Pathology of Challenging Melanocytic Neoplasms* (pp. 105-113).Springer New York.

Mei, B.C., Oh, E., Susumu, K., Farrell, D., Mountziaris, T.J. and Mattoussi, H., 2009. Effects of ligand coordination number and surface curvature on the stability of gold nanoparticles in aqueous solutions. *Langmuir*, *25*(18), pp.10604-10611.

Meier, F., Schittek, B., Busch, S., Garbe, C., Smalley, K., Satyamoorthy, K., Li, G. and Herlyn, M., 2005. The RAS/RAF/MEK/ERK and PI3K/AKT signaling pathways present molecular targets for the effective treatment of advanced melanoma. *Front Biosci*, *10*(2986–3001), pp.2986-3001.

Meng, H., Mai, W.X., Zhang, H., Xue, M., Xia, T., Lin, S., Wang, X., Zhao, Y., Ji, Z., Zink, J.I. and Nel, A.E., 2013. Codelivery of an optimal drug/siRNA combination using mesoporous silica nanoparticles to overcome drug resistance in breast cancer in vitro and in vivo. *ACS nano*, *7*(2), pp.994-1005.

Micali, G., Lacarrubba, F., Bongu, A. and West, D., 2001.The skin barrier.*The biology of the skin, 14*.

Mieszawska, A.J., Mulder, W.J., Fayad, Z.A. and Cormode, D.P., 2013. Multifunctional gold nanoparticles for diagnosis and therapy of disease. *Molecular pharmaceutics*, *10*(3), pp.831-847.

Mitra, A., Agarwal, P.N., Singh, R., Verma, S., Srivastava, V., Chugh, A. and Jain, V., 2014. Squamous cell carcinoma of the scrotum-still an occupational hazard. *Indian journal of occupational and environmental medicine*, *18*(3), p.150.

Mitragotri, S. and Kost, J., 2004. Low-frequency sonophoresis: a review.*Advanced drug delivery reviews*, *56*(5), pp.589-601.

Mitragotri, S., 2013. Devices for overcoming biological barriers: the use of physical forces to disrupt the barriers. *Advanced drug delivery reviews*, *65*(1), pp.100-103.

Mitragotri, S., Blankschtein, D. and Langer, R., 1995. Ultrasound-mediated transdermal protein delivery. *Science*, *269*(5225), pp.850-853.

Mitragotri, S., Burke, P.A. and Langer, R., 2014. Overcoming the challenges in administering biopharmaceuticals: formulation and delivery strategies. *Nature reviews Drug discovery*, *13*(9), pp.655-672.

Moghimi, S.M., Symonds, P., Murray, J.C., Hunter, A.C., Debska, G. and Szewczyk, A., 2005. A two-stage poly (ethylenimine)-mediated cytotoxicity: implications for gene transfer/therapy. *Molecular Therapy*, *11*(6), pp.990-995.

Montone, K.T., Van Belle, P., Elenitsas, R. and Elder, D.E., 1997. Proto-oncogene c-kit expression in malignant melanoma: protein loss with tumor progression. *Modern pathology: an official journal of the United States and Canadian Academy of Pathology, Inc*, *10*(9), pp.939-944.

Morille, M., Passirani, C., Vonarbourg, A., Clavreul, A. and Benoit, J.P., 2008. Progress in developing cationic vectors for non-viral systemic gene therapy against cancer. *Biomaterials*, *29*(24), pp.3477-3496.

Mout, R., Moyano, D.F., Rana, S. and Rotello, V.M., 2012. Surface functionalization of nanoparticles for nanomedicine. *Chemical Society Reviews*, *41*(7), pp.2539-2544.

Mura, S., Nicolas, J. and Couvreur, P., 2013. Stimuli-responsive nanocarriers for drug delivery. *Nature materials*, *12*(11), pp.991-1003.

Naik, A., Kalia, Y.N. and Guy, R.H., 2000. Transdermal drug delivery: overcoming the skin's barrier function. *Pharmaceutical science & technology today*, *3*(9), pp.318-326.

Namvar, F., Rahman, H.S., Mohamad, R., Rasedee, A., Yeap, S.K., Chartrand, M.S., Azizi, S. and Tahir, P.M., 2015. Apoptosis Induction in Human Leukemia Cell Lines by Gold Nanoparticles Synthesized Using the Green Biosynthetic Approach. *Journal of Nanomaterials, 2015*. doi:10.1155/2015/642621
Namvar, F., Rahman, H.S., Mohamad, R., Rasedee, A., Yeap, S.K., Chartrand, M.S., Azizi, S. and Tahir, P.M., 2015. Apoptosis Induction in Human Leukemia Cell Lines by Gold Nanoparticles Synthesized Using the Green Biosynthetic Approach. *Journal of Nanomaterials, 2015*.
Niemeyer, C.M., 2001. Nanoparticles, proteins, and nucleic acids: biotechnology meets materials science. *Angewandte Chemie International Edition*, *40*(22), pp.4128-4158.

Niu, G., Bowman, T., Huang, M., Shivers, S., Reintgen, D., Daud, A., Chang, A., Kraker, A., Jove, R. and Yu, H., 2002. Roles of activated Src and Stat3 signaling in melanoma tumor cell growth. *Oncogene*, *21*(46), pp.7001-7010.

Niu, G., Heller, R., Catlett-Falcone, R., Coppola, D., Jaroszeski, M., Dalton, W., Jove, R. and Yu, H., 1999. Gene therapy with dominant-negative Stat3 suppresses growth of the murine melanoma B16 tumor in vivo. *Cancer research*, *59*(20), pp.5059-5063.

Oh, K.S., Kim, R.S., Lee, J., Kim, D., Cho, S.H. and Yuk, S.H., 2008. Gold/chitosan/pluronic composite nanoparticles for drug delivery. *Journal of applied polymer science*, *108*(5), pp.3239-3244.

Pawar, R.G., Pawar, S.D., Gadhave, M.V., Jadhav, S.L. and Gaikwad, D.D., 2012. Microneedles: Novel approach to transdermal drug delivery system. *Journal of drug delivery and therapeutics*, *2*(1), pp.76-80.

Pfeifer, G.P. and Besaratinia, A., 2012. UV wavelength-dependent DNA damage and human non-melanoma and melanoma skin cancer. *Photochemical & Photobiological Sciences*, *11*(1), pp.90-97.

Philandrianos, C., Andrac-Meyer, L., Mordon, S., Feuerstein, J.M., Sabatier, F., Veran, J., Magalon, G. and Casanova, D., 2012. Comparison of five dermal substitutes in full-thickness skin wound healing in a porcine model. *Burns*, *38*(6), pp.820-829.

Pikal, M.J., 2001.The role of electroosmotic flow in transdermal iontophoresis. *Advanced drug delivery reviews*, *46*(1), pp.281-305.

Pissuwan, D. and Niidome, T., 2012, November. Gold nanoparticles for the development of transdermal delivery systems.In *American Chemical Society*. doi:10.1021/bk-2012-1113.ch005

Poole, R.M., 2014. Pembrolizumab: first global approval. *Drugs*, *74*(16), pp.1973-1981.

Pornpattananangkul, D., Olson, S., Aryal, S., Sartor, M., Huang, C.M., Vecchio, K. and Zhang, L., 2010. Stimuli-responsive liposome fusion mediated by gold nanoparticles. *ACS nano*, *4*(4), pp.1935-1942.

Prausnitz, M.R. and Langer, R., 2008. Transdermal drug delivery. *Nature biotechnology*, *26*(11), pp.1261-1268.

Proksch, E., Brandner, J.M. and Jensen, J.M., 2008. The skin: an indispensable barrier. *Experimental dermatology*, *17*(12), pp.1063-1072.

Prow, T.W., Grice, J.E., Lin, L.L., Faye, R., Butler, M., Becker, W., Wurm, E.M., Yoong, C., Robertson, T.A., Soyer, H.P. and Roberts, M.S., 2011. Nanoparticles and microparticles for skin drug delivery. *Advanced drug delivery reviews*, *63*(6), pp.470-491.

Ragelle, H., Vandermeulen, G. and Préat, V., 2013. Chitosan-based siRNA delivery systems. *Journal of Controlled Release*, *172*(1), pp.207-218.

Ragelle, H., Vanvarenberg, K., Vandermeulen, G. and Préat, V., 2016. Chitosan Nanoparticles for SiRNA Delivery In Vitro. *SiRNA Delivery Methods: Methods and Protocols*, pp.143-150.

Raj, R., Mongia, P., Ram, A. and Jain, N.K., 2015. Enhanced skin delivery of aceclofenac via hydrogel-based solid lipid nanoparticles. *Artificial cells, nanomedicine, and biotechnology*, pp.1-6.

Raza1, R., Mittal, A., Kumar, P., Alam, S., Prakash, S. and Chauhan, N., 2015. Approaches and evaluation of Transdermal drug delivery system. *International Journal of Drug Development* and Research, *7*(1), pp.222-233.

Rejman, J., Oberle, V., Zuhorn, I.S. and Hoekstra, D., 2004. Size-dependent internalization of particles via the pathways of clathrin-and caveolae-mediated endocytosis. *Biochemical Journal*, *377*(1), pp.159-169.

Rivera, R.S., Nagatsuka, H., Gunduz, M., Cengiz, B., Gunduz, E., Siar, C.H., Tsujigiwa, H., Tamamura, R., Han, K.N. and Nagai, N., 2008. C-kit protein expression correlated with activating mutations in KIT gene in oral mucosal melanoma. *Virchows Archiv*, *452*(1), pp.27-32.

Robert, C., Karaszewska, B., Schachter, J., Rutkowski, P., Mackiewicz, A., Stroiakovski, D., Lichinitser, M., Dummer, R., Grange, F., Mortier, L. and Chiarion-Sileni, V., 2015. Improved overall survival in melanoma with combined dabrafenib and trametinib. *New England Journal of Medicine*, *372*(1), pp.30-39.

Rosenberg, S.A., Yang, J.C., Topalian, S.L., Schwartzentruber, D.J., Weber, J.S., Parkinson, D.R., Seipp, C.A., Einhorn, J.H. and White, D.E., 1994. Treatment of 283 consecutive patients with metastatic melanoma or renal cell cancer using high-dose bolus interleukin 2. *Jama*, *271*(12), pp.907-913.

Rossi, M., Cupisti, A., Ricco, R., Santoro, G., Pentimone, F. and Carpi, A., 2004. Skin vasoreactivity to insulin iontophoresis is reduced in elderly subjects and is absent in treated non-insulin-dependent diabetes patients. *Biomedicine & pharmacotherapy*, *58*(10), pp.560-565.

Rossi, S., Di Stasi, M., Buscarini, E., Cavanna, L., Quaretti, P., Squassante, E., Garbagnati, F. and Buscarini, L., 1994. Percutaneous radiofrequency interstitial thermal ablation in the treatment of small hepatocellular carcinoma. *The cancer journal from Scientific American*, *1*(1), pp.73-81.

Rudzinski, W.E. and Aminabhavi, T.M., 2010. Chitosan as a carrier for targeted delivery of small interfering RNA. *International journal of pharmaceutics*, *399*(1), pp.1-11.

Ruiz, D., Berenguer, V., Soriano, A. and SáNchez, B., 2011. A decision support system for the diagnosis of melanoma: A comparative approach. *Expert Systems with Applications*, *38*(12), pp.15217-15223.

Russak, J.E. and Rigel, D.S., 2012. Risk factors for the development of primary cutaneous melanoma. *Dermatologic clinics*, *30*(3), pp.363-368.

Sachdeva, M.S. and Patlolla, R., Florida Agricultural and Mechanical University, 2014. *Nanoparticle formulations for skin delivery*.U.S. Patent 8,715,736.

Samad, A., Sultana, Y. and Aqil, M., 2007. Liposomal drug delivery systems: an update review. *Current drug delivery*, *4*(4), pp.297-305.

Satyamoorthy, K., Li, G., Gerrero, M.R., Brose, M.S., Volpe, P., Weber, B.L., van Belle, P., Elder, D.E. and Herlyn, M., 2003. Constitutive mitogen-activated protein kinase activation in melanoma is mediated by both BRAF mutations and autocrine growth factor stimulation. *Cancer research*, *63*(4), pp.756-759.

Schadendorf, D., Ugurel, S., Schuler-Thurner, B., Nestle, F.O., Enk, A., Bröcker, E.B., Grabbe, S., Rittgen, W., Edler, L., Sucker, A. and Zimpfer-Rechner, C., 2006. Dacarbazine (DTIC) versus vaccination with autologous peptide-pulsed dendritic cells (DC) in first-line treatment of patients with metastatic melanoma: a randomized phase III trial of the DC study group of the DeCOG. *Annals of Oncology*, *17*(4), pp.563-570.

Schneider, M., Stracke, F., Hansen, S. and Schaefer, U.F., 2009. Nanoparticles and their interactions with the dermal barrier. *Dermato-endocrinology*, *1*(4), pp.197-206.

Schramm, J. and Mitragotri, S., 2002. Transdermal drug delivery by jet injectors: energetics of jet formation and penetration. *Pharmaceutical research*, *19*(11), pp.1673-1679.

Schreier, H. and Bouwstra, J., 1994. Liposomes and niosomes as topical drug carriers: dermal and transdermal drug delivery. *Journal of controlled release*, *30*(1), pp.1-15.

Sekulic, A., Migden, M.R., Oro, A.E., Dirix, L., Lewis, K.D., Hainsworth, J.D., Solomon, J.A., Yoo, S., Arron, S.T., Friedlander, P.A. and Marmur, E., 2012. Efficacy and safety of vismodegib in advanced basal-cell carcinoma. *New England Journal of Medicine*, *366*(23), pp.2171-2179.

Senft, C., Priester, M., Polacin, M., Schröder, K., Seifert, V., Kögel, D. and Weissenberger, J., 2011. Inhibition of the JAK-2/STAT3 signaling pathway impedes the migratory and invasive potential of human glioblastoma cells. *Journal of neuro-oncology*, *101*(3), pp.393-403.

Seremet, T., Lienard, D., Suppa, M., Trepant, A.L., Rorive, S., Woff, E., Cuylits, N., Jansen, Y., Schreuer, M., Del Marmol, V. and Neyns, B., 2015. Successful (neo) adjuvant BRAF-targeted therapy in a patient with locally advanced BRAF V600E mutant melanoma. *Melanoma research*, *25*(2), pp.180-183.

Shaffer, M.P. and Belsito, D.V., 2000. Allergic contact dermatitis from glutaraldehyde in health-care workers. *Contact Dermatitis*, *43*(3), pp.150-156.

Shan, Y., Ma, S., Nie, L., Shang, X., Hao, X., Tang, Z. and Wang, H., 2011.Size-dependent endocytosis of single gold nanoparticles. *Chemical Communications*, *47*(28), pp.8091-8093.

Sharma, S., Parvez, N. and Sharma, P.K., 2015. Iontophoresis-Models and Applications: A Review. *African Journal of Basic & Applied Sciences*, *7*(1), pp.01-07.

Shim, M.S. and Kwon, Y.J., 2012.Stimuli-responsive polymers and nanomaterials for gene delivery and imaging applications. *Advanced drug delivery reviews, 64*(11), pp.1046-1059.

Shukla, R., Bansal, V., Chaudhary, M., Basu, A., Bhonde, R.R. and Sastry, M., 2005. Biocompatibility of gold nanoparticles and their endocytotic fate inside the cellular compartment: a microscopic overview. *Langmuir,21*(23), pp.10644-10654.

Silva, J., Fernandes, A.R. and Baptista, P.V., 2014.Application of nanotechnology in drug delivery. *Application of nanotechnology in drug delivery*.

Singh, P. and Maibach, H.I., 1993. Iontophoresis in drug delivery: basic principles and applications. *Critical reviews in therapeutic drug carrier systems*, *11*(2-3), pp.161-213.

Sinha, V.R. and Kaur, M.P., 2000. Permeation enhancers for transdermal drug delivery. *Drug development and industrial pharmacy*, *26*(11), pp.1131-1140.

Sintov, A.C., Krymberk, I., Daniel, D., Hannan, T., Sohn, Z.E. and Levin, G., 2003. Radiofrequency-driven skin microchanneling as a new way for electrically assisted transdermal delivery of hydrophilic drugs. *Journal of Controlled Release*, *89*(2), pp.311-320.

Smalley, K.S., Haass, N.K., Brafford, P.A., Lioni, M., Flaherty, K.T. and Herlyn, M., 2006. Multiple signaling pathways must be targeted to overcome drug resistance in cell lines derived from melanoma metastases. *Molecular cancer therapeutics*, *5*(5), pp.1136-1144.

Smalley, K.S., Haass, N.K., Brafford, P.A., Lioni, M., Flaherty, K.T. and Herlyn, M., 2006. Multiple signaling pathways must be targeted to overcome drug resistance in cell lines derived from melanoma metastases. *Molecular cancer therapeutics*, *5*(5), pp.1136-1144.

Solit, D.B., Garraway, L.A., Pratilas, C.A., Sawai, A., Getz, G., Basso, A., Ye, Q., Lobo, J.M., She, Y., Osman, I. and Golub, T.R., 2006. BRAF mutation predicts sensitivity to MEK inhibition. *Nature*, *439*(7074), pp.358-362.

Sudhakar, Y., Kuotsu, K. and Bandyopadhyay, A.K., 2006. Buccal bioadhesive drug delivery-a promising option for orally less efficient drugs.*Journal of controlled release*, *114*(1), pp.15-40.

Sumimoto, H., Imabayashi, F., Iwata, T. and Kawakami, Y., 2006. The BRAF–MAPK signaling pathway is essential for cancer-immune evasion in human melanoma cells. *The Journal of experimental medicine*, *203*(7), pp.1651-1656.

Sun, Q., Kang, Z., Xue, L., Shang, Y., Su, Z., Sun, H., Ping, Q., Mo, R. and Zhang, C., 2015. A collaborative assembly strategy for tumor-targeted siRNA delivery. *Journal of the American Chemical Society*, *137*(18), pp.6000-6010.

Svenson, S. and Tomalia, D.A., 2012.Dendrimers in biomedical applications-reflections on the field. *Advanced drug delivery reviews*, *64*, pp.102-115.

Szakács, G., Paterson, J.K., Ludwig, J.A., Booth-Genthe, C. and Gottesman, M.M., 2006. Targeting multidrug resistance in cancer. *Nature reviews Drug discovery*, *5*(3), pp.219-234.

Taberner, A., Hogan, N.C. and Hunter, I.W., 2012. Needle-free jet injection using real-time controlled linear Lorentz-force actuators. *Medical engineering & physics*, *34*(9), pp.1228-1235.

Taga, T. and Kishimoto, T., 1997. Gp130 and the interleukin-6 family of cytokines. *Annual review of immunology*, *15*(1), pp.797-819.

Tamjidi, F., Shahedi, M., Varshosaz, J. and Nasirpour, A., 2013. Nanostructured lipid carriers (NLC): A potential delivery system for bioactive food molecules. *Innovative Food Science & Emerging Technologies, 19*, pp.29-43.

Tan, W.B. and Zhang, Y., 2005. Surface modification of gold and quantum dot nanoparticles with chitosan for bioapplications. *Journal of biomedical materials research Part A, 75*(1), pp.56-62.

Tanner, T. and Marks, R., 2008. Delivering drugs by the transdermal route: review and comment. *Skin Research and Technology, 14*(3), pp.249-260.

Taratula, O., Kuzmov, A., Shah, M., Garbuzenko, O.B. and Minko, T., 2013. Nanostructured lipid carriers as multifunctional nanomedicine platform for pulmonary co-delivery of anticancer drugs and siRNA. *Journal of Controlled Release, 171*(3), pp.349-357.

Thillai, K., Ross, P. and Sarker, D., 2016. Molecularly targeted therapy for advanced hepatocellular carcinoma-a drug development crisis?. *World journal of gastrointestinal oncology*, *8*(2), p.173-174.

Thomas, C.E., Ehrhardt, A. and Kay, M.A., 2003. Progress and problems with the use of viral vectors for gene therapy. *Nature Reviews Genetics*,*4*(5), pp.346-358.

Thomas, H. and Coley, H.M., 2003. Overcoming multidrug resistance in cancer: an update on the clinical strategy of inhibiting p-glycoprotein. *Cancer control*, *10*(2), pp.159-159.

Tibbitt, M.W., Dahlman, J.E. and Langer, R., 2016. Emerging frontiers in drug delivery. *Journal of the American Chemical Society*, *138*(3), pp.704-717.

Touitou, E., Junginger, H.E., Weiner, N.D., Nagai, T. and Mezei, M., 1994. Liposomes as carriers for topical and transdermal delivery. *Journal of pharmaceutical sciences*, *83*(9), pp.1189-1203.

Tournebize, J., Boudier, A., Sapin-Minet, A., Maincent, P., Leroy, P. and Schneider, R., 2012. Role of gold nanoparticles capping density on stability and surface reactivity to design drug delivery platforms. *ACS applied materials & interfaces*, *4*(11), pp.5790-5799.

Tran, M.A., Gowda, R., Sharma, A., Park, E.J., Adair, J., Kester, M., Smith, N.B. and Robertson, G.P., 2008. Targeting V600EB-Raf and Akt3 using nanoliposomal-small interfering RNA inhibits cutaneous melanocytic lesion development. *Cancer research*, *68*(18), pp.7638-7649.

Tuan-Mahmood, T.M., McCrudden, M.T., Torrisi, B.M., McAlister, E., Garland, M.J., Singh, T.R.R. and Donnelly, R.F., 2013. Microneedles for intradermal and transdermal drug delivery. *European Journal of Pharmaceutical Sciences*, *50*(5), pp.623-637.

Tucci, M., Stucci, S., Passarelli, A., Giudice, G., Dammacco, F. and Silvestris, F., 2014. The immune escape in melanoma: role of the impaired dendritic cell function. *Expert review of clinical immunology*,*10*(10), pp.1395-1404.

Tursun, I., Tazegul, G., Bozbay, A., Ozdemir, S.K., Salim, O. and Coban, E., 2015. Psoriasis and Glucose-6 Phosphate Dehydrogenase Deficiency: A Rare Association?. *Journal of Medical Cases*, *6*(11), pp.493-497.

Tyle, P., 1986. Iontophoretic Devices for Drug Delivery. *Pharmaceutical Research*, *3*(6), pp.318-326.

Uchechi, O., Ogbonna, J.D. and Attama, A.A., 2014. Nanoparticles for dermal and transdermal drug delivery. *Application of nanotechnology in drug delivery. Rijeka: InTech*, pp.193-235. doi: 10.5772/58672.

Uchida, T., Kanazawa, T., Kawai, M., Takashima, Y. and Okada, H., 2011. Therapeutic effects on atopic dermatitis by anti-RelA short interfering RNA combined with functional peptides Tat and AT1002. *Journal of Pharmacology and Experimental Therapeutics*, *338*(2), pp.443-450.

Van der Molen, R.G., Spies, F.T., Van't Noordende, J.M., Boelsma, E., Mommaas, A.M. and Koerten, H.K., 1997. Tape stripping of human stratum corneum yields cell layers that originate from various depths because of furrows in the skin. *Archives of dermatological research*, *289*(9), pp.514-518.

Velema, W.A., Szymanski, W. and Feringa, B.L., 2014. Photopharmacology: beyond proof of principle. *Journal of the American Chemical Society*, *136*(6), pp.2178-2191.

Venkatesan, R., Pichaimani, A., Hari, K., Balasubramanian, P.K., Kulandaivel, J. and Premkumar, K., 2013. Doxorubicin conjugated gold nanorods: a sustained drug delivery carrier for improved anticancer therapy. *Journal of Materials Chemistry B*, *1*(7), pp.1010-1018.

Venkatpurwar, V., Shiras, A. and Pokharkar, V., 2011. Porphyran capped gold nanoparticles as a novel carrier for delivery of anticancer drug: in vitro cytotoxicity study. *International journal of pharmaceutics*, *409*(1), pp.314-320.

Venuganti, V.V., Sahdev, P., Hildreth, M., Guan, X. and Perumal, O., 2011. Structure-skin permeability relationship of dendrimers. *Pharmaceutical research*, *28*(9), pp.2246-2260.

Venuganti, V.V.K., Saraswathy, M., Dwivedi, C., Kaushik, R.S. and Perumal, O.P., 2015. Topical gene silencing by iontophoretic delivery of an antisense oligonucleotide–dendrimer nanocomplex: the proof of concept in a skin cancer mouse model. *Nanoscale*, *7*(9), pp.3903-3914.

Villanueva, J., Vultur, A., Lee, J.T., Somasundaram, R., Fukunaga-Kalabis, M., Cipolla, A.K., Wubbenhorst, B., Xu, X., Gimotty, P.A., Kee, D. and Santiago-Walker, A.E., 2010. Acquired resistance to BRAF inhibitors mediated by a RAF kinase switch in melanoma can be overcome by cotargeting MEK and IGF-1R/PI3K. *Cancer cell*, *18*(6), pp.683-695.

Vinod, K.R., Kumar, M.S., Anbazhagan, S., Sandhya, S., Saikumar, P., Rohit, R.T. and Banji, D., 2012. Critical issues related to transfersomes–novel vesicular system. *Acta Sci Pol Technol Aliment*, *11*(1), pp.67-82.

Vitorino, C., Almeida, A., Sousa, J., Lamarche, I., Gobin, P., Marchand, S., Couet, W., Olivier, J.C. and Pais, A., 2014. Passive and active strategies for transdermal delivery using co-encapsulating nanostructured lipid carriers: in vitro vs. in vivo studies. *European Journal of Pharmaceutics and Biopharmaceutics*, *86*(2), pp.133-144.

Wagle, N., Van Allen, E.M., Treacy, D.J., Frederick, D.T., Cooper, Z.A., Taylor-Weiner, A., Rosenberg, M., Goetz, E.M., Sullivan, R.J., Farlow, D.N. and Friedrich, D.C., 2014. MAP kinase pathway alterations in BRAF-mutant melanoma patients with acquired resistance to combined RAF/MEK inhibition. *Cancer discovery*, *4*(1), pp.61-68.

Wang, F., Wang, Y.C., Dou, S., Xiong, M.H., Sun, T.M. and Wang, J., 2011. Doxorubicin-tethered responsive gold nanoparticles facilitate intracellular drug delivery for overcoming multidrug resistance in cancer cells. *Acs Nano*, *5*(5), pp.3679-3692.

Wang, J., Lu, Z., Wientjes, M.G. and Au, J.L.S., 2010. Delivery of siRNA therapeutics: barriers and carriers. *The AAPS journal*, *12*(4), pp.492-503.

Wang, Y., Thakur, R., Fan, Q. and Michniak, B., 2005. Transdermal iontophoresis: combination strategies to improve transdermal iontophoretic drug delivery. *European journal of pharmaceutics and biopharmaceutics*, *60*(2), pp.179-191.

Welch, A.J., Motamedi, M., Rastegar, S., LeCarpentier, G.L. and Jansen, D., 1991. Laser thermal ablation. *Photochemistry and photobiology*, *53*(6), pp.815-823.

Wermeling, D.P., Banks, S.L., Hudson, D.A., Gill, H.S., Gupta, J., Prausnitz, M.R. and Stinchcomb, A.L., 2008. Microneedles permit transdermal delivery of a skin-impermeant medication to humans.*Proceedings of the National Academy of Sciences*, *105*(6), pp.2058-2063.

Whitehead, K.A., Langer, R. and Anderson, D.G., 2009. Knocking down barriers: advances in siRNA delivery. *Nature reviews Drug discovery*, *8*(2), pp.129-138.

Wiedersberg, S. and Guy, R.H., 2014. Transdermal drug delivery: 30+ years of war and still fighting!. *Journal of Controlled Release*, *190*, pp.150-156.

Williams, A.C. and Barry, B.W., 2012. Penetration enhancers. *Advanced drug delivery reviews*, *64*, pp.128-137.

Wittrup, A. and Lieberman, J., 2015. Knocking down disease: a progress report on siRNA therapeutics. *Nature Reviews Genetics*, *16*(9), pp.543-552.

Wong, T.W., 2014. Electrical, magnetic, photomechanical and cavitational waves to overcome skin barrier for transdermal drug delivery. *Journal of Controlled Release*, *193*, pp.257-269.

Wyman, K., Atkins, M.B., Prieto, V., Eton, O., McDermott, D.F., Hubbard, F., Byrnes, C., Sanders, K. and Sosman, J.A., 2006. Multicenter Phase II trial of high-dose imatinib mesylate in metastatic melanoma. *Cancer*, *106*(9), pp.2005-2011.

Xie, T.X., Huang, F.J., Aldape, K.D., Kang, S.H., Liu, M., Gershenwald, J.E., Xie, K., Sawaya, R. and Huang, S., 2006. Activation of stat3 in human melanoma promotes brain metastasis. *Cancer research*, *66*(6), pp.3188-3196.

Xie, T.X., Wei, D., Liu, M., Gao, A.C., Ali-Osman, F., Sawaya, R. and Huang, S., 2004. Stat3 activation regulates the expression of matrix metalloproteinase-2 and tumor invasion and metastasis. *Oncogene*,*23*(20), pp.3550-3560.

Xu, G., Zhang, W., Bertram, P., Zheng, X.F. and McLeod, H., 2004. Pharmacogenomic profiling of the PI3K/PTEN-AKT-mTOR pathway in common human tumors. *International journal of oncology*, *24*(4), pp.893-900.

Yadav, V., Zhang, X., Liu, J., Estrem, S., Li, S., Gong, X.Q., Buchanan, S., Henry, J.R., Starling, J.J. and Peng, S.B., 2012. Reactivation of mitogen-activated protein kinase (MAPK) pathway by FGF receptor 3 (FGFR3)/Ras mediates resistance to vemurafenib in human B-RAF V600E mutant melanoma. *Journal of Biological chemistry*, *287*(33), pp.28087-28098.

Yan, G., 2015. *Iontophoresis delivery of cationic prodrugs for topical treatment of musculoskeletal or skin diseases*. U.S. Patent Application 14/689,005.

Yan, K., Todo, H. and Sugibayashi, K., 2010. Transdermal drug delivery by in-skin electroporation using a microneedle array. *International journal of pharmaceutics*, *397*(1), pp.77-83.

Yang, J., Zhang, Q., Chang, H. and Cheng, Y., 2015. Surface-engineered dendrimers in gene delivery. *Chemical reviews*, *115*(11), pp.5274-5300.

Younes, I. and Rinaudo, M., 2015. Chitin and chitosan preparation from marine sources.Structure, properties and applications. *Marine drugs*, *13*(3), pp.1133-1174.

Yu, H., Kortylewski, M. and Pardoll, D., 2007. Crosstalk between cancer and immune cells: role of STAT3 in the tumour microenvironment. *Nature Reviews Immunology*, *7*(1), pp.41-51.

Yu, H., Pardoll, D. and Jove, R., 2009. STATs in cancer inflammation and immunity: a leading role for STAT3. *Nature Reviews Cancer*, *9*(11), pp.798-809.

Zhang, S., Gao, H. and Bao, G., 2015. Physical principles of nanoparticle cellular endocytosis. *ACS nano*, *9*(9), pp.8655-8671.

Zhang, S., Leem, G., Srisombat, L.O. and Lee, T.R., 2008.Rationally designed ligands that inhibit the aggregation of large gold nanoparticles in solution. *Journal of the American Chemical Society*, *130*(1), pp.113-120.

Zhang, S., Zhao, B., Jiang, H., Wang, B. and Ma, B., 2007. Cationic lipids and polymers mediated vectors for delivery of siRNA. *Journal of Controlled Release*, *123*(1), pp.1-10.

Zhang, Z., Tsai, P.C., Ramezanli, T. and Michniak-Kohn, B.B., 2013. Polymeric nanoparticles-based topical delivery systems for the treatment of dermatological diseases. *Wiley Interdisciplinary Reviews: Nanomedicine and Nanobiotechnology*, *5*(3), pp.205-218.

Zhao, Z. and Wu, F., 2010. Minimally-invasive thermal ablation of early-stage breast cancer: a systemic review. *European Journal of Surgical Oncology (EJSO)*, *36*(12), pp.1149-1155.

Zheng, D., Giljohann, D.A., Chen, D.L., Massich, M.D., Wang, X.Q., Iordanov, H., Mirkin, C.A. and Paller, A.S., 2012. Topical delivery of siRNA-based spherical nucleic acid nanoparticle conjugates for gene regulation. *Proceedings of the National Academy of Sciences*, *109*(30), pp.11975-11980.

Zheng, D., Giljohann, D.A., Chen, D.L., Massich, M.D., Wang, X.Q., Iordanov, H., Mirkin, C.A. and Paller, A.S., 2012. Topical delivery of siRNA-based spherical nucleic acid nanoparticle conjugates for gene regulation.*Proceedings of the National Academy of Sciences*, *109*(30), pp.11975-11980.

Zhu, H.B., Yang, K., Xie, Y.Q., Lin, Y.W., Mao, Q.Q. and Xie, L.P., 2013. Silencing of mutant p53 by siRNA induces cell cycle arrest and apoptosis in human bladder cancer cells. *World journal of surgical oncology*, *11*(1), p.1-3.

Zhu, T., Vasilev, K., Kreiter, M., Mittler, S. and Knoll, W., 2003. Surface modification of citrate-reduced colloidal gold nanoparticles with 2-mercaptosuccinic acid. *Langmuir*, *19*(22), pp.9518-9525.

Zorec, B., Becker, S., Reberšek, M., Miklavčič, D. and Pavšelj, N., 2013. Skin electroporation for transdermal drug delivery: the influence of the order of different square wave electric pulses. *International journal of pharmaceutics*, *457*(1), pp.214-223.

Zsebo, K.M., Williams, D.A., Geissler, E.N., Broudy, V.C., Martin, F.H., Atkins, H.L., Hsu, R.Y., Birkett, N.C., Okino, K.H., Murdock, D.C. and Jacobsen, F.W., 1990. Stem cell factor is encoded at the SI locus of the mouse and is the ligand for the c-kit tyrosine kinase receptor. *Cell*, *63*(1), pp.213-224.

Zuniga, R. and Nguyen, T., 2013. Skin conditions: emerging drug-resistant skin infections and infestations. *FP essentials*, *407*, pp.17-23.

LIST OF PUBLICATIONS AND PRESENTATIONS

From thesis

1. Labala, S., Jose, A. and Venuganti, V.V.K., 2016. Transcutaneous iontophoretic delivery of STAT3 siRNA using layer-by-layer chitosan coated gold nanoparticles to treat melanoma. *Colloids and Surfaces B: Biointerfaces*, 146, pp. 188-197.

2. Labala, S., Mandapalli, P.K., Kurumaddali, A. and Venuganti, V.V.K., 2015. Layer-by-layer polymer coated gold nanoparticles for topical delivery of imatinib mesylate to treat melanoma. *Molecular pharmaceutics*, *12*(3), pp.878-888.

3. Labala, S., Mandapalli, P.K., Bhatnagar, S. and Venuganti, V.V.K., 2015. Encapsulation of albumin in self-assembled layer-by-layer microcapsules: comparison of co-precipitation and adsorption techniques. *Drug development and industrial pharmacy*, *41*(8), pp.1302-1310.

Other publications

1. Mandapalli, P.K., Labala, S., Jose, A., Bhatnagar, S., Janupally, R., Sriram, D. and Venuganti, V.V.K., 2016. Layer-by-Layer Thin Films for Co-Delivery of TGF-β siRNA and Epidermal Growth Factor to Improve Excisional Wound Healing. *AAPS PharmSciTech*, pp.1-12.

2. Mandapalli, P.K., Labala, S., Chawla, S., Janupally, R., Sriram, D. and Venuganti, V.V.K., 2015. Polymer–gold nanoparticle composite films for topical application: Evaluation of physical properties and antibacterial activity. *Polymer Composites*. early online, DOI: 10.1002/pc.23885.

3. Mandapalli, P.K., Labala, S., Bojja, J. and Venuganti, V.V.K., 2016. Effect of pirfenidone delivered using layer-by-layer thin film on excisional wound healing. *European Journal of Pharmaceutical Sciences*, *83*, pp.166-174.

4. Mandapalli, P.K., Labala, S., Vanamala, D., Koranglekar, M.P., Sakimalla, L.A. and Venuganti, V.V.K., 2014. Influence of charge on encapsulation and release behavior of small molecules in self-assembled layer-by-layer microcapsules. *Drug delivery*, *21*(8), pp.605-614.

Papers accepted/presented in conference

From thesis

1. Suman Labala, Anup Jose, Mohammed Shareef Khan, Sumeet Chawla, Onkar Prakash Kulkarni, Venkata Vamsi Krishna Venuganti. Co-delivery of STAT3 siRNA, imatinib mesylate using layer-by-layer chitosan coated gold nanoparticles, National level symposium on Sipra innovative pharma research awards conducted by Sipra Labs Limited, Hyderabad, India. July' 2016.

2. Suman Labala, Venkata Vamsi K. Venuganti, STAT3 siRNA and chitosan layer-by-layer coated gold nanoparticles to treat melanoma. AAPS Annual Meeting and Exposition 2015, Orlando, USA. Oct' 2015.

3. Suman Labala, Praveen Kumar Mandapalli, Venkata Vamsi Krishna Venuganti. Layer-by-layer polymer coated gold nanoparticles for topical delivery of imatinib mesylate to treat melanoma. AAPS Annual Meeting and Exposition 2014, San Diego, USA. Nov' 2014.

4. Suman Labala, Praveen Kumar Mandapalli, Shubhmita Bhatnagar, Venkata Vamsi Krishna Venuganti. Preparation, characterization and protein deliverability of layer-by-layer microcapsules. AAPS Annual Meeting and Exposition 2014, San Diego, USA. Nov' 2014.

5. Suman Labala, Shubhmita Bhatnagar, Praveen Kumar Mandapalli, Venkata Vamsi Krishna Venuganti. Preparation and characterization of self-assembled layer-by-layer microcapsules to deliver model protein. 65th Indian Pharmaceutical Congress, Dec' 20-22, 2013, New Delhi, India.

Other presentations

1. Anup Jose, Suman Labala, Venkata Vamsi K. Venuganti. Preparation, characterization and in-vitro evaluation of ceramide containing liposome - STAT3 siRNA complex to treat skin cancer. AAPS Annual Meeting and Exposition 2015, Orlando, USA. Oct' 2015

2. Rahul Sonawane, Onkar Kulkarni, Suman Labala, Venkata Vamsi Venuganti. Nasal Delivery of Tetanus Toxoid Loaded Polymeric Nanoparticles with Additional Adjuvant Effect. AAPS Annual Meeting and Exposition 2015, Orlando, USA. Oct' 2015

3. Praveen Kumar Mandapalli, Jagadeesh Balija, Suman Labala, Venkata Vamsi Krishna Venuganti. Preparation, characterization and in vivo evaluation of pirfenidone loaded layer-by-layer films for dermal wound management. AAPS Annual Meeting and Exposition 2014, San Diego, USA. Nov' 2014.

4. P.K. Mandapalli, S. Labala, D. Sriram, J. Renuka, V.V.Venuganti. Polymeric composites containing gold nanoparticles as antimicrobial agents for topical applications. Biomaterials International, June 1-5, 2015, Kenting, Taiwan.

5. Praveen Kumar Mandapalli, Suman Labala, Venkata Vamsi Krishna Venuganti. Influence of charge on encapsulation and release of small molecules from PSS/PAH layer by layer microcapsules. 65th Indian Pharmaceutical Congress, Dec' 20-22, 2013, New Delhi, India.

6. S. Pawar, M. Akula, S. Labala, Venkata Vamsi K. Venuganti, A. Bhattacharya, A. Nag. Surfactant sensitized fluorescence sensing of Zn2+ in water and its application in bioimaging. 17th CRSI National Symposium in Chemistry, National Chemical Laboratory, Pune, India.

7. Praveen K. Mandapalli, Suman Labala, Sumeet Chawla, Venkata Vamsi K. Venuganti. Evaluation of anti-microbial activity of gold nanoparticle loaded polymer films for topical application. 66th Indian Pharmaceutical Congress, Jan' 23-24, 2015, Hyderabad, India.

AWARDS AND RECOGNITIONS

1. Awarded International Travel Support (ITS) Grant by Science and Engineering Research Board (SERB), Dept. of Science and Technology, Govt. of India to present a paper at AAPS Annual Meeting and Exposition 2015, Orlando, Florida. November, 2015.

2. Awarded International Travel Award by Indian Council of Medical Research (ICMR), Govt. of India to present a paper at AAPS 2014, San Diego, CA. October, 2014.

3. Awarded International Travel Award by Centre for International Co-operation in Science (CICS), Govt. of India to present a paper at AAPS Annual Meeting and Exposition 2014, San Diego, USA. November, 2014.

Biography of Suman Labala

Mr. Suman Labala has completed his B. Pharm (2007) from KVSR Siddhartha College of Pharmaceutical Sciences, Vijayawada, Andhra Pradesh. He obtained his M. Pharm (2009) from Manipal University, Manipal, Karnataka. Later, he worked as a formulation scientist in Research and Development, Biocon Limited, Bangalore. He joined BITS-Pilani, Hyderabad campus in July 2012 for pursuing his doctoral studies under the supervision of Dr. Venkata Vamsi Krishna Venuganti. He has authored/co-authored research papers in renowned international and national peer-reviewed journals. He was awarded gold medal from Indian Pharmaceutical Association (IPA) and scholarship from Ministry of Human Resource Development (MHRD), India. Mr. Suman received travel grants from Indian Council of Medical Research (ICMR) and Centre for International Co-operation in science (CICS) and Department of science and technology (DST) to present his research work.

Biography of Dr. Venkata Vamsi Krishna Venuganti

Dr. Venkata Vamsi Krishna Venuganti is currently working as Assistant Professor in Department of Pharmacy, BITS-Pilani, Hyderabad Campus. He received his B. Pharm degree (2004) from Kakatiya University, India. He was awarded with PhD degree from South Dakota State University, USA (2010) in Pharmaceutical Sciences. He has been working as a faculty member in BITS-Pilani, Hyderabad Campus since July, 2010. He has 1 Indian patent, 14 publications to his credit and authored a book chapter in “Nanosystems for skin drug delivery. In. Nanoparticulate delivery systems II. Formulation and Characterization” published by Informa Healthcare Inc, New York, NY, USA. Currently he has four government ongoing sponsored research projects. He has successfully completed two projects funded by BITS-Pilani (Research initiation grant) and Department of Science and Technology - SERB Young Scientist Award, India.